The evolution of the Archaean continental crust of Northern Zimbabwe

Thesis

The Evolution of the Archaean Continental Crust of Northern Zimbabwe

A thesis presented for the degree of Doctor of Philosophy

by

Jon Stanley Dougherty-Page
B.A. (Hons.) *Oxon.* 1989

Department of Earth Sciences

The Open University.

Submitted 22nd of April, 1994

EX12

HIGHER DEGREES OFFICE

LIBRARY AUTHORISATION FORM

Please return this form to the Higher Degrees Office with the bound library copies of your thesis. All students should complete Part 1. Part 2 applies only to PhD students.

Student: JON STANLEY DOUGHERTY-PAGE PI: M7063198

Degree: DOCTOR OF PHILOSOPHY

Thesis title: THE EVOLUTION OF THE ARCHAEAN CONTINENTAL CRUST OF NORTHERN ZIMBABWE

Part 1 Open University Library Authorisation (to be completed by all students)

I confirm that I am willing for my thesis to be made available to readers by the Open University Library, and that it may be photocopied, subject to the discretion of the Librarian.

Signed: Date: 26th April 1995

Part 2 British Library Authorisation (to be completed by PhD students only)

If you want a copy of your PhD thesis to be held by the British Library, you must sign a British Doctoral Thesis Agreement Form. You should return it to the Higher Degrees Office with this form and your bound thesis. *You are also required to supply a third, unbound copy of your thesis.* The British Library will use this to make their microfilm copy; it will not be returned. Information on the presentation of the thesis is given in the Agreement Form.

If your thesis is part of a collaborative group project, you will need to obtain the signatures of others involved for the Agreement Form.

The University has agreed that the lodging of your thesis with the British Library should be voluntary. Please tick either (a) or (b) below to indicate your intentions.

(a) ☐ I am willing for the Open University to supply the British Library with a copy of my thesis. A signed Agreement Form and 3 copies of my thesis are attached (two bound as specified in Section 9.4 of the Research Degree Handbook and the third unbound).

(b) ☑ I do not wish the Open University to supply a copy of my thesis to the British Library.

Signed: _____ Date: _____

Abstract

Granitoid clasts preserved in Late Archaean conglomerates indicate the presence of continental crust in Northern Zimbabwe prior to the ≈ 2.7 to ≈ 2.6 Ga "event" which terminated with the stabilisation of the Zimbabwe Craton. The "Kober Technique" (Kober, 1986, 1987) of direct thermal ionisation of zircons has been set up in order to investigate the geochronological record preserved in such clasts. Conglomerates were sampled from two localities, Shamva, within the central part of Northern Zimbabwe, and Chinhoyi, at the north-western boundary of the craton. The results from both localities demonstrate the presence of continental crust in Northern Zimbabwe with a long and complex history prior to the Late Archaean "event". The minimum age of continental crust in the Shamva region is 3.34 Ga (Sm-Nd model age), with further episodes of granitiod intrusion indicated by zircon crystallisation at 3,197 ± 10 Ma, 2,925 ± 10 Ma, and 2,800 ± 20 Ma (Pb-Pb zircon). The Chinhoyi region has a shorter, simpler history, with the earliest recorded continental crust at 2,875 ± 3 Ma and later intrusions of granitoids at 2,800 ± 20 Ma, and 2,720 ± 6 Ma (Pb-Pb zircon).

Chemically, the early crust was dominated by sodic, Tonalite-Trondhjemite-Granodiorite granitoids, whose formation may be modelled by the partial melting of metabasalts with residual hornblende and/or garnet. By contrast, the granitoids formed during the Late Archaean "event" which culminated in the stabilisation of the craton, dominantly follow calc-alkaline trends, and their formation may be modelled by the fractionation of basaltic magmas (combined with assimilation of pre-existing continental material) or intra-crustal remelting. This major switch in the origins (and hence chemistry) of granitoids may be attributed to mantle plume activity, the onset of which is recorded by the presence of greenstone belt volcanics derived from anomalously hot mantle, dated at 2,713 ± 15 Ma (U-Pb zircon Jelsma, 1993).

Acknowledgements

I would like to thank Chris Hawkesworth for his patient supervision and constructive comments on earlier versions of this thesis; Peter van Calsteren for his support in setting up the zircon technique; Mabs Johnston for her help in the lab; Steve Wyatt and Keith Parrish at Oxford University for carrying out X.R.F. analyses; Béatrice Luais for encouragement, Nd analyses and discussions about earlier versions of the text, which was also improved by comments from Simon Turner; Nick Rogers for INAA data; Trevor Lambert and Chris Jones for their help with statistics; Steven Moorbath for supplying samples of the Sesombi Tonalite; Hielke Jelsma for sending me a copy of his thesis, and J.D. Kramers for his support and hospitality during my fieldwork in Zimbabwe.

For my friends, most thanks of all has to go to Béatrice, for putting up with bits of engine in the sink, coping with some of my stranger ideas, and generally believing in me, amongst other things. And thanks to all the others I shared houses, offices, meals, beers and coffee with while I was in Milton Keynes - far too many to mention you all, but then I was there for *ages*. Some of the best bits seemed to involve Phil (git) Gravestock, Simon Lomas, Ned, Marcie, Jason Newton, Simon Turner and Kathy Stewart, Andy Sutton, Jessica Bartlett, Fran Garland, Mike Ayers, Helen Budgey, Linda Kirstein, Geoff Nowell, Beto de Souza, Penny King, Derek Vance and Graham Pearson. Special thanks really should go to Simon, Kathy and Beto for giving me a great place to stay, cake and the finest wines known to humanity for the last few months. And last of all, I'd like to thank my family for giving me a sane place to run to when I needed it.

Index

Lists of Captions

FIGURE CAPTIONS

CHAPTER ONE

Figure 1.1 A geological sketch map of the Archaean Craton of Zimbabwe, showing the major geological divisions, and the locations of the major greenstone belts (in italics), and some previously dated granitoids. (1) the Tokwe Gneiss; (2) the Mushandike Gneiss; (3) the Shabani Gneiss (4) the Mont d'Or Granodiorite; (5) the Chingezi Tonalite; (6) the Rhodesdale gneiss; (7) the Umwindsi Gneiss; (8) the Mashaba Tonalite; (9) the Gwenoro Migmatite; (10) the White Waters Tonalite; (11) the Sombula Tonalite (12) the Sesombi Tonalite; (13) the Chinamora Batholith. The "Wedza Suite" of syn-tectonic tonalites outcrop in the batholiths which surround the Harare-Shamva greenstone belt.

Figure 1.2 Previous Geochronological Work on Zimbabwean Granitoids. References to table 1.1: (1)Dodson et al, '88; (2)Moorbath et al, '76; (3)Taylor et al, '84; (4)Taylor et al, '91; (5)Compston et al, '90; (6)Moorbath et al, '87; (7)Moorbath, '77; (8)Moorbath et al,'86; (9)Hawkesworth et al, '75; (10)Baldock and Evans, '88; (11)NERC Geoscience Lab report '90-'92; (12)Jelsma, '93; (13)Kamber et al. '93; (14)Hickman, '78; (15)Hamilton et al, '77; (16)Hickman, '74; (17)Hawkesworth et al. '79; (18)Vinyu et al. '93

Figure 1.3 Previous geochronological work on Zimbabwean Greenstones. References given in table 1.2

Figure 1.4 CaO - Na_2O - K_2O diagram for Upper Bulawayan granitoids, showing the broad range of compositions for the Wedza and late tectonic (Mazowe) granitoids, and the restricted range in composition, and comparatively high K_2O/Na_2O ratio of the late granites of the Chilimanzi suite (after Jelsma, 1993).

CHAPTER 2

CHAPTER THREE

Figure 3.1 Geological sketch map of Northern Zimbabwe, showing the major geological divisions and the two clast sample localities, one at the Shamvaian type locality, on the Mazowe river near Shamva, and the other on the north-western margin of the craton, at Chinhoyi.

Figure 3.2 Geological sketch map of the Shamva sampling locality

Figure 3.3 Chondrite normalised REE plots of sediments from the Shamva type locality (89-S-3 analysed in this study, data for sample numbers 519, 534, 635 from Jelsma, 1993) compared with an average REE pattern for tonalitic clasts held within the basal conglomerate (this study) and an average REE pattern for basic volcanics from the Harare-Shamva greenstone belt (data from Jelsma, 1993).

Figure 3.4 Cr/Th vs age diagram (after Condie and Wronkiewickz 1990). The grey field defines the typical range of Cr/Th ratios through time. The Shamva sediments plot in the lower range of this field for their time (2.67 Ga), intermediate between an average Cr/Th ratio for TTG clasts (0.21) contained in the basal conglomerate of the Shamvaian and an average greenstone composition (72). This average composition was calculated using data from Jelsma (1993). The average Cr/Th ratio of felsic greenstone belt volcanics is 35.3, and the average Cr/Th ratio of mafic greenstone belt volcanics is 88.7. The ratio for felsic to mafic greenstones exposed at present is 1:2.2, and mixing these two components in this ratio gives the average value of 72. Simple lever rule mixing calculations suggest that the composition of the sediment is consistent with it being made up of a mixture of material derived from the TTG terrain in a range of ratios from approximately 1:1 to 2:1 (TTG: greenstone ratio).

Figure 3.5 Feldspar ratio plot using Anorthite-Albite-Orthoclase CIPW normative compositions for the Shamva clasts (after O'Connor, 1965)

Figure 3.6 Major elements vs. Silica for the Shamva Clasts, showing 2 clearly defined groups. Group 1 (dark shading) has better defined trends and a lower silica content than group 2 (light shading). The unshaded fields are from the Chingezi and Mashaba Tonalites of Southern Zimbabwe (data from Luais and Hawkesworth, 1984).

Figure 3.25 Chondrite normalised REE patterns of the Chinhoyi group 2 clasts compared with a "Low-Alumina Trondhjemite" (Barker and Arth, 1976) from the Ancient Gneiss complex of Swaziland (bold line)(Data from Condie and Hunter, 1976), and an experimentally produced "Low-Alumina Trondhjemite", produced by partial melting of a metabasite at 8 kbar pressure and 1000°C (dashed line) (Rapp et al. 1991).

Figure 3.26 Zircon data from the Chinhoyi group 1 clast 89-C-15 (a) Index of reliability of data *vs.* age scatter graph; (b) Frequency within a 10 Ma interval *vs.* age histogram; (c) Weighted frequency *vs.* age histogram. See Chapter 2:4 for a full explanation of the use of these diagrams

Figure 3.27 Frequency within a 10 Ma interval *vs.* age histogram for the Chinhoyi group 1 clasts 89-C-20 and 89-C-28. (a) data for 89-C-20 (b) data for 89-C-28 (c) combined data.

Figure 3.28 Zircon data from the Chinhoyi group 2 clast 89-C-21 (a) Index of reliability of data *vs.* age scatter graph; (b) Frequency within a 10 Ma interval *vs.* age histogram; (c) Weighted frequency *vs.* age histogram. See Chapter 2:4 for a full explanation of the use of these diagrams

Figure 3.29 Zircon data from the Chinhoyi group 2 clast 89-C-23 (a) Index of reliability of data *vs.* age scatter graph; (b) Frequency within a 10 Ma interval *vs.* age histogram; (c) Weighted frequency *vs.* age histogram. See Chapter 2:4 for a full explanation of the use of these diagrams

Figure 3.30 Geological sketch map of the Archaean craton of Zimbabwe, showing the major geological divisions, the boundary between the eastern and western successions of Upper Bulawayan greenstones, and the locations of granites and greenstones dated in previous work (table 4) and this study (table 5).

Figure 3.31 Zircon data from the Sesombi Tonalite (a) Index of reliability of data *vs.* age scatter graph; (b) Frequency within a 10 Ma interval *vs.* age histogram; (c) Weighted frequency *vs.* age histogram. See Chapter 2:4 for a full explanation of the use of these diagrams

Figure 3.32 A graph of $^{206}Pb/^{204}Pb$ *vs.* age for zircons from 89-H-1, a sample of the Chingezi Tonalite collected from a volcanic breccia in the Hokonui Formation. 2 of the samples "zircon 1" (10 zircons heated within a single filament) and "zircon 2", a single crystal, gave suites of ages up to a maximum value of 2,840 Ma. The third crystal, "zircon 3", gives a

clustering of data at 2660 Ma, and is rejected as a contaminant from the Sesombi Tonalite (figure 3.31)

Figure 3.33 A graph of $^{206}Pb/^{204}Pb$ and $^{208}Pb/^{206}Pb$ *vs.* age for a single zircon from the Mashaba Tonalite (sample 89Zb-12, supplied by B.Luais). There is a suite of ages up to 3,250 Ma. The shaded region indicates the possible crystallisation date of a high $^{208}Pb/^{206}Pb$ phase of zircon at ≈ 2.87 Ga, coincident with the Rb-Sr age of the rock. (2860 ± 60 Ma).

Figure 3.34 Shows the data presented in tables 3.5 and 3.5, comparing the zircon data obtained in this work (horizontal lines, with grey shading to represent error bars) with previously published data (black squares with vertical error bars)

CHAPTER FOUR

Figure 4.1 Potential temperatures of Archaean plumes estimated from komatiites. Plume temperatures are assumed to be ≈ 300°C higher than average mantle temperatures, thus closely relating the thermal evolution of the mantle to a secular cooling curve (after Nisbet et al. 1993).

Figure 4.2 A curve relating mantle potential temperature to thickness of oceanic crust (after Galer, 1991), predicting (A) 7 km thick oceanic crust for a modern upper mantle potential temperature of 1280°C, and (B) ≈ 22 km thick oceanic crust for a 170°C hotter Archaean mantle.

Figure 4.3 A non-uniformitarian model for Archaean plate tectonic processes (Davies, 1992) in which the inherent buoyancy of oceanic crust prevents it being easily returned to the mantle. Oceanic crust piles up over symmetrical "subduction" zones, and may only return into the mantle once it had entered the eclogite field.

Figure 4.4 An age map of the Zimbabwe craton, showing the ≥ 3.8 Ga Tokwe segment, the area within which rocks older than 2.9 Ga have been recognised, and the region of "Kwekwe" type leads (analysed from galenas, Richardson, 1975) which contain a component ≥ 3.5 Ga old (Kramers and Foster, 1982). These demonstrate that the craton grew first to the north, and then to towards the north-west. However, there is

LIST OF TABLE CAPTIONS

CHAPTER ONE

CHAPTER THREE

LIST OF PHOTOGRAPH CAPTIONS

CHAPTER ONE

Photograph 1.1 Liquid immicibility ocelli within the rim of a komatiitic pillow lava, basal Reliance formation, Upper Bulawayan of the Belingwe Greenstone belt.

CHAPTER TWO

Photograph 2.1 A single zircon crystal folded into an evaporation filament. Width of zircon crystal ≈ 0.2 mm.

Photograph 2.2 Half of a large red zircon crystal from 89-S-14 (length of crystal ≈ 0.3 mm), showing a complex crystal habit indicative of formation at high temperatures (see figure 2.1).

Photograph 2.3 White zircon crystals from 89-S-14, showing simple prismatic crystal forms indicative of formation a low temperatures (see figure 2.1). Same magnification as above.

CHAPTER THREE

Photograph 3.1 The Shamva sediments (the top of the main conglomeratic unit, where most of the samples were collected) showing conglomeratic horizons with well rounded clasts, interbedded with greywacke horizons. Sledge-hammer for scale.

Photograph 3.2 Photomicrograph of Shamva sediment. Scale bar = 0.5 mm. The rock contains the metamorphic minerals biotite, amphibole and chlorite. This specimen (from within a conglomeratic horizon) has undergone shearing, with "major"shears running vertically (eg. to the left of the scale bar) and a subsidiary set of shears running steeply up from left to right

Photograph 3.3 Photomicrograph of the Shamva group 1 clast 89-S-14, showing badly weathered feldspars, but comparatively fresh biotite. Scale bar ≈ 0.5 mm

Photograph 3.4 Photomicrograph of the Shamva group 2 clast 89-S-12. The alteration of this clast has been more intensive than for the group 1 clast pictured above, with replacement of biotite by chlorite. Scale bar ≈ 0.5 mm

Photograph 3.5 Zircons from 89-S-23. The field of view is ≈ 1 mm. The population is extremely heterogeneous, and several of the crystals have visible cores and rims.

Photograph 3.6 Zircons from the Shamva group 2 clast 89-S-19. The fragment of crystal to the right shows a well defined reddish core, with a white rim.

Photograph 3.7 A zircon from Shamva group 2 clast 89-S-12 which has been analysed by the Kober technique (zircon 89-S-12/2), and is now pseudomorphed by baddeleyite. The top of the crystal still clearly retains its original multi-faceted high S-number typology. The zircon is approximately 0.3 mm long.

Photograph 3.8 A large clast in the Eldorado conglomerate, with a sledge-hammer for scale. Note the tectonic deformation of the clast and the surrounding conglomerate

Photograph 3.9 Photomicrograph of the sediment from Chinhoyi. The metamorphic assemblage is dominated by greenish biotite (kinked by later deformation at the left of the picture) and chlorite. Scale bar ≈ 0.5 mm.

Photograph 3.10 Photomicrograph of the Chinhoyi group 1 clast 89-C-15, showing the severe low-grade alteration common to all the Chinhoyi clasts, with the breakdown of mafic phases to chlorite and opaques, and saussuritisation of plagioclase. Note the zircon crystals within the group of mafics at the top of the picture

Photograph 3.11 Zircons from the Chinhoyi group 1 clast 89-C-15. The zircons are of high quality, homogeneous in typology, with magmatic inclusions and magmatic growth zoning. Field of view ≈1 mm.

Photograph 3.12 Zircons from the Chinhoyi group 1 clast 89-C-20. The zircons are of poor quality, and many show irregular overgrowths of a second generation of zircon. Field of view ≈ 1mm.

Photograph 3.13 High quality zircons from Chinhoyi group 2 clast 89-C-21. Width of field of view ≈ 1mm.

Photograph 3.14 High quality zircons from Chinhoyi group 2 clast 89-C-23. Width of field of view ≈ 1mm.

Photograph 3.15 Large, multi-faceted zircons from the Sesombi Tonalite. The crystals are well formed, up to 0.4 mm in length, with magmatic zoning and inclusions.

Chapter One

Introduction

1:1 INTRODUCTION

There are major differences, both in bulk chemical composition and trace element ratios, between Archaean continental crust, average (modern) continental crust and juvenile material incorporated into the continental crust at the present day (Barker et al. 1981; Martin, 1986; Ellam and Hawkesworth, 1988; Drummond and Defant, 1990). Therefore an understanding of the processes responsible for crust generation in the Archaean should provide important insights into the growth of the present continental mass. Information on the chemical processes responsible for the development of continental crust in the Archaean is recorded in the geochemistry of Archaean granitoids. This thesis describes a study of the Zimbabwe craton, incorporating a combination of geochemical and high-precision geochronological analyses on such granitoids, allowing the following problems to be addressed: (i) the age of the earliest continental nucleii within a given region. (ii) Timing of significant chemical changes. (iii) Possible age polarity across a segment of early continental crust (modern sites of tectonic, as opposed to plume-related, volcanism are essentially linear, resulting in strong arc- or ridge-parallel age zonations. Therefore the presence of such age zonations would be strong evidence for the operation of plate tectonic processes in the Archaean). (iv) The length of time within which the area of continental crust under investigation was formed and stabilised, and

the number of magmatic "events" which occurred during this time, from which the rate at which the continent formed may be deduced.

Numerous studies of Archaean granitoids (Barker and Arth, 1976; Martin, 1986; Rudnick and Taylor, 1986; Arkani-Hamed and Jolly, 1989; Drummond and Defant, 1990; Rapp et al. 1991; Luais and Hawkesworth 1994), indicate that the processes by which granitoids were generated in the Archaean were significantly different to those operating today, producing a sodic, Tonalite-Trondhjemite-Granodiorite (TTG) suite, rather than the more potassic calc-alkaline suite dominant today. Geochronological data on these early TTG terrains indicate that their earliest histories have often been almost totally erased by later tectonic and magmatic activity, and are now only recorded as anomalously old isotopic model ages and zircon cores (Froude et al. 1983; Compston and Pidgeon, 1986; Black et al. 1986; Compston and Kröner, 1988; Dodson et al. 1988; Bowring et al. 1989; Wendt et al. 1993a). However, although such geochronological data may provide important information on the longevity of the early crust, little information is given on the chemistry of the crust. On the basis of Sm-Nd data, it has been proposed that this early enriched crust was basaltic (Chase and Patchett, 1988; Galer and Goldstein, 1991), and although extremely ancient (≈ 4.2 Ga) zircons from Mt. Narryer have rare earth element patterns consistent with their growth within a chemically evolved "granitic" source (Maas et al. 1992), it is possible that this source was small-volume felsic differentiates within mafic/ultramafic "oceanic" crust. Therefore a less contentious indication of the initiation of granitoid-dominated continental crust within a region would provide invaluable information on the chemistry, longevity, growth rates and extent of the now re-worked proto-continents which formed the nucleii of the cratons.

This thesis examines such proto-continental material, through the study of granitoid clasts in late Archaean conglomerates in northern

Zimbabwe. These conglomerates are polymict, and the granitoid clasts they contain are up to one metre in diameter. The study of the clasts provides a "window" onto the continental surface from which they were eroded, which was extensively re-worked in the late Archaean, and is now present only as rare migmatitic gneisses. The south of the Zimbabwe craton has a well established cross-cutting stratigraphy and complementary geochronology (Bickle et al. 1975; Hawkesworth et al. 1975; Nisbet et al. 1977; Moorbath et al. 1977; Hamilton, 1977; Hickman, 1978; Hawkesworth et al. 1979; Dodson et al. 1988; Wilson, 1979, 1981, 1990; Taylor et al. 1991) and a detailed geochemical study has been completed recently (Luais and Hawkesworth, 1994). However, little was known of the geochemistry or geochronology of the earliest history of the north of the craton, and this study provides the first evidence of the geochemical history of this portion of continental crust.

The major objectives of this thesis are the geochemical study of a proto-continent, through analysis of the major and trace element geochemistry of granitoid clasts derived from the surface of the early continent, combined with high resolution geochronology. In order to achieve this latter objective, a considerable proportion of this project has been devoted to setting up high-precision zircon dating, using the "Kober Technique" of direct thermal ionisation of zircons (Kober, 1986, 1987), in order to constrain the crystallization histories of the clasts. Sm-Nd isotopic analyses have also been carried out, to give "model ages" of the date at which these granitoids separated from the mantle reservoir (DePaolo and Wasserberg, 1976; Othman et al. 1984).

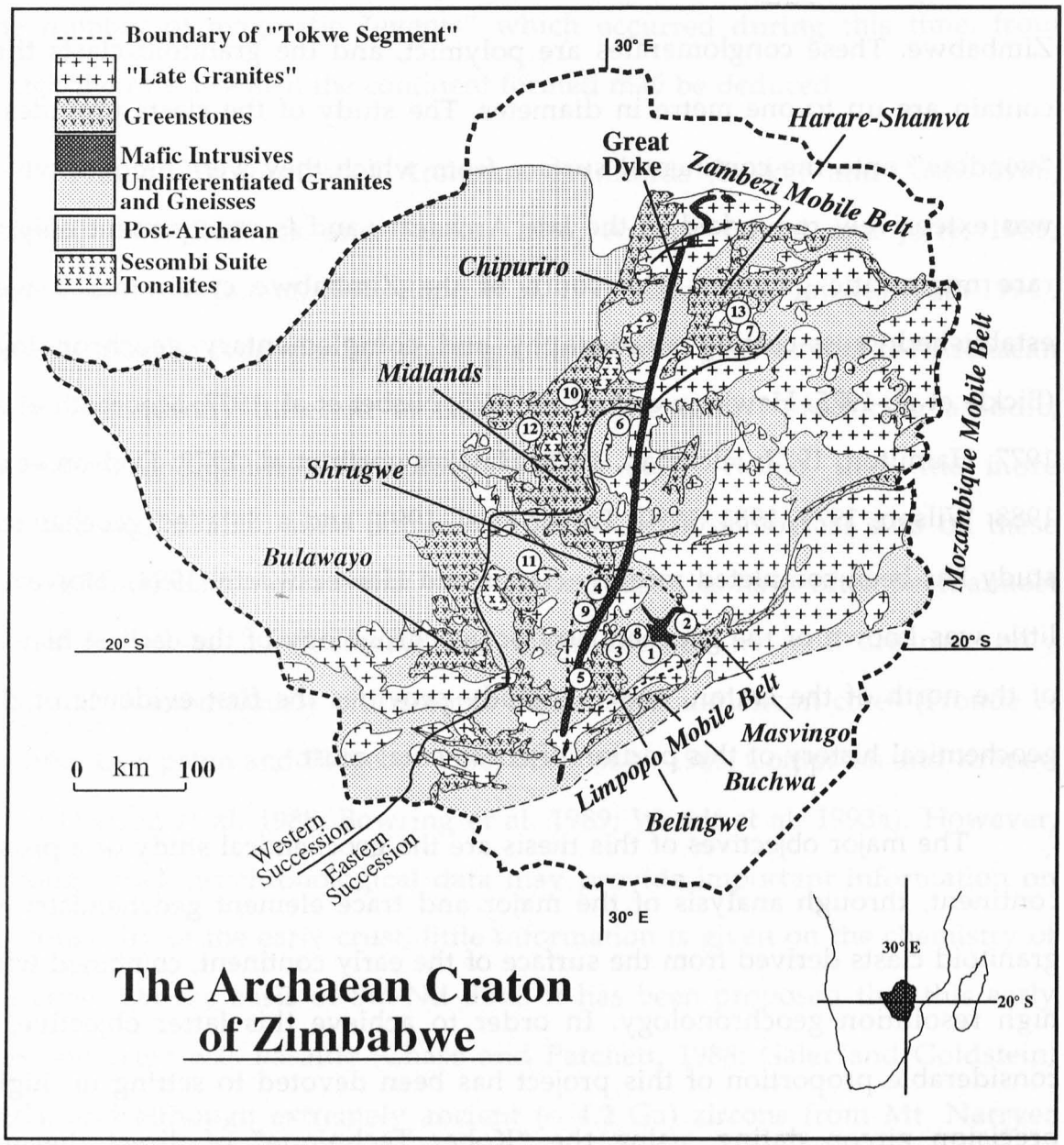

Figure 1.1 A geological sketch map of the Archaean Craton of Zimbabwe, showingthe major geological divisions, and the locations of the major greenstone belts (in italics) and some previously dated granitoids. (1) The Tokwe gneiss; (2) the Mushandikie gneiss: (3) the Shabani gneis; (4) the Mont d'Or granodiorite; (5) the Chingezi tonatite; (6) the Rodesdale gneiss; (7) the Umwindsi gneiss; (8) the Mashaba tonalite; (9) the Gwenoro migmatite; (10) the White Waters tonalite; (11) the Sombula tonalite; (12) the Sesombi tonalite; (13) the Chinamora batholith. The "Wedza Suite" of syn-tectonic tonalites outcrop in the batholiths which suround the Harare-Shamva greenstone belt.

GREAT DYKE (Craton Stabilised by this time)	Rb-Sr	2461± 16 (15)
LATE GRANITES		
Chinamora Syn-tectonic	Rb-Sr	2680±104 (10)
Wedza Suite	Zircon	2667±4 (12)
Chinamora Post-Tectonic	Zircon	2664±6 (18)
	Zircon	2649±9 (18)
	Zircon	2618±6 (18)
Chinamora Late	Zircon	2601±14 (12)
Chilimanzi	Rb-Sr	2570±25 (14)
Northern Marginal Zone Syn-Tectonic	Zircon	2620±108 (13)
SESOMBI SUITE TONALITES		
Sombula	Rb-Sr	2594±80 (7)
	Pb-Pb	2752±50 (4)
	Sm-Nd	2740 T_{Dm} (4)
Sesombi	Rb-Sr	2633±140 (9)
	Pb-Pb	2579±164 (4)
	Sm-Nd	2680 T_{Dm} (4)
White Waters	Sm-Nd	2648±81 (11)
MID-ARCHAEAN		
Chingezi Tonalite	Rb-Sr	2684±102; 2772±60 (4)
	Pb-Pb	2800±76; 2874±32; 2825±100; 2686±94 (4)
	Sm-Nd	2980; 3050; 2950 T_{Dm} (4)
Rhodesdale Gneiss	Rb-Sr	2700±80 (7)
	Pb-Pb	2976±125 (7)
	Sm-Nd	2990 T_{Dm} (4)
Umwindsi Gneiss	Rb-Sr	2860±135 (10)
Mashaba Tonalite	Rb-Sr	2860±60 (17)
Gwenoro	Rb-Sr	2720±60 (9)
	Pb-Pb	2705±62 (4)
EARLY ARCHAEAN		
Mont d'Or Granodiorite	Rb-Sr	3350±120 (2)
	Pb-Pb	3345±55 (3)
	Zircon	3350 (1)
	Sm-Nd	3640 T_{Dm} (4)
Mushandike	Rb-Sr	2917±171 (6)
	Pb-Pb	2946±135 (6)
	Rb-Sr	3445±260 (16)
	Zircon	"just under" 3400 (5)
	Sm-Nd	3540 T_{Dm} (4)
Shabani	Rb-Sr	3495±120 (7)
	Pb-Pb	3088±45 (4)
	Sm-Nd	3460 T_{Dm} (8)
Tokwe	Rb-Sr	3500±400 (9)
	Pb-Pb	3475±90 (4)
	Sm-Nd	3560 T_{Dm} (8)
Detrital Zircons		3200,3350, 3460, 3600, 3800 (1)

Table 1.1 Geochronology of Zimbabwean Granitoids. References given in caption to figure 1.2

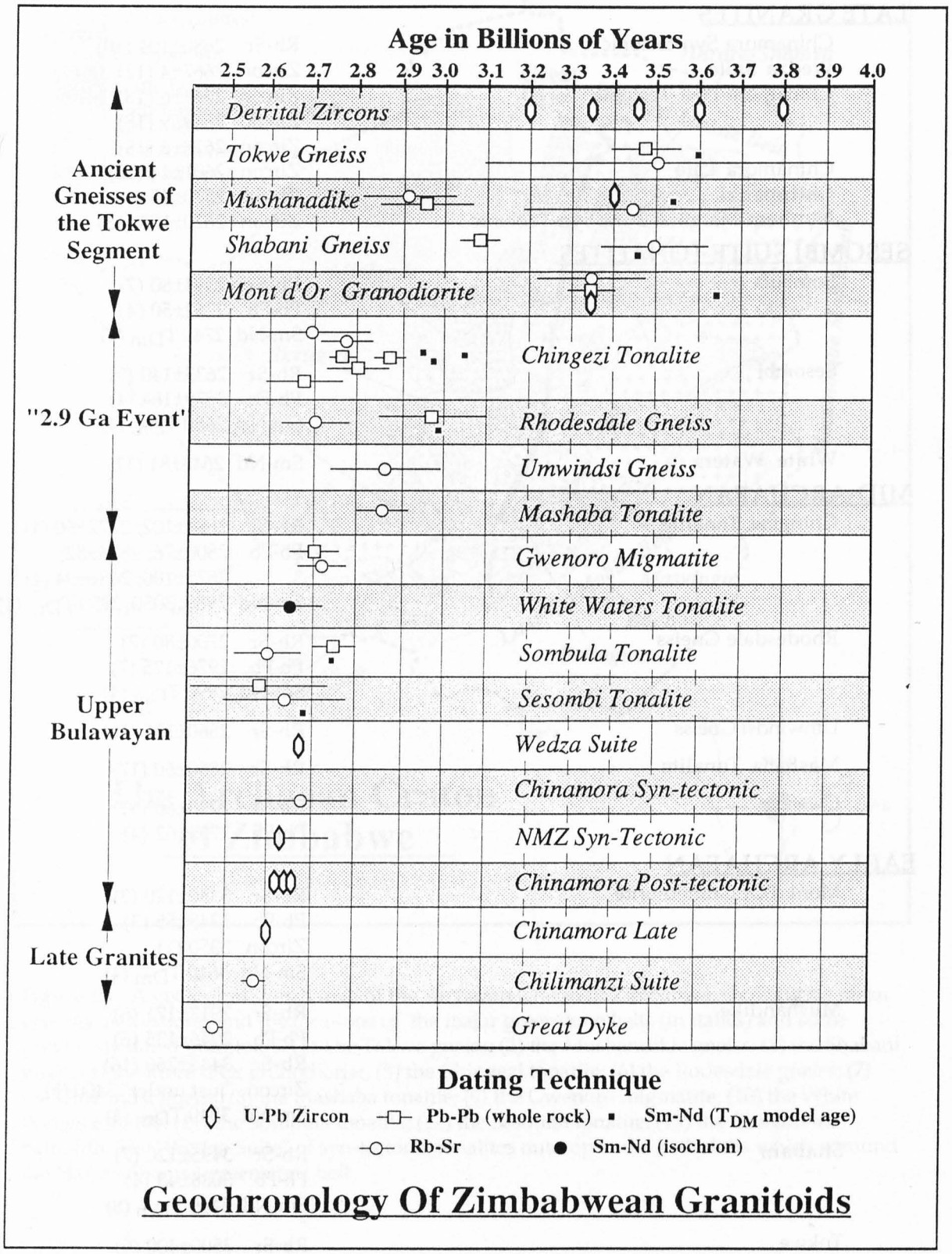

Figure 1.2 Previous Geochronological Work on Zimbabwean Granitoids. References to table 1.1: (1)Dodson et al, '88; (2)Moorbath et al, '76; (3)Taylor et al, '84; (4)Taylor et al, '91; (5)Compston et al, '90; (6)Moorbath et al, '87; (7)Moorbath, '77; (8)Moorbath et al,'86; (9)Hawkesworth et al, '75; (10)Baldock and Evans, '88; (11)NERC Geoscience Lab report '90-'92; (12)Jelsma, '93; (13)Kamber et al. '93; (14)Hickman, '78; (15)Hamilton et al, '77; (16)Hickman, '74; (17)Hawkesworth et al. '79; (18)Vinyu et al. '93

Geochronology of Zimbabwean greenstones.

Greenstone Belt	Method	Age
Harare-Shamva	Rb-Sr	2,512 ± 168 (1)
		2,670 ± 60 (2)
	Pb-Pb	2,659 ± 38 (3)
	Sm-Nd	2,910 T_{DM} (1); 2,810 Ga T_{DM} (1);
		2,850 T_{DM} (1); 2,870 T_{DM} (1);
		2,800 T_{DM} (3)
	Zircon	2,713 ± 15 (4)
		2,645 ± 4 (5)
		2,697 ± 9 (5)
		2,643 ± 8 (5)
Belingwe	Rb-Sr	2,700 ± 70 (2)
	Pb-Pb	2,692 ± 9 (6)
Bulawayo	Rb-Sr	2,615 ± 28 (3)
		2,485 ± 90 (7)
	Pb-Pb	2,867 ± 81 (3)
Kwekwe	Rb-Sr	2,480 ± 140 (7)
		2,660 ± 70 (7)
	Pb-Pb	2,867 ± 195 (3)
	Pb-Pb	2,380 ± 394 (3)
Mixed Suites	Rb-Sr	2,690 ± 90 (2)
	Sm-Nd	2,640 ± 140 (8)
Limestone at base of Masvingo belt		
	Pb-Pb	2,839 ± 33 (9)

Table 1. 2 Geochronology of Zimbabwean greenstones.
References - (1) Baldock and Evans, 1988; (2) Jahn and Condie, 1976; (3) Taylor et al. 1991; (4) Jelsma, 1993; (5) Nesbitt et al. unpublished data tabulated in Jelsma, 1993; (6) Chauvel et al. 1993; (7) Hawkesworth et al. 1975; (8) Hamilton et al. 1977; (9) Moorbath et al. 1987

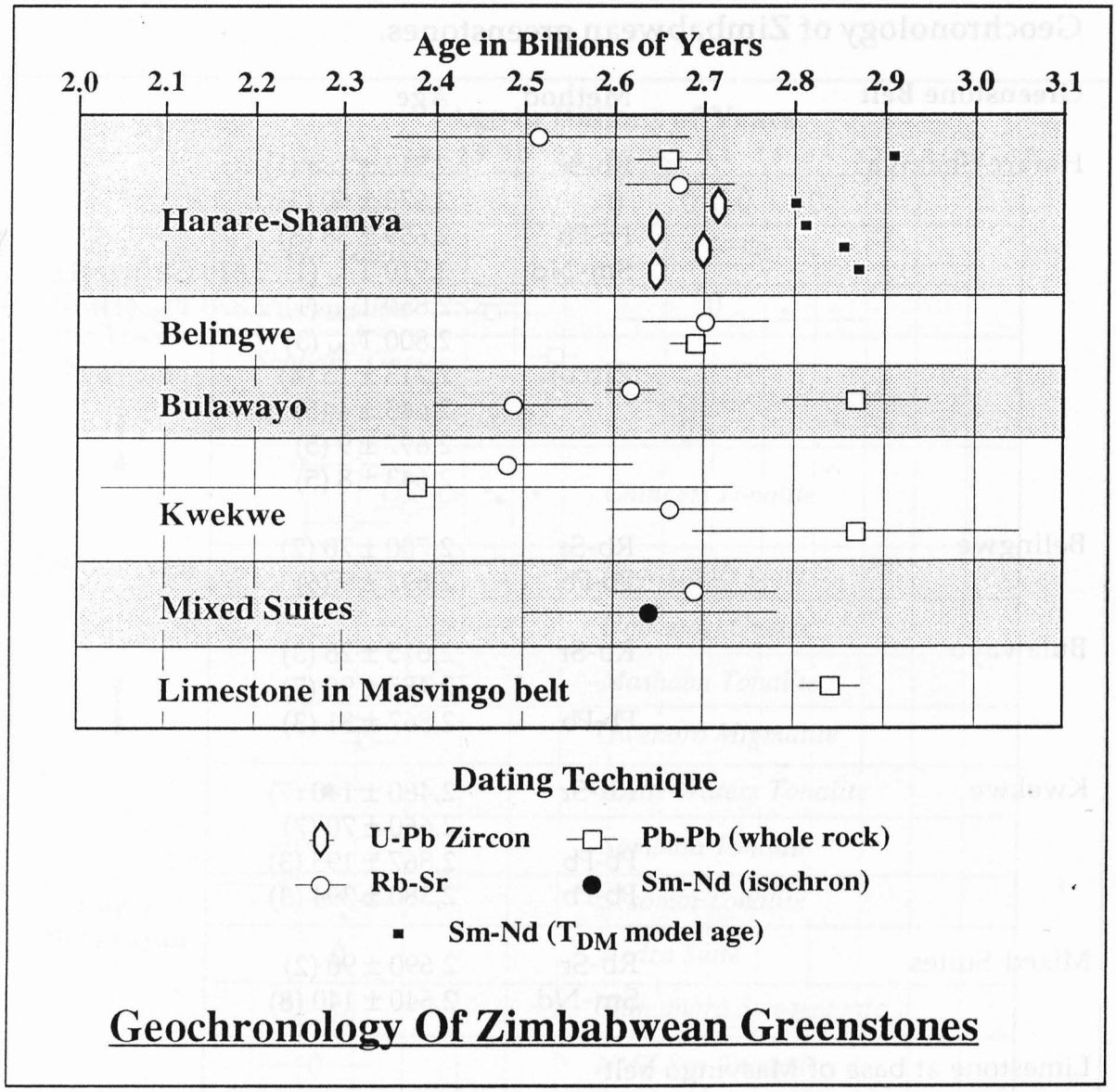

Figure 1.3 Previous geochronological work on Zimbabwean Greenstones. References given in table 1.2

1:2 THE ARCHAEAN CRATON OF ZIMBABWE- PREVIOUS WORK.

The Archaean craton of Zimbabwe is ellipsoid in shape, 750 km long and 400 km wide, and covers a total area of 312,700 km^2. The craton consists of a classic "granite-greenstone" terrain, of composite granite (*sensu lato*) batholiths, often containing several generations of granitoids of varying chemistry and grades of deformation, and greenstone belts (volcano-sedimentary supracrustal sequences) which generally form cuspate, synclinal structures between the batholiths. Metamorphic grades within the craton are generally low (greenschist to amphibolite facies), but the craton is bounded to the north, east and south by "mobile belts", the margins of which are defined by the onset of granulite facies metamorphism. To the south is the Archaean Limpopo mobile belt, which also contains the 10 km wide Proterozoic Triangle Shear Zone (Van Breemen & Hawkesworth, 1980; Kamber et al. 1993). To the north and east are the 500 Ma-old (Pan-African) Zambezi and Mozambique mobile belts. The west of the craton is bounded by the Proterozoic Magondi Mobile belt (Treloar, 1988), a thin-skinned fold and thrust terrain. Unique to the Zimbabwe Craton is the Great Dyke, a 500 km long, 11 km wide layered ultramafic intrusion, the intrusion date of which (2461 ± 16 Ma, Rb-Sr; Hamilton, 1977) is used define the Archaean-Proterozoic boundary world-wide (Nisbet, 1982). Although in the "snakes head" region at the North of the craton the Great Dyke is deformed by the Zambezi mobile belt, the dyke cross-cuts all the ductile features within the craton (Treloar et al. 1992), clearly demonstrating that by the time dyke was intruded, the Zimbabwe craton was fully assembled and stabilized, and acting as a rigid plate.

Several papers have been published which detail the statigraphy of the Zimbabwe craton (eg. Wilson, 1979, 1981, 1990). In brief, the history of the craton may be divided into three "super events", each responsible for the

formation of both granitoids and greenstones, and defined primarily on temporal groupings of granitoids (figure 1.2). The first of these "super events", referred to as the "Sebakwian", occurred between ≈ 3.8 and 3.2 Ga ago, and had been recognised only within the Tokwe segment (figure 1.1) of the south of the craton (figure 1.1). The second "event" was the "Lower Bulawayan" at ≈ 2.9 Ga. The effects of this event are recognised throughout the craton, from the Mashaba and Chingezi tonalites of the south of the craton, to the Umwindsi gneiss in the north, near Harare. The final "event" was the "Upper Bulawayan" from ≈ 2.7 to ≈ 2.6 Ga, which also produced magmatic effects over the entire craton. The (presumed) feeder dykes (which have yet to be dated) for Upper Bulawayan greenstones in the Tokwe segment have suffered very low levels of deformation, and this "Mashaba-Chibi" dyke swarm has been used to demonstrate that the Tokwe segment stabilised prior to the Upper Bulawayan event, unlike the rest of the craton, much of which underwent considerable deformation during the Upper Bulawayan. The early stabilisation of the Tokwe segment is also shown by the Lower Bulawayan granitoids, which are often unfoliated within the Tokwe segment (eg the Chingezi Tonalite; Taylor et al. 1991), but which were strongly deformed during the Upper Bulawayan in the north of the craton (eg the Umwindsi gneiss; Baldock and Evans, 1988)

Upper Bulawayan deformation has been explained in terms of the effects of the "Limpopo Orogeny" (eg Wilson, 1991, Treloar et al. 1992), the main phase of which occurred from ≈2.7 to ≈ 2.6 Ga (Barton and Van Reenen, 1992) during which the Limpopo mobile belt was formed by the collision of the Zimbabwe craton, the Kaapvaal craton, and the "Central Zone", an exotic crustal block (eg Roering et al. 1992). The study of this event is outside the sphere of this thesis, and the most recent information on research into the timing and processes of the orogeny may be found in a special volume of Precambrian Research (Volume 55, 1992). It is, however, worth noting that

since this volume was published, U-Pb zircon dating by Kamber et al. (1993) has confirmed a Sm-Nd age of 2.0 Ga (Van Breemen and Hawkesworth 1980) for the Triangle shear zone, a zone of mylonites up to 10 Km wide within the Limpopo mobile belt. Therefore the Limpopo mobile belt reached its present tectonic configuration in the Proterozoic, rather than the Archaean, and tectonic models for its development must now be re-assessed to take this into account.

1:2.1 The "Granite" terrain

Chemically, the granitoids of the ancient gneisses of the Tokwe segment, "2.9 Ga event" and the Sesombi and Wedza suites are dominantly members of the Tonalite-Trondhjemite-Granodiorite (TTG) suite (eg Taylor et al. 1991; Jelsma, 1993; Luais and Hawkesworth, 1994). Archaean TTG suite granitoids typically have low, mantle-like initial Sr isotope ratios (Moorbath and Taylor, 1981; Taylor et al. 1984; Martin, 1986; Harris et al. 1987; Taylor et al. 1991; Luais and Hawkesworth, 1994), and are regarded as the fundamental building materials of Archaean continental crust (Barker and Arth, 1976; Campbell and Taylor, 1983; Rapp, 1991; de Wit et al., 1992). The Archaean TTG suite is characterised by low HREE ($0.3 \leq (Yb)_N \leq 8.5$; Martin, 1993) and high LREE (generally $\approx$ 100 times chondritic values), resulting in highly fractionated REE patterns, in which $(La/Yb)_N$ ratios which may reach 150. Eu anomalies are generally small, and can be either positive or negative. Although fractional crystallisation models for the formation of Archaean TTG suites have been proposed (eg Arth et al. 1978) which may be applicable in certain circumstances, the model usually invoked for the formation of Archaean TTG suites is by partial melting of metabasite (Barker and Arth, 1976; Jahn et al. 1981; Hunter et al. 1984; Glikson and Jahn, 1985; Martin, 1986; Condie, 1986; Rudnick and Taylor, 1986; Harris et al. 1986; Johnston and Wyllie, 1988; Drummond and Defant, 1990; de Wit, 1992; Jelsma, 1993; Luais and Hawkesworth, 1994) with minimal residual plagioclase (and hence no

significant Eu depletion of the melt) and residual garnet and/or hornblende responsible for the low HREE.

The Sebakwian

The Sebakwian represents the most ancient material recorded in the Zimbabwe craton, and outcrops within the Tokwe segment of southern Zimbabwe (figure 1.1). The oldest ages yet recorded are from detrital zircons (Dodson et al. 1988) in Late Archaean (Tsomondo et al. 1992) sediments in the Shurugwe and Buchwa greenstone belts. However, material of this age has yet to be recognised in-situ, and the oldest gneisses (the Mushandike, Shabani and Tokwe gneisses) give ages that cluster between 3.4 Ga and 3.5 Ga (although the errors on these ages are large).

The Mont d'Or granodiorite has a depleted mantle model age distinctly older (3.65 Ga) than its well constrained crystallization age of 3.35 Ga (figure 1.2 and table 1.1), a high $^{87}Sr/^{86}Sr$ initial ratio (0.711 ± 0.002; Moorbath et al. 1976), and a high apparent μ_1 value (9.3; Moorbath et al, 1987). This granodiorite has therefore been interpreted (Taylor et al. 1991) as the earliest recorded ensialic intra-crustal remelt within the Zimbabwe craton.

The final effect of the "Sebakwian" is recorded as a 3.2 Ga abundance peak within detrital zircons (Dodson et al. 1988). However, as with the oldest detrital zircons, the source of these zircons has not been recognised.

Lower Bulawayan - the 2.9 Ga event.

Although granitoids of this age outcrop over the entire craton, they are more extensive in the south of the craton, where they are generally preserved at low metamorphic grades and are often unfoliated (eg Wilson, 1973; Taylor et al. 1991). By contrast, granitoids of this age in northern Zimbabwe, such as the Rhodesdale and Umwindsi gneisses are strongly deformed and migmatised.

Upper Bulawayan

The earliest Upper Bulawayan granitoids are the syn-tectonic Sesombi (figure 1.1) and Wedza suites (also referred to as the "gneissic granites" within the Chinamora batholith). The Wedza suite has been dated at 2,667 ± 4 Ma (U-Pb zircon; Jelsma, 1993). The Sesombi suite outcrops over a broad linear belt to the west of the craton (figure 1.1), and the Wedza suite (eg the Litchfield gneissic granite in the west of the Chinamora batholith; Snowden and Snowden, 1981) outcrops in batholiths surrounding the Harare-Shamva greenstone belt. As previously discussed, these granitoids are members of the Archaean TTG suite, and their formation has been modelled as being due to partial melting of a metabasite source rock (Jelsma, 1993; Luais and Hawkesworth, 1994)

There are major differences, both in terms of major and trace elements, between the Sesombi and Wedza suites, and the late syn- to post-tectonic Upper Bulawayan granitoids which were intruded subsequently. These younger granitoids have high K_2O/Na_2O ratios compared to the TTG suite, and plot on calc-alkaline, as opposed to sodic trends (Snowden and Snowden, 1981; Vinyu et al. 1993; Jelsma, 1993). The granitoids have non-minimum melt behaviour, and were emplaced at depths of between five and twelve kilometres (Vinyu et al. 1993). There is considerable chemical variation within these granitoids, and their formation has been modelled as resulting from interaction between basaltic melts and partial melts of pre-existing continental materials (Vinyu et al. 1993; Jelsma, 1993).

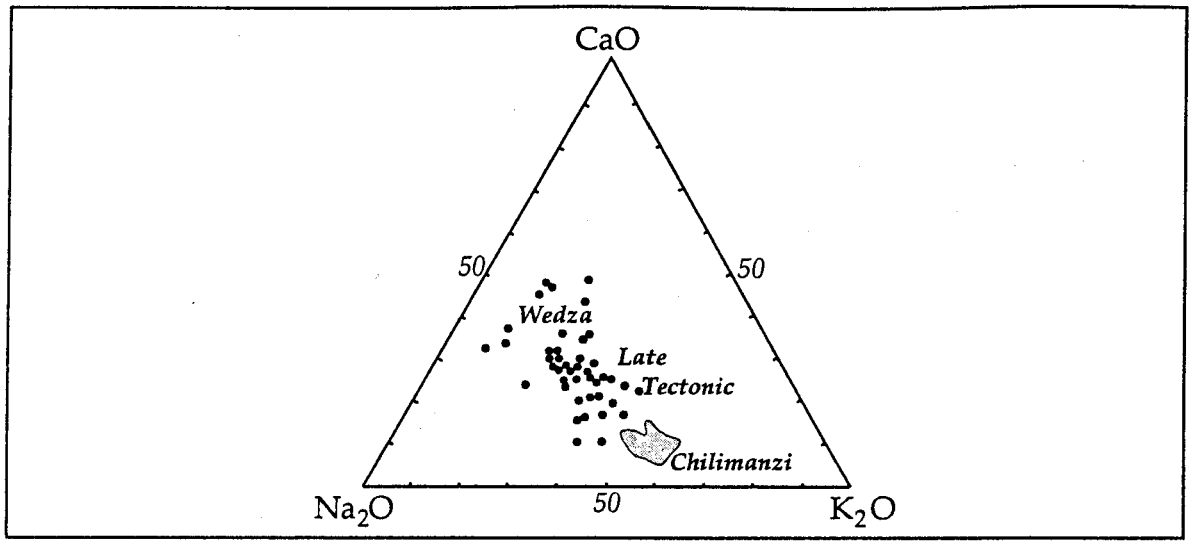

Figure 1.4 CaO - Na_2O - K_2O diagram for Upper Bulawayan granitoids, showing the broad range of compositions for the Wedza and late tectonic (Mazowe) granitoids, and the restricted range in composition, and comparatively high K_2O/Na_2O ratio of the late granites of the Chilimanzi suite (after Jelsma, 1993).

1:2.2 Greenstone Belts

Greenstone belts are volcano-sedimentary units present within most Archaean terrains. World-wide, their general stratigraphy is remarkably similar, with a mafic/ultramafic lower unit, passing up into a tholeiitic sequence, which may incorporate (bimodal) felsic volcanics, overlain by sedimentary sequences, generally preserved at low metamorphic grade (greenschist to amphibolite facies). Despite the similarities in their stratigraphy, it is probable that greenstone belts were developed in several different environments (de Wit et al. 1992). The ɔJamestown Ophiolite Complex within the Barberton greenstone belt (de Wit and Hart 1993), and the Kam group within the Yellowknife greenstone belt (Helmstaedt et al. 1986) contain sheeted dykes, indicative of considerable extension, and these belts have been interpreted as obducted pieces of oceanic crust. Other belts have basal contacts which have been mapped as unconformities (Bickle et al. 1975; Blenkinsop et al. 1993) and which show evidence for contamination by pre-existing continental crust (Compston et al. 1986; Taylor et al. 1991).

The Zimbabwe Craton contains a total of 32 greenstone belts, intruded in three major periods of greenstone belt formation, the "Sebakwian", the "Lower Greenstones" (or Lower Bulawayan) and the "Upper Greenstones" (or Upper Bulawayan). Figure 1.3 summarises published geochronological data on these greenstones. The dates of the Sebakwian and Lower Greenstones are poorly constrained, and are generally taken as ≈ 3.5 Ga and ≈ 2.9 Ga respectively, based on the assumption that they are cogenetic with suites of granitoids of those ages (figure 1.2). This assumption leaves considerable scope for error within the Sebakwian, where the ages of the granitoids, and possible contact relationships are comparatively poorly constrained. However, field relationships demonstrate that this assumption is valid within the Lower Greenstones. The base of the west of the Belingwe greenstone belt contains a formation of felsic vent agglomerate (the Hokonui formation) which both cross-cuts and is intruded by the Chingezi tonalite (Taylor et al. 1991), clearly demonstrating that the greenstones and the Chingezi tonalite were coeval.

As shown in figure 1.3, the Upper Greenstones are geochronologically far better constrained than the older greenstones. On the basis of their stratigraphy, the Upper Greenstones are divided into "Eastern" and "Western" successions (figure 1.1). The lower stratigraphic levels of both successions are of mafic-ultramafic volcanics. In the eastern succession these pass upwards into a sequence of interbedded tholeiites and pelite-dominated sediments, whereas the western succession passes up into a bimodal suite, with interbedded mafic/ultramafic and felsic (calc-alkaline) volcanics. These felsic volcanics may become dominant towards the top of the sequences. The eastern sedimentary unit, and its overlying and interbedded basalts, can be traced laterally into the western bimodal volcanic unit (Wilson, 1979), demonstrating that the the two successions were contemporaneous, confirmed by the similar ages obtained for the basal volcanics of the Harare-Shamva (western) and

Belingwe (eastern) of 2,713 ± 15 Ma (U-Pb zircon, Jelsma, 1993) and 2,692 ± 9 Ma (Pb-Pb, Chauvel et al. 1993) respectively.

The Upper Greenstones of the Belingwe greenstone belt have long been cited as an example of greenstones which were extruded on pre-existing continental crust (eg. Bickle et al. 1975). Recently, this has been challenged by Kusky and Kidd (1992) who suggested that shear zones at the base of the greenstones imply that the belt was an obducted oceanic plateau. This suggestion is supported by the whole-rock chemistry of komatiites (Bickle et al. 1993), ion-probe analyses of glassy inclusions within komatiites (McDonough and Ireland, 1993) and Pb isotope analyses (Chauvel et al. 1993) on the well preserved basal mafic/ultramafic volcanics of the belt (the Reliance formation), which showed that contamination of these volcanics by continental crust was minimal (<1 % by mass). However, recent detailed mapping of the area (Blenkinsop et al. 1993) strongly supports the suggestion that the greenstones were formed within an ensialic environment, with the thin shear zone (which is not mylonite as stated by Kusky and Kidd (1992)) at the base of the greenstones representing a local accommodation structure related to the folding of the greenstone belt. Perhaps one of the most graphic illustrations of the low strain that the basal greenstones have suffered (by analogy with more recent ophiolites, the Kusky and Kidd model requires that the lowermost greenstones are strongly deformed by the large tectonic forces involved in obduction) is the presence of very well preserved liquid immicibility ocelli within the rims of komatiitic pillow lavas within a few tens of metres of the base of the sequence which still preserve their original, spherical form (photograph 1.1).

Photograph 1.1 Liquid immicibility ocelli within the rim of a komatiitic pillow lava, basal Reliance formation, Upper Bulawayan of the Belingwe Greenstone belt.

The base of the Harare-Shamva greenstone belt has been extensively modified by later tectonism and magmatism, and therefore structural evidence cannot be used to determine if the belt is allochthonous or autochthonous. However, Sm-Nd T_{DM} model ages on the volcanics are consistently higher than their extrusion ages (figure 1.3), demonstrating contamination by pre-existing enriched (continental) material. Therefore, these greenstones are also assumed to have been extruded onto continental crust.

The arguments detailed above are considered to refute the Archaean ophiolite hypothesis for the Upper Greenstones of Zimbabwe, which are therefore considered to have formed within an ensialic environment in response to plume activity.

The Upper Greenstones are unconformably overlain by the "Shamvaian", a sequence of conglomerates and greywackes, syn-depositional

intrusions within which have been dated at 2,672 ± 12 Ma (U-Pb zircon; Jelsma 1993), coeval with the first (Wedza suite) Upper Bulawayan granitoids (2,667 ± 4 Ma; U-Pb zircon; Jelsma 1993). As these Upper Bulawayan granitoids were emplaced at depths of five to twelve kilometres (Vinyu et al. 1993), they are unlikely to have been unroofed at this time, and the granitoid clasts within basal Shamvaian conglomerates are therefore older than the Upper Bulawayan, and preserve a unique sample of the pre-Upper Bulawayan continental crust through which the Upper Greenstones were erupted.

1:2.3 Late Granites

The final felsic igneous activity recorded on the craton was the intrusion of the post-tectonic Chilimanzi suite of late granites at 2,601 ± 14 Ma (U-Pb zircon; Jelsma, 1993). These granitoids are presently exposed over approximately 50 % of the surface of Zimbabwe (Ridley, 1992). They are generally tabular or sheet-like in form (Snowden, 1984), and are exposed at close to their maximum extent by the present erosion level. They are comparatively enriched in heat producing elements such as U, Th, K and Rb (figure 1.5), and depleted in elements concentrated within feldspars, such as Sr (which is compatible in plagioclase) and Ba (which is compatible in potassium feldspar). It has therefore been proposed (eg Jelsma, 1993) that this suite was formed by intra-crustal re-melting.

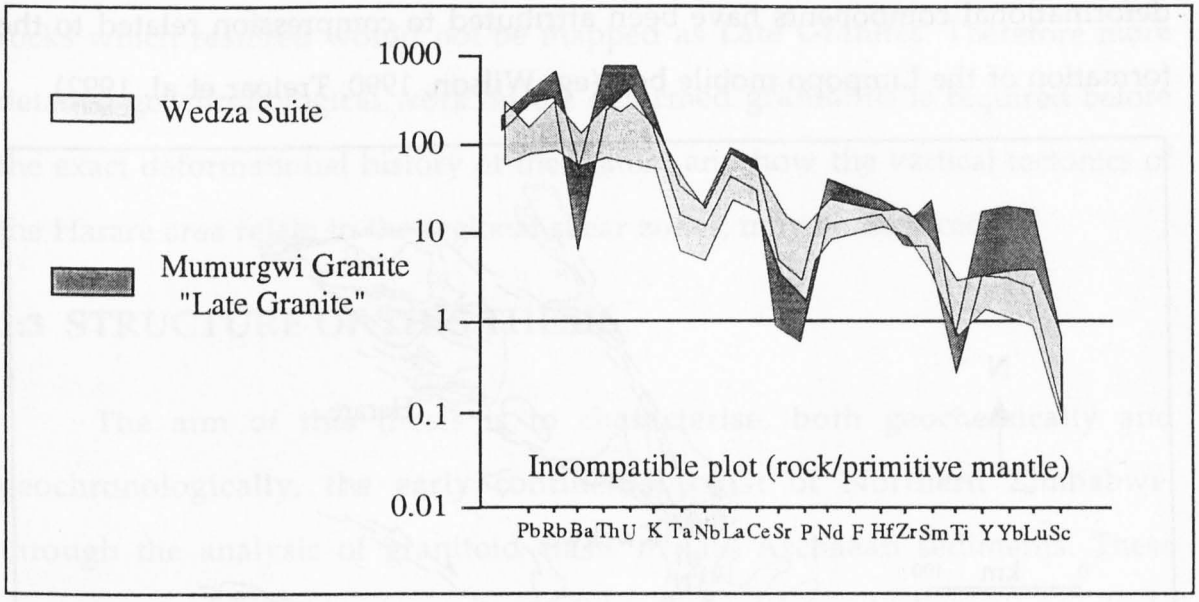

Figure 1.5 Incompatible element plot showing element patterns for the Wedza suite and the Mumurgwi granite, a "Late Granite" of the Chilimanzi suite, normalised to primitive mantle values of McDonough and Frey, 1989. (after Jelsma, 1993)

1:2.4 Deformation of the Granite-Greenstone terrain.

The Upper Bulawayan Granite-Greenstone terrain is deformed into a series of dome and basin structures, with granitoid batholiths occupying the domes, and the greenstone belts occupying the intervening basins. This pattern was initially ascribed to vertical tectonic processes, with the diapiric intrusion of "gregarious batholiths" (Macgregor, 1951), implying a comparatively weak crust. However, this model was questioned by authors (Snowden and Bickle, 1976; Snowden, 1984) who proposed that the deformation was a result of a fold interference pattern, in response to horizontal tectonic forces, which would require the crust to be comparatively strong. Recent mapping within the Chinamora Batholith and Harare-Shamva greenstone belt (Jelsma, 1993) strongly supports the vertical tectonic model in this area, with diapirism (or ballooning plutonism) as the dominant driving force of deformation. However, the presence of major shear zones (figure 1.6) indicates that a model of purely vertical tectonics cannot be invoked to explain all the deformational features of the Zimbabwe craton. The horizontal

deformational components have been attributed to compression related to the formation of the Limpopo mobile belt (eg. Wilson, 1990; Treloar et al. 1992).

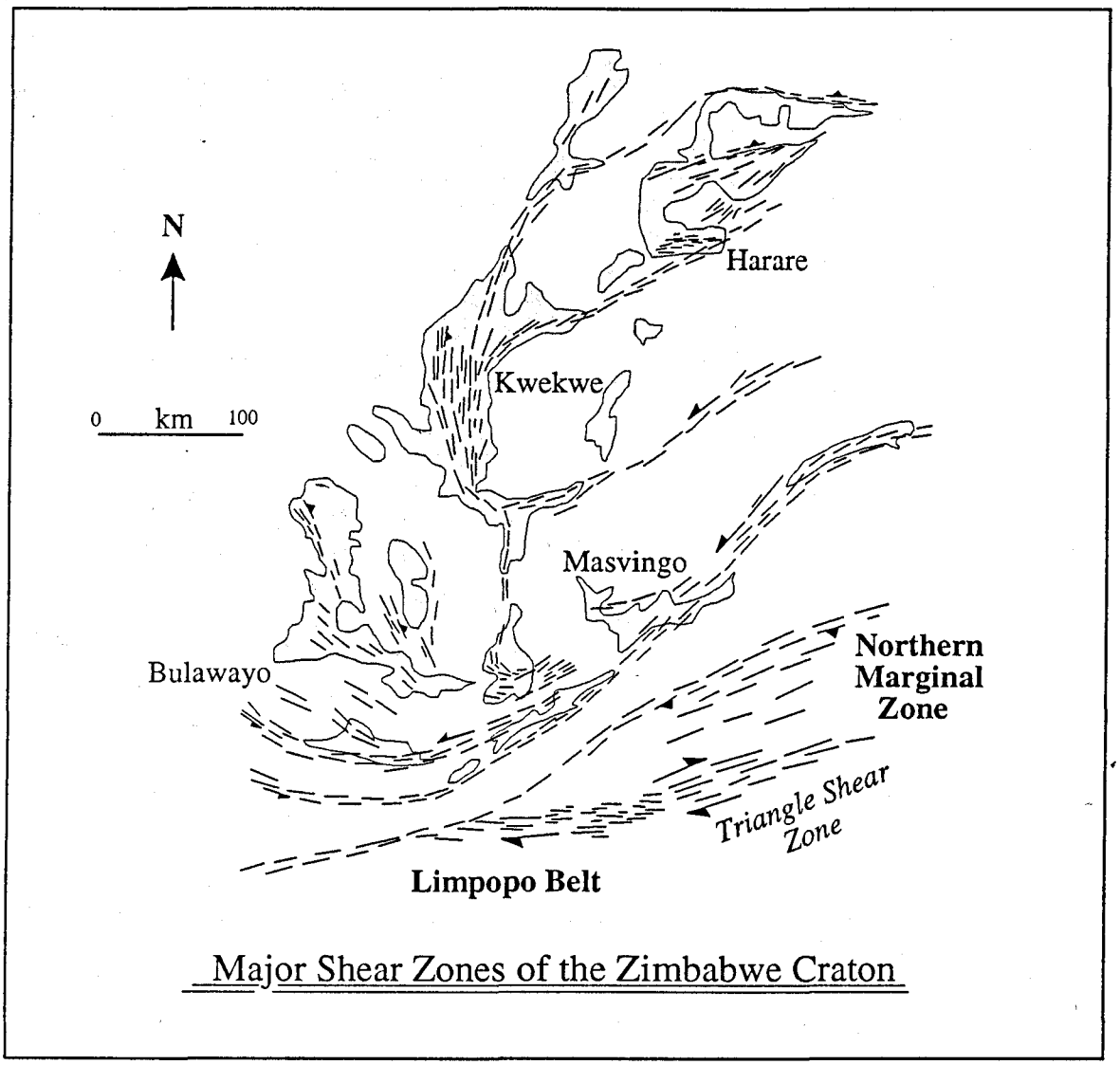

Figure 1.6 Shear zones within the Zimbabwe Craton (after Treloar et al. 1992)

The exact timing of the deformation of the craton which produced the major regional shears is only constrained to be between the 2,670 Ma syn-tectonic Wedza and Sesombi suites of tonalites, and the intrusion of the Great Dyke at 2,461 16 Ma, (Rb-Sr, Hamilton, 1977) which cuts all the ductile structures on the craton. Although the 2,600 Ma Chilimanzi suite of ǝLate Granites are regarded as post-tectonic, there is a strong probability that this assumption has been incorporated into the mapping of the craton, and that if members of the Chilimanzi suite were deformed by the shears, the gneissose

rocks which resulted would not be mapped as Late Granites. Therefore more detailed geochronological work on the deformed granitoids is required before the exact deformational history of the craton, and how the vertical tectonics of the Harare area relate to the regional shear zones, may be deduced.

1:3 STRUCTURE OF THIS THESIS

The aim of this thesis is to characterise, both geochemically and geochronologically, the early continental crust of Northern Zimbabwe, through the analysis of granitoid clasts in late Archaean sediments. These represent the least altered remnants of this early crust, which was extensively re-worked by ɔUpper Bulawayan igneous and tectonic activity. Knowledge of the chemistry and geochronology of this early continental crust will provide valuable insights into the formation and stabilisation of the continental crust.

The thesis is divided into four chapters. This first chapter is a general introduction to the Archaean of Zimbabwe.

The second chapter deals with zircon dating, covering first the physical and chemical properties of zircon, and then the principal methods of zircon dating which are in common use, concentrating on the ɔKober Technique of Pb-Pb zircon dating by direct thermal ionisation of zircon crystals, which has been applied in this thesis to samples from Zimbabwe.

The third chapter details the chemical and geochronological investigation of the early crust of the north of the Zimbabwe craton.

The fourth chapter discusses the history of the Zimbabwe craton within a context of various other models proposed for Archaean processes, and proposes models for the formation and stabilisation of continental crust in the Archaean.

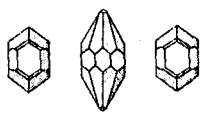

Chapter Two

U-Pb and Pb-Pb Zircon Dating

2:1 INTRODUCTION

Zircon is an extremely durable accessory mineral present within most crustal rock types. It is capable of remaining as a closed system to U, Th and radiogenic Pb through processes ranging from weathering, to partial melting, to diamond pressure metamorphism. Clearly, the study of such a durable material may provide invaluable information on the crystallisation history of igneous and metamorphic rocks. This chapter will discuss first the chemistry and physical properties of zircon, then U-Th-Pb systematics, and then finally the methods of zircon dating in most common use. Particular emphasis is given to the "Kober technique" of Pb-Pb dating by whole-grain evaporation of zircon crystals, which has been applied in this thesis (Chapter 3) to date Archaean granitoids in Northern Zimbabwe.

2:2 THE PHYSICAL PROPERTIES & CHEMISTRY OF ZIRCON

Zircon (tetragonal $ZrSiO_4$) acts as the major sink for zirconium within most crustal rocks, and as such, forms a near-ubiquitous phase within crustal igneous and metamorphic systems. Although zircon is generally of low abundance, it may reach modal abundances of several percent in certain alkaline igneous rocks, and it is an essential constituent of zircon syenite. In its purest forms, zircon is hard (hardness 7.5), dense (relative density 4.7), with

poorly developed cleavages ({110} imperfect, {111} poor). It is both mechanically and chemically extremely resistant to most geological processes. Due to its hardness and resistance to weathering, zircon is a common detrital mineral in clastic sedimentary rocks, becoming more concentrated within more mature sediments, where it may form placer deposits.

2:2.1 Zircon Typology

Zircon crystallises in the tetragonal system, in a wide range of crystal shapes. Pupin (1980) devised a classification system based upon 75 of the most common habits of magmatic zircon (Figure 2.1). By painstakingly extracting zircons held as inclusions within minerals of a known crystallisation sequence, Pupin demonstrated that the habit of the crystal depended upon both the chemistry of the enclosing magma, and upon the temperature at which the zircon crystallised. Therefore within a single magma body, the crystal habit of zircon evolves as the magma cools and crystallises. Thus the form (or typology) of zircon may be utilised both in the classification and discrimination of various granitoids, and as a geothermometer.

The Pupin system of zircon classification has been widely accepted, and geothermometery based on zircon morphology is often quoted in the literature (eg Jelsma 1993). Pupin's proposed sequences of zircon morphology have been used in studies of trace element concentration during the crystallisation of a magma (Barth et al. 1989; figure 2.2), and the modal abundances of the various crystal types have been used to distinguish mixed populations of zircons, such as the main phase of zircon crystallisation within a magma and xenocrystal zircons (Bossart et al. 1986).

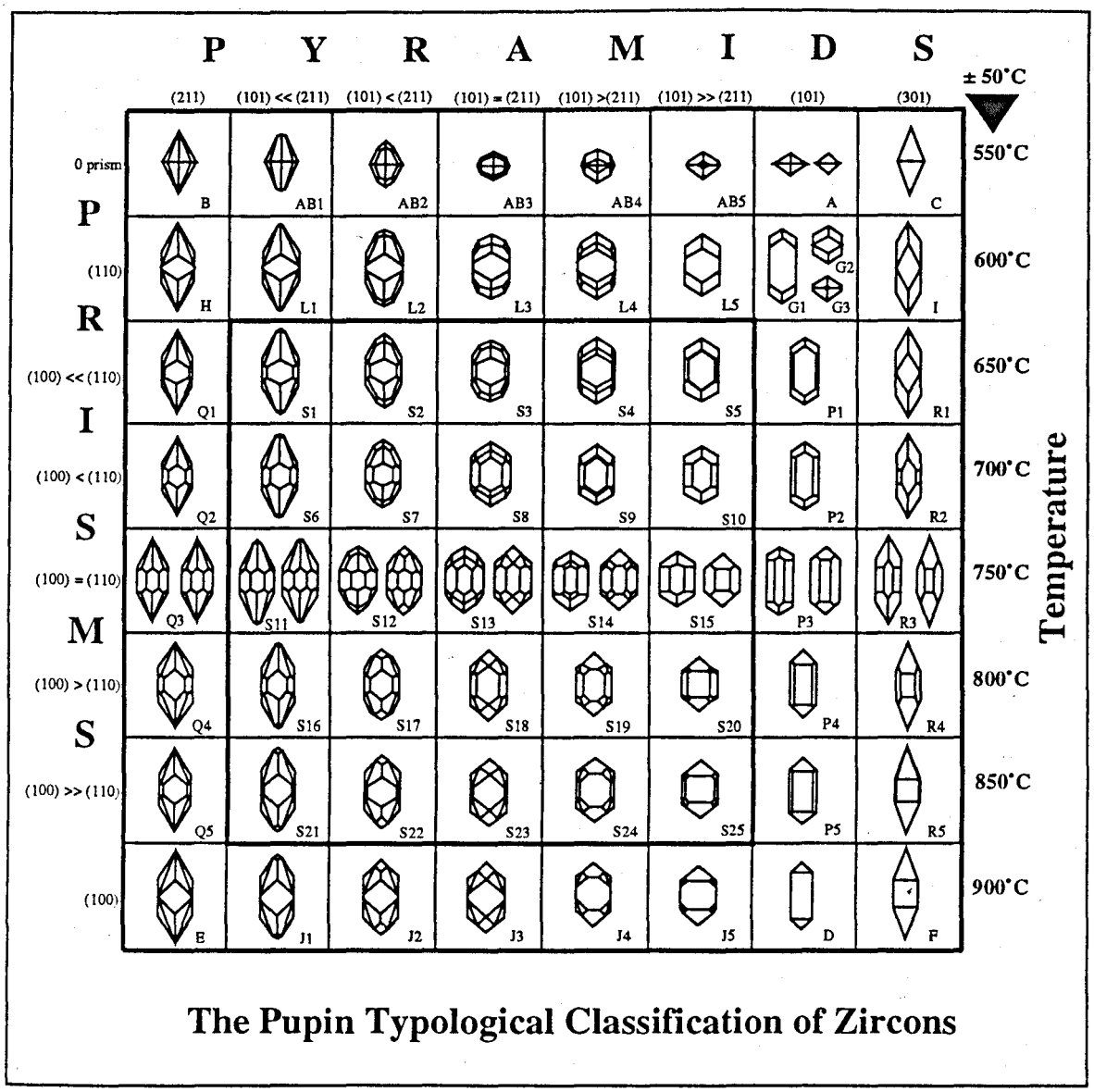

Figure 2.1 The Pupin (1980) typological classification of zircons based on crystal morphology.

It should be noted that the Pupin typological classification takes no account of the length to breadth ratio of the zircon crystal. This ratio is also extremely variable, with zircons tending to become more elongate with faster crystallisation (Speer 1980). Length to breadth ratios have been incorporated in systems used to distinguish different plutons of similar composition by the shapes of the zircons they contain (Byerly et al. 1975).

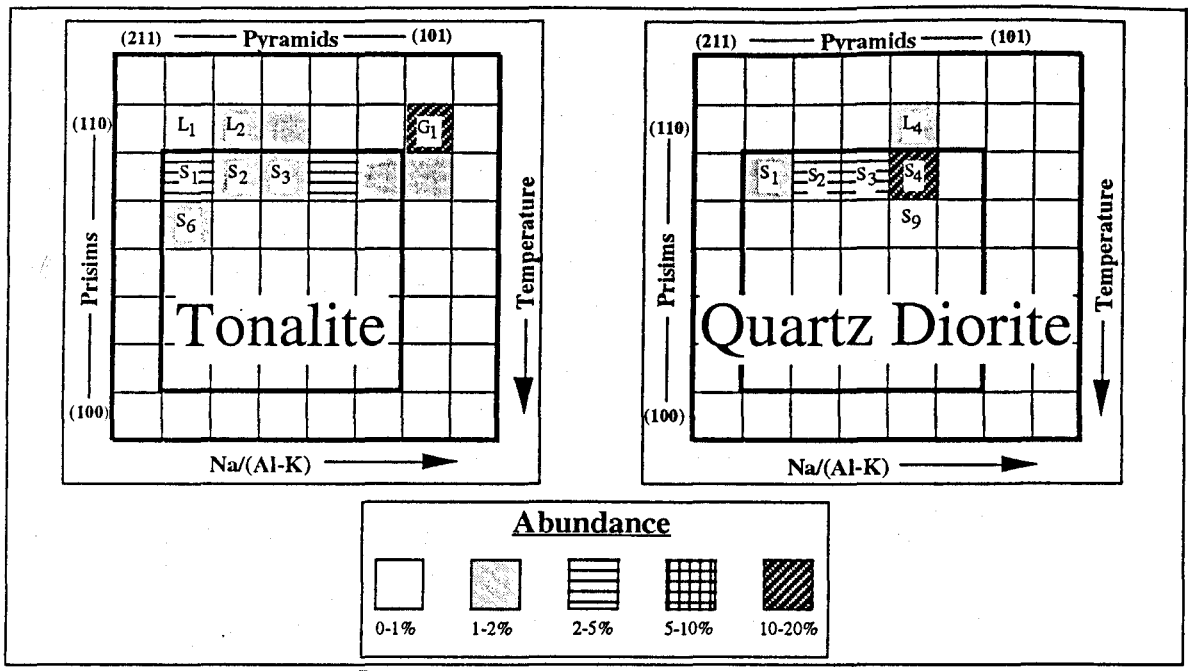

Figure 2.2. Typological frequency diagrams showing abundances of zircon morphology within different intrusions (Barth et al. 1989), illustrating how zircon typology may be used to distinguish between different granitoids.

More recently, Benisek and Finger (1993) concluded that the prism morphology of zircons in granitic systems does not constitute a reliable geothermometer as proposed by Pupin (1980), as crystal morphology is controlled by the trace element concentration within zircon, notably U, Th and Y (REE). The observed progressions of crystal forms are therefore due to progressive enrichment of these incompatible elements within the cooling magma, and Pupin's geothermometery using zircon should only be taken as a guide-line, based on the fact that cooler magmas tend to have higher contents of incompatible elements.

2:2.2 Zircon solubility in crustal melts and zircon xenocrysts.

Zirconium has relatively low solubility in most crustal melts, with saturation levels of only ≈ 50 to 350 ppm in granitoids (Watson and Harrison, 1983). Zirconium solubility depends on the temperature of the melt and its composition, increasing with increasing magma alkalinity (measured by the alkali/alumina ratio). Peralkaline melts are capable of holding large amounts of zirconium in solution, and pantellerites with up to 1800 ppm of Zr

of zirconium in solution, and pantellerites with up to 1800 ppm of Zr uniformly distributed within the glassy matrix have been recorded (Watson, 1979). The rate at which zircon dissolves within crustal melts is strongly dependant upon the water content of the magma. Rates of zircon dissolution in anhydrous (>0.2% H_2O) melts are very low, such that a 50 μm crystal will require in excess of 200 Ma to dissolve in an anhydrous granitic melt at 750°C. However, if 3-6 % of water is added to the system, the same crystal will dissolve geologically instantaneously, in less than 100 years (Harrison and Watson, 1983). Therefore the rate of dissolution of zircon is rarely a control on the Zr content of magmas produced by intra-crustal melting.

Most granites produced by intra-crustal melting will become saturated with Zr before all the zircon available in the source has been consumed (Watson and Harrison, 1984). The separating melt phase may entrain restitic zircon crystals, derived from the protolith from which the melt was generated. These xenocrysts will retain their original isotopic composition, and thus give the age of the protolith. An excellent example of this was studied by Zeitler and Chamberlain in 1991, working on young leucogranites in the Western Himalaya of Pakistan. In the Nanga Parbat region, they found zircons with high U (5000 to 40,000 ppm U) rims which they dated at ≤ 15 Ma. The xenocrystic cores to these zircons have much lower contents of U, and are far older, with 1800 Ma being the age of most of the population, although some crystals of late Archaean age (2,600 Ma) are present.

2:2.3 Zonation of Zircon

Zircons commonly show very fine scale zonation, individual zones having thicknesses down to one micron. This zonation may be highlighted by sectioning and polishing the crystal, and then either etching the surface with HF vapour, or by causing the crystal to fluoresce. Ono (1976) showed zoning defined by fluorescence under electron bombardment corresponds to chemical

zoning, with the areas of brightest fluorescence generally corresponding to areas richer in HfO_2 and poorer in YPO_4. However, because of the large number of substituting elements which may be present, no simple relationship exists between luminescent intensity, colour and chemistry (Speer, 1980). Therefore cathodoluminescence is a useful tool in highlighting the zonation within zircons, but it cannot be calibrated to give any estimate of the variations in chemistry between zones. This chemical variation is best studied by ion probe. However, as the size of spot analysed by ion probe is generally in the range 20-30μm, it should be remembered that such analyses may represent analyses of up to 30 separate zones.

Recent workers (Hanchar & Miller, 1992; Vavra, 1992) have used the zonation within zircon crystals, highlighted by differing intensity of cathodoluminescence, to trace the morphological growth history of individual crystals, without recourse to the method used by Pupin, which is extremely time consuming, and requires large amounts (several tens of kilos) of rock in order to extract sufficient zircon, followed by careful mineral picking, before a statistically valid analysis can be made.

Pidgeon (1992) has noted that many zircons with fine scale zonation also show a patchwork replacement of the zoned material by unzoned zircon. The zoned material often fades into unzoned material with faint traces of zonation still detectable at the margins of the zoned zircon. There are important chemical differences between the unzoned material and the primary, finely zoned material. The unzoned material is generally much "purer", with lower concentrations of trace elements such as U (up to 5 times less), Th (up to 10 times less), and Pb (also up to 10 times less), than the zoned material. How common this process is, and the time interval between the original crystallisation of the zircon and the replacement is still unclear. The main question that remains to be answered is whether the replacement occurs

soon after crystallisation, within the cooling igneous body, or whether the replacement reflects a later (thermal) event.

2:2.4 The Trace Element Chemistry of Zircon.

The principal structural unit of zircon is a chain of alternating, edge sharing [SiO_4] tetrahedra and [ZrO_8] triangular dodecahedra extending parallel to the c-axis (Speer, 1980). The zirconium ions are in the Zr^{4+} state, and have an atomic radius of 0.84 Å. The elements which have a similar charge and ionic radius, and which commonly substitute for zirconium include:-

Ion	*Ionic radius*
Hf^{4+}	0.83 Å
Y^{3+}	1.02Å
U^{4+}	1.00Å
Th^{4+}	1.05Å
Rare Earth Elements (REE) La^{3+} (1.16Å) to Lu^{3+} (0.98Å)	
Pb^{4+}	0.94Å

Si^{4+} has an ionic radius of 0.26Å, and the more common substituting ions include:-

Al^{3+}	0.39Å
P^{5+}	0.17Å

The mineral hafnon, [$HfSiO_4$] is isostructural with zircon, and, due to the similarity in size and charge of the Zr and Hf ions (see above), a complete solid solution series exists between the two minerals. The mean Zr:Hf ratio of zircons is around 40:1, (Speer, 1980) which is approximately the ratio between the abundances of these two elements in the Earth's crust, suggesting that most geological processes are incapable of fractionating these two elements from each other. However, Hf does seem to become relatively enriched in the

final stages of crystallisation of a magma (Ono, 1976; Kinny and Wyborn, 1990) and extreme fractionation of Hf from Zr does occur, notably in pegmatites containing Ta and Nb minerals. Hafnons from Zambezia, Moçambique, have been found with compositional zones of up to 97% hafnon, and bulk compositions of up to 78% hafnon (Speer, 1980). Conversely, zircons from magmas generated in continental rift settings (such as carbonatites or nepheline syenites) have anomalously low Hf concentrations, (<8000 ppm Hf, with Zr:Hf ratios >60; Heaman et al, 1990). The mechanisms by which Zr and Hf are fractionated are still unclear.

Xenotime [YPO_4] is also isostructural with zircon, but due to differences in the size of the unit cell, only about 3 wt% of xenotime may be incorporated in solid solution within the zircon lattice before xenotime starts to form a discreet phase intergrown within the zircon crystal. Other isostructural minerals commonly intergrown with zircon include thorite [$ThSiO_4$] and coffinite [$USiO_4$].

Zircon may contain up to 10 wt% Rare Earth Elements (REE), with average contents of around 1%. From simple deductions based upon the ionic radius, it can be seen that due to the lanthinide contraction, the smaller heavy REE (HREE) are more compatible within the zircon lattice than the light REE (LREE), resulting in HREE enrichment in the zircon crystal. As Eu is commonly reduced to the Eu^{2+} state within magmas, it is not as readily accepted into the zircon lattice as the other REE, resulting in a negative Eu anomaly. These simple deductions are bourne out by work on zircon distribution coefficients carried out by Nagasawa (1970) and Gromet and Silver (1983).

The differences in compatibility within zircon between Hf and Lu (a member of the HREE) have important implications for the Lu-Hf system of dating. Although the methodology and applications of this dating system lie

beyond the scope of this thesis, it provides a useful example of some of the implications of the trace element chemistry of zircon. ^{176}Lu decays to produce ^{176}Hf with a half-life of 3.5 (± 0.2) x 10^{10} years. Hf is far more strongly partitioned into zircon than are the HREE at the time of crystallisation of the melt. Typical Hf concentrations in zircon are ≈ 1.65 wt % (wt % of Hf in hafnon x typical zircon:hafnon ratio), while typical Lu concentrations are only ≈ 25 ppm (typical Lu abundance in zircon (≈1000 x chondrite) x the chondritic value (0.025 ppm)). Hf:Lu ratios in zircon are therefore ≈ 700:1. This fractionation of the parent isotope (^{176}Lu) from the daughter (^{176}Hf) means that little radiogenic Hf is formed within zircon, and therefore zircon may be used to provide an initial $^{176}Hf/^{177}Hf$ ratio of the source of the zircon's host rock, with corrections due to the decay of ^{176}Lu being negligible for rocks younger than ≈ 3.0 Ga old (G.Faure, 1986). In whole-rock dissolution analyses, complete dissolution of all the zircon present is therefore essential in order to obtain an accurate result, and furthermore, the presence of xenocrystic zircon cores may cause major errors in the interpretation of the data if their presence is not accounted for.

Figure 2.3 shows the REE contents of rims and cores of zircons from the Boggy Plain Adamellite determined by Kinny and Wyborn (1990) in an ion probe study. The cores have a classic magmatic HREE-enriched pattern, with a negative Eu anomaly and Ce-enrichment. However, the rims, which crystallised from late-stage hydrothermal fluids, have extremely high abundances for all the REE, and much flatter patterns. The rims were also found to be enriched in U, Th and Hf. The REE content of zircons (determined by ion-probe) has been used as a discriminant factor in dividing detrital zircons from sedimentary rocks into distinct populations (Gaudette et al. 1981) thus enabling the hinterland rocks from which the sediment was derived to be dated by multi-grain dissolution analysis.

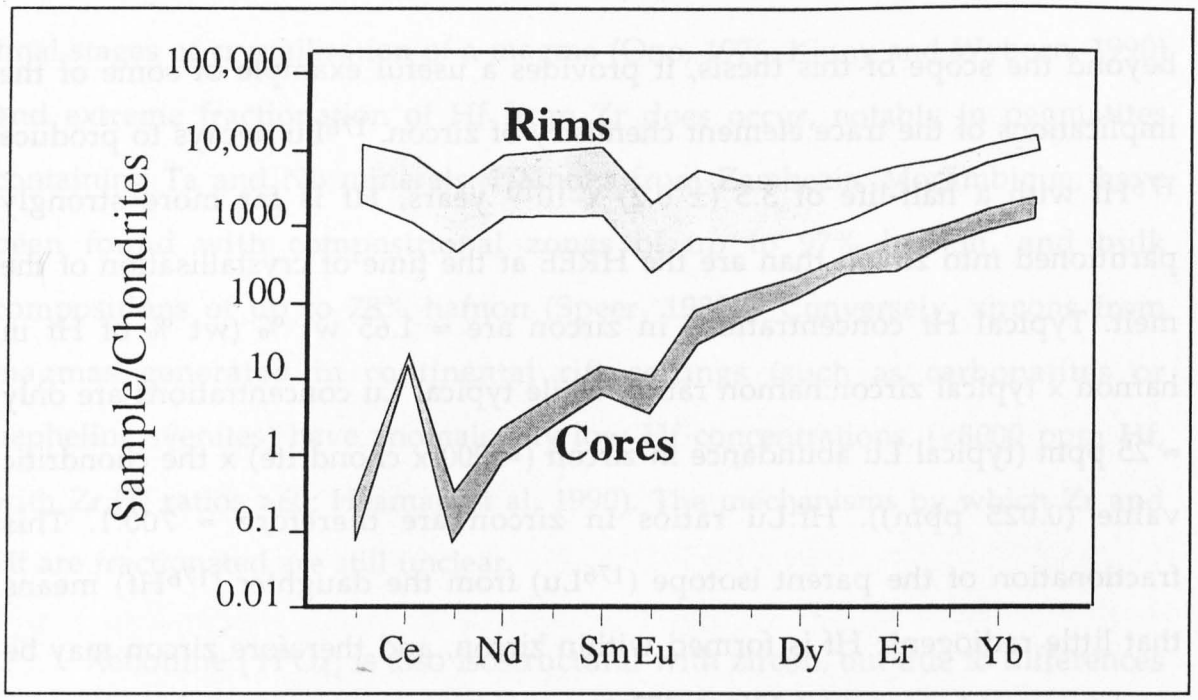

Figure 2.3. Chondrite normalised core and rim REE profiles for zircons from the Boggy Plain Adamellite (Kinny and Wyborn, 1990).

Hansen and Friderichsen (1989), carried out detailed X-ray investigations on populations of zircons from three granites. They found that the cell volume and lattice constants of their zircons increased with increasing amounts of incorporated trace elements, and thus a strong correlation exists between the level of impurities present and the ease with which the zircon crystal will become an open system with respect to radioactive parent isotopes and their daughter products.

Therefore, the purer a zircon is, the more reliable it is as a geochronometer.

2:2.5 Thorium, uranium & lead chemistry of zircon.

U^{4+} (1.00Å) and Th^{4+} (1.05Å) both may substitute for Zr^{4+} (0.84Å) within the lattice of zircon. Typical Th contents of zircons range from ≤ 2 ppm in zircons from kimberlites, up to 10 wt% in some metasomatic rocks. U contents range from ≤ 2 ppm in zircons from kimberlites, up to 7 wt% in some pegmatites. Evolution of zircon morphology is often linked to the fractionation trend of the host magma towards an incompatible element enriched residual melt, resulting in higher U contents in more evolved zircon forms. The more evolved zircon types typically show an inverse correlation between grain size and U-concentration, as the smallest crystals formed last, within the most U-rich environment.

The Th/U ratio of zircons is generally ≤ 1, in contrast to typical values of 3.5 to 4 for their igneous host rocks. This could be for two reasons. First, the U ions, being marginally smaller, fit better inside the zircon lattice than the Th ions, and thus may be taken up preferentially. Secondly, the Th could have been taken up by the crystallisation of phases such as thorite, allanite or monazite, all of which have a strong affinity for Th relative to U. A study of the U and Th contents of zircons during the crystallisation of a magma body (the Rensen Pluton in Northern Italy) was undertaken by Barth et al. (1989). Using Pupin's classification system, they showed that the U content of zircons increased progressively from the least evolved crystal shapes, which contained ≈610 ppm of U, up to 1760 to 2540 ppm in the more evolved crystals. The zircons also displayed a progressive decrease in Th/U from the least evolved types to the most evolved types, which they attributed to the crystallisation of allanite during the crystallisation sequence of zircon.

Pb within the magmas tends to be in the Pb^{2+} state, with an ionic radius of 1.29Å. The Pb ion is both far too large, and its charge too small, to be able to fit readily into the zircon lattice, and thus Pb is virtually excluded from the

zircon at the time of crystallisation. Therefore, the vast majority of Pb found in zircon is formed in-situ by the radioactive decay of U and Th. The "common lead" (Pb not generated by in-situ radioactive decay) content of "pure", high quality zircons has been estimated at ≤ 10 parts per billion (Compston et al. 1992).

The radiogenic Pb held within the zircon has a high activation energy - up to 7 eV (Bogolomov, 1991). Thus this Pb must be held in the 6- or 8-fold coordinated site usually occupied by Zr^{4+}, in the Pb^{4+} state. It has been speculated (Kober, 1987) that the highly oxidizing conditions necessary to oxidise the radiogenic Pb are set up within the crystal lattice as a result of the decay of the radioactive isotopes. The ß- particles released have ranges of up to 1mm, and thus may escape the crystal. The alpha-particles have much shorter ranges (0.01 to 0.03 mm), and as such will remain within the crystal. Therefore an excess of positive charge is set up, carried by He^{2+} or He^{4+}. These are very strong oxidizing agents, and electron donation from radiogenic nucleiides such as Pb^{2+} may be a prominent process of charge redistribution, oxidizing Pb^{2+} ions to Pb^{4+}, enabling them to become stabilised within the Zr^{4+} sites of the zircon lattice.

2:2.6 Zircon blocking temperatures

The high activation energy necessary to remove radiogenic Pb from the lattice of zircon has important implications for Pb retention by zircon during the geological processes which may affect zircons after their initial crystallisation. U-Pb dating on xenocrystal zircon cores has unequivocally demonstrated that the blocking temperature of zircon to open system behaviour of its parent and daughter isotopes is above the temperature of most magmatic systems, and zircon xenocrysts have even been recovered from komatiitic basalts within greenstone belts with probable extrusion

temperatures >1200°C (Compston et al. 1986). Claoue-Long et al. (1991) demonstrated that in the extreme, diamond-pressure, metamorphic compositions recorded in the Kokchetav massif, Russia (up to 40 kbar and 900 to 1000°C) although most of the zircon present was re-set to the time of the metamorphism, some xenocrystic cores to zircon crystals have at least partially retained their original isotope systematics, and give crystallisation ages of up to 2000 Ma. Zircons from kimberlites have also been found which have retained Archaean (≈2.8 Ga) isotopic signatures (Kinny et al. 1986), interpreted as the time at which the lithospheric mantle source region of these zircons (formed at ≈3.5 Ga) passed through a blocking temperature of ≥ 1100°C.

However, although zircon is capable of retaining closed-system behaviour at extreme temperatures and pressures, crystals (or portions of crystals) commonly show some degree of Pb or U loss (Pb loss is the more common) when subjected to metamorphic or magmatic events. When loss of U or Pb does occur, ion microprobe dating has demonstrated that zircons do not show an internal Pb loss pattern which might represent a diffusion gradient. Instead, the magnitude of the Pb loss varies from zone to zone within the crystal, bearing no systematic relationship to crystal edges (Williams et al. 1984). The degree of Pb loss suffered by a zircon crystal during a thermal "event" is dependant on the degree of order of its crystal lattice. This is controlled by two related factors. The first is the trace element content (section 2:2.4), and the second is the amount of radiation damage to the lattice caused by in-situ decay of the trace elements U and Th.

2:2.7 Metamict Zircon.

The decay of U and Th results in damage to the crystal lattice of zircon, forming metamict zircon. Metamict zircon has sufficiently different physical and optical properties to normal zircon to have been given separate names in the past, such as malacon or cyrtolite. Entire crystals may be metamict, or zones within a crystal, or more commonly, the rims of crystals (which often have the highest incompatible element concentrations - section 2:2.4).

Transmission Electron Microscope (TEM) studies (McLaren et al. 1990) have shown that radiation damage causes the zircon to break down into an extremely fine grained (< 10 nm) intergrowth of baddeleyite (ZrO_2) and silica glass. This alteration causes crystals to become "milky" or opaque, rather than transparent. As the breakdown reaction involves a volume increase (and density decrease), metamict zircon is less dense, and softer than pristine zircon. These differences in physical properties may be used to separate metamict zircons from undamaged crystals.

Metamict zircons have far lower activation energies before they become open systems with respect to radioactive elements and their daughter products than pristine, non-metamict zircons (4 eV as opposed to 7 eV for non-metamict crystals, Bogomolov, 1991). Therefore, metamict zircons are of less use than unaltered crystals in constraining the crystallisation age of a population of zircons, as their isotope systematics may be disturbed by relatively minor events, and steps are usually taken to exclude metamict material from analysed suites of zircons.

2:3 U-Pb & Pb-Pb GEOCHRONOLOGY USING ZIRCON

Possibly the most geologically useful isotopes present in zircon are ^{238}U, ^{235}U and ^{232}Th. These are present as Th^{4+} and U^{4+}ions, and occupy the Zr^{4+} site in the crystal lattice. They ultimately decay to ^{206}Pb, ^{207}Pb and ^{208}Pb respectively. Between them, these three decay series contain 43 isotopes of 12 elements as their intermediate daughter products, but each daughter product is specific to a single decay series.

$^{238}U \rightarrow {}^{206}Pb$ Half-Life = 4468 Ma

$^{235}U \rightarrow {}^{207}Pb$ Half-Life = 704 Ma

$^{232}Th \rightarrow {}^{208}Pb$ Half-Life = 14, 010 Ma

The radiogenic lead (Pb*) produced is retained within the crystal lattice, and thus Pb*/U, Pb*/Th and Pb*/Pb* ratios may be used to date the crystallisation of the mineral.

2:3.1 The concordia diagram

The decay of ^{238}U to $^{206}Pb^*$ and of ^{235}U to $^{207}Pb^*$ takes place according to the following equations:-

$$\frac{^{206}Pb^*}{^{238}U} = (e^{\lambda^{238}U \times \text{time of decay}})-1$$

$$\frac{^{207}Pb^*}{^{235}U} = (e^{\lambda^{235}U \times \text{time of decay}})-1$$

Where:

$\lambda^{238}U$ = The decay constant of $^{238}U = 1.55125 \times 10^{-10}\ a^{-1}$

$\lambda^{235}U$ = The decay constant of $^{235}U = 9.8485 \times 10^{-10}\ a^{-1}$

If the $^{206}Pb^*/^{238}U$ and $^{207}Pb^*/^{235}U$ ratios are determined for a range of ages, and the results plotted on a graph with $^{207}Pb^*/^{235}U$ on the X-axis, and $^{206}Pb^*/^{238}U$ on the Y-axis, a curve is constructed, connecting all the points for which these isotope systems have remained closed since the time of their formation. This curve is known as the concordia (Wetherill, 1956) and the zircons whose isotopic compositions plot along the curve are described as concordant.

For terrestrial samples, the $^{238}U/^{235}U$ ratio was set at a certain value at the formation of the Earth, and due to the differences in the half-lives of the two elements, this ratio has since evolved to a value of 137.88:1 (^{238}U: ^{235}U) at the present day. Therefore, as the relative abundances of these two isotopes are known, the ratio of $^{207}Pb^*/^{206}Pb^*$ may also be used to determine the age of a concordant sample, according to the equation:-

$$\frac{^{207}Pb^*}{^{206}Pb^*} = \frac{1}{137.88} \times \left(\frac{(e^{\lambda^{238}U \times \text{time of decay}})-1}{(e^{\lambda^{235}U \times \text{time of decay}})-1} \right)$$

2:3.2 Discordant Zircon

Loss or gain of U or Pb from zircon occurs, resulting in *discordancy*, when the isotopic composition of the crystal plots off the concordia curve. Such zircons are therefore referred to as *discordant.*

During a thermal "event", a population of zircons will lose radiogenic Pb as the zircons start to exhibit open system behaviour. Different crystals, or portions of crystals, will undergo different degrees of Pb-loss, depending upon

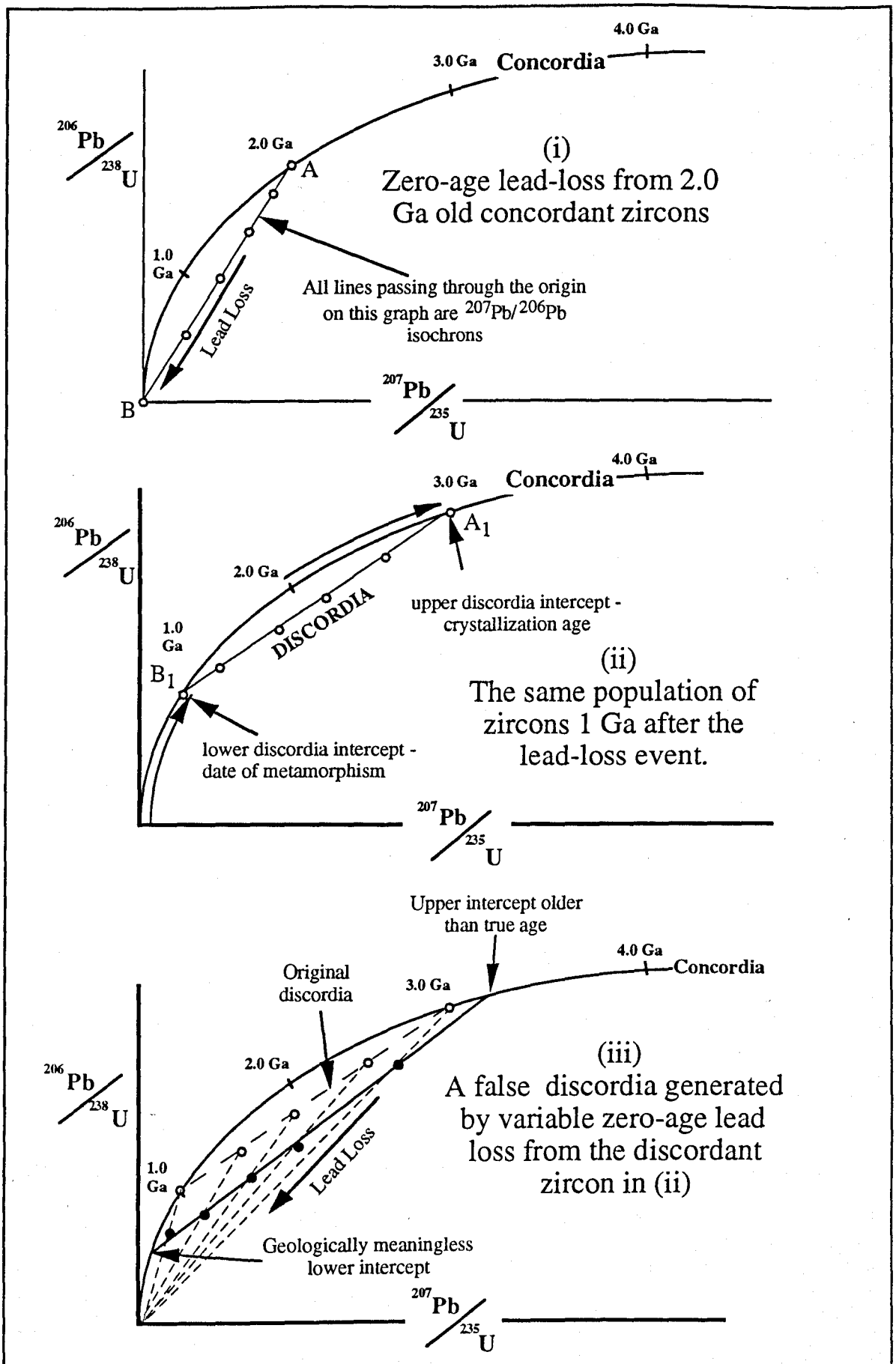

Figure 2.4 A series of diagrams illustrating the discordia method of dating. For explanation see text.

factors including their trace element content (section 2:2.4) and the degree of radiation damage that they have suffered (section 2:2.7).

On the concordia diagram (figure 2.4(i)) this Pb loss will cause the U-Pb ratios of individual zircons or batches of zircons to be displaced from the concordia (at A) and to plot towards the origin at B (where zircons which are completely re-set will plot) along a $^{207}Pb/^{206}Pb$ isochron (as all of the zircons have the same age).

Figure 2.4a(ii) shows same population of zircons 1 Ga after the "zero age" Pb-loss event in figure 2.4(i). The initial crystallisation age and Pb-loss events are now 1 Ga older (at 3 Ga and 1 Ga respectively) and therefore the U/Pb isotopic ratios of the two end-member "concordant" components A and B have evolved along the concordia curve to A_1 and B_1 respectively. The zircons which were only partially re-set in the thermal event behave as two-component mixtures between these end-members, and plot along a chord known as a *discordia* (no longer a $^{207}Pb/^{206}Pb$ isochron). If no concordant zircon is present, the intercepts of the discordia with the concordia curve may therefore be used to determine the original crystallisation age and the age of the Pb-loss event.

However, if the zircons undergo more than one episode of Pb-loss, then dating by the discordia method may produce inaccurate, or even geologically meaningless results. Figure 2.4(iii), shows a situation where the discordant zircons from figure 2.4(ii) undergo a second period of zero-age Pb-loss. Again, lead loss results in each point being displaced along a line back towards the origin. If a chord is drawn through these points, a false discordia is produced, the upper intercept of which is older than the true crystallisation age, while the lower intercept is younger than the true age of the first lead loss event. Although the scatter of points along this line is usually greater than for a true discordia, this may not be recognised if only a limited data set is available. If it

is suspected that the zircons have undergone more than two episodes of lead loss, then the $^{207}Pb/^{206}Pb$ age of the oldest sample analysed will provide a *minimum* age of the older phase, and the $^{207}Pb/^{206}Pb$ age of the youngest analysis will provide a *maximum* crystallisation age of the younger phase of zircon present.

Radiation damaged, metamict material is the discordant component within most zircon analyses, and within most zircon populations there is a general correlation between the degree of discordance and the U content. Due to the large number of possible variables apart from the U content, this correlation tends to be rather poor, and U content and discordance are rarely correlated between separate suites of zircon (Hansen and Friderichsen, 1989). Therefore, as most of the error in zircon dating is due to the difficulty of interpreting discordant zircon, and in uncertainty over the composition of "common lead" (Pb not produced by in-situ radioactive decay) which contaminates the samples, most dating work attempts to eliminate these factors as far as possible by removing metamict zircon.

2:3.3 Daughter isotope fractionation.

As the U decay series contain so many intermediate members, many of which have relatively long half-lives, it is important to note that the intermediate members of the decay sequence may have been out of equilibrium due to fractionation when the zircon crystallised. This disequilibrium of isotopes will result in an incorrect "age" if the effect is not corrected. By the time several half-lives of the intermediate daughters have passed, equilibrium is restored in the decay sequence, and the anomaly in the daughter isotopes is "diluted" through time as progressively more daughter isotopes are generated at equilibrium. Therefore, these effects are particularly noticeable in younger zircons. The ^{232}Th to ^{208}Pb decay sequence is a very

useful check on the U decay sequences, as its intermediate daughters all have comparatively short half-lives, meaning that they are unlikely to build up to levels where disequilibrium becomes a serious problem, and that even if they do become fractionated, equilibrium is quickly restored.

In the ^{235}U to $^{207}Pb^*$ decay scheme, the most likely source of error is the enrichment of the daughter isotope ^{231}Pa with respect to ^{235}U in the zircon. ^{231}Pa is a member of the ^{235}U decay sequence, with a half-life of 33 thousand years ($\lambda_{231} = 2.116 \times 10^{-5}$), thus decaying almost entirely to ^{207}Pb within 0.5 Ma - instantaneously on the scale of most zircon dating. The $^{231}Pa^{5+}$ ion substitutes for Zr^{4+}, resulting in an excess of $^{207}Pb^*$ upon the decay of the Pa. This leads to anomalously old $^{207}Pb^*/^{235}U$ and $^{207}Pb^*/^{206}Pb^*$ ages. A case where this has occurred was reported by Mortensen et al. (1992). They found high-quality zircon crystals in a peraluminous pegmatite which contained up to 20% excess "unsupported" ^{207}Pb. The zircons gave scattered $^{207}Pb^*/^{206}Pb^*$ ages between 233 and 961 Ma, whereas the $^{206}Pb^*/^{238}U$ ages were tightly clustered around the true crystallisation age of 191.3 ± 0.6 Ma.

Figure 2.5 shows the effect of the addition of 1 ppm of ^{231}Pa to a zircon containing 1000 ppm of ^{238}U (corresponding to a total of ≈ 1010 ppm U at the present day, and ≈ 1200 ppm U at 4 Ga). It may be clearly seen that the effects of the addition of excess Pa are extremely marked in recent zircons, with an excess age of 1748 Ma for a zircon 100 Ma old, whereas a zircon 3700 Ma old gives an apparent age only 10 Ma with the same initial addition of 1 ppm of Pa.

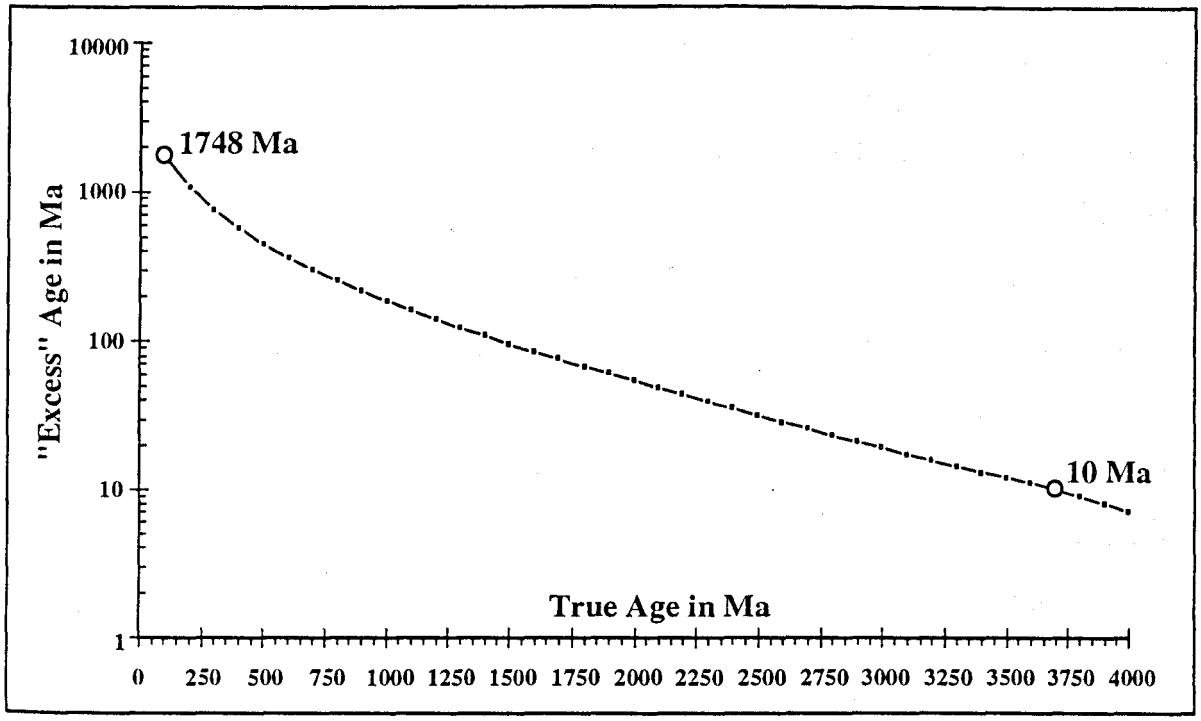

Figure 2.5 A diagram illustrating the effect of the addition of 1 ppm of ^{231}Pa to a zircon containing 1000 ppm of ^{238}U (and the appropriate quantity of ^{235}U) through time. Quantity of radiogenic ^{206}Pb calculated according to the equation $D^* = N_0 (1 - e^{-\lambda t})$, where D^* = quantity of radiogenic daughter; N_0 = original quantity of parent ^{238}U (1000 ppm); λ = decay constant of ^{238}U. Quantity of radiogenic ^{207}Pb derived at equilibrium from ^{235}U calculated from true $^{207}Pb/^{206}Pb$ ratio for each 100 Ma interval, apparent ages then calculated after 1 ppm of ^{207}Pb was added. "Excess" age = apparent age - true age.

Techniques where a full set of U and Pb isotope ratios are not available, such as the Kober technique (section 2:4.5) must therefore view data from zircons with anomalously high 207Pb/206Pb ratios with caution, and the possibility that their "ages" are due to an initial excess of Pa, rather than the presence of older xenocrystic cores, must be considered. However, the effect is rare (it has only been reported once), and more information on both possible mechanisms by which Pa may reach sufficient concentrations for the effect to become significant, and the distribution coefficients of Pa into zircon and other phases is required before the degree to which this effect must be taken into account may be fully evaluated.

2:3.4 Common lead corrections

With the U-Pb and Pb-Pb methods of dating, it is important that Pb not produced by radioactive decay within the sample, referred to as common lead, is either removed prior to analysis, or corrected for (figure 2.6). Due to the decay of U and Th, the composition of common lead has evolved through time. Various attempts have been made to define the isotopic evolution of common Pb, using the isotopic compositions of galena (PbS) from ore deposits of known age (galena contains no U, and thus its Pb isotopic composition is fixed at the time that the galena crystallises). Of the various models proposed (see G. Faure, 1986 for a more complete list), the most commonly used (and applied in this thesis) is the "two-stage Pb evolution model" of Stacey and Kramers (1975).

Within a zircon analysis, common lead is supplied from two sources, the sample and laboratory contamination. Where possible, the proportion of common lead due to laboratory contamination (modern common lead) is determined by running through the full procedure without any zircon present, to give the "total procedure blank" that may be expected. Common lead is also present in the sample itself. This Pb has either been held in the lattice of the zircon crystal since the time of its crystallisation, generally an extremely small component, estimated at $\leq$ 10 parts per billion (Compston et al. 1992), or on the surface and within cracks of the zircon crystals in the sample. Lead held in this latter way is often the largest component of common lead in the analysis, and is the hardest to correct for, as it may have been introduced at any time since the formation of the crystal. It is, however, the easiest to remove by cleaning procedures. If this Pb component cannot be eliminated, common Pb corrections are often made using the whole rock Pb isotopic composition of the zircon's host rock.

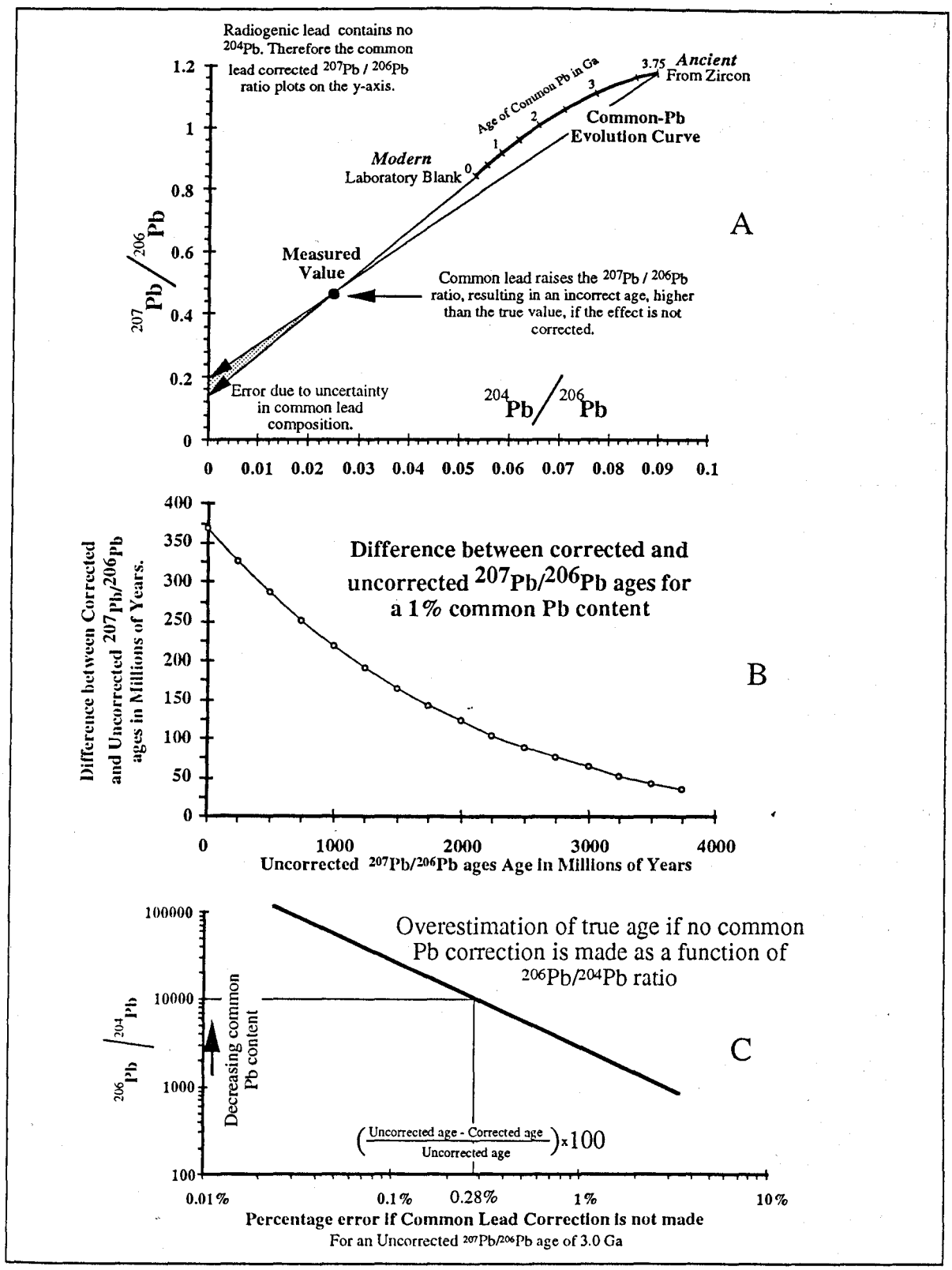

Figure 2.6 A series of diagrams illustrating common Pb corrections to the $^{207}Pb/^{206}Pb$ ratio. (A) $^{207}Pb/^{206}Pb$ vs $^{204}Pb/^{206}Pb$ diagram, to show that failing to make a common Pb correction results in an over-estimation of the $^{207}Pb/^{206}Pb$ ratio, and differences between corrections for modern and ancient common Pb. (B) Difference between corrected and uncorrected $^{207}Pb/^{206}Pb$ ages as a function of age (the age of the common Pb = the uncorrected age). (C) Difference between corrected and uncorrected $^{207}Pb/^{206}Pb$ ages as a function of $^{204}Pb/^{206}Pb$

However, whole rock systematics are comparatively easy to alter, and making this correction assumes that the common Pb content of the zircon was open to the same possible alterations up until the time of analysis, which is probable if this Pb is held within cracks. Alternatively, the assumption may be made that the common Pb was incorporated in the zircon at the time that the host rock crystallized, and thereafter remained closed to further alteration, which may be the case if the common Pb is held within inclusions within zircon crystals, and within the zircon crystal lattice itself. In this instance, the Pb isotopic composition of a phase such as feldspar (which contains Pb but no U, and thus records the initial Pb isotopic composition of the rock) is used to make the common Pb correction.

Once the relative proportions of contamination due to ancient and modern common lead have been determined, the common lead correction is made. This is achieved by subtracting the common ^{206}Pb and ^{207}Pb from the raw data. The quantity of material to subtract is generally determined by the amount of ^{204}Pb present in the analysis. ^{204}Pb is present in common lead, but is not produced by the decay of either U or Th. Therefore, the proportion of ^{204}Pb, usually expressed as the $^{206}Pb/^{204}Pb$ ratio, is a measure of the quantity of common lead present. In order to correct for common lead, first the composition of common lead is determined from the Stacey and Kramers (1975) curve, and then the quantity of common lead necessary to reduce the ^{204}Pb content (and hence the common lead) of the sample to zero is subtracted from the raw data, according to the equation:-

$$\frac{^{207}Pb^*}{^{206}Pb^*} = \left(\frac{^{207}Pb}{^{206}Pb}\right)_m \times \left[\frac{1-\frac{(^{207}Pb/^{204}Pb)_t}{(^{207}Pb/^{204}Pb)_m}}{1-\frac{(^{206}Pb/^{204}Pb)_t}{(^{206}Pb/^{204}Pb)_m}}\right]$$

Where the subscript m denotes measured value, and the subscript t denotes common lead values at time t (Cocherie et al. 1992).

Figure 2.6a demonstrates this common Pb correction by subtraction of non-radiogenic ^{206}Pb and ^{207}Pb from the analysed composition on the basis of ^{204}Pb content. From this diagram, it may be seen that correcting to "ancient" common lead compositions results in a higher $^{207}Pb/^{206}Pb$ common Pb corrected age than if the correction is made to modern common Pb. Therefore inaccuracy in the determination of common Pb composition will result in an error in the common lead corrected age. However, this effect is comparatively small ($\approx$ 0.1%) and decreases with decreasing common Pb content. Failing to make a common Pb correction has a far larger effect, resulting in an overestimate of the age of the zircon. Due to the shape of the common Pb evolution curve (and the fact that younger zircons have lower $^{207}Pb/^{206}Pb$ ratios) the over-estimation of age if common Pb is not corrected for (for the same level of common Pb contamination) increases as the age of the zircons decreases (figure 2.6b). Obviously, the over-estimation of true age due to uncorrected common Pb is proportional to the common Pb content, and figure 2.6c shows this relationship for an uncorrected $^{207}Pb/^{206}Pb$ age of 3.0 Ga. For low blank Pb analyses, the $^{206}Pb/^{204}Pb$ ratio is often greater than 10,000. If only small amounts of lead are being analysed, this can mean that ^{204}Pb is close to background levels, and therefore cannot be precisely analysed. It is often quoted in published papers that $^{206}Pb/^{204}Pb$ was >10,000, and therefore no common Pb correction is necessary (eg. Fryer et al. 1993). However, figure 2.6c shows that this may result in an over-estimation of the true age by up to 0.28% at 3.0 Ga, (increasing for younger zircons). This overestimate of the age may be larger than the quoted error.

In order to reduce this possible error due to the very small amounts of ^{204}Pb present when only small amounts of zircon are analysed, an alternative system of common Pb correction is possible, using the Th/U and $^{208}Pb/^{206}Pb$

ratios (Compston et al. 1992). If the zircon has had closed system behaviour, then the $^{208}Pb/^{206}Pb$ ratio and the Th/U will be correlated. As ^{208}Pb is much more abundant than ^{204}Pb, it may be much more accurately measured.

Concordant zircons will plot along a line defined by the equation:-

$$\frac{^{208}Pb^*}{^{206}Pb^*} = \frac{^{232}Th}{^{238}U} \times \left(\frac{(e^{\lambda^{232}Th \times \text{time of decay}})-1}{(e^{\lambda^{238}U \times \text{time of decay}})-1} \right)$$

The distance the total $^{208}Pb/^{206}Pb$ lies above this line is a measure of the amount of common lead in the sample. Should the $^{208}Pb/^{206}Pb$ plot below this line, then the Th/U ratio has been altered at some point, and the method is not applicable.

2:4 U-Pb AND Pb-Pb ZIRCON DATING TECHNIQUES

There are three methods of dating zircon currently widely in use; dissolution, followed by chemical separation of U and Pb, and thermal ionisation solid source mass spectroscopy; Sensitive High Resolution Ion MicroProbe (SHRIMP) dating of small portions of individual grains, and Pb-Pb dating using direct thermal ionisation of whole zircon grains (the Kober technique).

2:4.1 Sample selection and preparation for zircon dating

Although zircon is an almost ubiquitous phase in crustal rocks, it rarely reaches modal abundances greater than 0.5%. Therefore, complex concentration procedures are necessary. The hardness and density of zircon are exploited in most techniques for its extraction. After the rock has been ground to individual grains, lighter minerals are removed in a two-stage floatation process (see appendix B for method) using overflow type centrifuges which were built for this project. The first stage is carried out in a very large capacity (4.5 litre) centrifuge, using sodium polytungstate solution (specific gravity 2.8), and the second stage is carried out using methyl iodide (specific gravity 3.3) in a small (400 cc) centrifuge. The residual dense separate is then passed through a Frantz magnetic separator to remove magnetic minerals. As discussed in section 2:2.7, metamict zircons are more likely to show discordant behaviour than pristine crystals. Therefore, the precision of the analysis is improved if such material is separated and discarded. The separation of metamict zircon may be achieved by several techniques.

Metamict zircon is less dense than pure zircon (pure zircon has a density of 4.66, metamict zircon often has a density as low as 3.9), so separation in an extremely dense liquid is a possible first step in eliminating the

metamict component. The main problem with this method of separation is that most very dense liquids, such as Clerici's solution, are extremely toxic, and they also contain Pb, thus adding to the procedural blank. Therefore this stage is best avoided.

Metamict zircon is considerably softer than non-metamict zircon. To exploit this, Krogh (1982a), devised an apparatus in which zircons are mixed with pyrite and agitated in a current of compressed air. The result of this air abrasion is to remove the softer, metamict and discordant crystals and rims. Metamictisation also involves a volume increase, so if there are any crystals with metamict interiors, the outer layers will tend to be cracked and weakened, and thus these grains are also destroyed, and removed by the abrasion process. A further use of the abrasion technique is that rims of later overgrowth may be removed from xenocrystic cores, enabling the cores to be dated accurately by conventional dissolution techniques.

Aleinikoff et al. (1990) published details of a modified air abrasion device, which allowed collection of fragments of "rim" material for dating. The usefulness of this technique is rather doubtful, as the fragments of overgrowth will be contaminated with; fragments of metamict, discordant, material; material from the cores of any xenocrystal grains which have been broken; and material from around cracks, rich in common lead. In a situation where a population of zircons with obvious cores and rims is to be dated, the best course of action is to abrade the material with visible cores, which are then released for dissolution, and to carefully pick out core-free grains which formed at the time of the crystallisation of the rims, to allow the dating of this event. A further point to note is that following abrasion, the degree of concordancy is very poorly correlated with U-content, so it appears that only near-surface U is involved in the usual correlation of discordance and U content (Krogh, 1982a).

Krogh (1982b) also noted that iron oxides and hydroxides were commonly deposited within metamict zircon, which has an expanded, spongy texture. Neither Fe^{2+} nor Fe^{3+} is easily accommodated within the lattice of zircon, so the iron content and the degree of metamictisation are commonly well correlated. Krogh designed an electromagnetic grid which creates an extremely intense magnetic field, and is capable of processing large quantities of samples quickly, retaining any magnetic grains. To process smaller samples, the same effect can be obtained by placing the sample in a dish over a strong magnet. The zircons are then touched with a soft iron wire point attached to a bar magnet of opposite polarity to the one under the dish. Only the least magnetic zircons will not be moved by the intense field generated at the tip of the pointer.

Air abrasion, combined with magnetic separation, should be capable of eliminating 90 to 100% of the discordance of a zircon sample, and most of the common lead.

For multi-zircon analyses in which the zircons are expected to be discordant, it is usual to dissolve fractions of the population of zircon, with the individual fractions selected on criteria related to the degree of discordance, such as magnetic susceptibility or size. This ensures that they are well spaced along the discordia, and so facilitates accurate estimates of the upper and lower intercept dates. For single zircon dating (using any technique), the zircons are usually selected on the grounds that they are likely to be concordant (clear, crack and inclusion free crystals with low magnetic susceptibility).

When looking at detrital zircons of varied provenance, the population from the sediment is split into groups, based on factors such as colour, length to width ratio, REE profiles or the most common sub-populations of habit for any given grain size, according to the Pupin classification scheme. This

minimises the number of analyses which have to be carried out, and validates the use of multi-grain dissolutions within heterogeneous populations.

2:4.2 Dissolution, followed by isotope dilution and thermal ionisation mass spectrometry.

In this technique the zircon is dissolved in HF and HNO_3 in a teflon dissolution vessel at temperatures of up to 220°C. There are various dissolution vessels in common use, most of which are based on a design by Krogh (1973). Of the refinements suggested to this design, perhaps the most significant is the use of "micro-capsules" within a larger dissolution vessel (Parrish, 1987), which allows very high temperature (and thus short dissolution time) low-blank analyses on small quantities of zircon. Once the zircon has been dissolved, U and Pb are separated by column chromatography, and analysed by thermal ionisation mass spectrometry. Mass fractionation within the mass spectrometer may be corrected by comparison with internationally available standards, such as NBS 981 or NBS 983, and these standards also allow different laboratories to corroborate each others' data. At the start of the dissolution process, a known quantity of "spike" solutions of Pb and U (solution sufficiently isotopically different to the sample to be easily recognised in the final analysis) is introduced. By comparison between the known concentration of Pb in the spike and the Pb from the zircon, the concentration of Pb in the zircon may be determined to high precision. With the micro-capsule dissolution technique, routine blank levels in the order of 10-50 pg of Pb before corrections for reagents and loading (Roddick et al. 1987), and ≤ 5 pg of Pb after correction for reagents and loading (Parrish, 1987), on sample sizes ranging from several hundred grains (several mg) down to fragments of a single grain (>0.05 mg, eg Schärer and Allègre, 1985). The precision of these analyses is ≤ 0.1% (1 σ errors) for samples which supply 1 ng

of Pb, falling to ± 1% on samples which supply 300 pg (the amount of Pb depends on the size, age, and initial U content of the zircons).

Obviously, the more U and Pb that is present in the zircon dissolved, the more precise the analysis will be, suggesting that the most accurate ages should be obtained from dissolutions of large numbers of zircons. However, zircon populations (and often individual zircons) are frequently extremely heterogeneous in terms of their ages, and picking hundreds (several mg) of zircons of a single age component is rarely either possible or practical. Therefore, it is desirable that only very small quantities of carefully selected zircon are analysed to avoid mixing different age components of the zircon population, using only very small quantities of reagents (thus with very low levels of laboratory contamination).

Using dissolution techniques, combined with Krogh's selection procedures, extremely precise dates may be determined. U and Pb isotope ratios allow disequilibrium corrections, and strong constraints may be placed on the sources of common Pb. The technique is capable of providing dates with a precision of ≤ 0.1% on zircons ranging from only 10 Ma old to early Archaean zircons, and sample sizes ranging from hundreds of crystals down to fragments of a single grain.

2:4.3 The Sensitive High Resolution Ion MicroProbe (SHRIMP)

The technique, as described in Compston et al. (1992) is as follows. Selected zircons are mounted on thin sections in epoxy resin, along with fragments of "standard zircons" of known age (standards are selected which are close to the presumed age of the sample) and polished down until the zircons are cross-sectioned. The sample is then cleaned, photographed, and gold coated for maximum surface conductivity. Selected sites are then ablated

with a beam of oxygen ions, creating a pit 20-30 μm in diameter, most of the material from which is totally ionised, and which may then be analysed for the isotopes of U, Pb and Th. SHRIMP is the only zircon dating technique in which Th is routinely analysed, allowing Th/U - $^{208}Pb/^{206}Pb$ common Pb corrections. The total weight of the analysed sample is less than 10 ng, more than three orders of magnitude less than for a typical single zircon dissolution analysis. The mass spectrometer scans through Zr_2O^+, Pb isotopes, $^{238}U^+$, ThO^+, and UO^+. A problem unique to SHRIMP analyses is the presence of hydrides, which are generated by the bonding of H^+ in the ion beam and Pb from the sample. This creates ions such as $(^{206}Pb^1H^+)^+$, which are then misinterpreted as $^{207}Pb^+$ ions, resulting in an error in the $^{207}Pb/^{206}Pb$ ages recorded. The precautions taken against this effect include a mass filter in the primary beam, and a very high vacuum at the sample. The raw data obtained on samples are then processed by first correcting for common Pb, and then determining the best-fit "calibration curve" relating Pb^+/U^+ and UO^+/U^+ for the sample with the standard. Thus the accuracy of the analysis is determined by the reproducibility of data from the standard, and the precision to which the composition of the standard is known. Revisions of the ratios given by standards caused the age of 3,930 ± 10 Ma obtained on Mount Somes in Antarctica by Black et al. (1986), then the oldest date obtained on a terrestrial rock, to be revised down to 3,870 ± 10 Ma (Bowring et al. 1989).

A common Pb blank is introduced into SHRIMP analyses as the sample is polished and etched. Common Pb, either from the ground up portion of the zircon, or from the etching and grinding reagents, is smeared across the surface, to be vaporised along with the sample. This may partly explain the concentration of common lead in cracks in zircon which is normally seen by SHRIMP. The common Pb correction in SHRIMP analyses is performed using the $^{208}Pb/^{206}Pb$ vs. Th/U technique described in section 2:3.4, expressed as "percentage of ^{206}Pb which is common Pb". Typical common Pb percentages

are ≈ 0.65 % (taken from the average of 84 analyses published in Compston et al. 1992), corresponding to a $^{206}Pb/^{204}Pb$ ratio of ≈ 3,000 (the $^{206}Pb/^{204}Pb$ ratio calculated from percentage of common Pb depends on the age of common Pb used in the calculation). Natural $^{206}Pb/^{204}Pb$ ratios in unaltered zircon are many tens of thousands to one (Corfu and Davis, 1991), so the lower ratios obtained by SHRIMP indicate the presence of a considerable amount of common Pb, the age of which cannot be determined and must be estimated. The common Pb correction usually performed on SHRIMP analyses uses the common Pb composition corresponding to the $^{206}Pb/^{238}U$ age of the zircon. This practice has been questioned by some authors (Corfu and Davis, 1991) who regard modern common Pb as the most likely contaminant. However, the effect is generally small, with possible errors of ≈ 0.1%, and these errors decrease on samples which contain below average concentrations of common Pb.

The errors on individual analyses by SHRIMP are higher, at ≈ ± 1%, than for conventional dissolution techniques (± 0.1%). However, the precision of analysis may be improved by repeated analysis of the sample, and errors of ≈ ± 0.1% may be achieved in this way.

SHRIMP dating analyses very small amounts of material, and therefore the technique works best on ancient zircons with reasonably high U contents (which therefore also contain large amounts of radiogenic Pb) but due to the extremely high U contents of some young zircons in S-type granites, SHRIMP dating may even be applied to samples as young as a few tens of millions of years (eg Zeitler and Chamberlain, 1991).

2:4.4 Laser Probe - Inductively Coupled Plasma Mass Spectrometry (LP-ICPMS)

Recently, a technique has been developed (Fryer et al. 1993; Feng et al. 1993) in which 20 to 80 μm pits are ablated in zircons by laser, and the ions released are analysed in an Inductively Coupled Plasma Mass Spectrometer (ICPMS). Although the technique is still in its developmental stages, zircons have been analysed with precisions of ± 1%, and the results agree closely with dates on the same zircons obtained by conventional techniques. Zircons from the Otto Stock, previously dated at 2680 ± 1 Ma by dissolution have been dated by LP-ICPMS at 2,686 ± 8 Ma (Fryer et al. 1993), identical within error, and clearly demonstrating the potential of the technique. Problems with constraining inter-element fractionation between U, Th and Pb have meant that as yet, the dates are determined solely by the $^{207}Pb/^{206}Pb$ method of dating. The technique has a significant advantage over SHRIMP, in that the surface of the sample may be cleaned by low-energy laser ablation before data acquisition commences, and therefore there is a low potential for common lead contamination of the sample. However, unlike SHRIMP, the common Pb correction has to be performed using the $^{206}Pb/^{204}Pb$ ratio, and the large inaccuracies in the measurement of (close to background) ^{204}Pb will result in inaccuracies in the calculated age. Due to the small quantities of Pb analysed, the threshold $^{206}Pb/^{204}Pb$ ratio below which ^{204}Pb may no longer be detected is ≈ 10,000 with this technique, and it is not sufficient (as Fryer al. stated) to simply state that "no common lead was detected (the $^{206}Pb/^{204}Pb$ ratio was >10,000), and therefore no common Pb correction was made" as this may potentially overestimate the age by up to ≈ 0.3 % (figure 2.6c). It is interesting to note that this potential over-estimation is close to the difference (0.22 %) between the conventional and LP-ICPMS results on the Otto Stock zircons (discounting the error bars).

With refinement, this technique should prove to be a very powerful analytical tool in zircon geochronology, potentially equal to the resolution of SHRIMP in the study of zircons with complex crystallisation histories. Important factors to in favour of the technique are that the required machinery is comparatively (to SHRIMP) cheap, no complex ultra-clean chemical procedures are required (unlike conventional dissolution) and the analysis is very fast, the date on the Otto Stock zircons being obtained in just 2 hours of machine time.

2:4.5 Zircon crimping - the Kober technique.

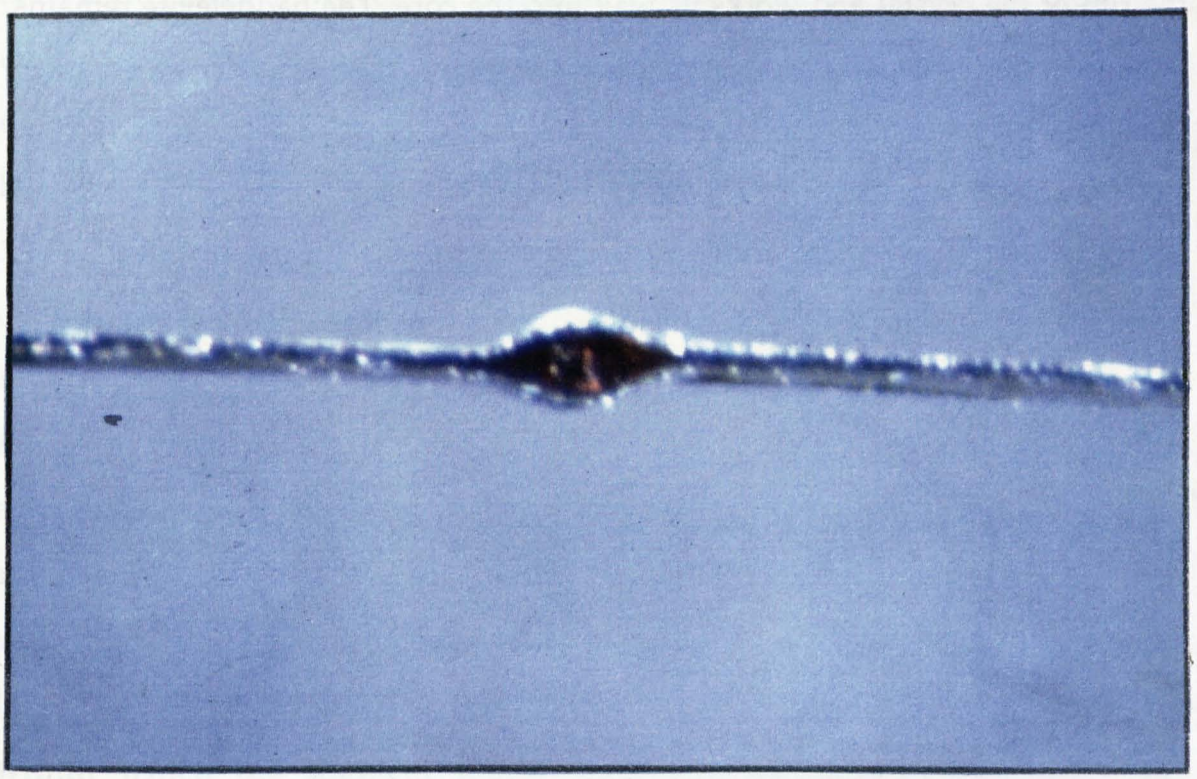

Photograph 2.1 A single zircon crystal folded into an evaporation filament. Width of zircon crystal ≈ 0.2 mm.

This technique of zircon geochronology is based on the analysis of Pb isotopes emitted by direct thermal ionisation of zircons, to give a Pb-Pb age. This technique was first attempted, using ground zircon on single filaments, as early as 1965 (Kosztolanyi). Gentry et al. (1982) developed an improved

technique - crimping entire zircon crystals within filaments. However, single filaments result in very poor ionisation, with resultant weak and unstable beams. Kober (1986) improved both the strength and stability of the beam of Pb ions, using a double filament technique, in which ionisation of material emitted from the evaporation filament is ensured with a very hot (≈2000°C) ionisation filament, adjacent to the evaporation filament.

Heating of the zircon causes it to break down into baddeleyite and silica, in the reaction:

$$ZrSiO_4 \longrightarrow ZrO_2 + SiO_2$$

(Ansdell and Kyser, 1993; Chapman & Roddick, 1994). This reaction starts at the rim of the crystal and works its way into the core. The baddeleyite remains within the filament, pseudomorphing the original zircon crystal, and the silica is emitted with the Pb ions. If this material is deposited on a (cold) ionisation filament, then it forms an emitter compound capable of giving extremely stable Pb beams of long duration, allowing very precise analyses to be made. The emitter compound, probably $PbHfSiO_5$, has Pb retention and ionisation properties very similar to those of the Si-gel method of Pb loading (Kober, 1987). Therefore, although the samples cannot be spiked, they can be run against international standards, (the standard used in this thesis was NBS 983, loaded in 2 µl silica gel and 1 µl phosphoric acid) in order to confirm the accuracy of the analysis, and to constrain the effects of mass fractionation within the mass spectrometer.

The technique has been applied in this thesis, on a Finnegan-MAT 261 mass spectrometer, equipped with faraday cups and a Secondary Electron Multiplier (SEM). The samples were either run dynamically at low beam intensities, (in dynamic analyses the four Pb isotope beams are alternately targeted into the SEM) or if the beam was sufficiently intense, then the sample was analysed statically. In static data collection, the smallest beam of ions (the

^{204}Pb beam) is collected in the SEM, while the ^{206}Pb, ^{207}Pb and ^{208}Pb are collected in the faraday Cups. This technique is several times faster than dynamic running, and allows very precise measurement of sub-nanogram levels of Pb (Roddick et al. 1987).

2:4.5a Procedure for the Kober Technique.

The zircon is loaded onto a de-gassed rhenium (Re) filament, which is then wrapped as tightly as possible around the crystal (as in photograph 2.1) to ensure even heating (see appendix B for the method). Only a small aperture is left, directly facing the ionisation filament, also of de-gassed Re. The filaments used in this study were 0.7 mm wide (the same width used by Kober). Kröner and Todt (1988) however, recommend 1 mm wide filaments, as these are capable of catching more of the emitter compound as it is released from the evaporation filament, especially if the evaporation filament twists when it is heated, and filaments 2mm wide have been used (Chapman & Roddick, 1994)). However, although the wider filaments are capable of retaining more of the emitter compound, they have a larger source area than smaller filaments, and this results in less well focused beams. Also, the wider filaments have lower resistance, and thus have to be run at higher currents to attain the same temperatures. When an attempt to run 2mm wide filaments was made in this study, it was found that in order to attain temperatures at which the emitter compound gives the strongest, most stable beam of ions (1260 to 1275°C), the filament current had to be turned up to the upper limits within which the filament temperature was stable, and that even the maximum current (8 amps) only raised the temperature of the filament to 1600°C, too low to ensure that the filament is fully "cleaned" between deposition cycles.

After the filaments are loaded into the mass spectrometer, the ionisation filament is turned up to 2000°C, and then the evaporation filament

is slowly heated up to 1350 to 1380°C to "condition" the zircon by removing common lead. At these temperatures, the breakdown of zircon to baddeleyite is relatively slow, and the first material to be lost from the crystal is that held on the crystal surface, or within metamict zircon. Metamict zircon is often a fine intergrowth of silica glass and baddeleyite (McLaren et al. 1990), and this silica and the associated Pb is lost very rapidly during the "conditioning" process. The reaction also propagates along any cracks within the zircon crystal, and therefore zircons with cracks are not selected, as step heating of such crystals will not give a true series of analyses from the rim to the core. The duration of conditioning varies with the size and quality of the crystal, and where possible is determined by the $^{206}Pb/^{204}Pb$ ratio of the Pb emitted during the process. Once the $^{206}Pb/^{204}Pb$ ratio has risen to 5,000 or so, the vast majority of the remaining Pb should be radiogenic $^{208}Pb^*$, $^{207}Pb^*$ and $^{206}Pb^*$, produced within the crystal lattice and the conditioning is assumed to be complete.

This radiogenic Pb is held in high activation energy Zr^{4+} sites within the lattice of zircon (section 2:2.5). Numerous studies (see section 2:2.6) have shown that the U-Pb systematics of high quality zircon crystals are retained through processes ranging from weathering to the partial melting of the rocks containing the zircons, to diamond pressure metamorphism. Therefore, it may be assumed that the Pb emitted following conditioning is concordant. This assumption of concordancy is the basis of the analysis.

Two situations where this assumption of concordancy is not valid have been recorded. In the first of these, a SHRIMP study identified zircons which contained unsupported radiogenic Pb (Williams et al. 1984). These zircons had concentrations of radiogenic Pb up to 50% higher than could have been produced by decay since the time that the zircon crystallised. This "reverse discordance" was caused by a gain of radiogenic Pb during a metamorphic event when portions of the crystal gained the Pb lost by other portions of the

same crystal. Unfortunately, as SHRIMP works by totally ionizing a small pit, it is impossible to say whether this Pb was actually held within the crystal lattice of zircon and would therefore have been analysed by the Kober technique as radiogenic Pb. A study by McLaren (1990) revealed that annealing of metamict zircon in a thermal event will result in the formation of silica glass, either exsolved from recrystallised zircon, or intergrown with zircon or baddeleyite. Silica glass is capable of holding very large quantities of Pb, and it could therefore be speculated that the reverse discordance was caused by silica glass which absorbed radiogenic Pb during the metamorphic event. The second situation where the assumption of concordancy is not valid is where there was a strong initial disequilibrium in the U and Th to Pb decay schemes as the zircon crystallised, and the crystal was depleted in ^{230}Th, or enriched in ^{231}Pa (See section 2:3.3 on daughter isotope fractionation). Data from only one zircon obtained by the Kober technique should therefore be viewed with caution, as the U-Pb systematics of the crystal analysed may have been disturbed. However, the recorded instances of non-concordancy all affect different crystals, and even different domains within those crystals, to different degrees. This will cause scatter in the data from more than one crystal, and therefore where the data from several crystals are in agreement, the assumption of concordancy is taken to be valid. Furthermore, daughter isotope fractionation will also be reflected by unusual Th/U ratios, and therefore unusual $^{208}Pb/^{206}Pb$ ratios, which serve to warn of the possibility of non-concordancy. Therefore, although the Kober technique analyses single zircons, it should not be regarded as a single-zircon dating technique, but rather as a multiple-zircon dating technique in which the zircons are dated one at a time.

The extremely small concentrations of common lead present after conditioning is complete are assumed to have been held within the Zr^{4+} sites of the crystal lattice, and thus must have been present since the zircon

crystallised. This knowledge of the age of common lead removes a source of potential uncertainty in zircon analysis. It is advisable to use the cleaning procedures conventional in dissolution analysis on zircons to be analysed by the Kober technique, as although it makes no difference to the final result, cleaning the zircons both shortens the conditioning time, and avoids the possibility of contaminating other samples in the magazine which do not undergo a conditioning process (such as lead standards) with common lead.

After the conditioning is completed, the ionisation filament is turned off, and the evaporation filament turned up to the first deposition temperature, usually in the range 1400 to 1410°C, and allowed to deposit material for up to 10 minutes, the exact duration of the deposition depending on the size of the zircon. After this deposition cycle, the evaporation filament is turned off, and the ionisation filament is slowly turned up to 1260 to 1275°C, when, if there is sufficient Pb present, a Pb beam is produced, which may then be analysed either statically or dynamically, depending on its intensity. After the beam intensity has dropped below acceptable levels, the filaments are cleaned of any residual material by returning them to their conditioning temperatures. The deposition cycle is repeated, at a temperature 2 to 10°C higher. This incremental heating is continued until no more Pb is left in the zircon, which is generally after 15 to 20 heating steps for a 0.3 mm zircon crystal.

In this thesis, common lead corrected $^{207}Pb^*/^{206}Pb^*$ ages are calculated on sets of 10 Pb isotope ratios taken from each heating step using the ^{204}Pb correction described in section 2:3.4, and these common Pb corrected ages are then used to calculate the true age of the zircon (see section 2:4.5b).

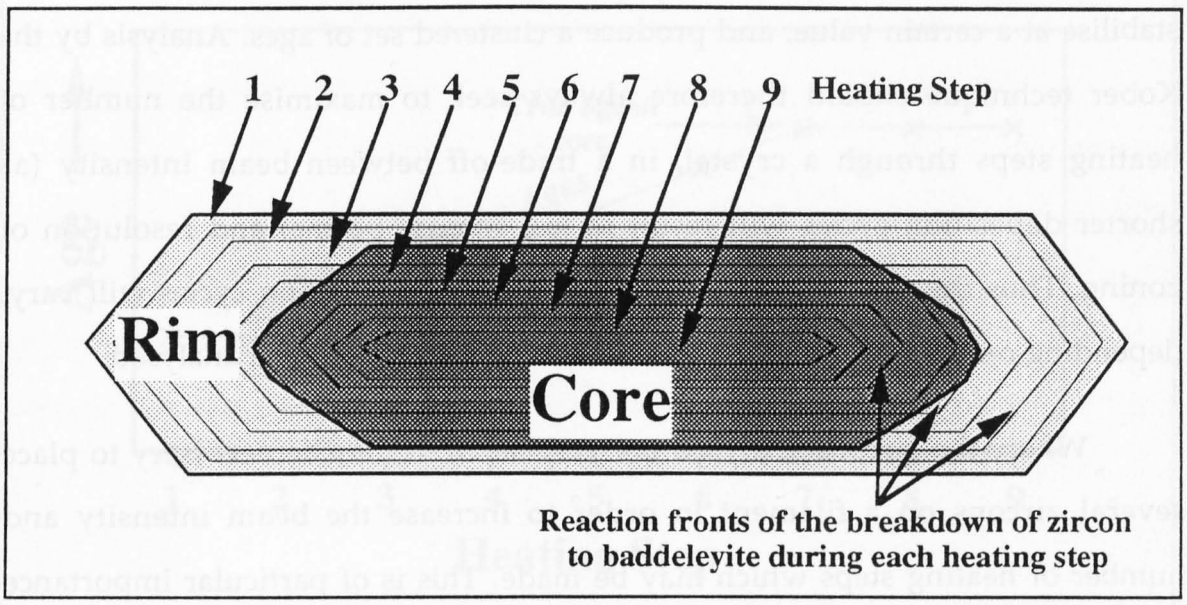

Figure 2.7 A schematic zircon crystal with a core and later rim. This diagram illustrates how material from the core and the rim may be mixed as the reaction front of the breakdown of zircon to baddeleyite progresses through the crystal in a number of heating steps.

The reason for incremental heating, rather than simply depositing all the Pb from the crystal in one prolonged deposition cycle, is that different parts of the zircon may have crystallised at different times, resulting in a single zircon crystal with a core and rim (figure 2.7). As the zircon to baddeleyite reaction front progresses through such a crystal, the Pb deposited on the ionisation filament may incorporate material derived from both the core and the rim (heating cycles 3 to 6 in figure 2.7), resulting in *mixed ages* (figure 2.8), intermediate between the true ages of the core and the rim. Therefore, where few data are available, the ages produced by the Kober technique should be regarded as *minimum* ages, as the possibility exists that the age recorded represents mixing between older and younger components. To constrain the true crystallisation age, it is desirable to select single phase zircons which give uniform $^{207}Pb^*/^{206}Pb^*$ throughout the stepped heating, indicating that they only contain one age component. If these zircons are rare, or unavailable, the core age may be constrained by the maximum ages obtained from zircons which do show a suite of mixed ages, but in which the older component was larger, so that the $^{207}Pb^*/^{206}Pb^*$ ratios produced by the final few heating steps

stabilise at a certain value, and produce a clustered set of ages. Analysis by the Kober technique should therefore always seek to maximise the number of heating steps through a crystal, in a trade-off between beam intensity (as shorter deposition cycles will result in less intense beams) and resolution of zoning. Thus the exact times and temperatures of deposition cycles will vary, depending on the size, quality and zonation of the crystal to be analysed.

Where the zircons analysed are very small, it may be necessary to place several zircons on a filament in order to increase the beam intensity and number of heating steps which may be made. This is of particular importance if the zircons are suspected to contain more than one phase of zircon. In this instance, single zircons would be consumed within a very few heating steps, resulting in meaningless, low resolution mixed ages intermediate between the two true ages. If several zircons are placed on the filament, the duration of the heating cycle may be decreased (and thus the number of heating steps may be increased) allowing the true age of at least the volumetrically larger age component within the zircons to be resolved with greater accuracy. This age component should be discernible in data from several filaments, confirming it is not an artificial effect produced by the proportion of crystals of various ages present, as the proportions of crystals of various ages are likely to vary between filaments. However, although loading multiple zircons onto filaments is capable of producing moderately well constrained data, it should be regarded as a "last resort", only used where single zircon analyses have failed to produce a well defined crystallisation age.

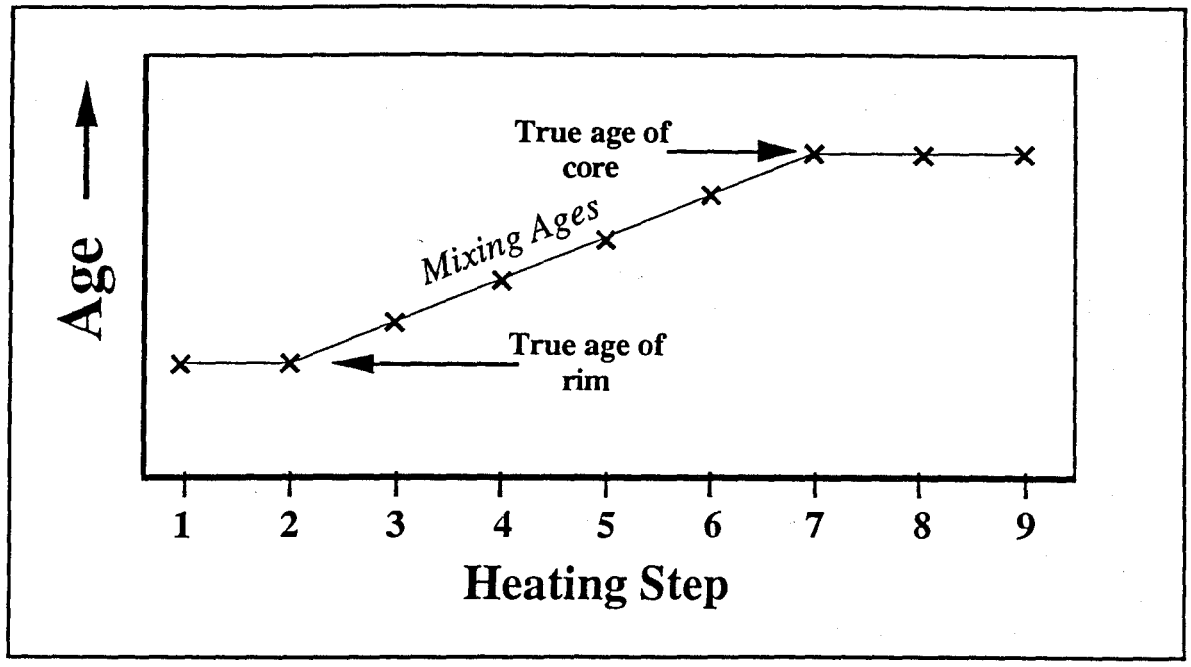

Figure 2.8 A schematic graph of age vs. heating step for the zircon in figure 2.7, illustrating that heating steps 3 to 6 give mixed ages, intermediate between the true ages of the core and rim of the zircon.

2:4.5b Graphical representation of data and determination of ages and errors with the Kober Technique.

Common Pb corrected ages calculated from individual heating steps will give $^{207}Pb^*/^{206}Pb^*$ ages with an internal error of less than one million years (see figure 2.11). However, this "age" may merely represent a point on a mixing line between different age components within the crystal. Therefore, a system of filtering the data to find these endpoints is required.

There are three main variables that determine the reliability of the data produced by the Kober technique. The first of these is the reproducibility of the data, and this is the basis of age calculation and graphical representation of data used by Kober, who determined the age of the sample from frequency histograms of sets of $^{207}Pb^*/^{206}Pb^*$ ratios where the corresponding $^{206}Pb/^{204}Pb$ ratio is greater than 5,000. In this case, the most frequently occurring age is regarded as the true age of the sample. The second variable is the precision of the analysis, related to beam intensity, a good indicator of which is the one standard error on the $^{207}Pb/^{206}Pb$ ratio for each given set of 10 ratios. However,

the fact that a beam is intense, and producing data with small errors, is no guarantee that the $^{207}Pb^*/^{206}Pb^*$ ratio recorded is not a mixed age between two components of the zircon crystal. The third variable is the "purity" of the zircon analysed, recorded by the $^{206}Pb/^{204}Pb$ ratio. Usually in a Kober analysis, data from heating steps which give a $^{206}Pb/^{204}Pb$ ratio above 5,000 are regarded as coming from "pure" zircon, and are used with equal weighting in the construction of frequency histograms. However, $^{206}Pb/^{204}Pb$ ratios in zircons may exceed 100,000, and simply declaring that above a cut-off value zircon is deemed to be "pure" ignores the fact that some phases of zircon are demonstrably purer than others, and the possible reasons for this.

Zoned crystals will obviously contain contacts between crystal domains of different ages, and the disruption to the crystal lattice in these contact regions means that they are capable of holding more common lead than the lattice of unzoned, single-phase crystals, which contain very low concentrations of common lead. Heating steps which contain Pb from more than one crystal domain will therefore tend to have lower $^{206}Pb/^{204}Pb$ ratios than those from a single domain.

It is therefore proposed that the accuracy of the dating of a sample may be improved by the use of a *reliability index*. The reliability index proposed in this study divides the $^{206}Pb/^{204}Pb$ ratio (a measure of the "purity" of the zircon) by 1 standard error in the $^{207}Pb/^{206}Pb$ ratio (a measure of the precision of the analysis)

$$\textbf{Reliability Index} = \frac{\left(\frac{^{206}Pb}{^{204}Pb}\right)}{1 \text{ std error in } \left(\frac{^{207}Pb}{^{206}Pb}\right)} \quad \text{calculated for each heating step}$$

Common Pb corrected ages and reliability indices are calculated for each heating step. For an ideal single-stage population of zircons, this produces a single, well defined peak on a graph of reliability index vs age (figure 2.9). The

age of the sample is then calculated as a weighted average using the equation below:

$$\text{Weighted Average Age} = \frac{\Sigma(\text{Age x Index})}{\Sigma(\text{Index})}$$ for all the heating intervals.

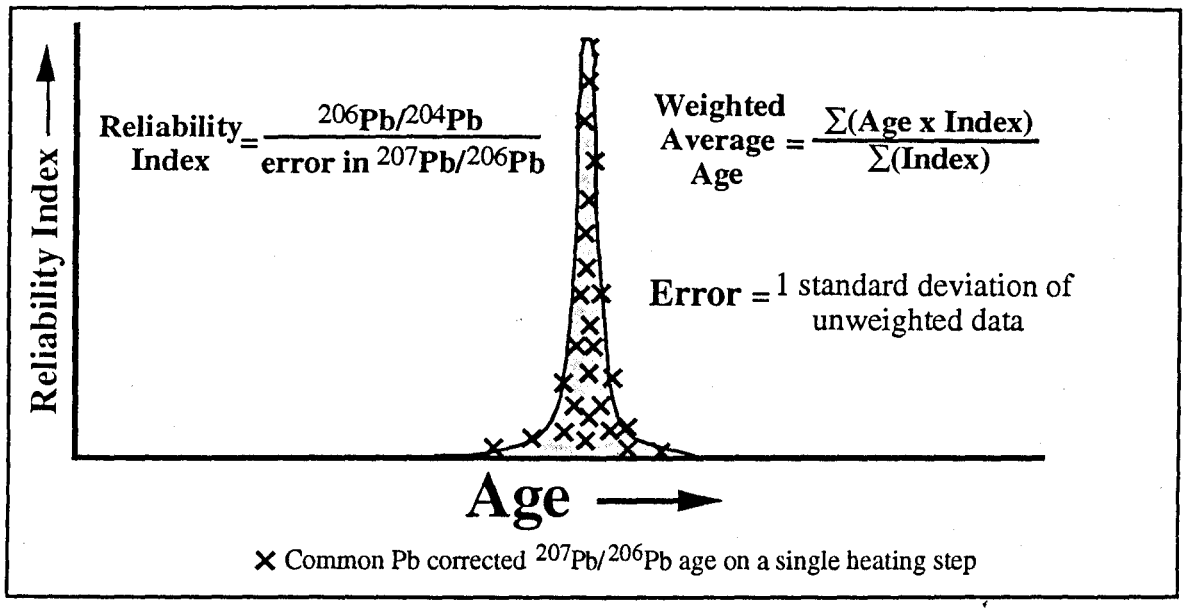

Figure 2.9 A graph of reliability index vs. $^{207}Pb/^{206}Pb$ age for an idealised single-age population of zircons.

The error on the weighted average age is then determined by taking 1 standard deviation of the *unweighted* data, as taking a standard deviation on the weighted data would effectively be increasing the number of analyses upon which a standard deviation is calculated, which is not justifiable.

For zircons with a two stage history, such as those in figure 2.7 and 2.8, two peaks are generated on a graph of reliability index vs age, one at the date of crystallisation of the core of the zircon, and one at the date of crystallisation of the rim (figure 2.10). Intermediate mixed ages between these two peaks contain larger amounts of common lead, and thus have lower values of the reliability index. Note that the peaks are skewed towards the age of the other component that they are mixed with. However, although figure 2.10a allows easier visual interpretation of the data than the frequency graph used by Kober (figure

2.10b), the curve drawn over the data is just a freehand sketch, with no statistical significance. The reliability index is therefore used to "weight" the age frequency data such that the heating steps which resulted in the high reliability points in figure 2.10a, which each have a reliability index of 6, are counted as six points each, and so on. By summing the reliability indexes of all the points (heating steps) within each age interval, a weighted frequency graph may be constructed. Figure 2.10c is a weighted frequency graph of the same information displayed in figures 2.10a and 2.10b. The weighted frequency graph has advantages over both the frequency graph (figure 2.10b), in that it allows easier visual interpretation of the data; and over the reliability index graph, in that the graphical representation of the data is statistically valid. As the three graphs each have some useful attributes, data presented in this thesis will be generally displayed in all three graphs.

The exact determination of ages and errors from multi-stage zircons is a far more complex statistical problem than for single stage populations, especially if the data set is limited. Simply taking the age of the highest reliability analysis ignores the possibility that this point may be erroneous - either a mixed age with an unusually low common Pb content, or with an anomalous isotopic composition due to initial disequilibrium of the decay sequence. Therefore, if a high reliability point is to be taken as the crystallisation age, it must be supported by a clustering of lower reliability data, preferably derived from several zircons.

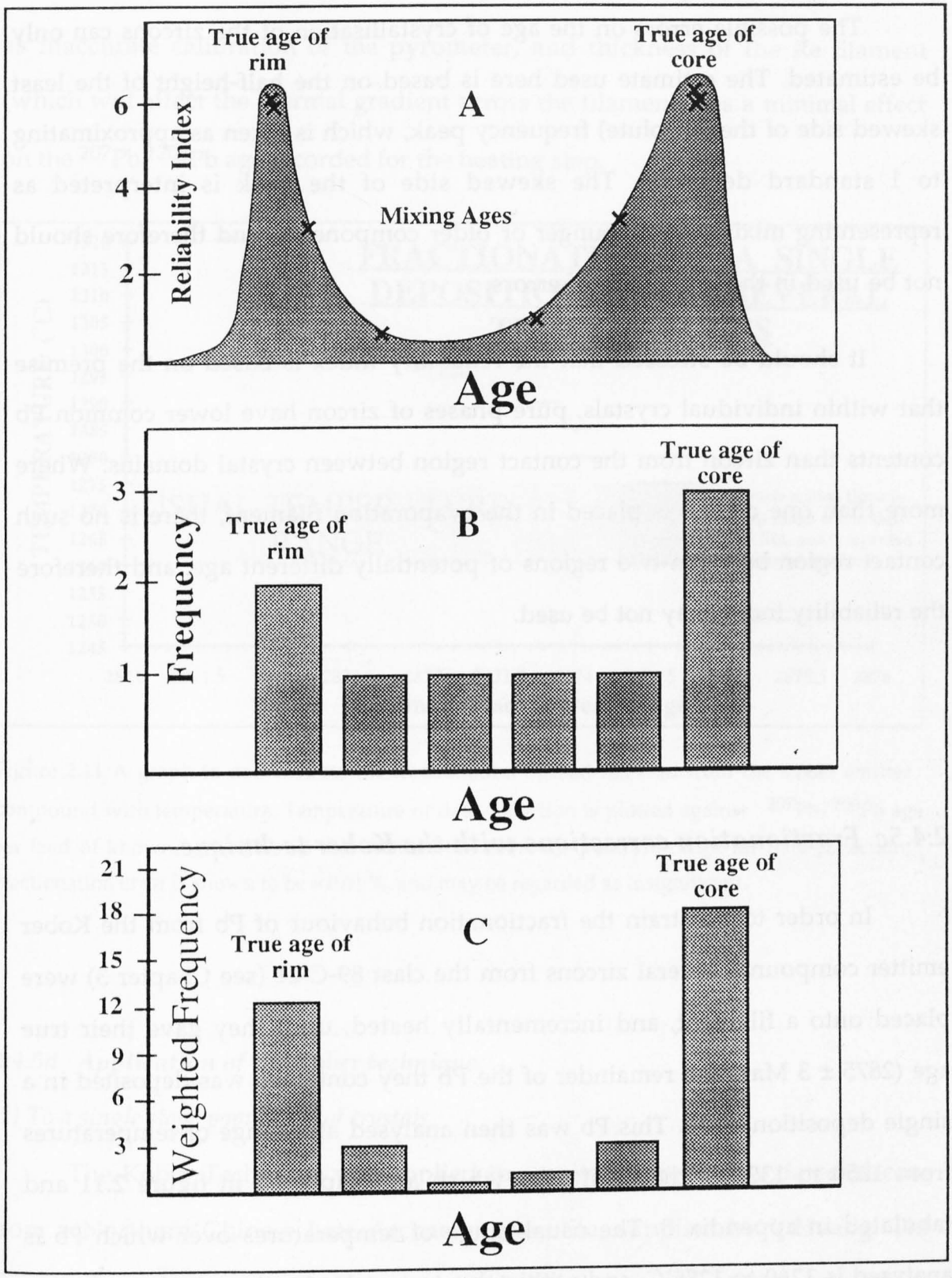

Figure 2.10 Three graphs representing idealised data from the 9 heating steps in figures 2.7 and 2.8. **2.10a.** Age vs. reliability index scatter graph. **2.10b.** Frequency (within an age interval) vs age interval histogram. **2.10c.** Weighted frequency within age interval vs age interval histogram. The weighted frequency is calculated by summing the reliability indices within each age interval from figure 2.10b.

The possible errors on the age of crystallisation of the zircons can only be estimated. The estimate used here is based on the half-height of the least skewed side of the (absolute) frequency peak, which is taken as approximating to 1 standard deviation. The skewed side of the peak is interpreted as representing mixing with younger or older components, and therefore should not be used in the estimation of errors.

It should be stressed that the reliability index is based on the premise that within individual crystals, pure phases of zircon have lower common Pb contents than zircon from the contact region between crystal domains. Where more than one crystal is placed in the evaporation filament, there is no such contact region between two regions of potentially different age, and therefore the reliability index may not be used.

2:4.5c Fractionation corrections with the Kober technique.

In order to constrain the fractionation behaviour of Pb from the Kober emitter compound, several zircons from the clast 89-C-21 (see Chapter 3) were placed onto a filament, and incrementally heated, until they gave their true age (2875 ± 3 Ma). The remainder of the Pb they contained was deposited in a single deposition cycle. This Pb was then analysed at a range of temperatures from 1250 to 1320°C, the results for which are displayed in figure 2.11 and tabulated in appendix B. The usual range of temperatures over which Pb is analysed is 1260 to 1275°C, and within this range, the fractionation error is less than 0.01%, and may therefore be regarded as insignificant. Although this argument is circular, in that the age of the clast was originally determined by the Kober technique, this experiment demonstrates that the temperature at which Pb from a heating step is analysed, which may vary due to effects such

as inaccurate calibration of the pyrometer, and thickness of the Re filament (which will affect the thermal gradient across the filament) has a minimal effect on the $^{207}Pb/^{206}Pb$ age recorded for the heating step.

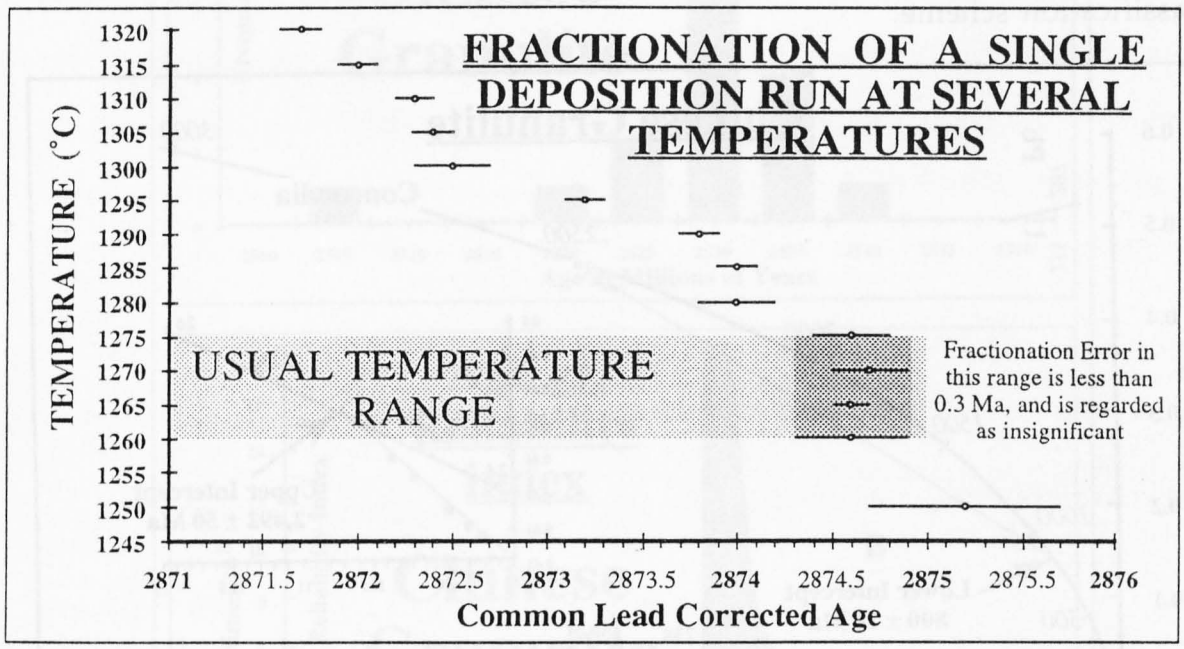

Figure 2.11 A graph to demonstrate the fractionation of lead released from the Kober emitter compound with temperature. Temperature of data collection is plotted against $^{207}Pb/^{206}Pb$ age for lead of known age (2875 ± 3 Ma). Within the usual temperature range for data collection, fractionation error is shown to be ≈ 0.01 %, and may be regarded as insignificant.

2:4.5*d* *Application of the Kober technique*

(1) To a single stage population of crystals

The Kober Technique was applied to a suite of previously dated zircons from a Northern Chinese Late Archaean granulite, supplied by Y.Huang. The sample, (sample number 8336), had yielded slightly discordant zircons, with an upper intercept to the discordia of 2492 ± 50 Ma, and a lower intercept of 800 ± 16 Ma (figure 2.12). Internal errors on the analyses were in the order of ± 1% (Y.Huang, pers. comm.). The zircons had been air-abraded, sieved into size fractions, and then into magnetic fractions, using a Frantz isodynamic

magnetic separator. For this study, the largest, least magnetic fraction (0.22-0.17 mm, Frantz at an inclination of 15° and a pitch of 1°) was selected as being the easiest to handle. Air abrasion had obscured the crystal typology of the zircons, but they appeared to be rounded, high S-number types on the Pupin (1980) classification scheme.

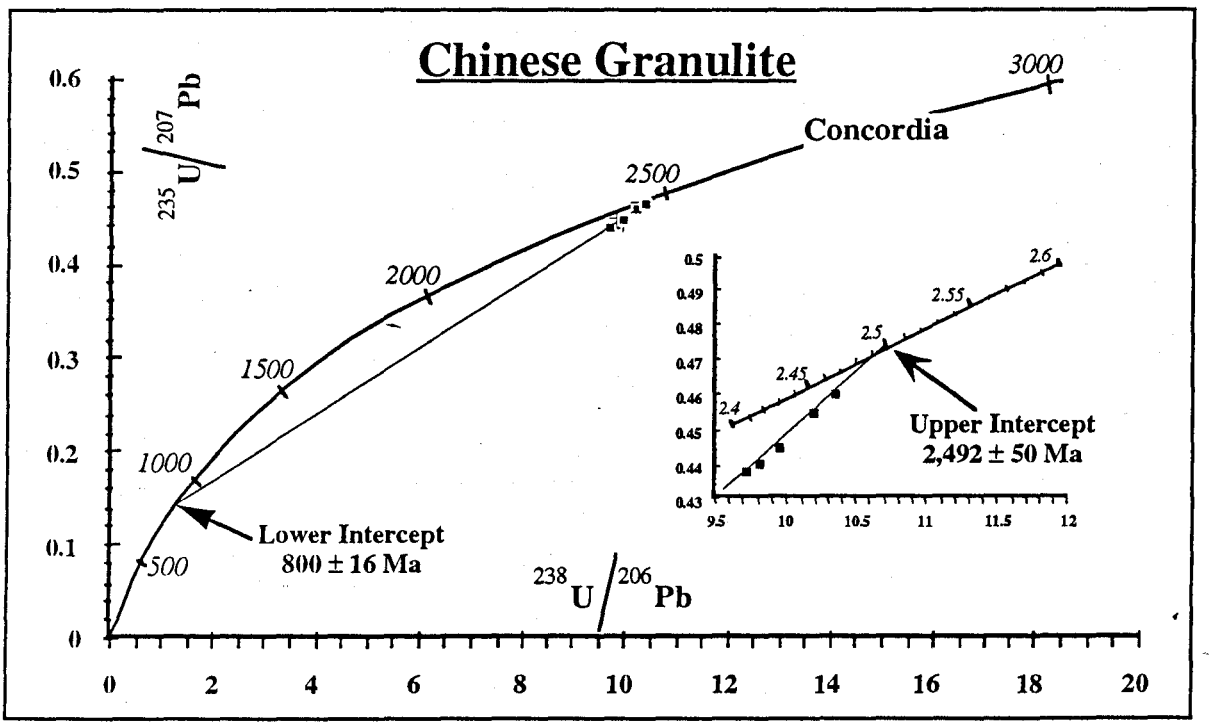

Figure 2.12 U-Pb concordia diagram for zircons from a Chinese granulite (data supplied by Y. Huang, pers. comm)

Seven clear, inclusion free crystals, dark violet in colour, were selected and loaded onto Re filaments (six in February of 1993, one in October of 1993). They were then analysed in a Finnigan MAT 261, by the step heating method described in section 2:4.5a. Common Pb corrected ages and reliability indices were calculated for each heating step, according to the equations previously described in this chapter. Common lead corrections were made according to the equation in section 2:3.4, using a common Pb composition of 2,500 Ma, determined from the Stacey and Kramers 2-stage curve.

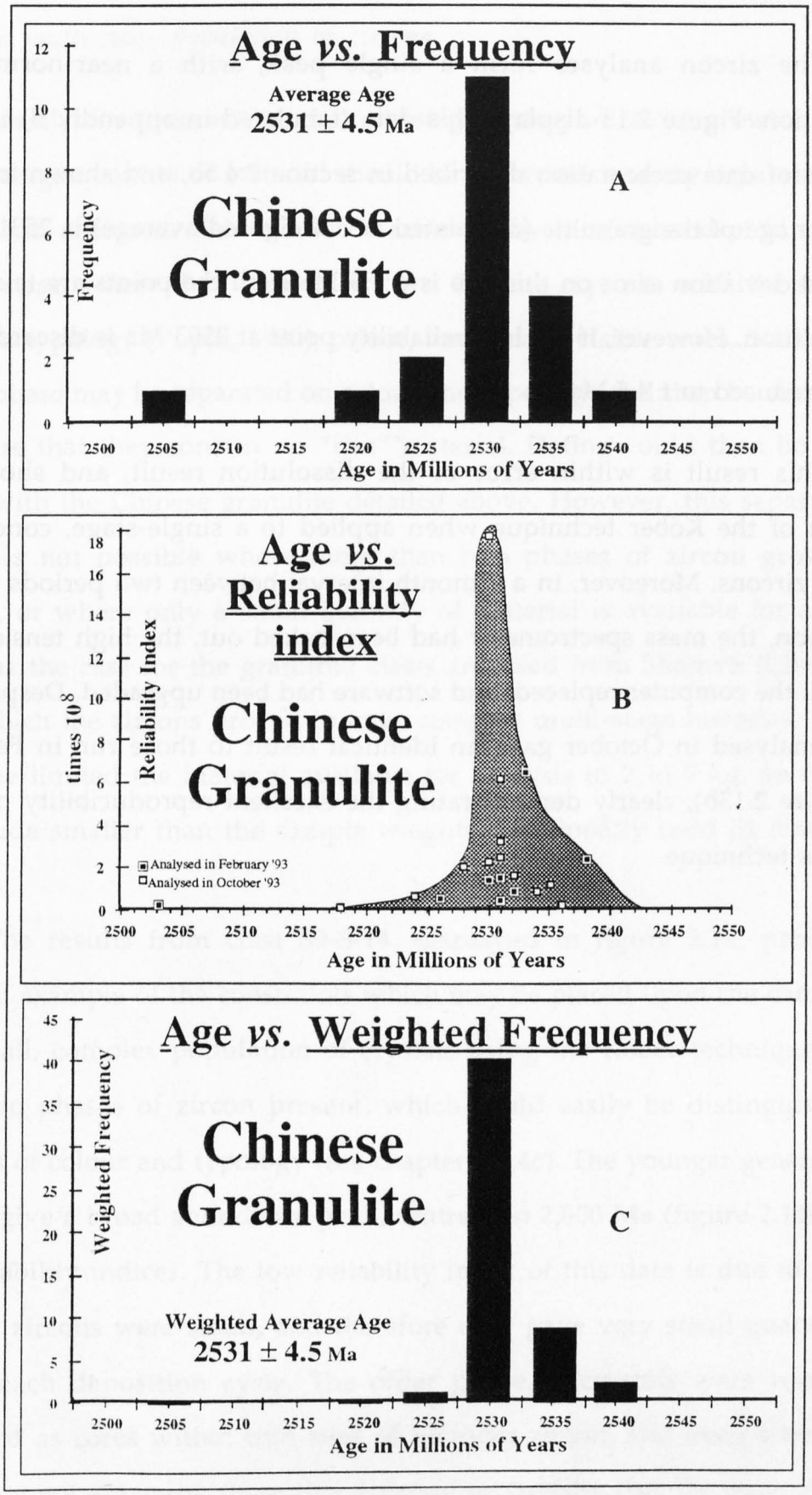

Figure 2.13. Data for zircons from a Late Archaean Chinese granulite, displayed in the three methods of data presentation used in figure 2.10. **2.13a.** Age vs frequency histogram; **2.13b.** Age vs reliability of data scatter graph; and **2.13c.** Age vs weighted reliability histogram.

The zircon analyses form a single peak, with a near-normal age distribution. Figure 2.13 displays this data (tabulated in appendix B) in the 3 methods of data presentation described in section 2:4.5b, and shown in figure 2.10. The age of the granulite (calculated as a weighted average) is 2531. The 1 standard deviation error on this age is ± 7.5 Ma if all the points are taken into consideration. However, if the low reliability point at 2503 Ma is discarded, the error is reduced to ± 4.5 Ma.

This result is within error of the dissolution result, and shows the strength of the Kober technique when applied to a single-stage, concordant suite of zircons. Moreover, in a 7 month interval between two periods of data acquisition, the mass spectrometer had been baked out, the high tension unit changed, the computer replaced, and software had been upgraded. Despite this, zircon analysed in October gave an identical result to those run in February (see figure 2.13b), clearly demonstrating the excellent reproducibility possible with this technique.

(2) To a multi-stage population of zircons

Ideally, for rocks with a multiple-stage history of zircon growth, a larger than average quantity of material should be separated, and the separate phases picked and analysed. This would be achieved by careful hand-picking of the "rim" phase, where they form their own discrete crystals, with the selection based on typology (Pupin, 1980), colour, and lack of visible cores. Similarly the "core" phase may be separated on colour and typology, and then be air abraded to ensure that they contain no "rim" material. Dating could then be carried out as with the Chinese granulite detailed above. However, this separation of phases is not possible where more than two phases of zircon growth are present, or where only a small quantity of material is available for analysis. This was the case for the granitoid clasts analysed from Shamva (Chapter 3), from which the zircons proved to have complex multi-stage histories, and the clast size limited the material available for analysis to 2 to 5 kg, an order of magnitude smaller than the sample weights traditionally used in dissolution analysis.

The results from clast 89-S-14, displayed in figure 2.14, provide an excellent example of the constraints which may be placed upon the chronology of a small, complex population of crystals using the Kober technique. There were two phases of zircon present, which could easily be distinguished on grounds of colour and typology (see chapter 3:2.4c). The younger generation of zircons give a broad abundance peak, centred on 2,800 Ma (figure 2.14b), with low reliability indices. The low reliability index of this data is due to the fact that the zircons were small, and therefore only gave very small quantities of Pb for each deposition cycle. The older phase of crystals were commonly contained as cores within thin rims of younger zircon, and even where such rims were not apparent, there was a strong probability that the outer portions of the grains would have had their U-Pb systematics at least partly re-set at the

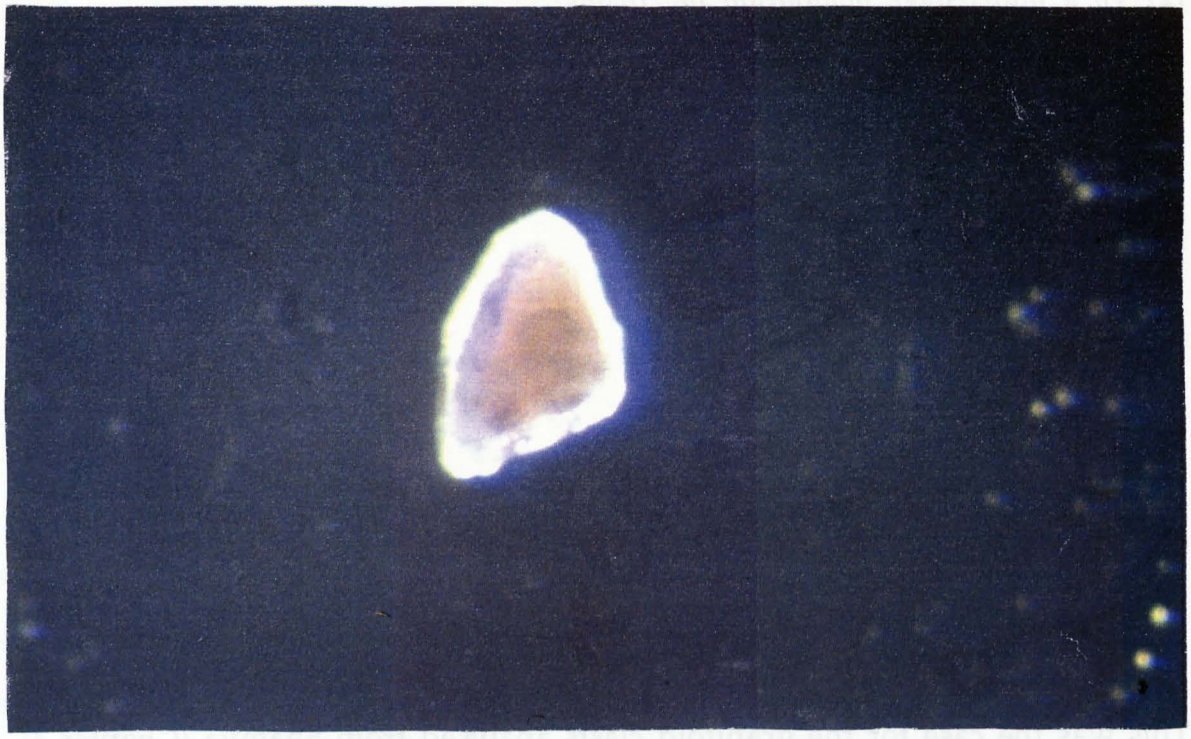

Photograph 2.2 Half of a large red zircon crystal from 89-S-14 (length of crystal ≈ 0.3 mm), showing a complex crystal habit indicative of formation at high temperatures (see figure 2.1).

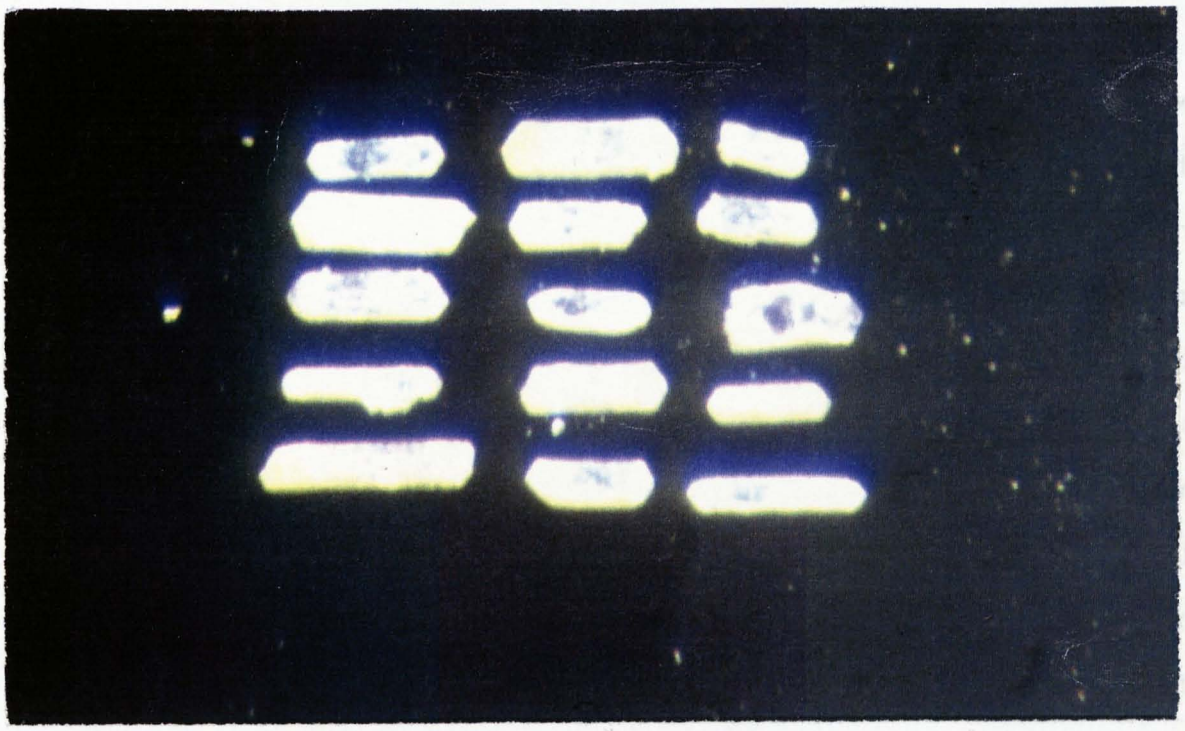

Photograph 2.3 White zircon crystals from 89-S-14, showing simple prismatic crystal forms indicative of formation a low temperatures (see figure 2.1). Same magnification as above.

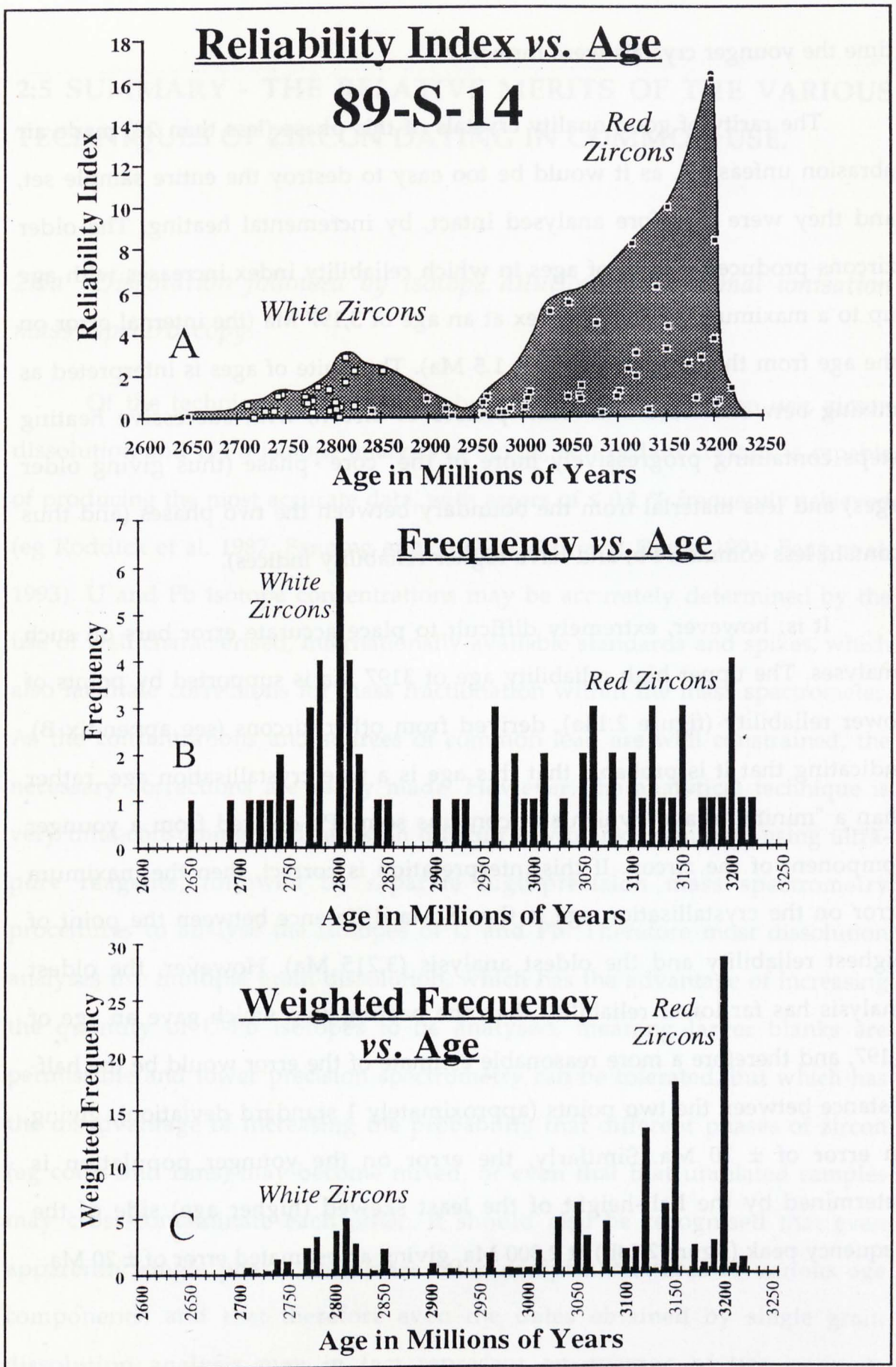

Figure 2.14 Data for zircons from a Late Archaean Tonalite clast from Zimbabwe, displayed in the three methods of data presentation used in figure 2.10. 2.14a. Age vs frequency histogram; 2.14b. Age vs reliability of data scatter graph; and 2.14c Age vs weighted reliability histogram.

time the younger crystals were formed.

The rarity of good quality crystals of this phase (less than 20) made air abrasion unfeasible, as it would be too easy to destroy the entire sample set, and they were therefore analysed intact, by incremental heating. The older zircons produced a suite of ages in which reliability index increases with age up to a maximum reliability index at an age of 3,197 Ma (the internal error on the age from this heating step is ± 1.5 Ma). This suite of ages is interpreted as mixing between "core and "rim" phases of zircon, with successive heating steps containing progressively more of the "core" phase (thus giving older ages) and less material from the boundary between the two phases (and thus contain less common Pb, and have higher reliability indices).

It is, however, extremely difficult to place accurate error bars on such analyses. The upper high reliability age of 3197 Ma is supported by points of lower reliability (figure 2.14a), derived from other zircons (see appendix B), indicating that it is probable that this age is a true crystallisation age, rather than a "minimum age" which still contains some Pb derived from a younger component of the zircon. If this interpretation is correct, then the maximum error on the crystallisation age is the 18 Ma difference between the point of highest reliability and the oldest analysis (3,215 Ma). However, the oldest analysis has far lower reliability than the heating step which gave an age of 3,197, and therefore a more reasonable estimate of the error would be the half-distance between the two points (approximately 1 standard deviation), giving an error of ± 10 Ma. Similarly, the error on the younger population is determined by the half-height of the least skewed (higher age) side of the frequency peak (figure 2.14b) at 2,800 Ma, giving an estimated error of ± 20 Ma.

2:5 SUMMARY - THE RELATIVE MERITS OF THE VARIOUS TECHNIQUES OF ZIRCON DATING IN COMMON USE.

2:5a Dissolution followed by isotope dilution and thermal ionisation mass spectroscopy.

Of the techniques of zircon analysis currently in common use, zircon dissolution and U-Pb isotope analysis of single, concordant crystals is capable of producing the most accurate data, with errors of ≤ 0.1 % frequently achieved (eg Roddick et al. 1987; Fanning et al. 1990; Corfu and Davis, 1991; Feng et al. 1993). U and Pb isotope concentrations may be accurately determined by the use of well characterised, internationally available standards and spikes, which also facilitate corrections for mass fractionation within the mass spectrometer. As the concentrations and sources of common lead are well constrained, the necessary corrections are easily made. However, the analytical technique is very time consuming, and relies on difficult low blank chemistry, using ultra-pure reagents, followed by separate high-precision mass spectrometry procedures to analyse the isotopes of U and Pb. Therefore most dissolution analyses use multiple grain dissolution, which has the advantage of increasing the quantity of U-Pb isotopes to be analysed, meaning larger blanks are permissible and lower precision spectrometry can be tolerated, but which has the disadvantage of increasing the probability that different phases of zircon (eg cores and rims) may become mixed, or even that that unrelated samples may cross-contaminate each other. It should also be recognised that even apparently single phase zircons are often complex mixtures of various age components, and that therefore even the dates obtained by single grain dissolution analysis may in fact represent an average of two or more components.

2:5b *The Sensitive High Resolution Ion MicroProbe (SHRIMP)*

SHRIMP analyses a 20 - 30 μm pit within a zircon crystal, allowing individual crystal domains to be carefully targeted, thus avoiding the problem of averaging the isotopic compositions of complex zircons. Studies of zircons with multi-phase histories may be carried out, and SHRIMP has made an invaluable contribution to the study of ancient provinces with complex histories (eg Froude et al. 1983; Black et al. 1986; Bowring et al. 1989). The precision of data produced from a single pit is ≈ ± 1% (Compston et al. 1984), considerably poorer than the 0.1% precision possible on individual dissolution analyses. However, the accuracy of the date may be improved by repeated analysis of individual zircons, and by this method, dates with an accuracy of ≤ ± 0.1% have been achieved, for instance the dating of the Acasta Gneisses at 3,962 ± 3 Ma (Bowring et al. 1989).

Therefore while conventional zircon dating is capable of providing more accurate dates on zircons with single stage histories, SHRIMP is able to constrain complex crystallisation histories with more accuracy than the dissolution technique, which may only be able to provide a minimum ($^{207}Pb/^{206}Pb$) age for the sample (see section 2:4.3). Again, the Acasta gneisses provides an example of this, as conventional U-Pb dating was only capable of constraining the minimum age of the intrusion of the protolith of the gneiss as 3,842 Ma, 120 Ma younger than the SHRIMP date on zircon cores (Bowring et al. 1989).

As SHRIMP analyses cannot be "spiked", element concentrations must be determined using an empirical calibration curve calculated by analysis of zircon standards, and therefore depend on the reproducibility of data from these standard zircons. As has been discussed in sections 2:2.3 and 2:2.4, individual zircon crystals are often heterogeneous, and as yet no zircons are in

use as international standards, so SHRIMP data may not be easily corroborated by other laboratories.

The practice of SHRIMP users to perform common Pb corrections using common Pb with a composition of the age of the sample, rather than the composition of modern common Pb, has also led to some debate over the errors usually quoted by SHRIMP (section 2:4.3). However, despite these concerns, the main problem with SHRIMP analysis is that there is currently only one operational machine, on which machine time is both of limited availability and expensive.

2:5c Pb-Pb dating by direct thermal ionisation of zircons (The Kober Technique).

The Kober technique is capable of providing high-resolution analyses on zircons with a single-stage crystallisation history, with errors close to ± 0.1% - for example are dating of a felsite within the Onverwacht Group of the Barberton Greenstone belt at 3,438 ± 6 Ma (Kröner and Todt, 1988). However, the errors on crystallisation dates of phases within zircons of complex history are difficult to assess (section 2:4.5b). The Kober technique provides only Pb isotope ratios, basing the analysis on the premise that above a certain temperature, Pb emitted by the thermal decomposition of zircon is derived from concordant zircon. The lack of U-Pb isotope ratios means that effects such as initial disequilibrium and reverse discordance may lead to incorrect interpretation of the data, as these effects may only be recognised by unusual degrees of scatter in the age data from analyses with low $^{206}Pb/^{204}Pb$ ratios, or anomalous $^{208}Pb/^{206}Pb$ ratios. However, the Kober technique has several advantages, including: the minimal sample preparation involved; the absence of a laboratory-induced blank; and the fact that the technique produces

sequential analyses through single grains of zircon, which is invaluable in the study of small populations of zircons with complex, multi-stage histories.

Once a zircon separate has been prepared, an analysis by the dissolution technique requires an average of 11 days of sample preparation, breaking down as follows: 2 days bomb cleaning: 1 day to weigh and spike each sample; one week for dissolution; 1 day of column chemistry and finally five minutes per sample to load onto filaments. By contrast, the time taken for the preparation of the samples using the Kober technique is just five minutes per sample to load them onto the filaments, so the advantage in speed that this technique has over the conventional dissolution technique is evident.

The accuracy of the Kober technique compared with conventional dissolution techniques has been confirmed in this study by the correspondence of the dissolution and Kober technique results on a Chinese Granulite (2:4:5d), and the error obtained on this analysis of ± 0.1% confirms that the Kober technique is capable of precisions equal to the best dissolution analyses on single stage zircons. Also, as the Kober technique produces incremental analyses on single zircon grains, zircon cores and "stray" contaminant zircons may be more easily recognised, and the data disregarded in the calculation of the crystallisation age of the main phase of zircon under consideration. Multi-grain dissolution on the same zircons would be unable to perform such corrections.

The relative speed and ease of the Kober technique makes it ideal for studies investigating old detrital zircons of low abundance. Kober et al. (1989) studied 42 zircons from a quartzite from the Jack Hills, Australia, and were able to confirm the presence of zircons up to 4.17 Ga old, which had previously been dated by SHRIMP (Compston and Pidgeon 1986), also confirming the accuracy of the Kober method compared with SHRIMP. The correspondence of SHRIMP and Kober technique dating on the same samples was also

demonstrated by Compston and Kröner (1988), who recorded ages within error of each other of 3,644 ± 4 Ma (SHRIMP) and 3,622 ± 23 Ma (Kober technique) on a sample from the Ancient Gneiss complex of Swaziland. Although the Kober technique produces results comparable with SHRIMP or dissolution where zircons have simple histories, or large quantities of separates are available, SHRIMP dating is superior to the Kober technique in dating small populations of zircons with extremely complex histories, as the availability of U/Pb isotope ratios allows clear distinction of minimum ages and true ages, and the accurate calculation of errors.

As the Kober technique determines the age of a sample purely by $^{207}Pb^*/^{206}Pb^*$ ratios, the most accurate ages are determined on Archaean zircons, as these have had plenty of time to accumulate Pb. The dating of young zircons (younger than 100 Ma) by the Kober technique is difficult, as such material has had little time to accumulate radiogenic Pb. The crystals which are capable of providing the largest numbers of $^{207}Pb^*/^{206}Pb^*$ ratios within such young material are the crystals which had the highest initial U contents. Unfortunately, these crystals are also the most likely to be metamict, and to show incorrect ages due to initial disequilibrium in the decay chains.

A possible solution to this problem is measurement of the $^{210}Pb^*/^{206}Pb^*$. ^{210}Pb is produced by the decay of ^{238}U, and obviously has the same ionisation rate as ^{206}Pb. Therefore the $^{210}Pb^*/^{206}Pb^*$ may be used to calculate the $^{238}U/^{206}Pb$ ratio, and as the evolution of terrestrial $^{238}U/^{235}U$ is known, then the $^{235}U/^{207}Pb$ ratio may also be calculated. However, the short half life of the ^{210}Pb (22.3 years) results in extremely low ^{210}Pb concentrations, and therefore very low $^{210}Pb^*/^{206}Pb^*$ ratios, of around one part of ^{210}Pb in 200 million of ^{206}Pb. Wendt et al. (1992 & 1993b) have succeeded in measuring $^{210}Pb^*/^{206}Pb^*$ ratios from zircon, with Pb extracted from large quantities of zircon (7-15 mg) by the dissolution technique. However, the errors on the $^{210}Pb/^{206}Pb$ ratios are large, (1 to 7%), and compare poorly with conventional

dating techniques. Therefore, a combination of the Kober technique and ^{210}Pb measurement is beyond the resolution of present mass spectrometry. However, further research could produce a very powerful technique which combines the advantages of both the Kober and dissolution techniques of zircon analysis.

Chapter Three

Chemistry and Geochronology of the Early Continental Crust of Northern Zimbabwe

3:1 INTRODUCTION

The Shamvaian is a sequence of greywackes and conglomerates which unconformably overlie the Western succession of Upper Bulawayan Greenstones (see Chapter 1). U-Pb zircon dating of syn-depositional dykes and sills within the Shamvaian sediments at the type locality by Jelsma (1993) has determined the age of deposition to be 2672 ± 12 Ma, within error of the Wedza (2667± 4 Ma, Jelsma, 1993) suite of syn- to post-tectonic tonalites. Tectonism at the time of the intrusion of these tonalites re-worked the pre-existing continental crust of Northern Zimbabwe to the extent that the only in-situ remnants of material older than the Upper Bulawayan are rare, strongly migmatised gneisses, such as the Umwindsi Gneiss within the Chinamora Batholith. Clearly, the intense metamorphism these rocks were subjected to in the late Archaean makes interpretation of the chemistry, geochronology and extent of the early crust of Northern Zimbabwe exceedingly difficult. However, the Shamvaian sediments contain coarse conglomeratic horizons, derived from the Upper Bulawayan land surface at 2.67 Ga. Granitoid clasts contained in these horizons only underwent low (greenschist) grades of metamorphism, and they preserve a unique record of the pre-Upper Bulawayan crust of Northern Zimbabwe. These clasts therefore provide insights into the chemistry, longevity and rate of formation of an Archaean proto-continent, prior to its stabilisation in the Late Archaean.

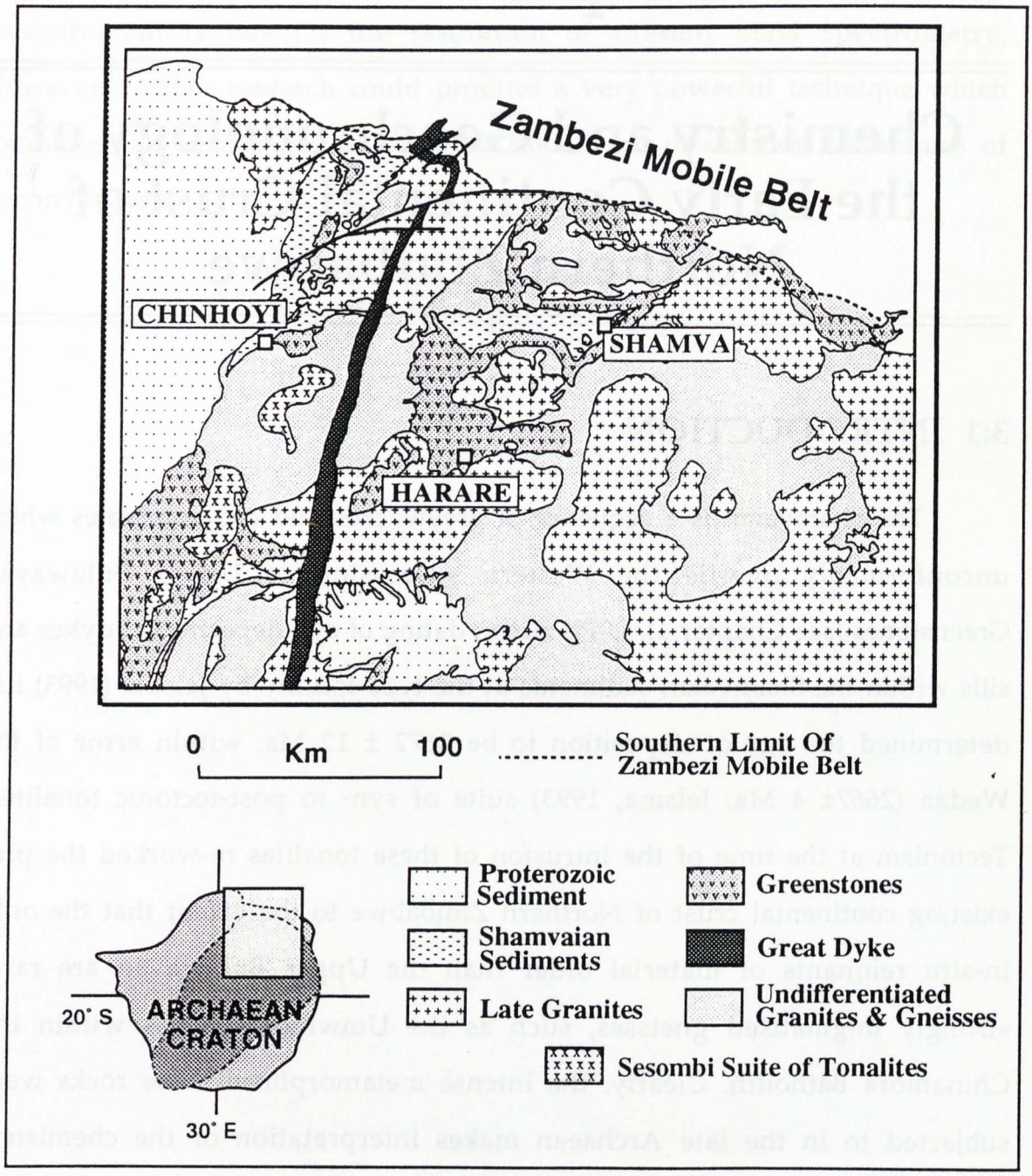

Figure 3.1 Geological sketch map of Northern Zimbabwe, showing the major geological divisions and the two clast sample localities, one at the Shamva type locality, on the Mazowe river near Shamva, and the other on the north-western margin of the craton, at Chinhoyi

3:2 LOCALITY 1 - SHAMVA

This locality is in the bed of the Mazowe River, on the Tipperary estate near the town of Shamva (figure 3.2). A sharp bend in the river marks the contact between pillowed basaltic lavas of the Panmure formation, and the overlying Shamvaian sediments. Here, the contact is a poorly exposed fault (J.D. Kramers, pers. comm) but elsewhere the contact has been mapped as an unconformity (Stidolph, 1977), which was locally exploited by faulting related to folding of the greenstone belt.

Photograph 3.1 The Shamva sediments (the top of the main conglomeratic unit, where most of the samples were collected) showing conglomeratic horizons with well rounded clasts, interbedded with greywacke horizons. Sledge-hammer for scale.

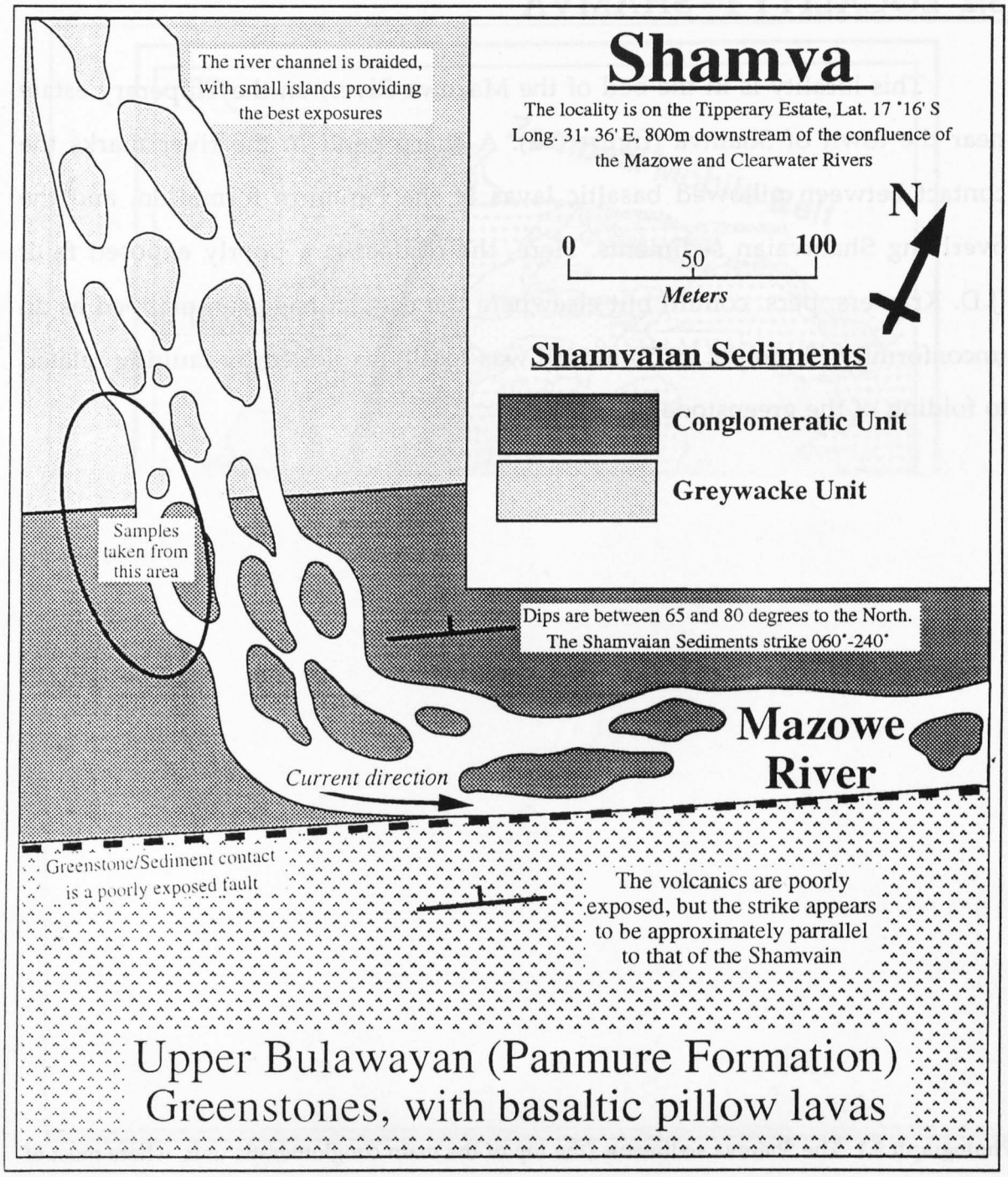

Figure 2. Geological sketch map of the Shamva sampling locality.

3:2.1 The Shamva Sediments.

Both the greenstone belt volcanics and the Shamvaian sediments dip steeply to the north, at an angle of 65° to 80°, striking at 060°. The lowermost unit of the sedimentary sequence consists of clast-supported polymict conglomerates interbedded with coarse greywackes (photograph 3.1). The conglomerate dominated unit is up to 200m thick, and may be traced along strike for a distance of 7 km. Working up-sequence greywackes become dominant, and the conglomerate horizons become progressively thinner, with smaller clasts. The coarse greywackes pass up into progressively finer sediments, in a sequence which has been interpreted as representing the inundation of an alluvial fan or braided delta (Jelsma, 1993) (table 3.1).

Shamvaian Group	Interpretation	Thickness
Graded Unit *Fine to very fine-grained*		Less than 500 m
Turbiditic Unit {AB(CD)E} individual units up to 4m thick *Medium to fine grained*	Turbidites	300-500 m
Horizontally stratified, massive, cross -bedded and trough cross-bedded *medium to coarse grained*	Downslope part of a fan or braided delta	≈ 800 m
Matrix supported Pebble beds, massive and stratified unit *coarse grained*	Flood Deposits	3-400 m
Basal clast supported polymict conglomerate *very coarse grained*	Alluvial fan or braided delta	100-200 m

Table 3.1 Lithostratigraphy of the Shamvaian Group Metasediments at the type locality (after Jelsma, 1993)

The clasts in the basal sequence are well rounded, with an average diameter of 10 to 15 cm, although they range in size from small pebbles to boulders over 50 cm in diameter. The clasts are predominantly medium to coarse grained, unfoliated granitoids, but a wide range of materials are present, including chert, quartzite, feldspar porphyry, vein quartz, mafic greenstone,

banded ironstone, limestone and rare granitic gneiss. The presence of large, well rounded clasts, set within a much finer matrix may indicate that some of the clasts were inherited from an earlier conglomerate (R. Butler, pers. comm). The conglomerate horizons are laterally continuous, with a weak preferred orientation of the clasts along strike. There are, however, no sedimentary structures such as channeling, cross-bedding or clast imbrication which could be used to determine palaeocurrent directions. The conglomeratic horizons are interbedded with horizons of coarse greywackes. Lithologically, the greywackes consist of poorly sorted angular grains of quartz, saussuritised plagioclase and lithic fragments set in a fine grained matrix of quartz, feldspar, carbonate, chlorite and opaques. The unit has undergone lower-amphibolite grade metamorphism, and mafic phases have re-crystallised to produce chlorite, brown biotite and subordinate blue-green sodic amphibole.

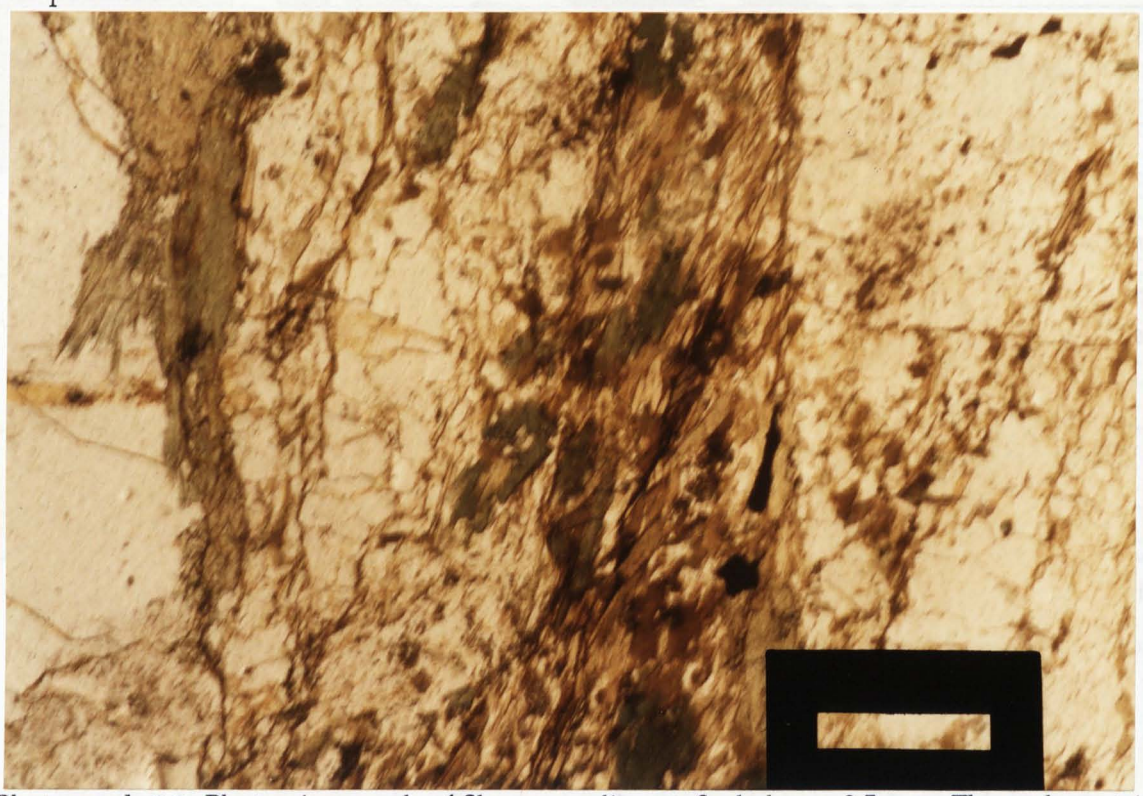

Photograph 3.2 Photomicrograph of Shamva sediment. Scale bar = 0.5 mm. The rock contains the metamorphic minerals biotite, amphibole and chlorite. This specimen (from within a conglomeratic horizon) has undergone shearing, with "major"shears running vertically (eg. to the left of the scale bar) and a subsidiary set of shears running steeply up from left to right.

Quartz grains have undergone dynamic recrystallisation to strained sub-grains, but within the greywacke horizons, planar fabrics and preferred orientation of metamorphic minerals are not developed, indicating a low strain regime. Within the conglomeratic horizons however, tectonic compaction of the sediment was accommodated preferentially by the matrix rather than the clasts, and a foliation defined by biotite and amphibole wraps around the clasts. The higher strain within the conglomerate matrix has also led to localised shearing, with the development of C- and S-fabrics (Lister and Snoke, 1984) defined by biotite and dynamically recrystallised quartz. This shearing indicates that the clasts have rotated during tectonism, and the weak preferred orientation of the clasts along strike is probably a tectonic, rather than sedimentary feature.

Chemistry and Petrography of the Shamva Sediments

Three samples of the greywacke matrix were analysed for major and trace elements. Chemically, (chemical data is tabulated in appendix A) the sediments are notable for their extremely sodic nature, indicated by the presence of sodic metamorphic amphibole (riebeckite). The sediments have very high Na_2O/Al_2O_3 ratios (0.20 to 0.24), well above average values in both Archaean (0.19) and post-Archaean (0.13) sediments. This enrichment of Na_2O is not accompanied by an increase in K_2O, and K_2O/Na_2O ratios in the sediment are lower, at 0.52 to 0.56, than an average Archaean value of 0.76 (average sedimentary compositions from Taylor and McLennan, 1985). The high Na_2O content of the sediments is likely to reflect a large input of material derived from a sodic TTG terrain, samples of which are preserved as granitoid clasts in the conglomeratic horizons (the chemistry of which is discussed in section 3:2.2). The derivation of the Shamvaian sediments from a TTG terrain is supported by the good correlation of average HREE patterns of granitoid clasts from the conglomerate and REE patterns of Shamvaian sediments

(figure 3.3). However, the sediments are less enriched in LREE than the clasts, due to the presence of another component in the sediment. Rare clasts of greenstone in the conglomeratic horizons indicate that this second component could have been derived from the underlying greenstone belt volcanics.

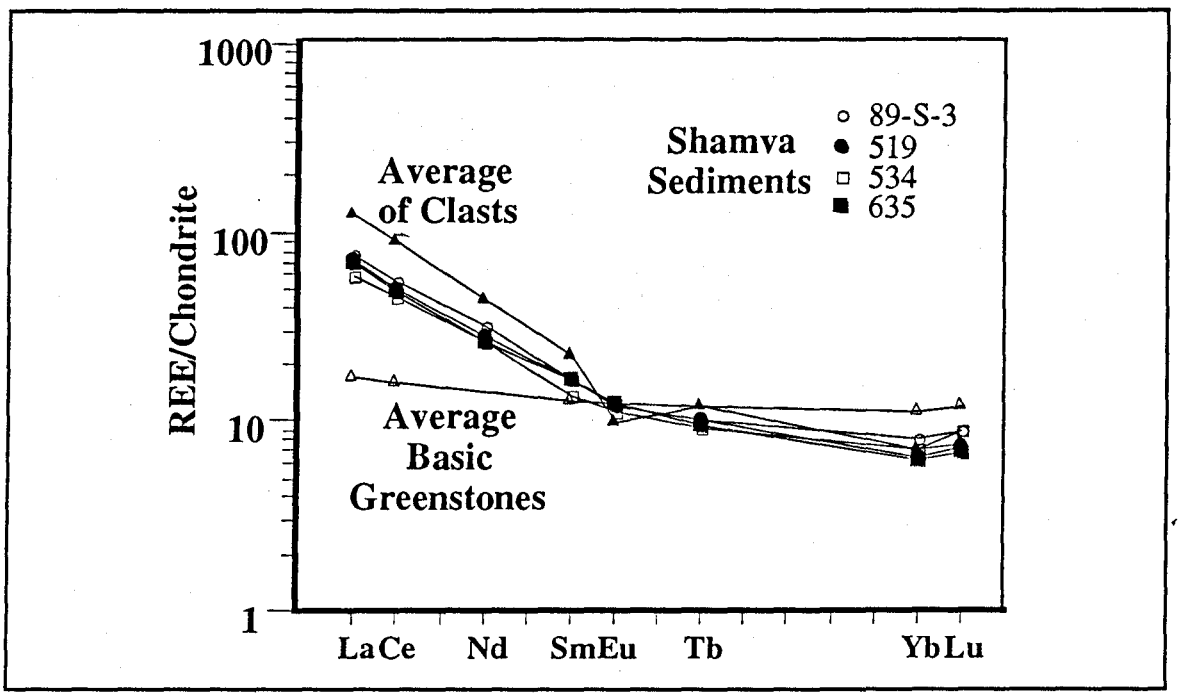

Figure 3.3 Chondrite normalised REE plots of sediments from the Shamva type locality (89-S-3 analysed in this study, data for sample numbers 519, 534, 635 from Jelsma, 1993) compared with an average REE pattern for tonalitic clasts held within the basal conglomerate (this study) and an average REE pattern for basic volcanics from the Harare-Shamva greenstone belt (data from Jelsma, 1993).

Condie and Wronkiewickz (1990) proposed the use of Cr/Th ratios to monitor the source composition of sediments, specifically to investigate changes in the composition of basic volcanics through time. Both elements are immobile in sedimentary systems, and therefore reflect the composition of the sources of the sediment, rather than any sedimentary or weathering processes. Th behaves incompatibly in most igneous systems, but Cr is compatible in mafic minerals (such as pyroxene and spinel) common in the source regions of basic melts, and therefore the Cr content of a basic rock

(excluding the effects of fractionation) is an indicator of the degree of partial melting that a source region underwent in order to produce a basic magma. As the Earth has cooled through time, the average degree of partial melting (and therefore Cr content) involved in the production of basic rocks has decreased, and Condie and Wronkiewickz (1990) tabulated data which shows that the average Cr/Th ratio of sediments has decreased through time, with a sharp drop in the Late Archaean/Early Proterozoic (Figure 3.4). The Cr/Th ratio of the Shamva sediments ranges from 24.3 to 32.2, within the lower limits of the normal range of Cr/Th ratios (25 to 100) for sediments of this age (2.67 Ga) (Figure 3.4).

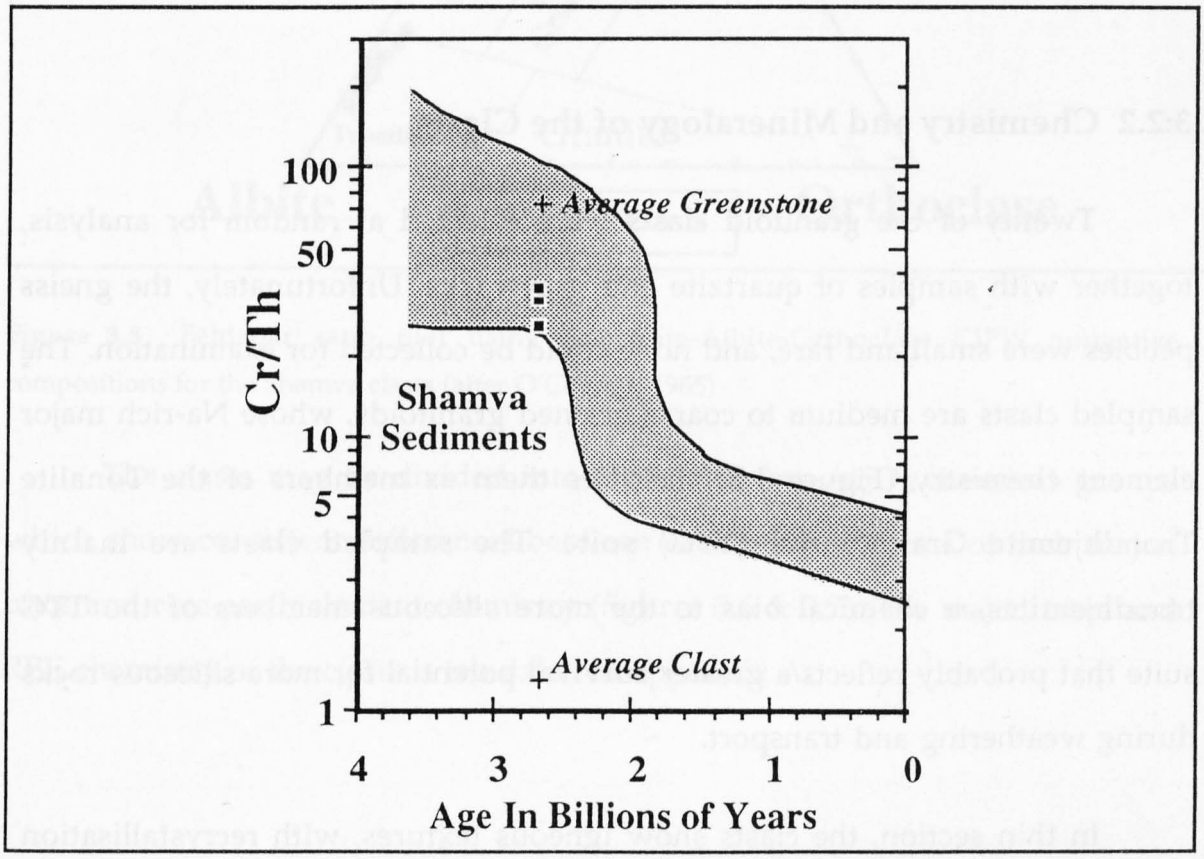

Figure 3.4 Cr/Th vs age diagram (after Condie and Wronkiewickz 1990). The grey field defines the typical range of Cr/Th ratios through time. The Shamva sediments plot in the lower range of this field for their time (2.67 Ga), intermediate between an average Cr/Th ratio for TTG clasts (.21) contained in the basal conglomerate of the Shamvaian and an average greenstone composition (72). This average composition was calculated using data from Jelsma (1993). The average Cr/Th ratio of felsic greenstone belt volcanics is 35.3, and the average Cr/Th ratio of mafic greenstone belt volcanics is 88.7. The ratio for felsic to mafic greenstones exposed at present is 1:2.2, and mixing these two components in this ratio gives the average value of 72. Simple lever rule mixing calculations suggest that the composition of the sediment is consistent with it being made up of a mixture of material derived from the TTG terrain in a range of ratios from approximately 1:1 to 2:1 (TTG: greenstone ratio).

The average Cr/Th ratio of Upper Bulawayan greenstone volcanics from the Harare-Shamva area is 72 (calculated using the average compositions of felsic and mafic volcanics, mixed in their present day relative proportions, using data given in Jelsma, 1993), and the average Cr/Th ratio of the Shamva clasts is 0.21. Simple lever rule mixing calculations suggest that the composition of the sediment is consistent with it being made up of a mixture of material derived from the TTG terrain that supplied the clasts, and a greenstone terrain in a range of ratios from approximately 1:1 to 2:1 (TTG:greenstone ratio), this range reflecting the poor homogenisation common in immature sediments.

3:2.2 Chemistry and Mineralogy of the Clasts

Twenty of the granitoid clasts were selected at random for analysis, together with samples of quartzite and greywacke. Unfortunately, the gneiss pebbles were small and rare, and none could be collected for examination. The sampled clasts are medium to coarse-grained granitoids, whose Na-rich major element chemistry (Figure 3.5) classifies them as members of the Tonalite Trondhjemite Granodiorite (TTG) suite. The sampled clasts are mainly trondhjemites, a chemical bias to the more siliceous members of the TTG suite that probably reflects a greater survival potential for more siliceous rocks during weathering and transport.

In thin section, the clasts show igneous textures, with recrystallisation of quartz to strained granular sub-domains as the only indication of tectonism. In contrast to their matrix, they do not contain well-developed metamorphic minerals, the only metamorphic mineral present being rare epidote. Their mineralogy is dominated by plagioclase feldspar and quartz, with much smaller quantities of alkali feldspar and biotite, and accessory minerals including zircon, sphene, apatite, allanite and opaques including magnetite,

pyrite, and in one case, molybdenite. All the clasts have undergone severe weathering, with saussuritisation of the plagioclase and breakdown of biotite to chlorite and opaques.

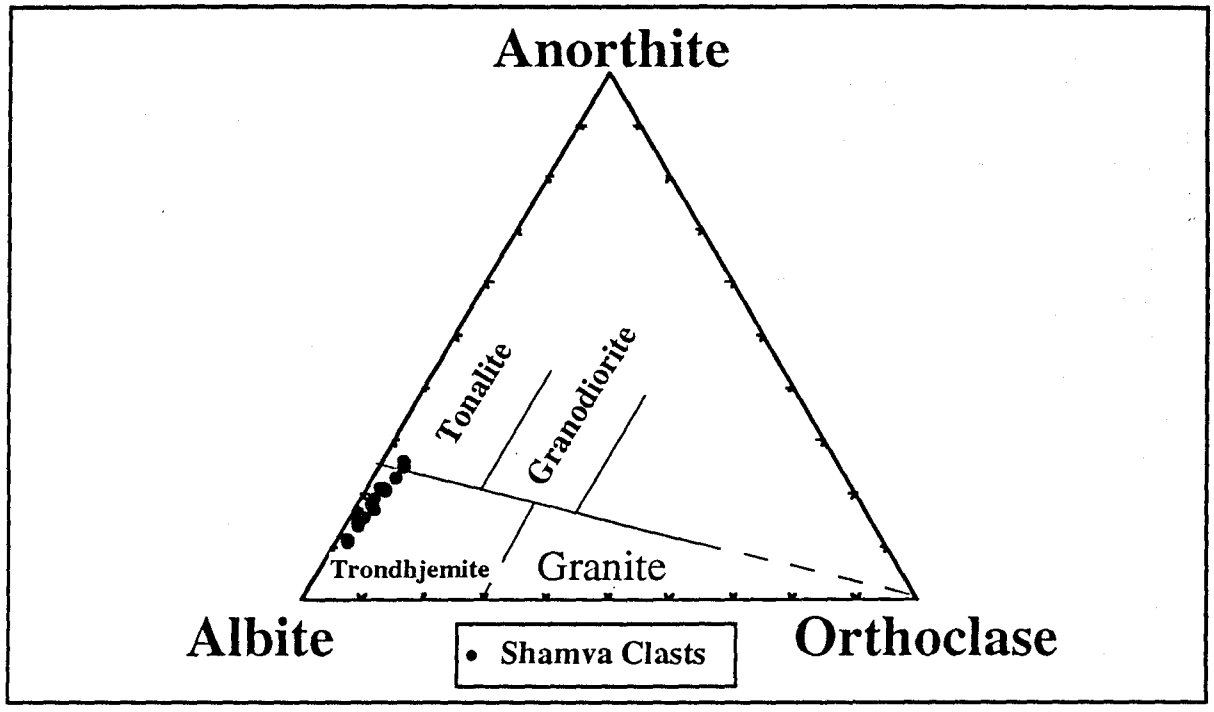

Figure 3.5 Feldspar ratio plot using Anorthite-Albite-Orthoclase CIPW normative compositions for the Shamva clasts (after O'Connor, 1965)

The clasts may be divided into high- and low-Al_2O_3 chemical groups which show consistent differences between each other in terms of their major, trace and rare-earth element chemistry (figures 3.6 & 3.7). The major, trace and REE chemistry of the clasts is tabulated in appendix A.

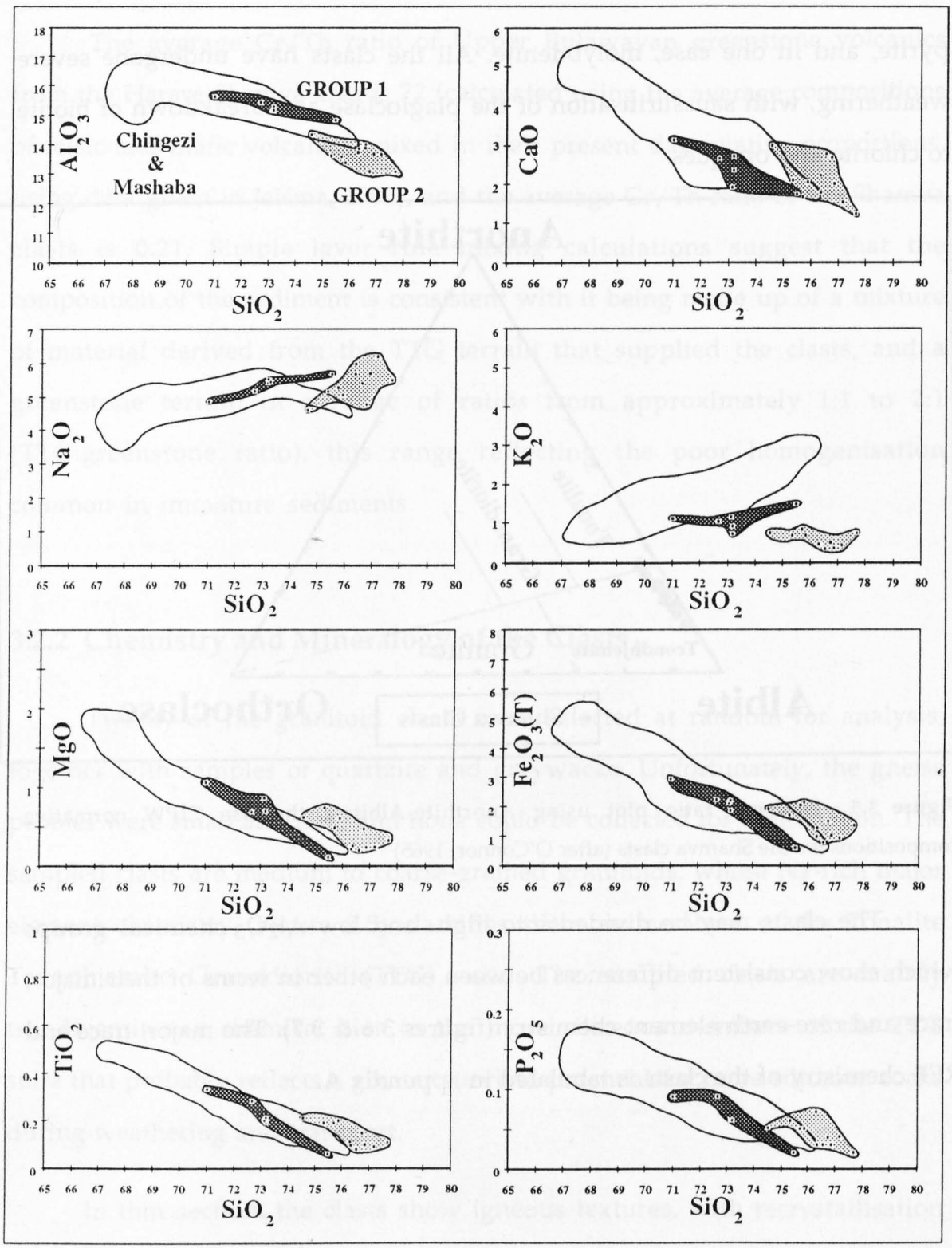

Figure 3.6 Major elements vs. Silica for the Shamva Clasts, showing 2 clearly defined groups. Group 1 (dark shading) has better defined trends and a lower silica content than group 2 (light shading). The unshaded fields are from the Chingezi and Mashaba Tonalites of Southern Zimbabwe (data from Luais and Hawkesworth, 1994).

3:2.2 a The Group 1 Clasts

There are 6 samples in this group, ranging in SiO_2 content from 71 to 75.5%. They show well defined trondhjemitic trends for major elements against silica (Figure 3.6), with increasing Na_2O and K_2O, and decreasing Al_2O_3, CaO, MgO, Fe_2O3, TiO_2 and $P2O_5$.

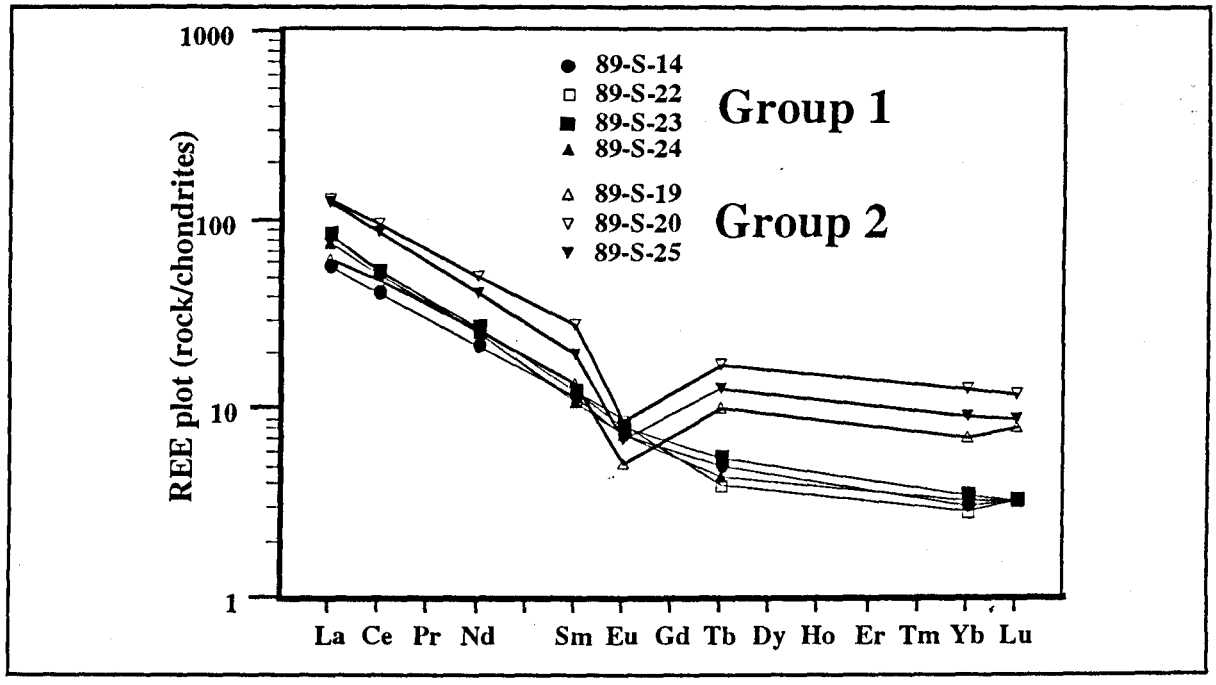

Figure 3.7 Chondrite normalised REE plots for the group 1 and 2 Shamva clasts

The group has a projected Al_2O_3 content of >15 % Al_2O_3 at 70 % SiO_2, making these clasts members of the Archaean high-alumina trondhjemite group of Barker and Arth (1976). Total content of ferromagnesian elements is low, with (Fe_2O_3(T)+MgO+TiO_2) ranging from 0.77 to 4.33, well within the normal range for Archaean TTG suites of ≤ 5 % (Martin, 1993). The clasts follow a K_2O-poor fractionation trend, with low (< 0.2) K_2O/Na_2O ratios, and they plot on the lower, sodic margin of the sodic trend seen in TTG terrains such as the grey-gneiss complex of Swaziland (Hunter et al. 1978, 1984) (figure 3.8). In common with most Archaean granitoids the clasts have strongly fractionated rare-earth element profiles with $(La/Yb)_N$ ratios from 20.2 to 32.4, no significant Eu anomaly and low HREE contents (figure 3.7 and 3.9). $(Yb)_N$

values in the clasts range from 3.6 to 4.4, within the typical range of $(Yb)_N$ values for Archaean TTG suites of $0.3 \leq (Yb)_N \leq 8.5$ (Martin, 1986).

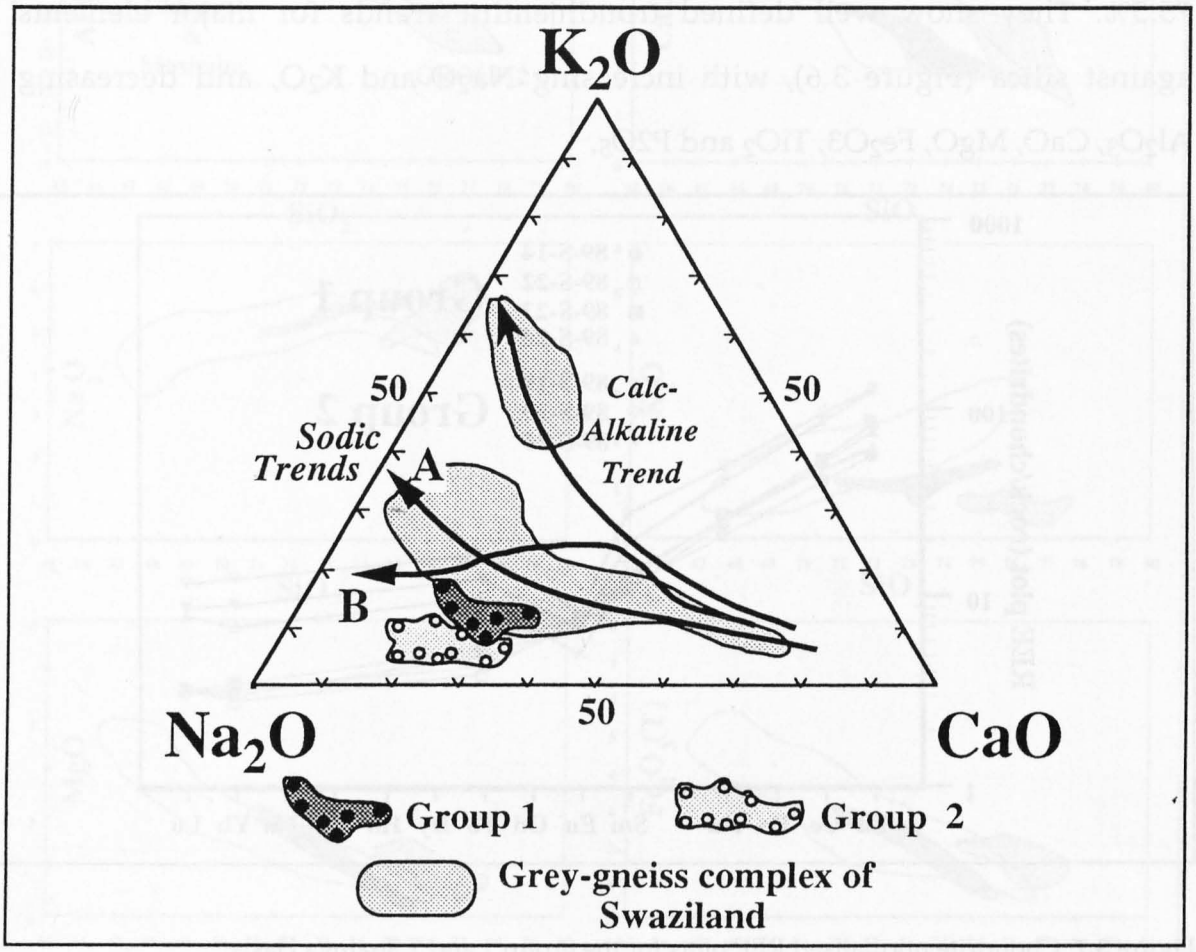

Figure 3.8 K_2O-Na_2O-CaO plot for the group 1 and group 2 Shamva clasts, showing the sodic (A) and calc-alkaline trends (Luais and Hawkesworth, 1994) and the trondhjemitic trend (B) of Barker and Arth (1976). Data fields of the grey-gneiss complex of Swaziland (Hunter et al. 1978 & 1984) are plotted for comparison. Group 2 is notably displaced towards the Na_2O axis, reflecting a K_2O-loss due to weathering.

3:2.2 b The Group 2 Clasts

There are 11 members of this group, ranging in silica content from 75.7 to 77.7%. When silica is plotted against immobile elements, such as Al_2O_3 or TiO_2 (figure 3.6), the group forms a well defined array, with a trend running subparallel to group 1. However, when more mobile elements, such as K_2O, Na_2O or CaO are considered, the trends are lost, and the group merely shows a poorly defined scatter. The group is displaced from the sodic trend usually

seen in TTG terrains (figure 3.8). Group 2 is more siliceous than group 1, and therefore should have an higher K_2O content within a trondhjemitic differentiation sequence (figure 3.6). However, the K_2O content of group 2 is lower than that of group 1 suggesting that the displacement seen in figure 3.8 may be due to a relative loss of K_2O, rather than a gain of Na_2O. Loss of K_2O is also indicated by the fact that although Rb/Sr ratios should increase in a trondhjemitic differentiation sequence, on average the group 2 clasts have a lower Rb/Sr ratio (an average of 0.05) than the group 1 clasts (which have an average ratio of 0.09).

Most of the K_2O within tonalitic rocks is held within potassic feldspar and biotite. Biotite is less resistant to weathering than plagioclase, whereas potassic feldspar is more resistant (Nesbitt and Young, 1984). Therefore, for a preferential loss of K_2O to have occurred, weathering must have proceeded to a stage at which biotite had been altered in group 2, and not in group 1. This does appear to be the case, as the biotites in group 2 have greater degrees of alteration than those in group 1, and have largely broken down to chlorite and opaques. As the clasts will have simultaneously undergone the same processes once the two groups were incorporated in the sediment together, this differential weathering between group 1 and group 2 must have occurred in the Archaean, suggesting that the area from which the group 2 clasts were derived had been exposed for longer, and thus weathered more deeply, than that of the group 1 clasts. Despite the greater weathering of the clasts in group 2, there is no correlation between clast size, degree of rounding, and the group to which the clasts belong. The group 2 clasts have higher REE contents than the group 1 clasts and a strong negative Eu anomaly (figure 3.7). The REE profiles are distinctly less fractionated than those of group 1,with $(La/Yb)_N$ ratios ranging from 9.6 to 14.5, in contrast to 20.2 to 32.4 for group 1. The lower La/Yb ratios are due to less HREE depletion, and $(Yb)_N$ values range from 9.1 to 16.5, above the usual range for Archaean granitoids of ≤ 8.5 (Martin, 1986).

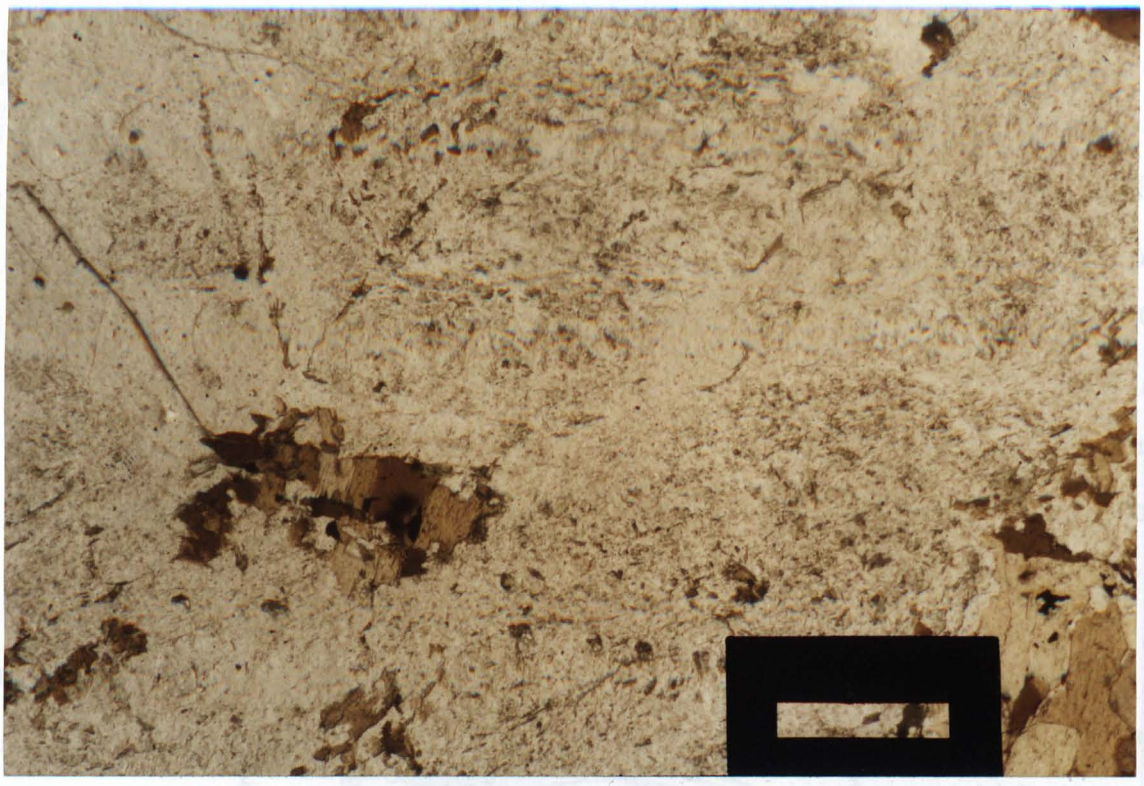

Photograph 3.3 Photomicrograph of the Shamva group 1 clast 89-S-14, showing badly weathered feldspars, but comparatively fresh biotite. Scale bar ≈ 0.5 mm

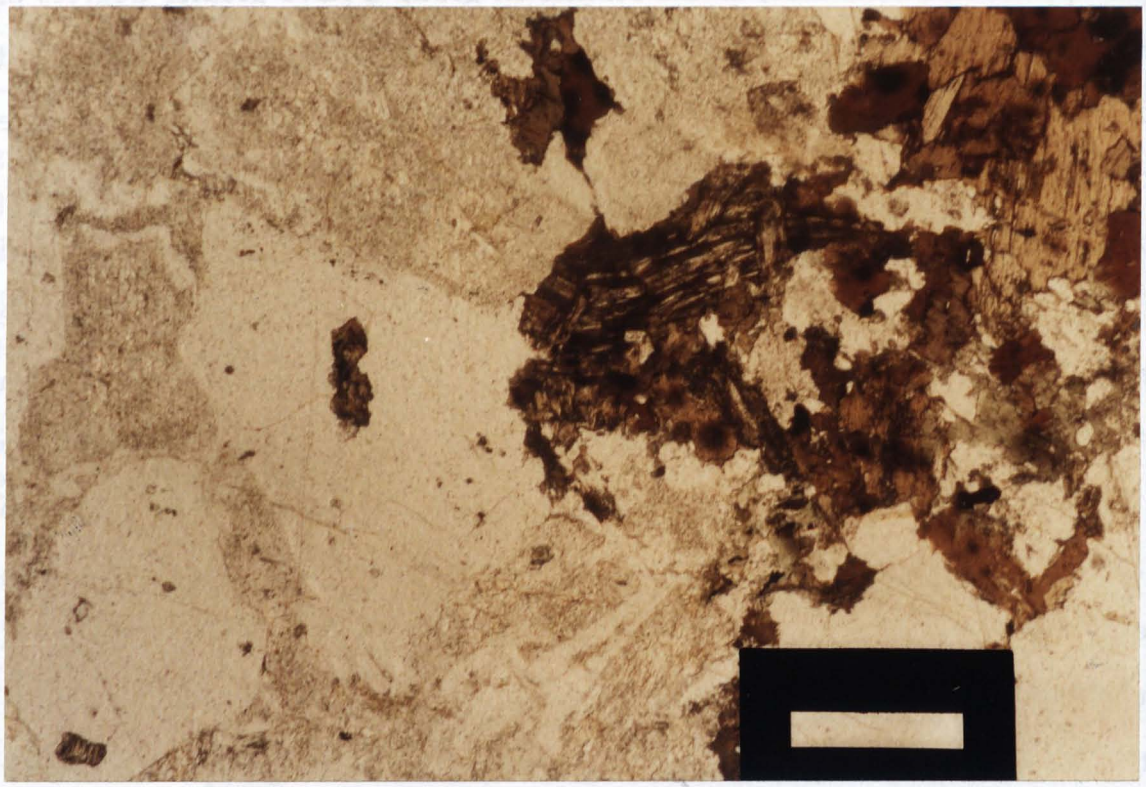

Photograph 3.4 Photomicrograph of the Shamva group 2 clast 89-S-12. The alteration of this clast has been more intensive than for the group 1 clast pictured above, with replacement of biotite by chlorite. Scale bar ≈ 0.5 mm

3:2.3 Petrogenetic Models for the Formation of the Group 1 and 2 Clasts

The group 1 clasts conform closely in terms of major elements, trace elements, and REE, to some Archaean TTG granitoids described in previous studies, such as the Ancient Gneiss Complex of Swaziland (Hunter et al. 1978) and the Chingezi-Mashaba tonalites of Southern Zimbabwe (Luais and Hawkesworth 1994) (figures 3.6, 3.8 & 3.9). Both geochemical modelling and experimental petrology indicate that such granitoids are formed by 10 to 40% partial melting of amphibolite-facies metabasalt at pressures ≈16 kbar, with residual garnet (± hornblende) buffering the HREE content of the melt at a low level (Barker and Arth, 1976; Martin 1986; Drummond and Defant, 1990; Rapp et al., 1991; Luais and Hawkesworth 1994). The group 1 clasts were therefore sourced at sub-crustal depths, and represented a new addition of material to the continental crust.

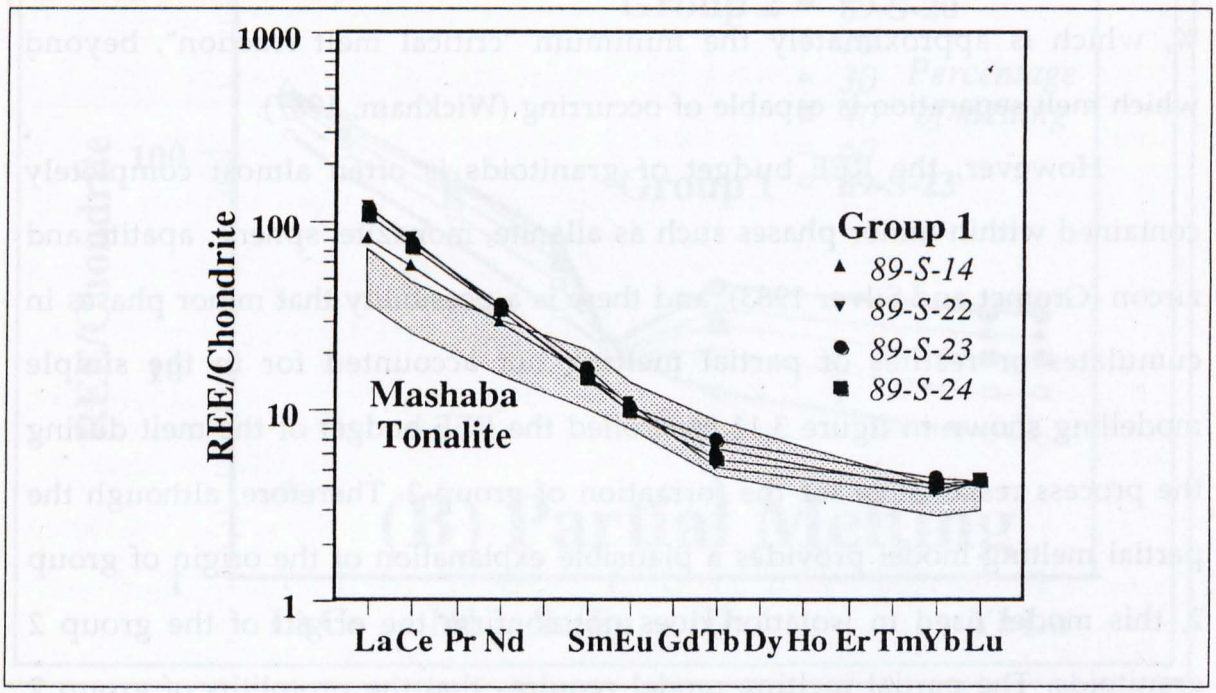

Figure 3.9 Chondrite normalised REE plots of the Shamva group 1 clasts compared to the Mashaba Tonalite (shaded field) (Luais and Hawkesworth, 1994).

The extreme weathering of the group 2 clasts means that little can be inferred of their origins from their major element chemistry. However, REE patterns are not fractionated by weathering processes (Taylor and McLennan, 1985) and using the REE profiles of the clasts, deductions on the origins of

group 2 may be made. The REE patterns of the group 2 clasts have negative Eu anomalies, indicating that plagioclase was an important phase in their formation. As plagioclase is only stable at crustal depths, this indicates that intra-crustal processes were important. As the siliceous portion of the early continental crust was largely constructed from group 1 type granitoids (Martin, 1993), there are two basic models for the formation of group 2; either partial melting of a group 1 tonalite, or fractionation of a group 1 melt. Figure 3.10 shows simple REE modelling of a group 2 composition by both partial melting and fractional crystallisation, from a group 1 starting composition. Both processes can produce REE patterns with a very close fit to the group 2 clast, with ≈ 20 % of liquid formed/remaining from the starting composition involved in both models. 80% fractional crystallisation is rather extreme, and the partial melting model offers a more plausible explanation of the origin of the clasts, with a restite of tonalitic composition and a degree of melting of ≈20 %, which is approximately the minimum "critical melt fraction", beyond which melt separation is capable of occurring (Wickham, 1987).

However, the REE budget of granitoids is often almost completely contained within minor phases such as allanite, monazite, sphene, apatite and zircon (Gromet and Silver 1983), and there is a possibility that minor phases in cumulates or restites of partial melting not accounted for in the simple modelling shown in figure 3.11 controlled the REE budget of the melt during the process responsible for the formation of group 2. Therefore, although the partial melting model provides a plausible explanation of the origin of group 2, this model used in isolation does not confirm the origin of the group 2 granitoids. The partial melting model requires that the protoliths of group 2 had a crustal history prior to a partial melting event, whereas the fractional crystallisation model suggests that like group 1, group 2 represents an addition of new material to the continental crust. Geochronological work detailed in the next section of this chapter will provide clear evidence of the crustal histories of the clasts, serving to support the partial melting hypothesis.

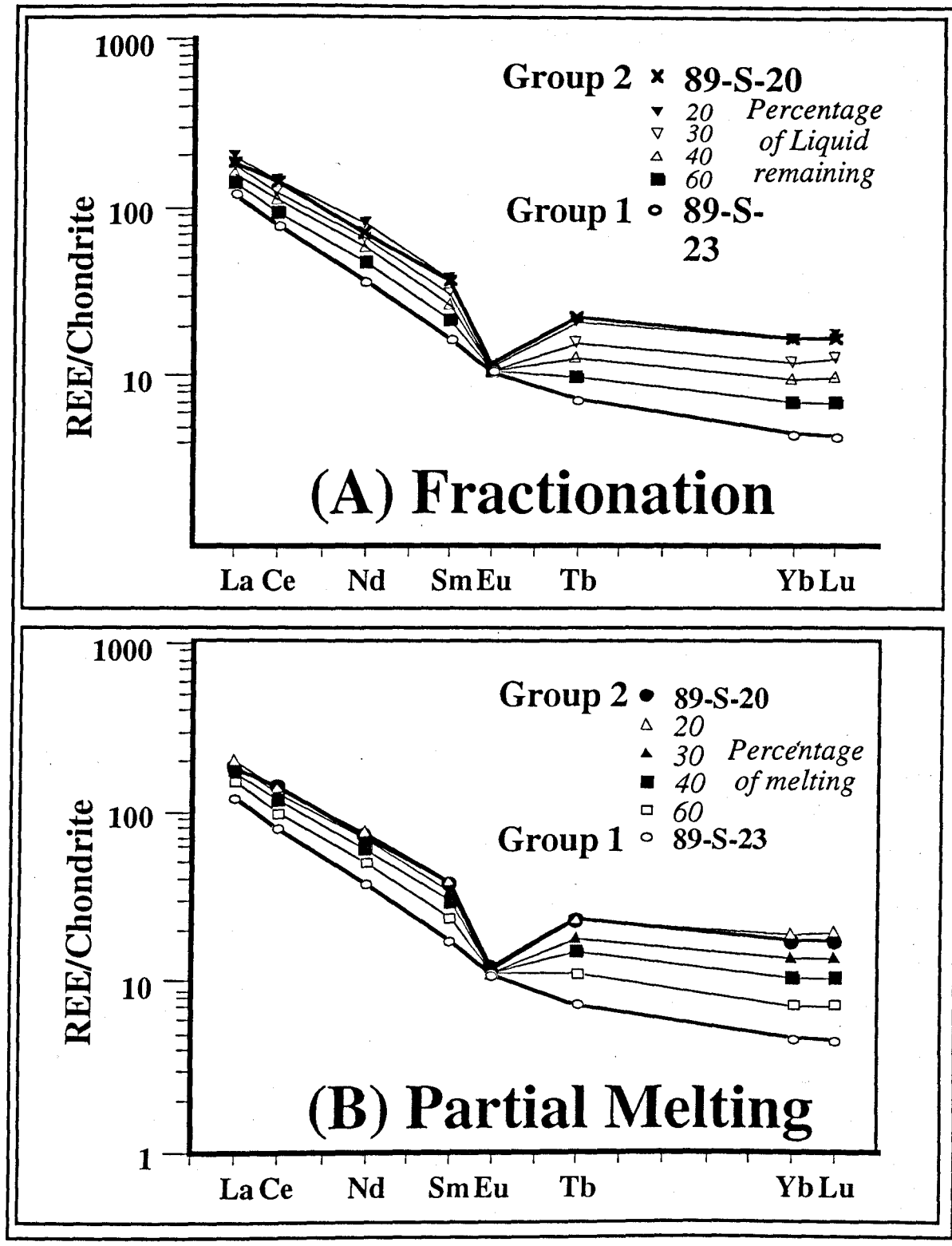

Figure 3.10 REE modelling of the formation of the group 2 granitoids of Shamva from a group 1 protolith (a) by 80% fractional crystallisation of a group 1 melt, leaving a cumulate of 40% plagioclase, 1.5% amphibole, 0.05% allanite and 58.5% quartz. (b) by 20% partial melting of a group 1 tonalite, leaving a residue of 70% plagioclase, 1% amphibole, 0.04% allanite and 29% quartz. Distribution coefficients are listed in appendix A.

3:2.4 Geochronology of the Shamva Clasts

3:2.4 a Geochronological methods used

The granitoid clasts had no known relationships to each other, were badly weathered, and had been metamorphosed to lower amphibolite grade. The geochronological techniques applied to them therefore had to be capable of providing accurate data from single clasts, to avoid the possibility of constructing meaningless "isochrons" from unrelated samples, and furthermore the chosen isotope systematics had to be resistant to disturbance by metamorphism and weathering processes. The U-Pb systematics of zircon are extremely resistant to alteration, and a major aspect of this thesis has been to set up Pb-Pb single zircon dating by the Kober technique (see Chapter 2) in order to constrain the crystallisation history of the clasts. Whole rock Sm-Nd systematics are resistant to alteration during low grades of metamorphism and weathering, and are used to give the "model age" of the extraction from the mantle of the material which makes up the clasts. ^{147}Sm has a long half-life (1.06×10^{11} years), and therefore in the Archaean there were only small differences between continental crust and mantle reservoirs of Nd. Therefore extremely high precision analysis of $^{147}Sm/^{144}Nd$ ratios, and thus of the Sm and Nd contents and isotopic compositions are required in order to accurately constrain "model ages". The Sm-Nd budget of granitoids such as these is virtually entirely contained within minor phases such as; zircon, allanite, sphene and apatite (Gromet and Silver, 1983). Both the concentrations and isotope ratios of Sm and Nd have been measured on the *same dissolution of sample* to avoid the possibility of differing proportions of REE-rich minor phases within separate dissolutions. Therefore the single dissolution for each sample has to be spiked with a solution of isotopes of Sm and Nd of known concentration and isotope ratios at the beginning of the dissolution procedure, in order to account for fractionation of Sm from Nd during the analytical

procedure (residual fluorides after dissolution in HF will fractionate Sm and Nd). As this procedure was not routinely carried out at the Open University these samples were analysed for Sm and Nd at Clermont-Ferrand. The measured $^{143}Nd/^{144}Nd$ ratios were corrected using a natural $^{145}Nd/^{144}Nd$ ratio of 0.348417 (corresponding to a $^{146}Nd/^{144}Nd$ ratio of 0.7219), and model ages were calculated according to the depleted mantle evolution curve detailed in Othman et al. (1984). Internal errors on individual Sm-Nd analyses were ≤ 0.25 %, corresponding to a possible error on the T_{DM} model age of ≤ ± 0.008 Ga at 3.0 Ga. As the model ages are only quoted to 2 decimal places, errors for the model ages are not given in the following text, although they are tabulated in table 3.2.

3:2.4 b Sample selection and preparation.

Criteria for selecting which clasts were to be analysed were primarily the size of the clast, and the presence of zircon in thin section, to maximise the possibility that sufficient zircon was going to be present to allow an accurate age determination to be made. Two clasts from group 1 were selected, (sample numbers 89-S-14, and 89-S-23), and three from group 2 (sample numbers 89-S-12, 89-S-19, 89-S-25). A clast which could not be placed in either group, 89-S-26, and two large quartzite clasts (for analysis of detrital zircon populations) were also selected. Unfortunately, 89-S-26 and the quartzites proved to have insufficient zircon of suitable quality to enable an analysis to be made. Zircon separates were prepared by heavy liquid and magnetic separation (see appendix B), single crystals were then hand-picked for analysis by the the Kober technique, as described in Chapter 2. The data from these clasts are discussed individually below, and tabulated in table 3.2. The calculation of ages and estimation of errors on Kober data is described in Chapter 2.

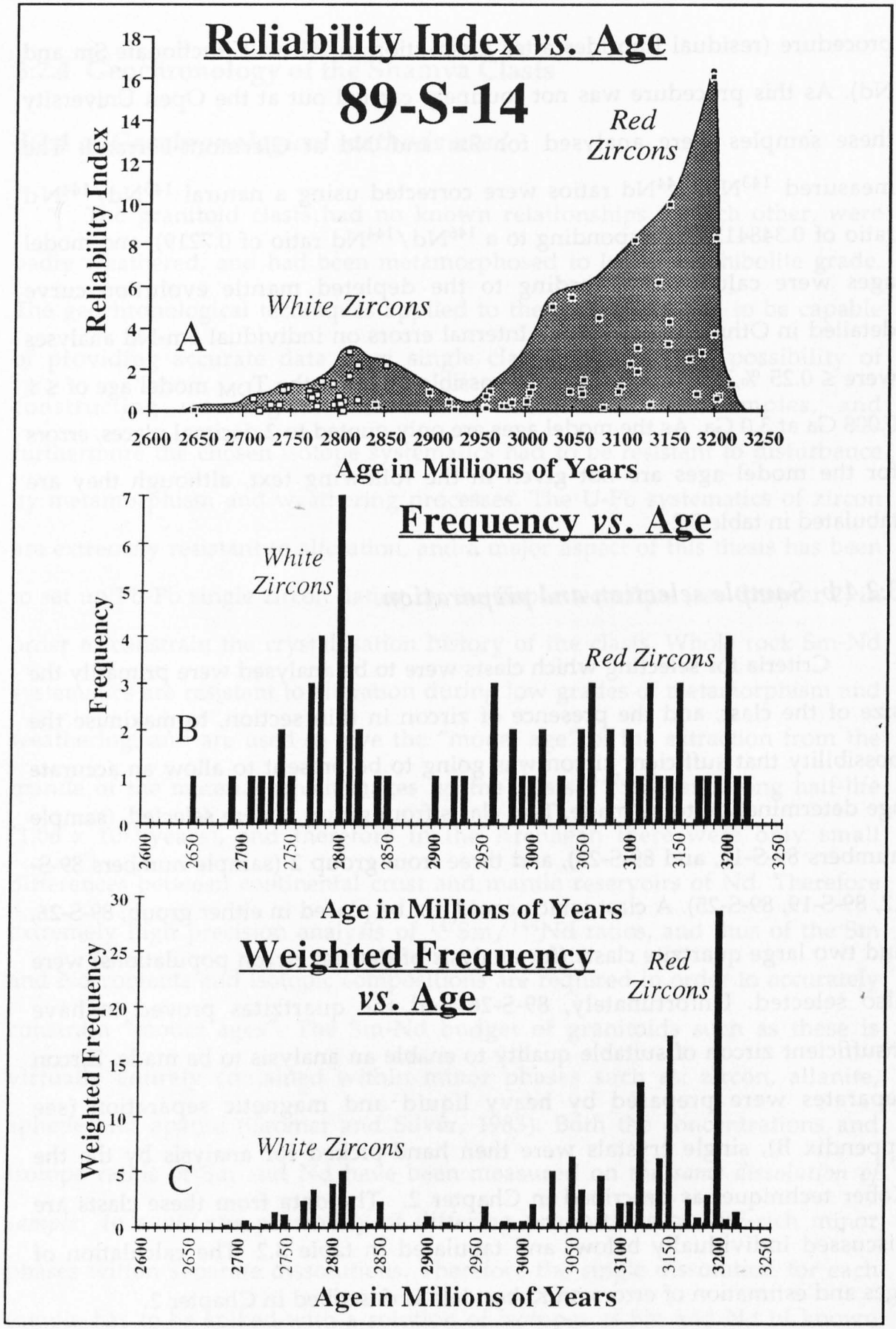

Figure 3.11 Zircon data from the Shamva group 1 clast 89-S-14 (a) Index of reliability of data vs. age scatter graph; (b) Frequency within a 10 Ma interval vs. age histogram; (c) Weighted frequency vs. age histogram. See Chapter 2:4 for a full explanation of the use of these diagrams

3:2.4 c Group 1 Clasts

89-S-14

This 3 kg clast produced a separate of approximately one hundred zircon crystals, with 2 obvious phases of crystallisation, an early reddish phase, and a later colourless phase. Photographs of the zircons are shown in Chapter 2 (photographs 2.2 and 2.3). Both phases of crystallisation provided zircons of suitable quality for dating. As with all of the Shamva clasts, the zircon population was too small to allow a full typological analysis, but the two phases were distinctly different. The reddish phase of crystals are multi-faceted, with high S-number typology on the Pupin (1980) typological classification of zircons (up to S-17, see Chapter 2, figure 2.1) and an average length to breadth ratio of 2.4, whereas the white phase is more elongate, with average length to breadth ratios of 3.7, and simpler crystal forms. Common-Pb corrected ages were calculated for each heating step, and these results for analyses on both the early and late phases are displayed in figure 3.13, and tabulated in appendix B. The determination of ages and errors on the zircons from this rock is discussed in Chapter 2:4.5d(2). The red crystals give an age of 3,197 ± 10 Ma, and the white crystals give an age of 2,800 ± 20 Ma

The Sm-Nd (T_{DM}) model age for this clast is 2.98 Ga, intermediate between the older (red) phase of zircons (3,197 ± 10 Ma), and the younger (white) phase (2,800 ± 20 Ma). There are two possible mechanisms which could have caused this; either the original melt separated from the mantle reservoir at ≈3.2 Ga, and the resultant rock had its Sm-Nd systematics partially re-set in an intense metamorphic event at ≈2.8 Ga, or a melt which separated from the mantle reservoir at ≈2.8 Ga assimilated pre-existing crustal material dating from ≈3.2 Ga, and retained an inherited component of xenocrystal zircon cores. As the clast is unfoliated, with an igneous texture, and no evidence of high grade metamorphic minerals, the latter explanation is preferred.

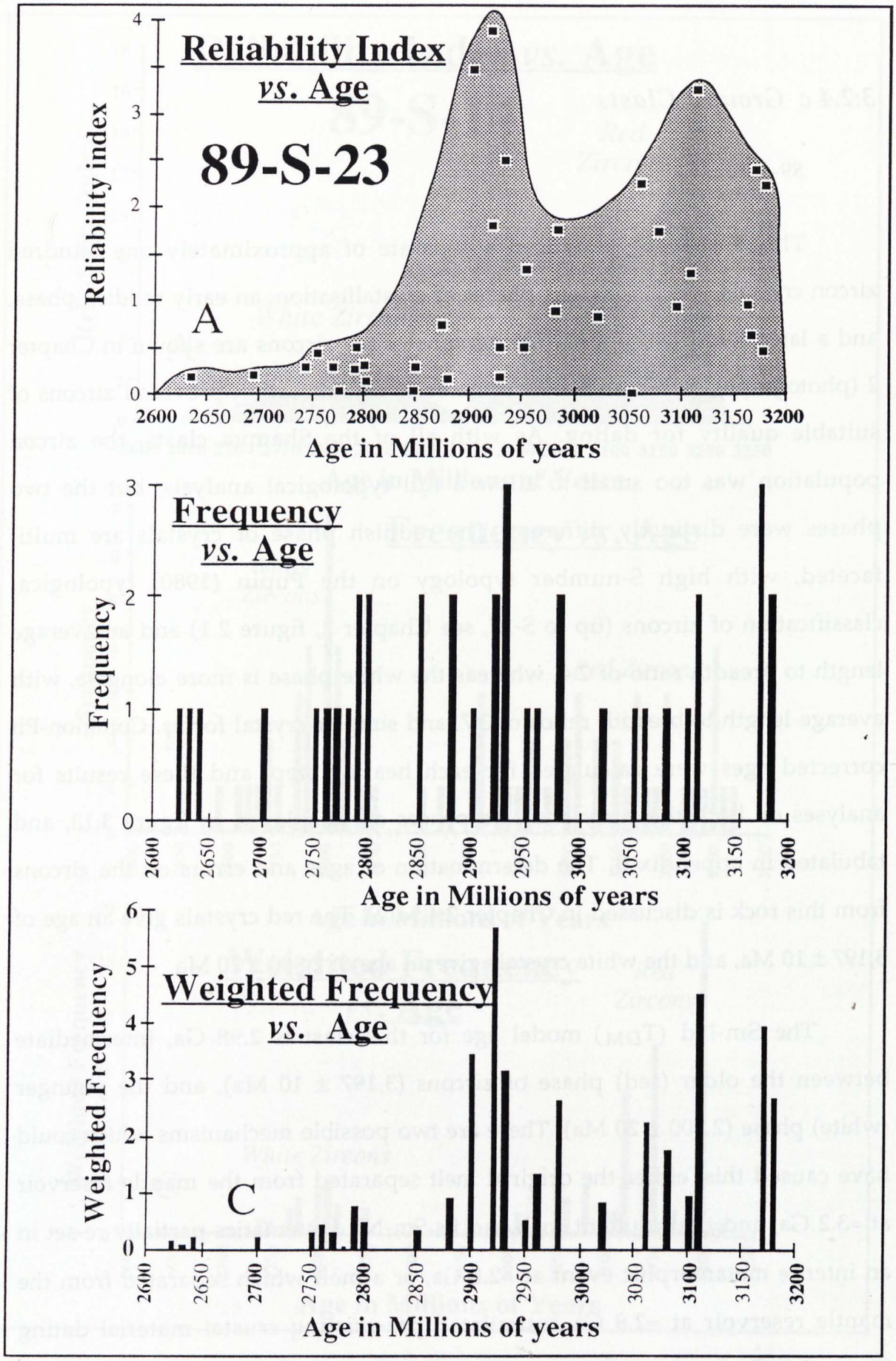

Figure 3.12 Zircon data from the Shamva group 1 clast 89-S-23 (a) Index of reliability of data vs. age scatter graph; (b) Frequency within a 10 Ma interval vs. age histogram; (c) Weighted frequency vs. age histogram. See Chapter 2:4 for a full explanation of the use of these diagrams.

89-S-23

This 2.7 kg clast provided a small, moderate quality separate of exceedingly diverse types of zircon (photograph 3.5), most with visible cores and rims.

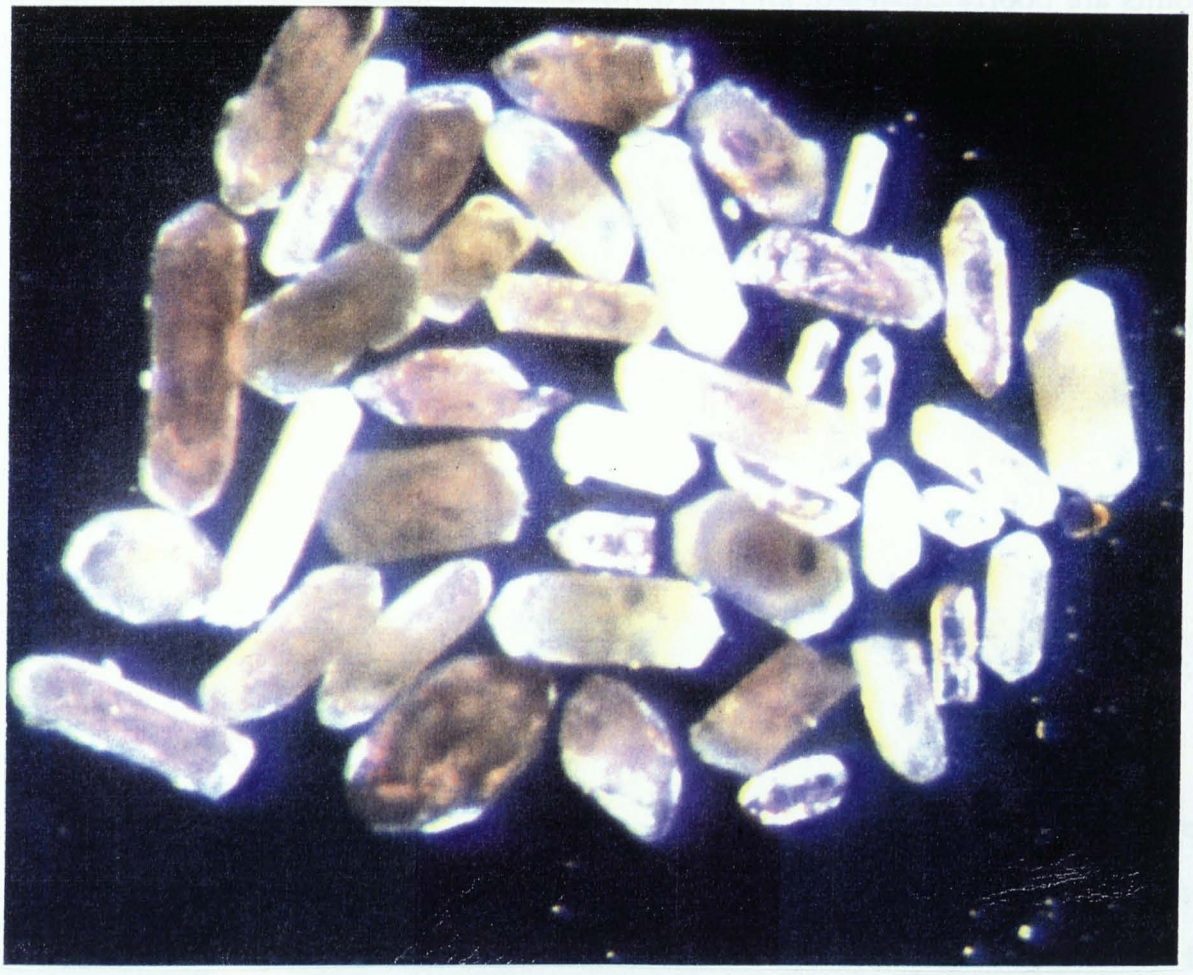

Photograph 3.5 Zircons from 89-S-23. The field of view is ≈ 1 mm. The population is extremely heterogeneous, and several of the crystals have visible cores and rims.

The diversity of the zircon population was borne out by the results from step heating Kober technique analyses of zircons. Common-Pb corrected ages were calculated for each heating step, and these results are plotted in figure 3.12 and tabulated in appendix B. A suite of ages up to 3,182 Ma is recorded, with a cluster of low reliability data points between 2,750 - 2,800 Ma, and a clustering of higher reliability points around 2,920 Ma, this latter grouping containing the point with the highest recorded reliability index, at

2,922 Ma. The history of this clast is therefore exceedingly complex, with at least 3 phases of zircon crystallisation present. None of the recorded groupings of data are sufficiently well defined to allow accurate crystallization dates to be determined from this clast in isolation, but the main clusterings are concident with well defined crystallisation dates in other clasts. The oldest recorded data points are poorly clustered, and the 3,182 Ma age is taken as the minimum age for the oldest zircon cores in this clast. The grouping of data points between 2,750 and 2,800 Ma probably represents the same 2,800 ± 20 Ma crystallisation recorded in clast 89-S-14, and the clustering of data centred on 2,922 Ma is coincident with the main phase of crystallisation recorded in the group 2 clasts 89-S-12, 89-S-19, and 89-S-25.

The Sm-Nd T_{DM} model age of this clast is 3.16 Ga, similar to the minimum age for the oldest zircon cores.

3:2.4 d Clast number 89-S-26

This clast was initially included in group 2 due to its low K_2O content, (probably due to severe weathering) but it has very strongly fractionated REE patterns, with strong HREE depletion, characteristic of group 1 (Figure 3.13). However, unlike the rest of the clasts in group 1, 89-S-26 has a very pronounced negative Eu anomaly. Therefore, as this clast does not belong to either group, it has not been included in previous discussions.

The zircon separate provided only a few turbid, obviously multi-phase zircons, which could not be dated. However, the clast was analysed for Sm-Nd, and gave a T_{DM} model age of 3.34 Ga, the oldest model age yet recorded from Northern Zimbabwe.

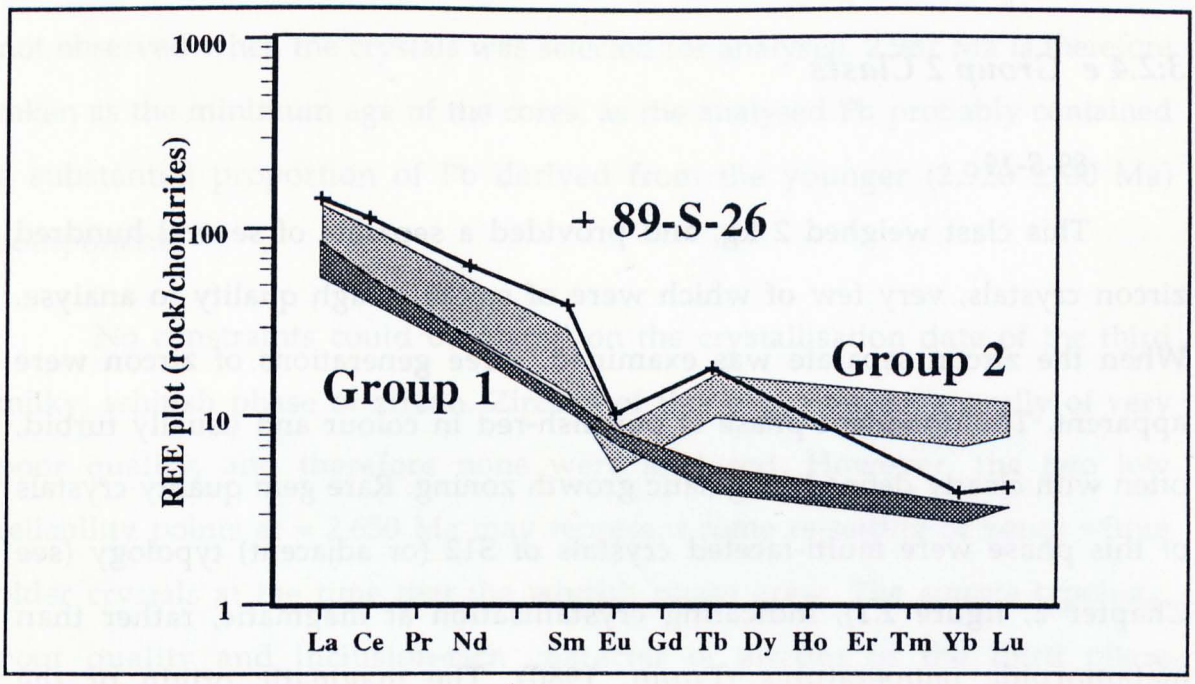

Figure 3.13. Chondrite normalised REE plot for the clast 89-S-26, showing fields for the group 1 (dark shading) and group 2 (light shading) clasts.

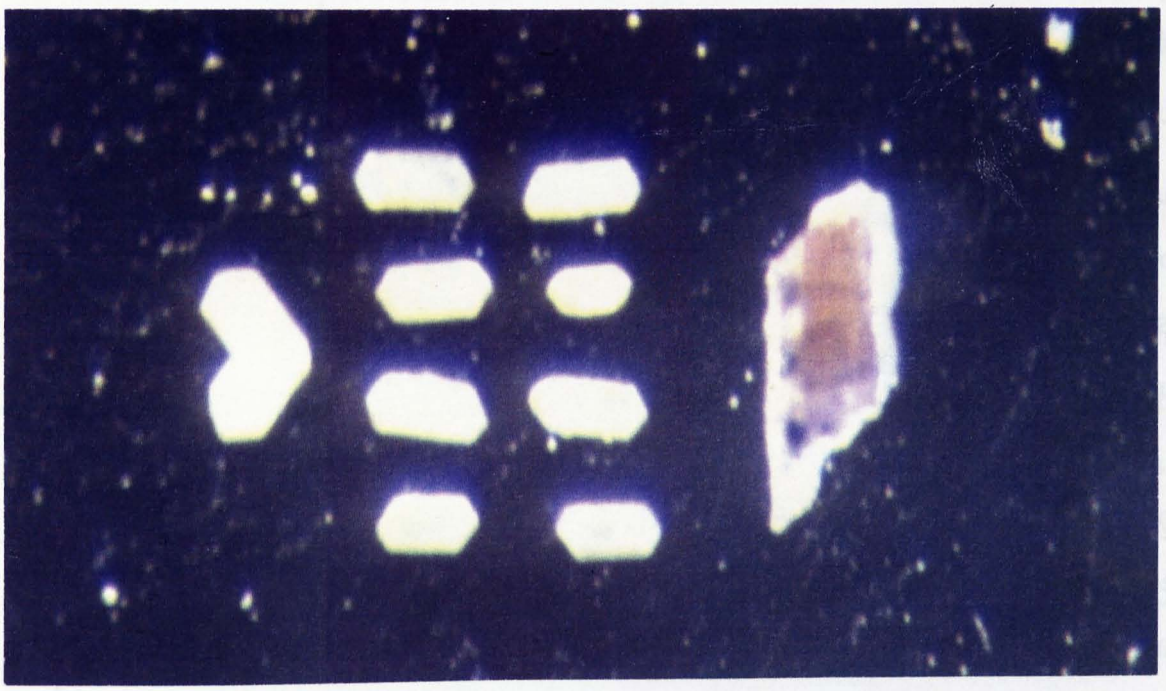

Photograph 3.6 Zircons from the Shamva group 2 clast 89-S-19. The fragment of crystal to the right shows a well defined reddish core, with a white rim.

3:2.4 e Group 2 Clasts

89-S-19

This clast weighed 2 kg, and provided a separate of several hundred zircon crystals, very few of which were of suitably high quality to analyse. When the zircon separate was examined, three generations of zircon were apparent. The dominant phase is purplish-red in colour and usually turbid, often with clearly defined magmatic growth zoning. Rare gem quality crystals of this phase were multi-faceted crystals of S12 (or adjacent) typology (see Chapter 2, figure 2.1), indicating crystallisation at magmatic, rather than metamorphic temperatures (Pupin, 1980). The magmatic origin of the dominant phase of zircon may also be demonstrated by the presence of magmatic growth zoning within some crystals. Zircons of this phase contain rare, rounded cores, and milky, whitish overgrowths of S5 to G1 typology. Where this last phase forms its own crystals, these are notably more elongate than those of the purplish phase.

Only the main phase of zircon provided crystals of sufficient quality to analyse, and of these, crystals with visible cores or rims were not selected. Common-Pb corrected ages were calculated for each heating step, and these results are displayed in figure 3.14, and tabulated in appendix B. The data confirm the complexity of crystallisation history indicated by the three phases of zircon which were observed. The date of crystallisation of the main, magmatic, phase of zircon is given by the highest frequency interval on the frequency vs. age graph (figure 3.14b) which occurs in the interval 2,915 - 2,925 Ma. The age of crystallisation of this main phase of zircon is therefore taken as 2,920 Ma, with an estimated error of ± 30 Ma (the half-height of the least skewed (older) side of the frequency peak). Ages were recorded up to a maximum of 2,987 Ma, interpreted as representing mixed ages between the main phase of zircon crystallisation and older core components (which were

not observed when the crystals was selected for analysis). 2,987 Ma is therefore taken as the minimum age of the cores, as the analysed Pb probably contained a substantial proportion of Pb derived from the younger (2,920 ± 30 Ma) component.

No constraints could be placed on the crystallisation date of the third milky, whitish phase of zircon. Zircons of this phase were generally of very poor quality, and therefore none were analysed, However, the two low reliability points at ≈ 2,650 Ma may represent some re-setting of zones within older crystals at the time that the whitish phase grew. The simple typology, poor quality and inclusion-rich character of zircons of the third phase indicates that these crystals grew under metamorphic, rather than magmatic conditions, and that they are therefore of minor importance in the crystallisation history of this clast.

The Sm-Nd depleted mantle model age of the clast is 3.17 Ga, indicating that material now within the clast had a crustal history of at least 250 Ma prior to the main phase of zircon crystallisation, during which time the observed cores were formed.

89-S-25

This clast weighed 5 kg, and provided a separate of large, generally poor quality crystals. As with S-19, there are 3 phases of crystallisation, with rounded cores, a main reddish phase, and thin white, milky overgrowths. Common-Pb corrected ages were calculated for each heating step for zircons from this clast, the results for which are displayed in figure 3.15 and tabulated in appendix B . Constraints were able to be placed on the date of crystallisation of all three phases of zircon. The youngest phase is represented by a frequency peak of low-reliability data at ≈ 2,670 Ma. As with the zircons from 89-S-19, this phase of zircons probably grew under metamorphic conditions, and this frequency peak is interpreted as indicating the date of metamorphism of the

Shamvaian sediments. Heating steps from the zircon which gave the highest reliability point (zircon 2) gave ages of 2,917, 2,918 Ma and 2,925 Ma, the reproducibility of data on several heating steps strongly indicating that this zircon was predominantly made up of a single concordant component. These four heating steps give a weighted average age of 2,924 Ma, taken to be crystallisation age of the main phase of zircon, with a 1 standard deviation error of ± 5 Ma. The age of the main phase of zircon is taken as the age given by the zircon 2, rather than the age interval with the greatest frequency (2,890 Ma) which is interpreted as indicating that most of the crystals of the main phase analysed contained components which became closed systems to U and Pb at the time that the white phase of zircon grew during lower amphibolite facies metamorphism at ≈ 2,670 Ma. A zircon crystal with a visible core was dated for this clast, which gave ages of up to 3,116 Ma. This represents the minimum age, as the analysed lead could still contain a component derived from a younger crystallisation phase.

The Sm-Nd depleted mantle model age of the clast is 3.20 Ga, and the true age of the cores may be close to this value.

89-S-12

This clast, weighing 2.5 kg, provided a small (a few 10's of crystals) separate of low quality crystals, with two distinct phases present - larger, purplish-red crystals and a later whitish phase present mainly as rims to the purplish phase, although a few discrete crystals were present. This whitish phase was relatively abundant, but of poor quality, and could not be dated. The results are tabulated in appendix B, and displayed in figure 3.16. The age of the crystallisation of the purplish-red phase is well constrained, with a single peak skewed to the left (younger ages). The skewing of this peak is interpreted as mixing between two phases of zircon, an older one at ≈ 2.92 Ga, and a younger component. The bimodality of the peak is due to the results from zircon 2, which gave a suite of mixed ages, getting progressively older with each

heating step, but which was totally evaporated before its true age had been reached. The most reliable analysis for the clast gives an age of 2921 Ma, a date supported by 6 other analyses of moderate reliability. The estimated error on this date is ± 10 Ma, based on the half peak height of the least skewed (right) side of the frequency graph (figure 3.16 b).

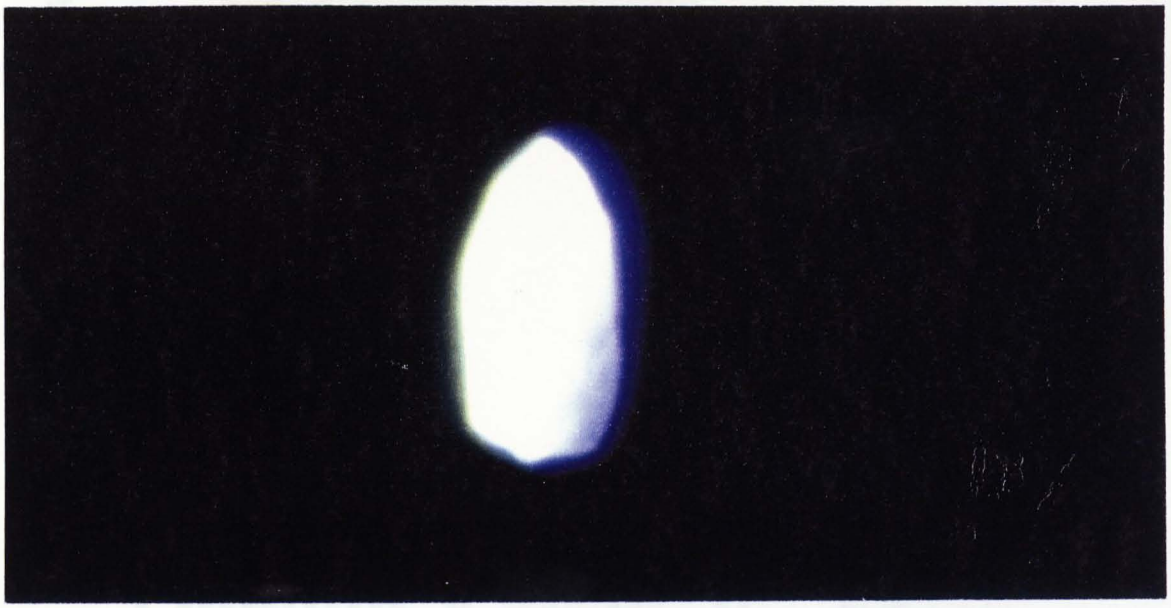

Photograph 3.7 A zircon from Shamva group 2 clast 89-S-12 which was analysed by the Kober technique (zircon 89-S-12/2), and is now pseudomorphed by baddeleyite. The top of the crystal still clearly retains its original multi-faceted high S-number typology. The zircon is approximately 0.3 mm long.

There is no conclusive evidence for the date of crystallisation of the white phase of zircon, as although there are two peaks on the reliability index, these are unsupported. However, these peaks do occur at ages which are recorded elsewhere in the Shamva area, at 2679 Ma (close to the age of the Wedza Suite and syn-depositional intrusions in the Shamvaian (Jelsma 1993)), and at approximately 2.8 Ga (also recorded in clasts from Chinhoyi and 89-S-14). The Sm-Nd (T_{DM}) model age for this clast is 3.13 Ga, indicating that despite the fact that no cores were observed within the ≈ 2.92 Ga purplish phase of zircon, as with the other group 2 clasts analysed, material now contained within the clast had a crustal history of several hundred million years prior to the growth of the main phase of zircon at ≈ 2,925 Ma.

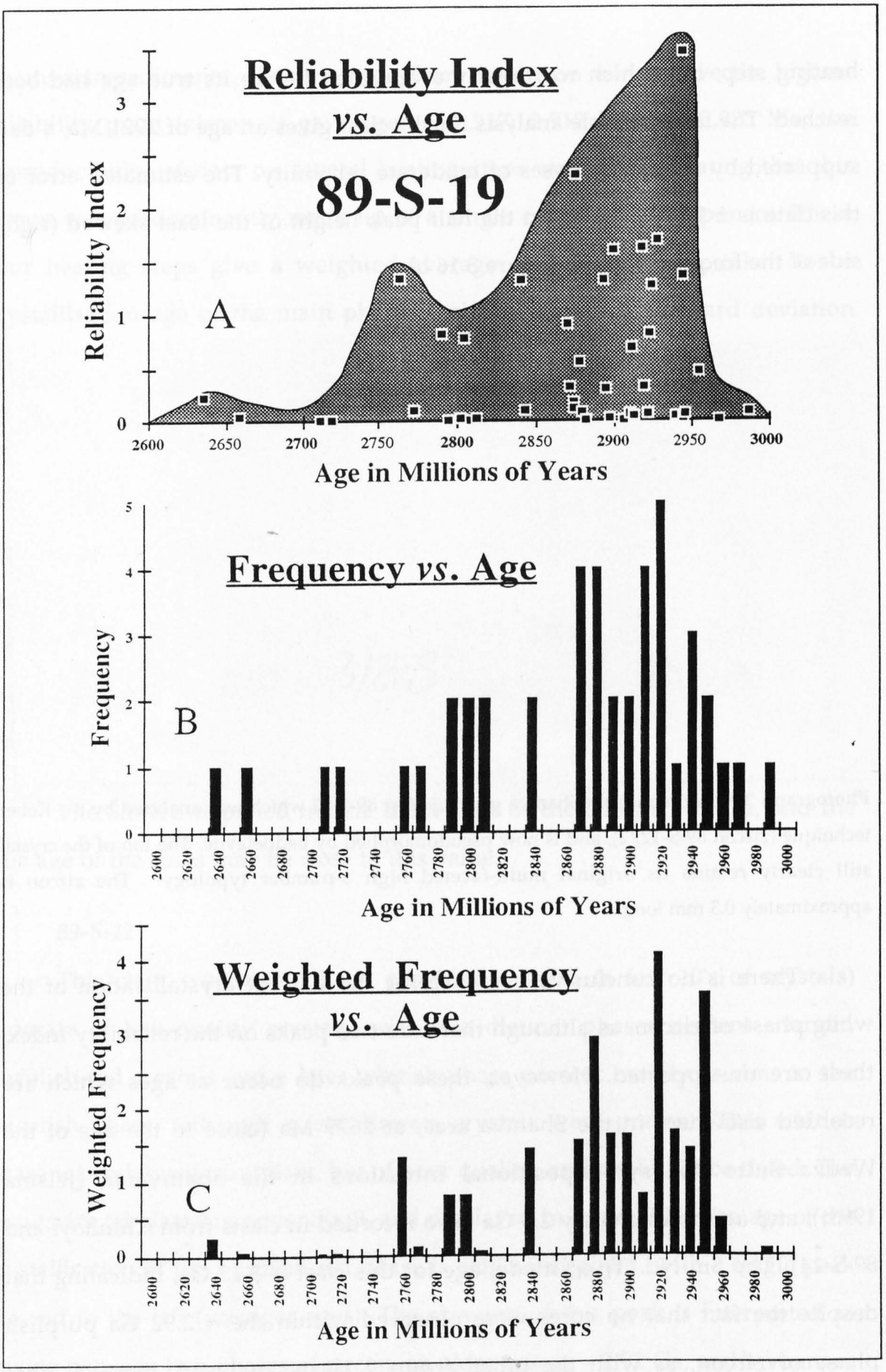

Figure 3.14 Zircon data from the Shamva group 2 clast 89-S-19 (a) Index of reliability of data vs. age scatter graph; (b) Frequency within a 10 Ma interval vs. age histogram; (c) Weighted frequency vs. age histogram. See Chapter 2:4 for a full explanation of the use of these diagrams

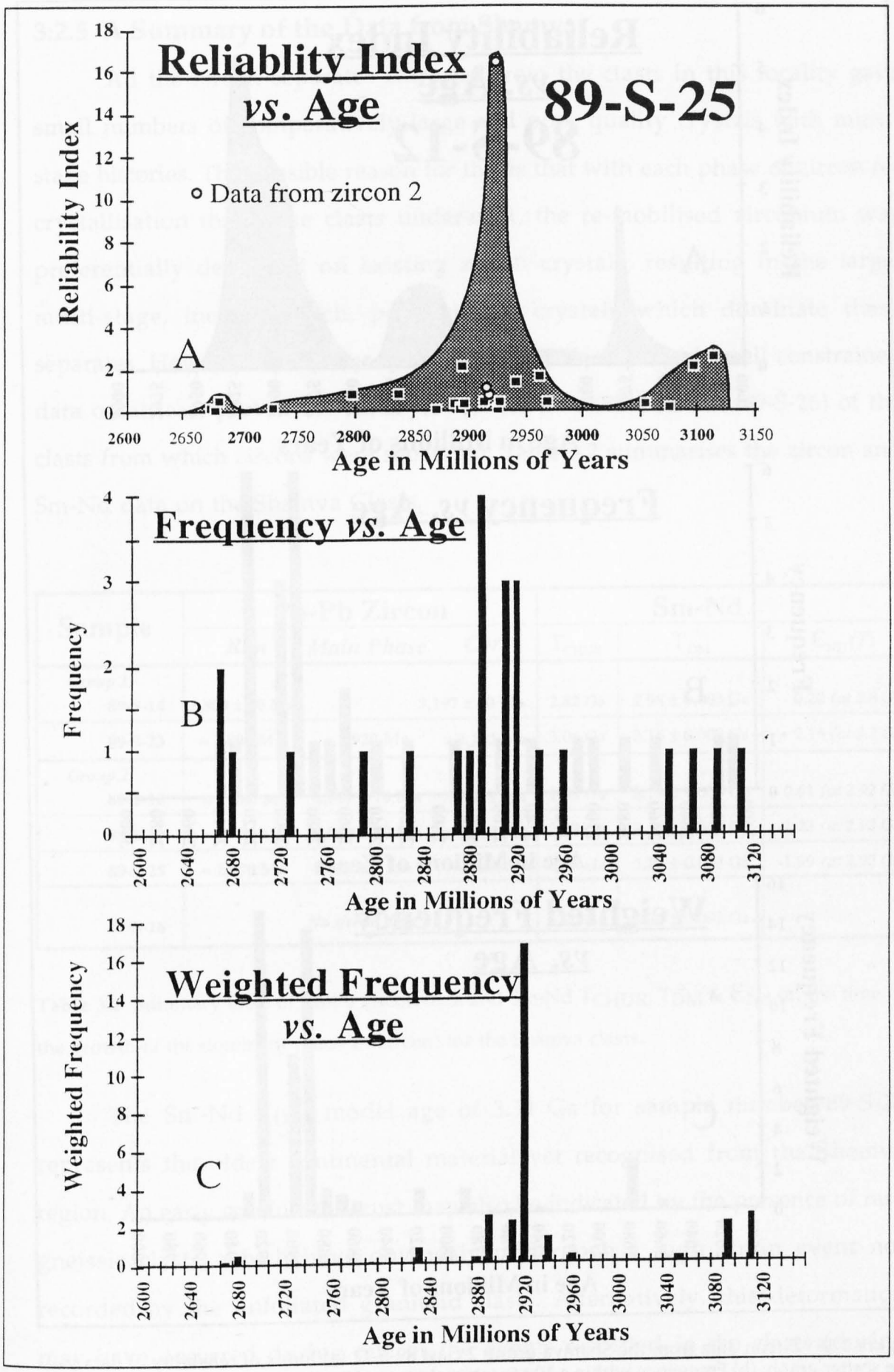

Figure 3.15 Zircon data from the Shamva group 2 clast 89-S-25 (a) Index of reliability of data vs. age scatter graph; (b) Frequency within a 10 Ma interval vs. age histogram; (c) Weighted frequency vs. age histogram. See Chapter 2:4 for a full explanation of the use of these diagrams

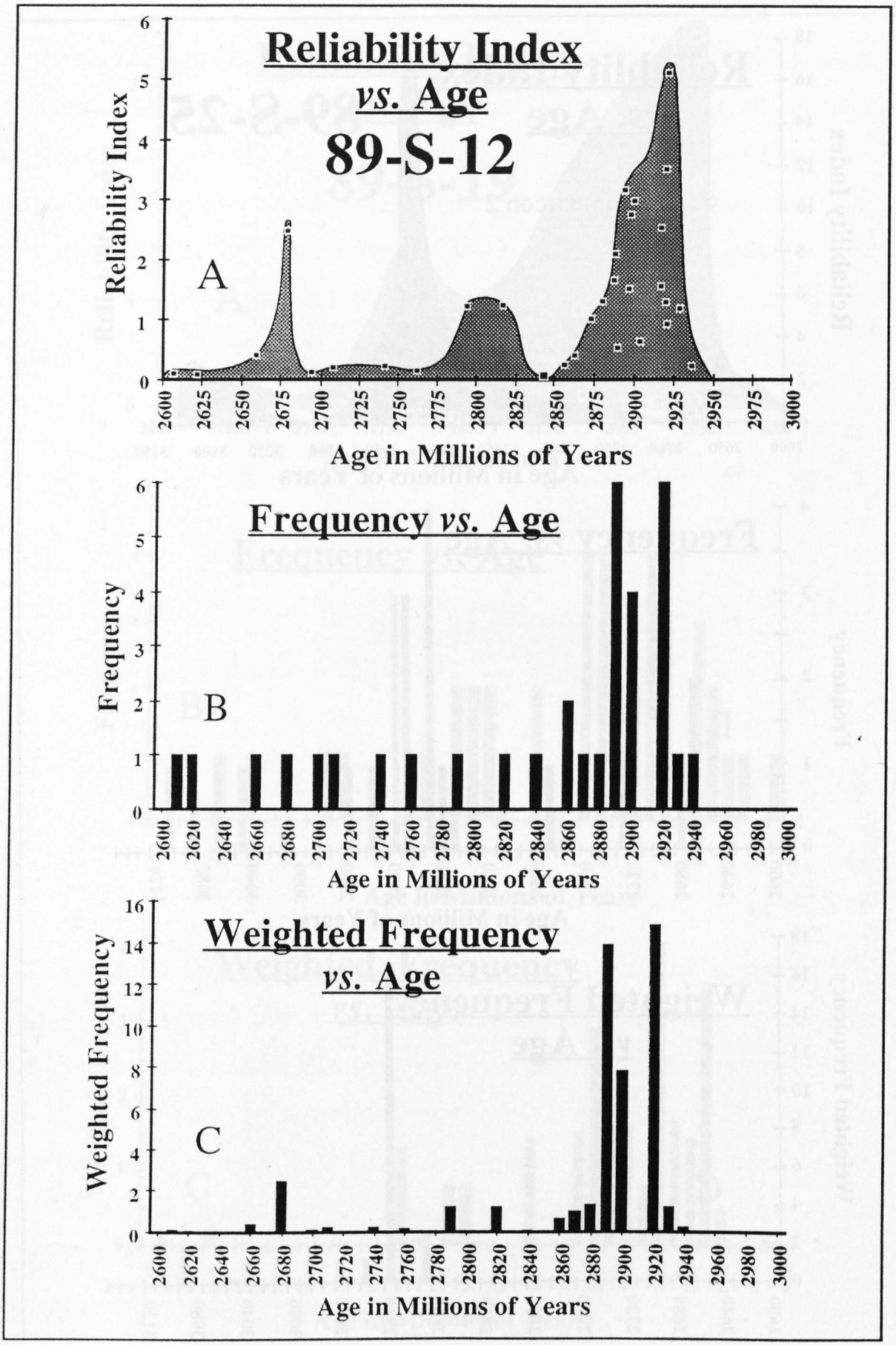

Figure 3.16 Zircon data from the Shamva group 2 clast 89-S-12 (a) Index of reliability of data vs. age scatter graph; (b) Frequency within a 10 Ma interval vs. age histogram; (c) Weighted frequency vs. age histogram. See Chapter 2:4 for a full explanation of the use of these diagrams

3:2.5 A Summary of the Data from Shamva

All the zircon separates extracted from the clasts in this locality gave small numbers of comparatively large and poor quality crystals with multi-stage histories. The possible reason for this is that with each phase of zircon re-crystallisation that these clasts underwent, the re-mobilised zirconium was preferentially deposited on existing zircon crystals, resulting in the large, multi-stage, inclusion rich, poor quality crystals which dominate these separates. However, the Kober technique was able to provide well constrained data on at least part of the history of all but two (89-S-23 and 89-S-26) of the clasts from which zircons were separated. Table 3.2 summarises the zircon and Sm-Nd data on the Shamva Clasts.

Sample	Pb-Pb Zircon			Sm-Nd		
	Rim	*Main Phase*	*Core*	T_{CHUR}	T_{DM}	$\varepsilon_{ND}(T)$
Group 1						
89-S-14	2,800 ± 20 Ma		3,197 ± 10 Ma	2.82 Ga	2.98 ± 0.003 Ga	- 0.20 *(at 2.8 Ga)*
89-S-23	≈ 2,800 Ma	≈ 2,920 Ma	> 3,182 Ma	3.04 Ga	3.16 ± 0.008 Ga	+ 2.16 *(at 3.2 Ga)*
Group 2						
89-S-12	≈ 2,680 Ma	2,921 ± 10 Ma	*Not Present*	2.98 Ga	3.13 ± 0.004 Ga	- 0.61 *(at 2.92 Ga)*
89-S-19	≈ 2,650 Ma	2,920 ± 30 Ma	> 2,987 Ma	3.03 Ga	3.17 ± 0.003 Ga	-1.23 *(at 2.92 Ga)*
89-S-25	≈ 2,670 Ma	2,924 ± 5 Ma	> 3,116 Ma	3.08 Ga	3.20 ± 0.003 Ga	-1.99 *(at 2.92 Ga)*
89-S-26	*No zircon data*			3.20 Ga	3.34 ± 0.002 Ga	

Table 3.2 Summary table of Pb-Pb zircon data and Sm-Nd T_{CHUR}, T_{DM} & ε_{Nd} (at the time of the growth of the dominant phase of zircon) for the Shamva clasts.

The Sm-Nd T_{DM} model age of 3.34 Ga for sample number 89-S-26 represents the oldest continental material yet recognised from the Shamva region. An early continental crust may also be indicated by the presence of rare gneissic clasts, which have obviously undergone a high strain event not recorded by the unfoliated granitoid clasts. Alternatively, this deformation may have occurred during one of the events recorded in the clasts (during which time the source granitoids of the clasts were in a low-strain regime),

and the rarity and small size of gneissic clasts may reflect the lower survival potential of foliated rocks during weathering and transport, rather than their derivation from a rare, older source.

Zircon core ages and Sm-Nd T_{DM} model ages in both groups of clasts from Shamva suggest that ≈ 3,200 Ma ago, there was a period of continental growth, with the intrusion of high-alumina TTG granitoids. The Sm-Nd model age of clast 89-S-26 suggests that this event represented growth of a pre-existing continental nucleus, rather than the formation of a new continental mass.

As Archaean high-alumina TTG suites represented new additions of material to the continental crust (Barker and Arth, 1976; Martin, 1986; Rapp et al., 1991; Luais and Hawkesworth, 1994), it should be possible to use the ε_{Nd} values of the clasts to investigate the degree of depletion of the Archaean mantle. For the clast 89-S-23, the Sm-Nd T_{DM} (3.16 Ga) and zircon ages (≥ 3.17 Ga) are in good agreement with each other, and this clasts' depleted ε_{Nd} value of +2.16 is typical for mid-Archaean mantle derived material (Chase and Patchett, 1988). However, 89-S-14 contains two populations of zircons, one representing the crystallisation age of the clast at 2,800 ± 20 Ma, and cores dating back to 3,197 ± 10 Ma. The Sm-Nd T_{DM} model age of the clast is intermediate between the two zircon ages, at 2.98 Ga. One model is that the material now making up the clast was added to the continental crust in two stages, the first at 3.2 Ga, which was then assimilated into a magma added to the crust at 2.8 Ga. It may be speculated that the ≈3.2 Ga and ≈2.8 Ga components were both Archaean high-alumina TTG granitoids, and the resulting mixture simply produced an average, typical Archaean high-alumina TTG granitoid, apparently derived from the mantle in a single event. The age data for this clast therefore emphasises the need for caution where data from only one isotopic dating system is available, especially in the construction of models for the growth (and rates of growth) of continental

crust through time. Although this rock was formed by mixing of at least two separate components, derived from the mantle 400 Ma apart, a more limited data set might have been erroneously interpreted as representing a single, large, crust forming event.

The group 2 clasts record a major magmatic event at ≈ 2,925 Ma, with ages of 2,921 ± 10 Ma (89-S-12) 2,920 ± 30 Ma (89-S-19), 2,924 ± 5 Ma (89-S-25) (table 3.2), all identical within error. The combination of the similar chemistry and crystallisation ages of these clasts strongly indicates that they were formed during the same event, and justifies combining the data from all 3 of these clasts. Figure 3.17 shows this combined data, from which the date of crystallisation is determined to be 2,925 ± 10 Ma. The presence of zircon cores in group 2 clasts with minimum ages of 3,116 Ma, enriched ε_{Nd} at 2,925 Ma, and whole rock Sm-Nd T_{DM} model ages of up to 3.20 Ga conclusively demonstrates that protoliths of these clasts had crustal histories of several hundred million years before the magmatic event they record at 2,925 Ma.

REE modelling in section 3:2.3 suggested that the group 2 clasts were formed by partial melting of group 1. However, as one of the group 1 clasts (89-S-14) contains a large component dating from ≈ 2,800 Ma, 125 Ma younger than the main phase of crystallisation in the group 2 clasts, the geochronology of these clasts has shown that Shamva group 2 cannot have been produced by the melting of Shamva group 1, but the melting of material compositionally similar (high Al TTG) granitoids is consistent with the data, which requires the incorporation of older material within the group 2 clasts at the time of the main (magmatic) phase of zircon crystallisation that they record at 2,925 Ma. However, ε_{Nd} for the group 2 clasts ranges from -0.61 to -1.99 at 2.925 Ga (table 3.2), suggesting that all these clasts cannot have been derived by partial melting of the same source.

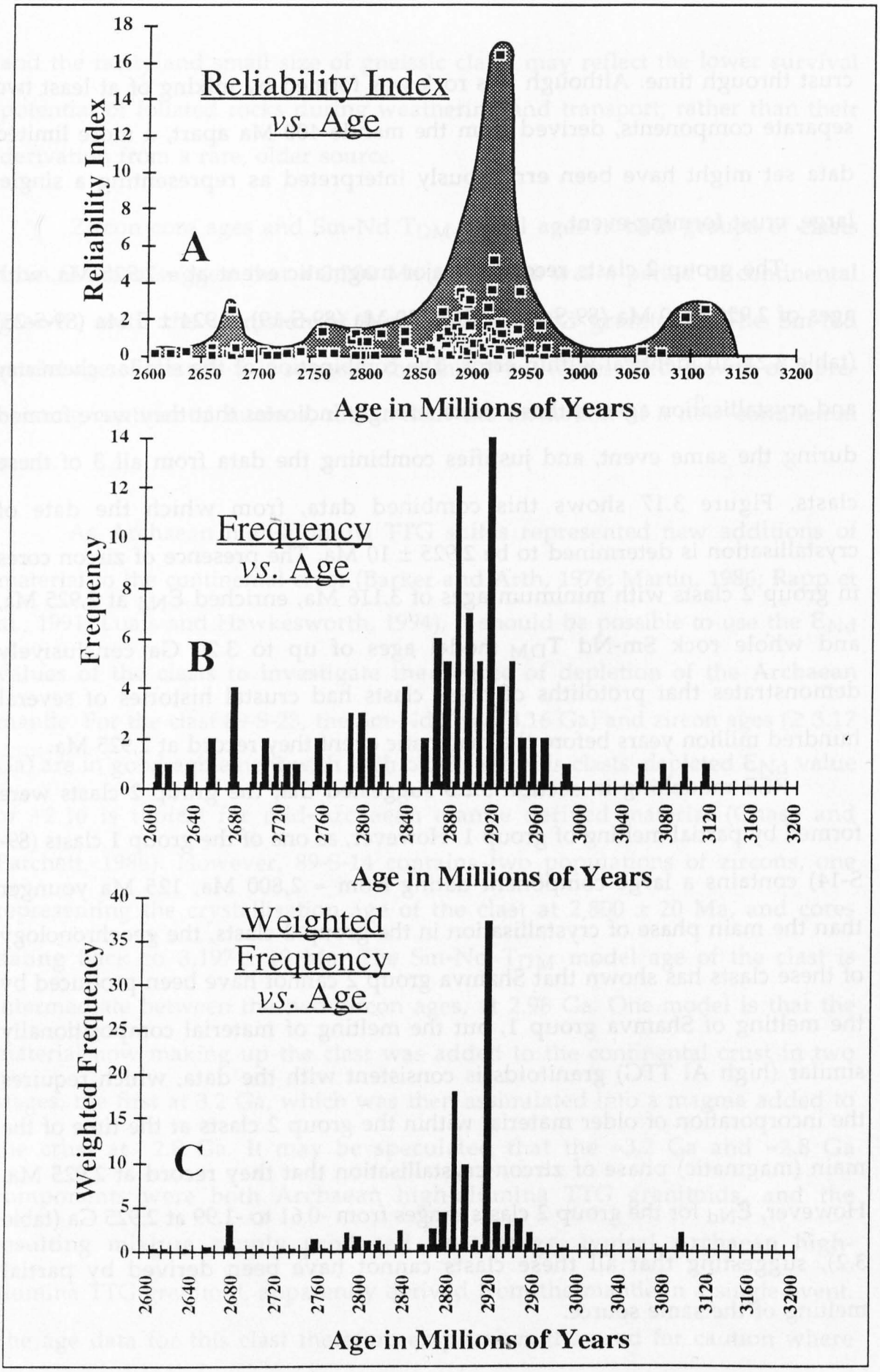

Figure 3.17 Combined zircon data for the Shamva group 2 clasts (a) Index of reliability of data vs. age scatter graph; (b) Frequency within a 10 Ma interval vs. age histogram; (c) Weighted frequency vs. age histogram.

Therefore, possible mechanisms for their formation are derivation of crustal re-melts from a source region which included varying proportions of granitoids chemically similar to those of group 1 intruded between 3.2 and 2.925 Ga, but not present in the sample set of clasts, or mixing of crustal re-melts with varying proportions of magmas derived from the mantle during the 2.925 Ga event.

There is a broad correlation between ε_{Nd} values and the abundance of zircon cores in the samples, with the sample with the most negative ε_{Nd} at 2.925 Ga, 89-S-25, also containing the most abundant cores, which have a minimum age of 3,115 Ma. Therefore, mixing between crustal re-melts and mantle derived melts is the preferred origin of these clasts, as the correlation between core abundance and ε_{Nd} would not exist if the clasts were entirely produced by intra-crustal re-melting.

The 2.925 Ga event was followed by a further magmatic event at 2,800 ± 20 Ma. This event involved an input of new material into the continental crust, and was responsible for the formation of the group 1 clast 89-S-14 (figure 3.11). This clast contains two populations of zircons, one representing the crystallisation age of the clast at 2,800 ± 20 Ma, and an inherited population of zircons, dating back to 3,197 ± 10 Ma which, as has already been discussed, appears to have been a major period of continental growth in Northern Zimbabwe. This is the only clast in which the white "rim" phase, present in most of the clasts could be accurately dated. It should not be assumed that all the rims were formed at the same time, or by the same process, as in this clast. For example, in some clasts the rims may represent late stage hydrothermal growth in the same event that caused the crystallisation of the main phase of zircon. Such late stage rims (or discrete crystals) are often rich in incompatible elements such as U and Th, and therefore become metamict and turbid, and thus of different appearance to "core" phases formed slightly earlier in the crystallisation of a magma body.

The group 2 clasts all indicate a (poorly defined) crystallisation event which occurred between ≈2,650 and≈ 2,680 Ma. Zircons of this age typically had simple typologies, and were of very low quality - turbid in appearance and rich in inclusions, consistent with their growth under metamorphic, rather than magmatic conditions. This age corresponds well to lower amphibolite facies metamorphism to which the sediments were subjected, the peak of which has been estimated to have occurred at ≈ 2,650 Ma (Jelsma, 1993). Alternatively, this final episode of zircon crystallisation may have been from hydrothermal fluids related to the gold mineralisation which also occurred in Shamva at this time.

3:3 LOCALITY 2 - CHINHOYI

The second area from which samples were collected is located on the north-western margin of the Archaean craton of Zimbabwe, near the town of Chinhoyi (see figure 3.1 for the location of Chinhoyi, and figure 3.18 for a locality map). Samples were collected from the "Eldorado Conglomerate" in basal Shamvaian sediments (see section 3:1) exposed on the bed of the Hunyani River, 1 mile to the east of Chinhoyi (Figure 3.18). This locality is within 5 km of the front of the Early- to Mid-Proterozoic (Treloar, 1988) Magondi Mobile Belt, and was chosen in order to study any possible chemical and geochronological differences between the central (at Shamva) and marginal (at Chinhoyi) portions of the North of the Zimbabwe craton at the time that the Shamvaian sediments were deposited (2.67 Ga, Jelsma, 1993).

Photograph 3.8 A large clast in the Eldorado conglomerate, with a sledge-hammer for scale. Note the tectonic deformation of the clast and the surrounding conglomerate.

The surface of the exposure is water smoothed, and often covered in a brown desert varnish of oxides released by weathering. Sediments at this

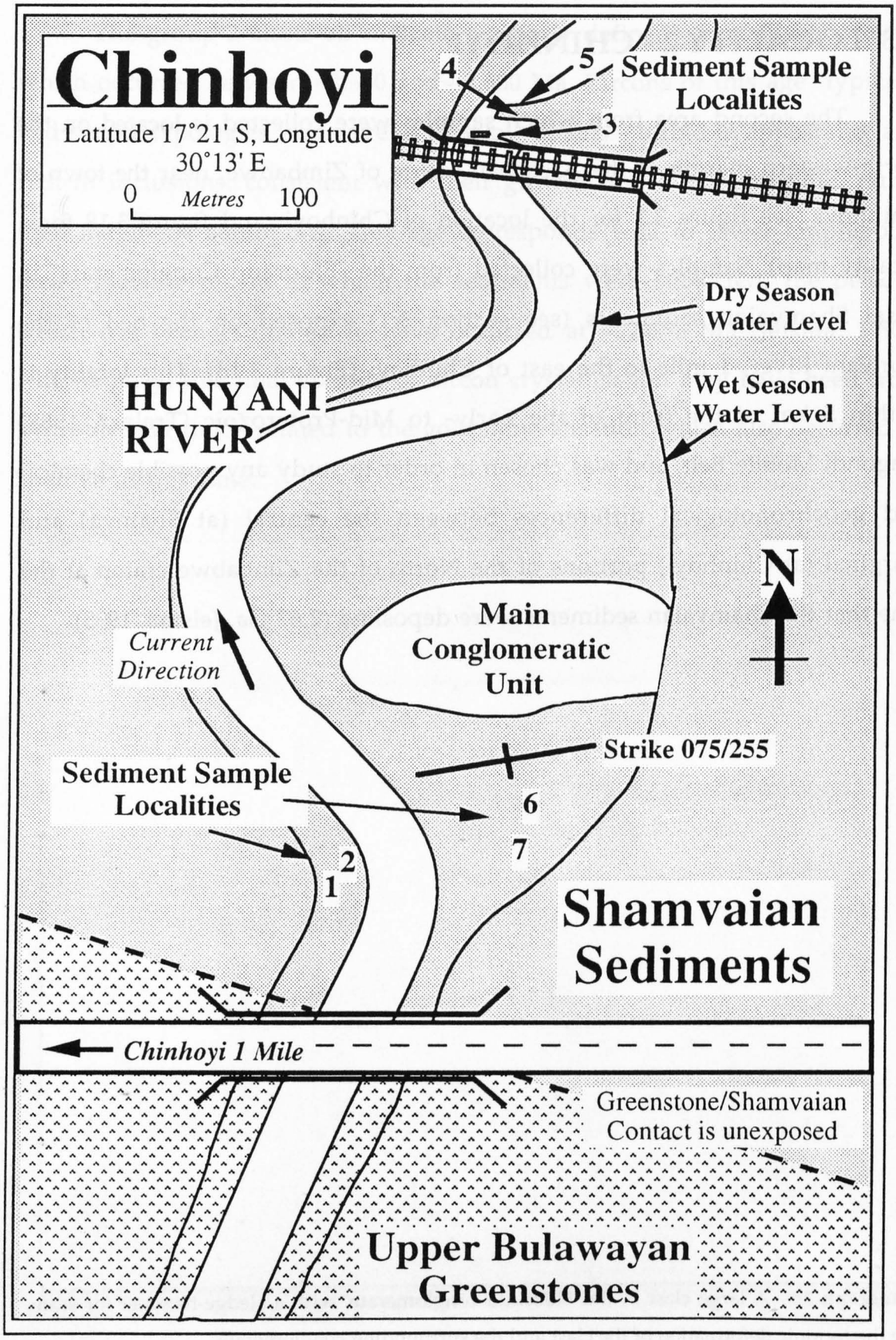

Figure 3.18 Geological sketch map of the Chinhoyi sample locality

locality are vertically bedded and strike at 075/225°. In contrast to the sediments at Shamva (section 3:2), those at Chinhoyi are strongly tectonised, with a variable degree of deformation across the outcrop. The more strongly deformed portions of the conglomerate are host to gold mineralisation, and the Eldorado mine was once one of the largest in Zimbabwe, producing a total of 486,790 ounces of gold before its closure in 1941 (Stagman, 1961). The deformation of the conglomerate makes a determination of whether it was originally matrix or clast supported difficult, but the high proportion of matrix material present does suggest that the conglomerate was originally matrix supported. The clasts are elongated in the direction of strike, often boudinaged, and may even be wrapped around some of the larger boulders (photograph 3.8). A foliation is present, which varies from a fine, slatey cleavage in the fine grained sediments at the base of the sequence (sample locality 1) to an anastomosing, slickensided set of fractures wrapping around the clasts within the coarse conglomeratic horizons. The clasts range in size from small pebbles only a few cm in diameter to boulders 70 cm in diameter. The larger clasts are dominantly medium to coarse grained, unfoliated granitoids, with subsidiary fine grained siliceous rocks (which shall be referred to as felsites so as not to make implications about their origins by nomenclature), banded ironstone, vein quartz, and rare greenstone clasts. There are no foliated granitoid clasts. 11 clasts were collected, dominantly of coarse-grained granitoids, but including banded ironstone and felsite. The clasts were selected primarily on the grounds of minimal deformation and shearing, together with a requirement that the granitoids should be of sufficient size (≥ 1.5 kg) to supply a reasonable quantity of zircons for dating.

3:3.1 The Chinhoyi Sediments

The sediments at Chinhoyi consist of a single conglomeratic horizon set within poorly sorted greywackes (figure 3.18). The greywackes (and matrix within the conglomeratic horizon) are composed of angular grains of quartz,

saussuritised plagioclase and lithic fragments set in a turbid, fine grained matrix of quartz, feldspar, carbonate, chlorite, clay minerals and opaques. The metamorphic grade is low, with green biotite as the dominant metamorphic mineral. Other metamorphic minerals present include muscovite, chlorite and epidote. The degree of deformation seen in thin section is variable, from extremely well developed c-and s-fabrics (defined by metamorphic biotite) in the fine grained sediments of locality 1, indicating a considerable amount of shearing, to irregularly spaced anastomosing fractures, again infilled with biotite, together with chlorite, carbonate and dynamically recrystallised quartz, within the coarser horizons.

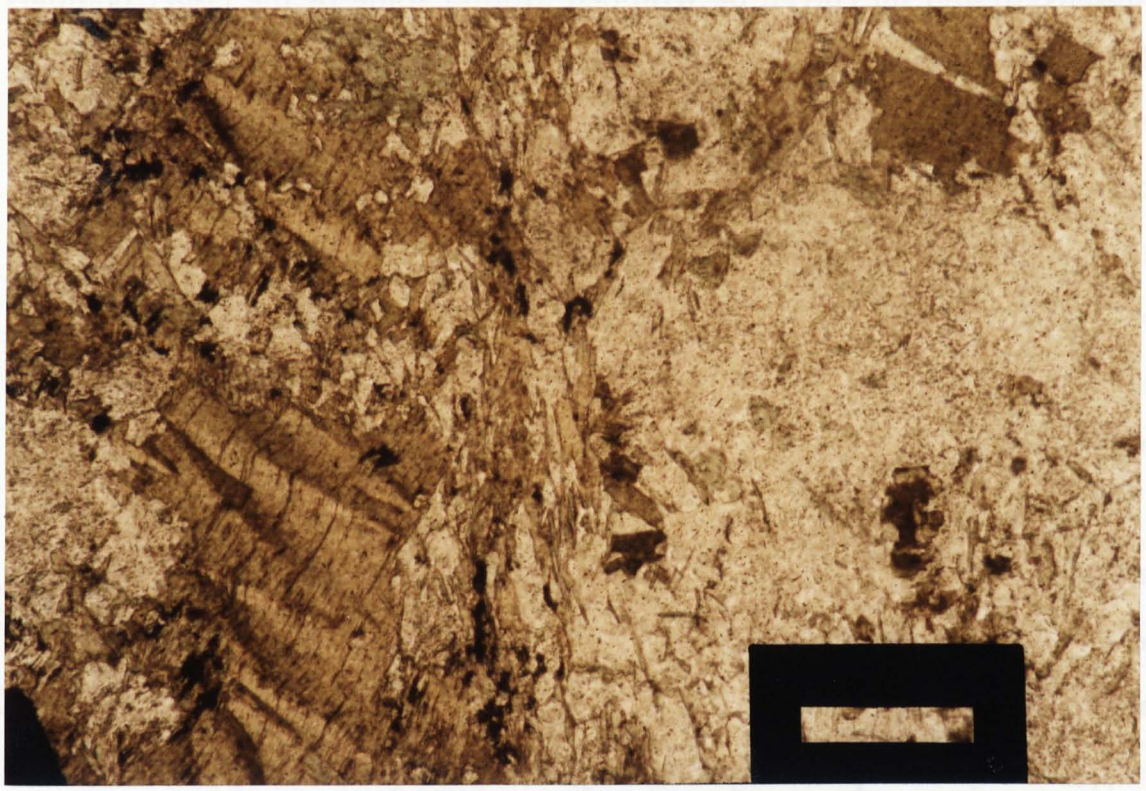

Photograph 3.9 Photomicrograph of the sediment from Chinhoyi. The metamorphic assemblage is dominated by greenish biotite (kinked by later deformation at the left of the picture) and chlorite. Scale bar ≈ 0.5 mm.

Eight samples of the sediments were analysed for their major and trace elements (data tabulated in appendix A) from three stratigraphic levels. Four samples were collected from below the conglomeratic unit, one sample of matrix from the conglomeratic horizon was analysed, and three samples of

sediment from above the conglomerates were also collected. The sample from the conglomerate itself and below are notable for their extreme heterogeneity. Silica contents vary from 54.3 to 69.2%, total ferromagnesian contents (Fe_2O_3(T)+MgO+TiO_2) vary from 7.3 to 22.5%. Samples collected from within a few metres of each other vary from extremely Na_2O-rich (89-C-2 contains 7.0% Na_2O) to having Na_2O contents below the detection limits of XRF analysis (89-C-1). Cr/Th ratios vary from 3.4, an order of magnitude below the typical range of mid-Archaean values (25 to 110, Condie and Wronkiewickz, 1990 - see section 3:2.1 for a discussion on the use of this ratio) to 252, a high value for the mid-Archaean. By contrast, the samples collected from above the conglomerate are relatively homogeneous, both in terms of major and trace elements. They are more siliceous, with a restricted range in SiO_2 (71.3 to 73.3% SiO_2) and total ferromagnesian content (5.2 to 6.0%). They are Na_2O-rich, with Na_2O/Al_2O_3 ratios from 0.23 to 0.28 (well above an average Archaean value of 0.19) and K_2O/Na_2O ratios from 0.48 to 0.62 (below the average Archaean value of 0.76 - average sedimentary compositions from Taylor and McLennan, 1985), making them more sodic than the Shamva sediments, for which Na_2O/Al_2O_3 ratios range from 0.20 to 0.24 and K_2O/Na_2O ratios from 0.52 to 0.56. Cr/Th ratios are low (18.6 to 19.7) for sediments of this age, indicating a smaller than average contribution to these sediments from greenstone-belt derived mafic rocks (Condie and Wronkiewickz, 1990). There is therefore a progression within this sedimentary sequence from an initial highly immature, chaotic mixture of coarse material derived from both the underlying greenstones and a surrounding terrain of sodic granitoids, to a finer, more mature, texturally better sorted and chemically more homogeneous sediment, with a greater average contribution from the granitoid terrain. A simple model for the increasing maturity of the sediment is deepening of the basin in which the sediment was deposited, resulting in increasing distances of sediment transport, and deposition in progressively lower energy environments at this

site of sedimentation. A similar model has also been invoked for the progression of sedimentary sequences at Shamva (section 3:2.1).

3:3.2 Chemistry and Petrography of the Chinhoyi Clasts

The granitoid clasts are coarse grained, with mineralogy dominated by plagioclase feldspar and quartz with minor amounts of alkali feldspar (microcline) and perthites. Biotite is the dominant mafic phase. Accessory minerals include zircon, sphene, apatite, magnetite and pyrite. The clasts are heavily weathered, with saussuritisation of plagioclase and breakdown of biotite to chlorite and opaques. Deformation of the clasts was accommodated plastically, largely through dynamic recrystallisation of quartz, but some brittle deformation of the clasts has also occurred. Fracture zones, infilled with biotite, chlorite and dynamically recrystallised quartz cut the clasts, and in some clasts these fractures have opened and the clasts have boudinaged.

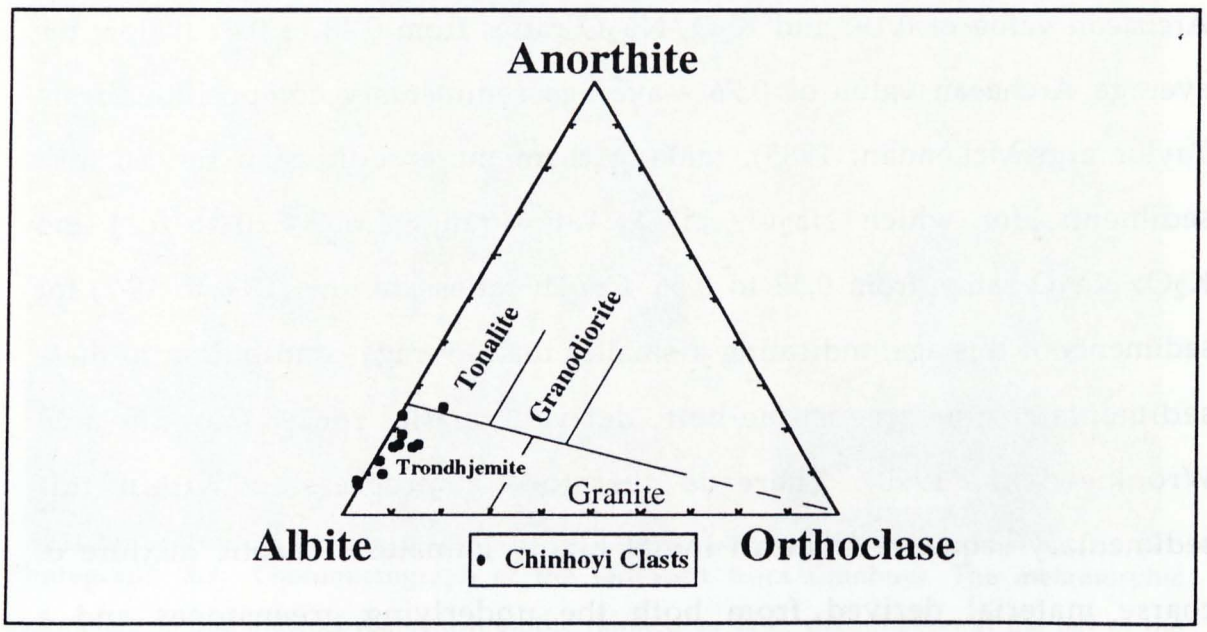

Figure 3.19 Feldspar ratio plot using Anorthite-Albite-Orthoclase CIPW normative compositions for the Chinhoyi clasts (after O'Connor, 1965)

The major element chemistry of the clasts (tabulated in appendix A, along with trace element and REE analyses) shows them to be members of the TTG-Suite (figures 3.19 and 3.20). They may be divided into two groups on the basis of their silica content.

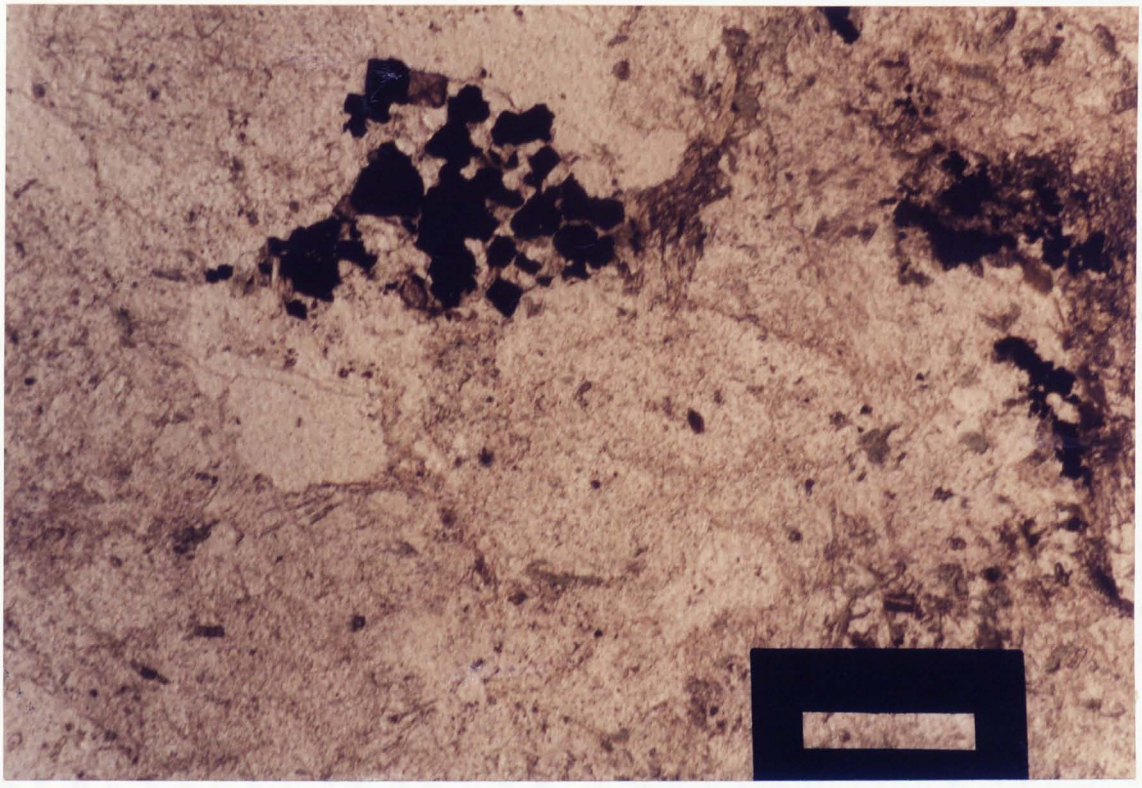

Photograph 3.10 Photomicrograph of the Chinhoyi group 1 clast 89-C-15, showing the severe low-grade alteration common to all the Chinhoyi clasts, with the breakdown of mafic phases to chlorite and opaques, and saussuritisation of plagioclase. Note the zircon crystals within the group of mafics at the top of the picture.

3:3.2 a Group 1

There are 6 samples in this group, with SiO_2 contents ranging from 68.1 to 72.2 % SiO_2. Al_2O_3 and CaO contents both decrease with increasing SiO_2 but all the other elements show rather flat trends. The group has an Al_2O_3 content of > 15% at 70% SiO_2, which classifies these clasts as members of the high-alumina Archaean TTG group of Barker and Arth (1976). The total content of ferromagnesian elements (Fe_2O_3(T)+MgO+TiO_2) is low, ranging from 4.0 to 5.3%, although at the upper limit for Archaean TTG suites of ≤ 5% (Martin, 1986). The less mobile major elements (Al_2O_3, TiO_2, P_2O_5) have trends which closely follow those of Shamva group 1 (figure 3.20).

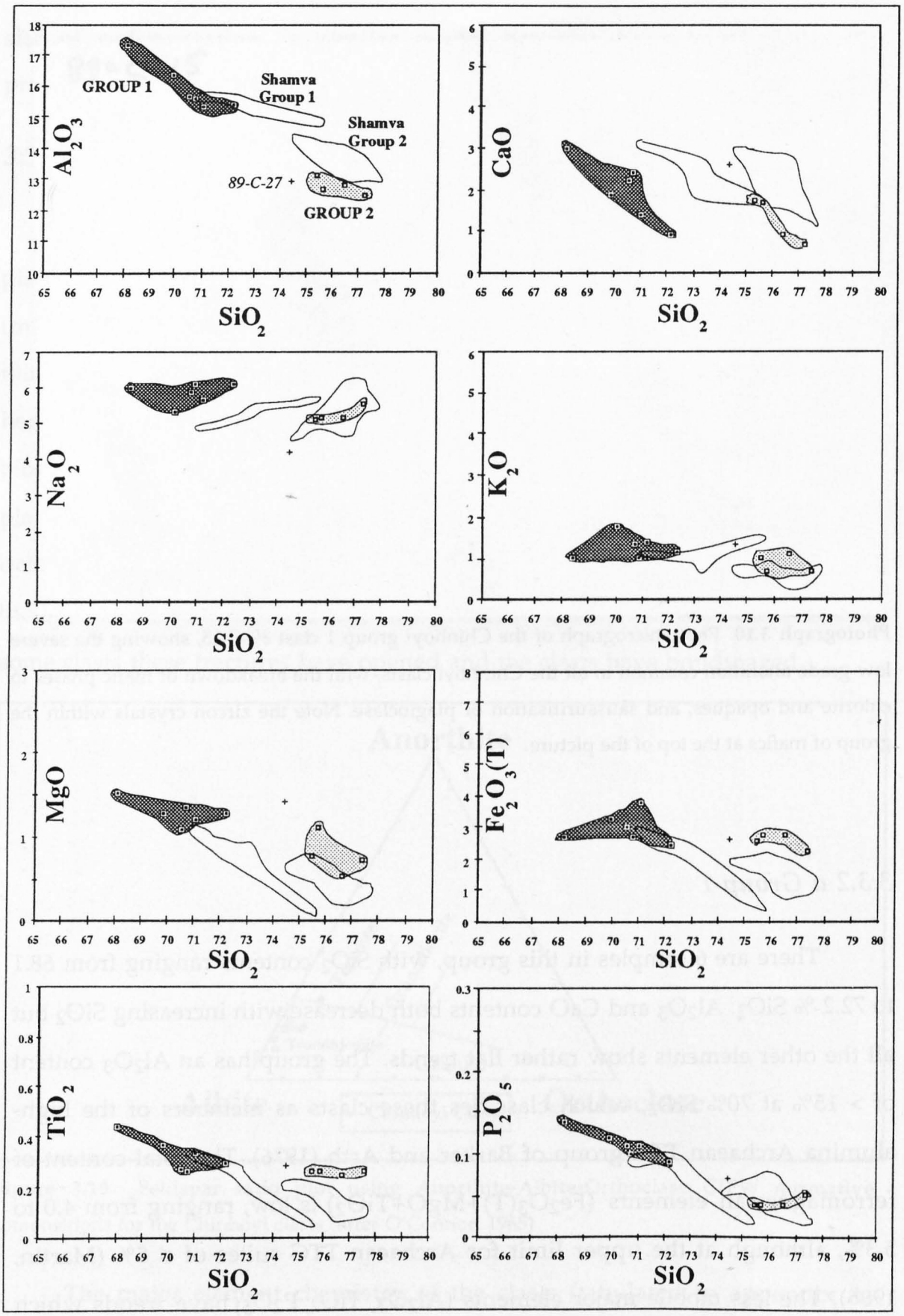

Figure 3.20 Major elements vs. silica for the Chinhoyi clasts, showing 2 clearly defined groups in terms of silica content, and the fine grained "felsite clast 89-C-27, which plots with apparent affinities to group 2. The unshaded fields are the Shamva group one and two clasts.

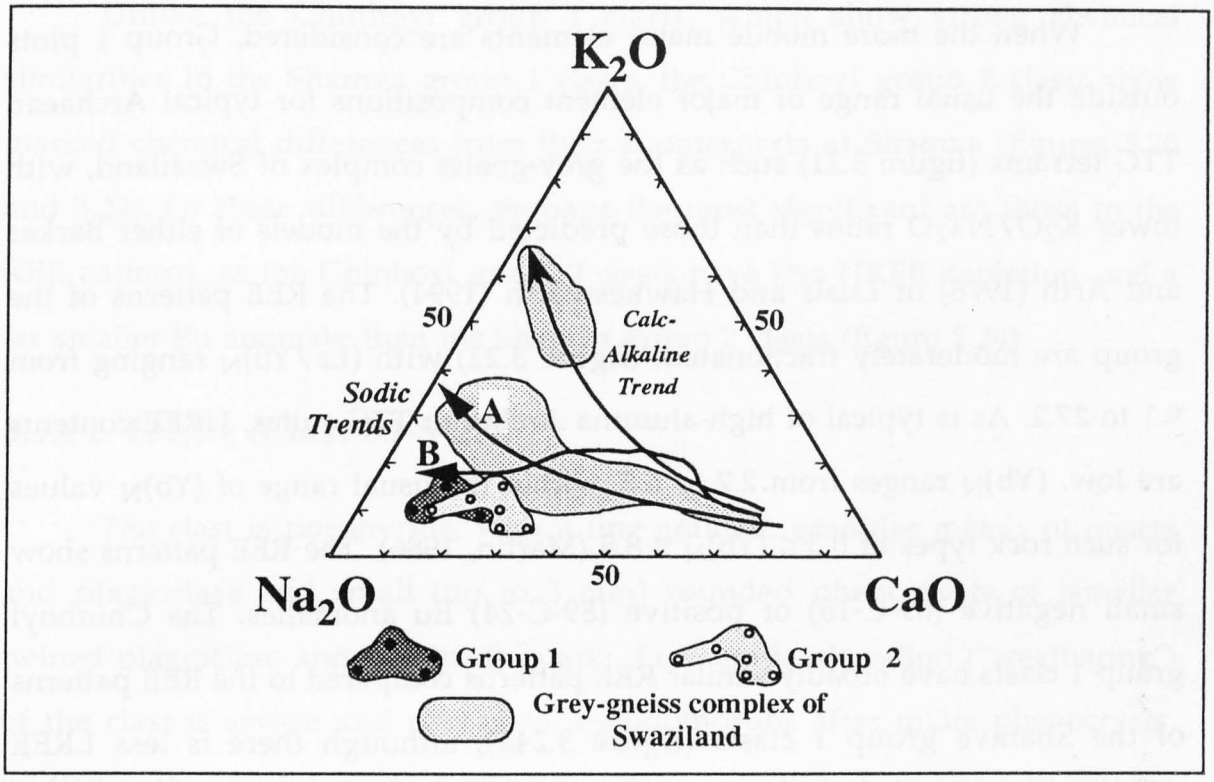

Figure 3.21 K_2O-Na_2O-CaO plot for the group 1 and group 2 Chinhoyi clasts, showing the sodic (A) and calc-alkaline trends (Luais and Hawkesworth, 1994) and the trondhjemitic trend (B) of Barker and Arth (1976). Data fields of the grey-gneiss complex of Swaziland (Hunter et al. 1978 & 1984) are plotted for comparison. Both groups are notably displaced towards the Na_2O axis, reflecting a K_2O-loss due to weathering.

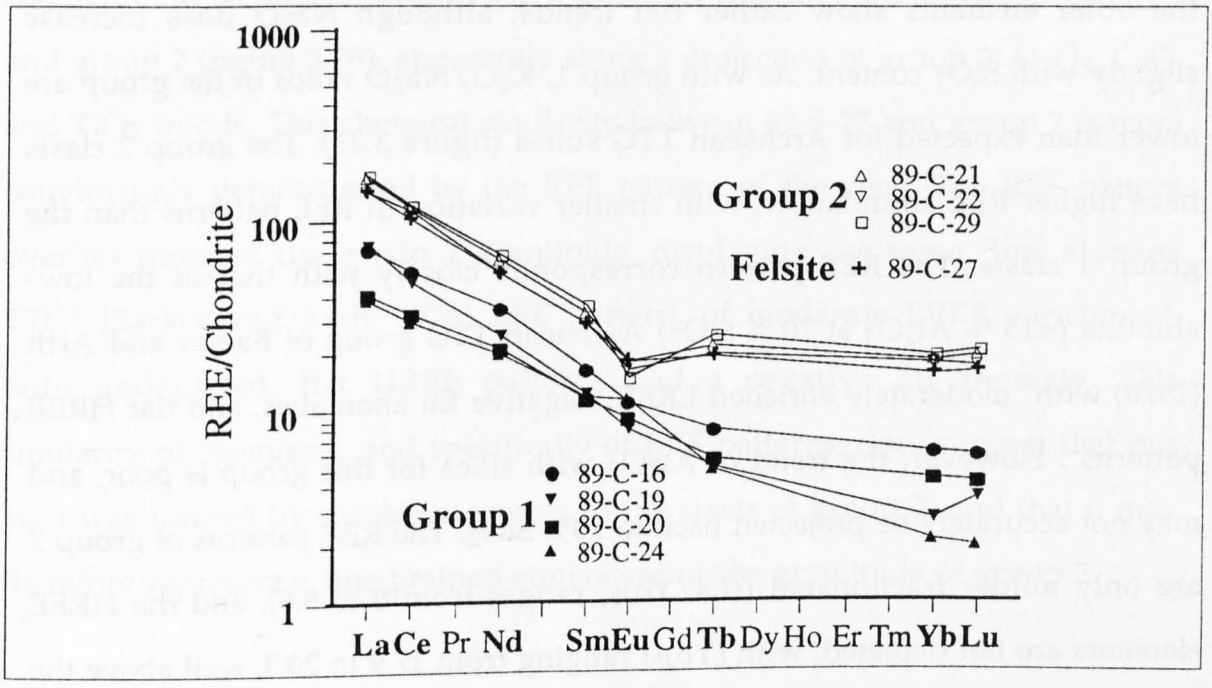

Figure 3.22 Chondrite normalised REE plots for the group 1 and 2 Chinhoyi clasts, together with the "felsite" clast 89-C-27, which has a very similar REE pattern to the group 2 clasts.

When the more mobile major elements are considered, Group 1 plots outside the usual range of major element compositions for typical Archaean TTG terrains (figure 3.21) such as the grey-gneiss complex of Swaziland, with lower K_2O/Na_2O ratios than those predicted by the models of either Barker and Arth (1976) or Luais and Hawkesworth (1994). The REE patterns of the group are moderately fractionated, (figure 3.22) with $(La/Yb)_N$ ranging from 9.1 to 27.2. As is typical of high-alumina Archaean TTG-suites, HREE contents are low. $(Yb)_N$ ranges from 2.7 to 6.2, within the usual range of $(Yb)_N$ values for such rock types of $0.3 \leq (Yb)_N \leq 8.5$ (Martin, 1986). The REE patterns show small negative (89-C-16) or positive (89-C-24) Eu anomalies. The Chinhoyi group 1 clasts have broadly similar REE patterns compared to the REE patterns of the Shamva group 1 clasts (figure 3.24a), although there is less LREE enrichment, and a greater range of HREE contents.

3:3.2 b Group 2

There are four clasts in this group, with SiO_2 contents ranging from 75.5 to 77.4% SiO_2. Al_2O_3 and CaO contents both decrease with increasing SiO_2, and the other elements show rather flat trends, although Na_2O does increase slightly with SiO_2 content. As with group 1, K_2O/Na_2O ratios in the group are lower than expected for Archaean TTG suites (figure 3.21). The group 2 clasts have higher REE abundances, with smaller variation in REE patterns than the group 1 clasts. The REE pattern corresponds closely with that of the low-alumina (<15 % Al_2O_3 at 70 % SiO_2) Archaean TTG group of Barker and Arth (1976) with "moderately enriched LREE, negative Eu anomalies, and flat HREE patterns". However, the trend of Al_2O_3 with silica for this group is poor, and may not accurately be projected back to 70% SiO_2. The REE patterns of group 2 are only mildly fractionated ($(La/Yb)_N$ ranges from 8 to 8.8), and the HREE elements are not depleted, with $(Yb)_N$ ranging from 17.9 to 20.3, well above the usual range of $(Yb)_N$ values for Archaean TTG suites.

Unlike the Chinhoyi group 1 clasts, which show strong chemical similarities to the Shamva group 1 clasts, the Chinhoyi group 2 clasts show marked chemical differences from their counterparts at Shamva (figures 3.20 and 3.24). Of these differences, perhaps the most significant are those in the REE patterns, as the Chinhoyi group 2 clasts have less HREE depletion, and a far smaller Eu anomaly than the Shamva group 2 clasts (figure 3.24).

3:3.2 c Felsite (Clast 89-S-27).

The clast is porphyritic, with a fine grained, granular matrix of quartz and plagioclase and small (up to 3 mm) rounded phenocrysts of lamellar twined plagioclase and (strained) quartz. Low grade alteration ("weathering") of the clast is severe and pervasive. Pseudomorphs after mafic phenocrysts, infilled with a turbid mixture of green biotite, quartz, calcite and fine-grained clay minerals are present, but none of the original phenocryst material remains. Given the severity of the low grade alteration, little may be inferred from the major element chemistry of this sample, other than to say that the clast appears to represent a member of a sodic, rather than calc-alkaline fractionation sequence, occupying a position intermediate between group 1 and group 2 (figure 3.20), apparently along a projection of group 2 Al_2O_3, CaO, and TiO_2 trends. This chemical similarity between 89-S-27 and group 2 is more convincingly demonstrated by the REE pattern of the clast. The REE pattern overlies those of the group 2 granitoids, displaying the same "low alumina TTG" (Barker and Arth, 1976) REE pattern, of moderate LREE enrichment, with undepleted, flat HREE patterns and a negative Eu anomaly. This similarity of chemistry, and specifically of REE patterns, does suggest that this clast was formed by similar processes to the clasts of group 2, and that it may therefore represent a fine-grained equivalent of the granitoids of group 2.

3:3.3 Petrogenetic Model for the Formation of the Chinhoyi Group 1 and 2 Clasts

Figure 3.21 shows that the clasts from both groups have anomalously low K_2O/Na_2O ratios compared with other Archaean TTG suites, such as the Ancient Gneiss complex of Swaziland. The low K_2O content in the clasts from both groups suggests that the low K_2O/Na_2O ratios are due to a loss of K_2O rather than a gain in Na_2O. K_2O loss is supported by the low Rb/Sr ratios of all the clasts (within the range 0.06 to 0.27 for group 1 and 0.07 to 0.27 for group 2) which are normally expected to rise with increasing silica content within a trondhjemitic sequence. Unlike the clasts analysed from Shamva, where the greatest K_2O-loss is confined to a single group, and therefore must have occurred before the sediment was deposited (section 3:2.2), all of the clasts at Chinhoyi have undergone similar degrees of alteration. This alteration may have been in response to one or more of three factors: (a) Archaean weathering, (b) metamorphism, or (c) hydrothermal alteration of the conglomerate at the time that the gold mineralisation occurred. In view of this severe alteration, and possible mobilisation of major elements such as Na, K and Ca, the proposed models are based on the relatively immobile REE.

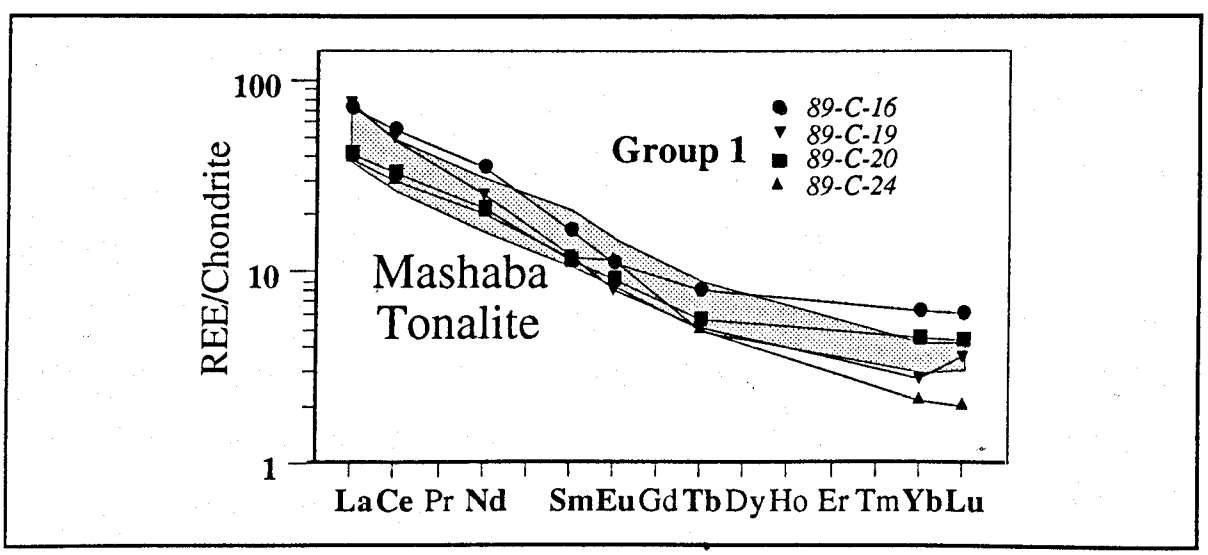

Figure 3.23 Chondrite normalised REE plots of the Chinhoyi group 1 clasts compared to the Mashaba Tonalite (shaded field) (Luais and Hawkesworth, 1994).

Group 1

The similarity in REE and (immobile) major element chemistry (figures 3.24a and 3.20) for the Chinhoyi group 1 clasts and the Shamva group 1 clasts strongly suggests that these two groups of clasts were formed by very similar processes. The REE patterns of these two groups correspond closely to typical Archaean high-alumina TTG granitoids such as the Mashaba Tonalite of Southern Zimbabwe (Figure 3.23). The most widely accepted models proposed for the generation of such granitoids suggest that they are formed by 10 to 40% partial melting of amphibolite-facies metabasalt at pressures of ≈16 Kbar, with residual garnet (± hornblende) buffering the HREE content of the melt at a low level (Barker and Arth, 1976; Martin 1986; Drummond and Defant, 1990; Rapp et al., 1991; Luais and Hawkesworth, 1994).

The involvement of hornblende in the formation of the Chinhoyi group 1 clasts is indicated by the positive Eu anomaly of 89-Ć-24, and the higher (chondrite normalised) abundance of Lu than Yb in 89-C-19, characteristic of a process of melt formation in which the melt was separated from hornblende, which has a negative Eu anomaly, and a lower partition coefficient for Lu than Yb (Hanson, 1978). This could have been achieved by either partial melting or fractional crystallisation. This model for the generation of the melts which eventually formed the group 1 clasts requires that they originated at depths greater than the thickness of average continental crust, by partial melting of a mafic precursor. Therefore, the group 1 clasts represented a new addition of material to the continental crust.

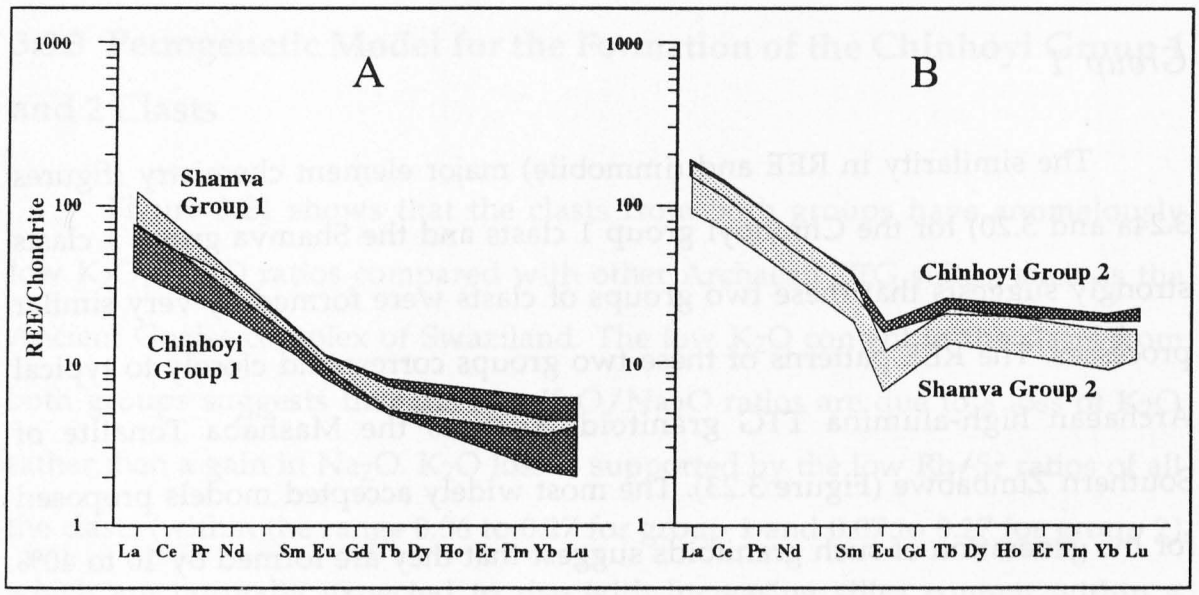

Figure 3.24 Chondrite normalised REE patterns of the Chinhoyi and Shamva (A) group 1 and (B) group 2 clasts, clearly showing the greater HREE enrichment and smaller negative Eu anomaly of the Chinhoyi group 2 clasts compared to the Shamva group 2 clasts.

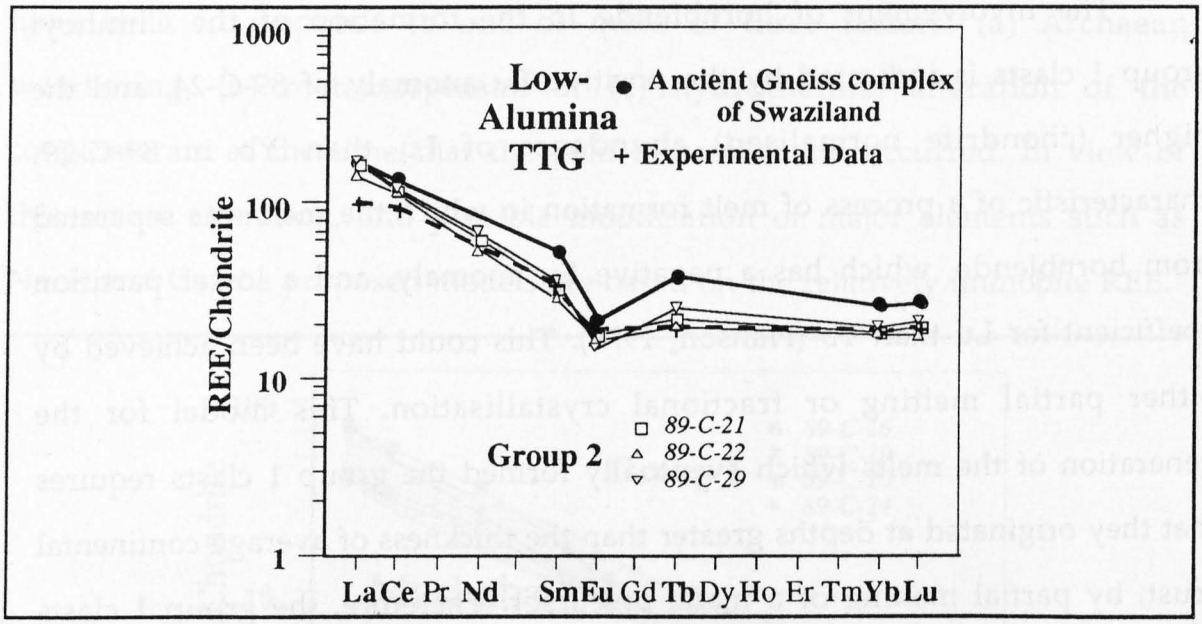

Figure 3.25 Chondrite normalised REE patterns of the Chinhoyi group 2 clasts compared with a "Low-Alumina Trondhjemite" (Barker and Arth, 1976) from the Ancient Gneiss complex of Swaziland (bold line)(Data from Condie and Hunter, 1976), and an experimentally produced "Low-Alumina Trondhjemite", produced by partial melting of a metabasite at 8 kbar pressure and 1000°C (dashed line) (Rapp et al. 1991).

Group 2

In terms of major elements, most notably CaO, the group 2 clasts lie on a separate trends to those of the group 1 clasts (Figure 3.20), indicating that the two groups are unlikely to be members of the same suite separated by an artificial silica gap produced by sampling bias. The group 2 clasts of Chinhoyi have higher HREE abundances and smaller Eu anomalies than the group 2 clasts of Shamva (figure 3.24), strongly suggesting that the two groups were formed by different mechanisms. Due to the enriched, flat HREE patterns and small Eu anomaly of Chinhoyi group 2, REE modelling cannot produce the REE patterns of Chinhoyi group 2 from a Chinhoyi group 1 protolith by partial melting or fractional crystallisation processes, without appealing to either minor phase control or high oxygen fugacity (such that Eu was largely oxidised to Eu^{3+} and thus not partitioned into plagioclase). Figure 3.25 shows that the REE patterns of group 2 correspond to those of the low-alumina TTG suite (Barker and Arth, 1976), and therefore the model proposed by these authors for the generation of such granitoids has been applied to these clasts. In their model, Barker and Arth attribute the formation of the Archaean low-alumina suite to partial melting of metabasalts, at pressures within the stability field of plagioclase. The major residual phases are plagioclase and hornblende, and the presence of plagioclase within the restite depletes the melt in Eu, although Eu depletion due to the positive Eu anomaly of restitic plagioclase is slightly counterbalanced by the negative Eu anomaly of restitic hornblende. As garnet is not a major residual phase, the HREE are not depleted. Recent experimental petrology (Rapp et al., 1991) has confirmed that 10% partial melting of a metabasalt at a pressure of 8 kbar does indeed produce a low-alumina TTG melts, with REE patterns very similar to group 2 (figure 3.25) leaving a restite dominantly composed of plagioclase (up to half the total restite) with lesser amounts of amphibole and orthopyroxene. Therefore, like the group 1 clasts, the group 2 clasts also represented a new addition of material to the

continental crust from a mafic protolith, but the partial melting processes which formed the TTG-melts occurred at a higher level.

3:3.4 Zircon Geochronology of the Chinhoyi Clasts.

Samples were selected from each of the groups for zircon geochronology on the basis of sample size (the largest available) and observed zircon in thin section, in order to maximise the quantity of zircons separated. Zircon separates were then prepared from four clasts from group 1 (samples 89-C-15, 20, 24 and 28) and two from group 2 (samples 89-C-21 and 89-C-23), first by heavy liquid floatation, then magnetic purification of the dense separates, by the techniques described in appendix B. Unfortunately, the largest (4.2 kg) of the group 1 clasts, 89-C-24, did not contain sufficient zircon for an accurate age determination to be made. The data from these clasts are discussed individually below, and tabulated in table 3.3 The calculation of ages and calculation (or estimation) of errors is dealt with in Chapter 2.

3:3.4 a Group 1 Clasts

89-C-15.

This 2.1 kg clast provided a large separate of several hundred clear, pinkish crystals with well developed crystal faces and primary (magmatic) inclusions. No cores or rims were observed to this single phase of zircon crystallisation. Six zircons were analysed, in a total of 48 heating steps. Common lead corrected ages were calculated for each heating step, and the results are plotted on figure 3.26 and tabulated in appendix B. These common lead corrected ages produce a single peak, the weighted average of which is 2720 Ma , with a 1 standard deviation error of ± 6 Ma (ages younger than 2,700 Ma were not used in the standard deviation calculation as they are assumed to contain a younger age component).

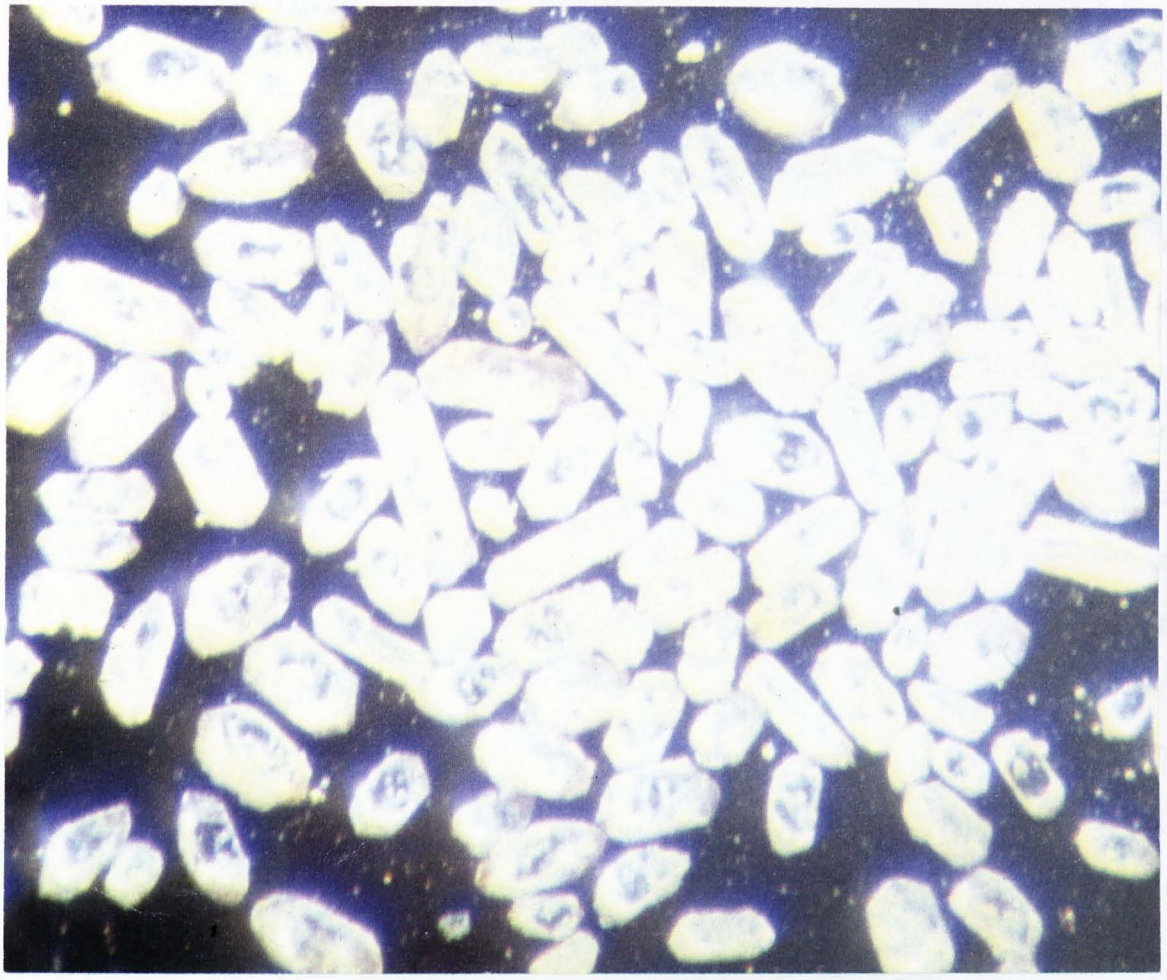

Photograph 3.11 Zircons from the Chinhoyi group 1 clast 89-C-15. The zircons are of high quality, homogeneous in typology, with magmatic inclusions and magmatic growth zoning. Field of view ≈1 mm.

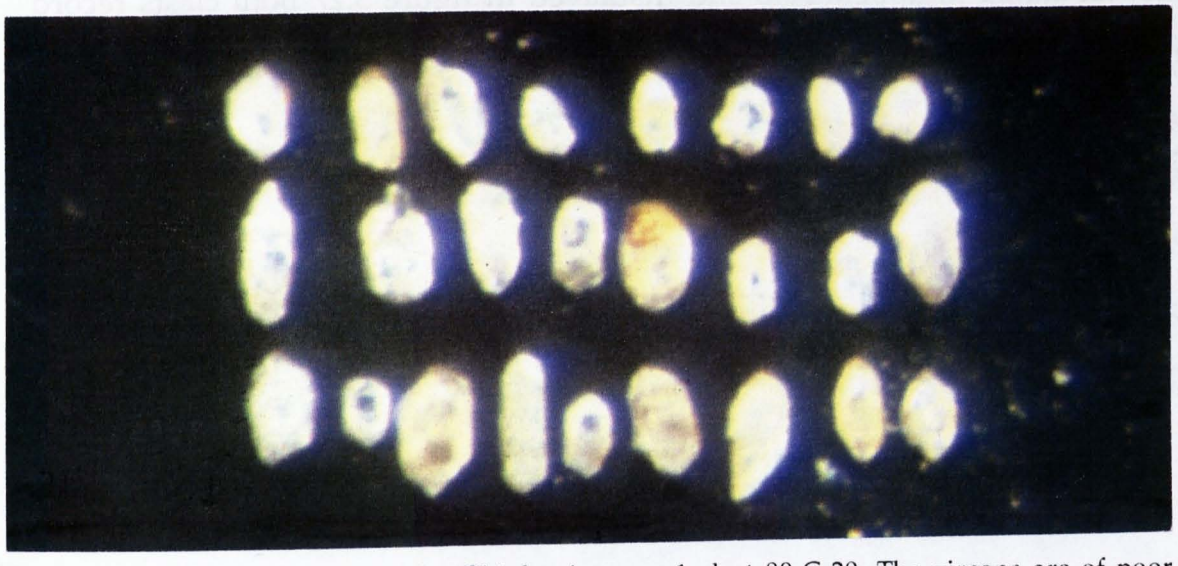

Photograph 3.12 Zircons from the Chinhoyi group 1 clast 89-C-20. The zircons are of poor quality, and many show irregular overgrowths of a second generation of zircon. Field of view ≈ 1mm.

89-C-20 and 89-C-28

These clasts (1.8 and 1.5 kg respectively) produced only small quantities of low-quality zircons, poorly faceted, and with internal reflections which suggested the presence of cores. The small size of the crystals meant that a large proportion of the crystal had to be broken down to baddeleyite in each heating step if sufficient Pb was to be emitted for an accurate analysis to be made. Therefore, with only one to three heating steps possible from each zircon, the possibility of resolving the true ages of the cores and rims was very much reduced. In order to increase the resolution of the core and rim ages by increasing the number of heating steps, it was necessary to decrease the duration of the heating steps. Therefore, several (up to 8) zircons were loaded onto each filament so that a very short heating step emitted sufficient lead for an accurate analysis to be made. The reliability index may not be used for multiple zircon evaporations (see Chapter 2), and therefore only the frequency of common lead corrected ages within a particular age interval may be considered in the determination of the crystallisation age of the clasts.

Zircons analysed from both clasts produced extremely similar sets of data, tabulated in appendix B and displayed in figure 3.27 Both clasts record only a few, scattered ages below an abundance peak at 2,800 Ma, above which a further suite of ages are recorded - up to 2,880 Ma in 89-C-20 and 2,870 Ma in 89-C-28. These data are interpreted as representing mixing of two age components in the zircons, the younger of which is corresponds to the abundance peak at 2,800 Ma. The estimated error on this 2,800 Ma crystallisation age is ± 20 Ma. The abrupt termination of the older suite of ages at ≈2,880 Ma indicates that the age of the older component is probably close to this value, but no accurate constraints may be placed upon this.

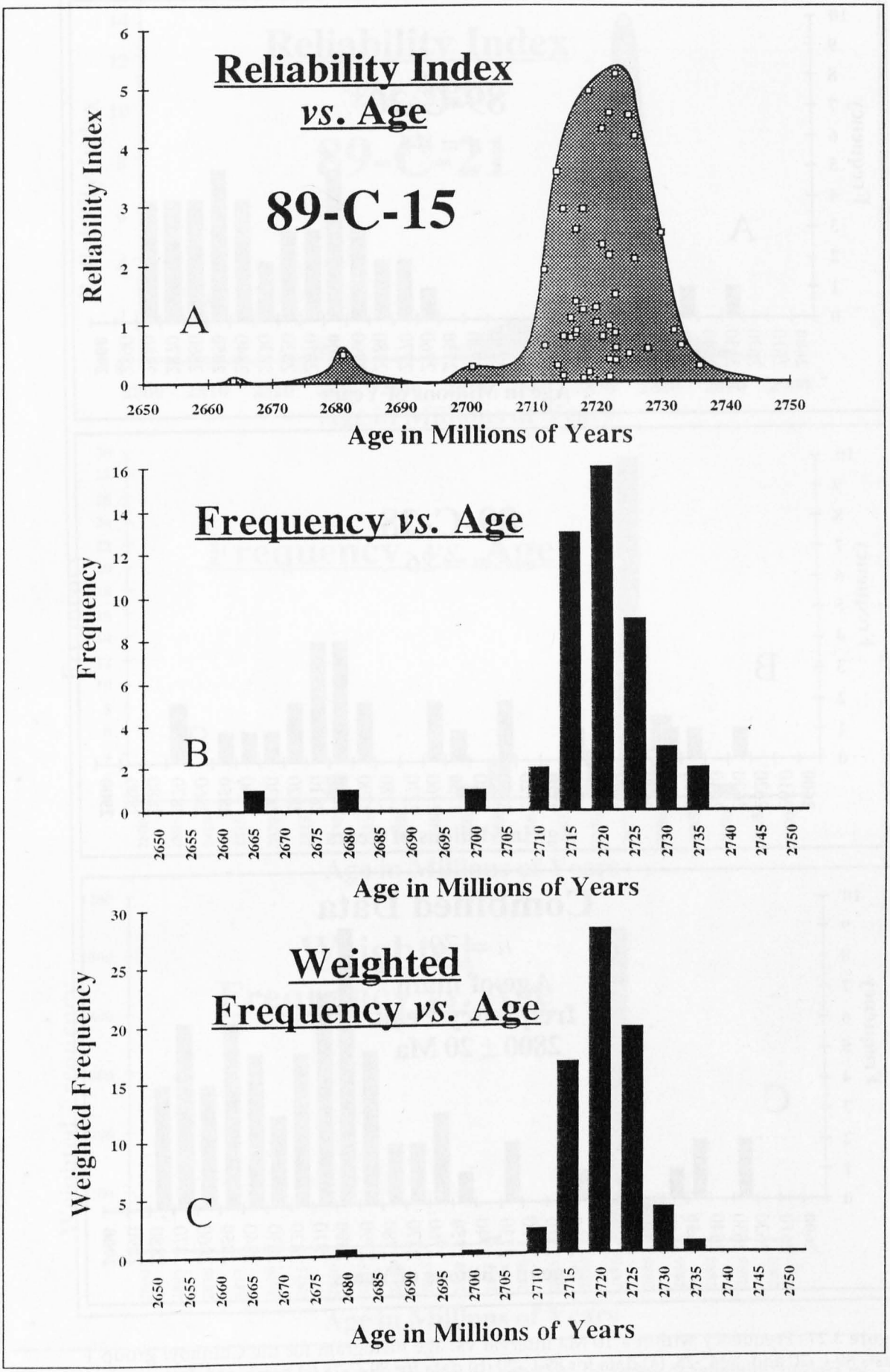

Figure 3.26 Zircon data from the Chinhoyi group 1 clast 89-C-15 (a) Index of reliability of data vs. age scatter graph; (b) Frequency within a 10 Ma interval vs. age histogram; (c) Weighted frequency vs. age histogram. See Chapter 2:4 for a full explanation of the use of these diagrams

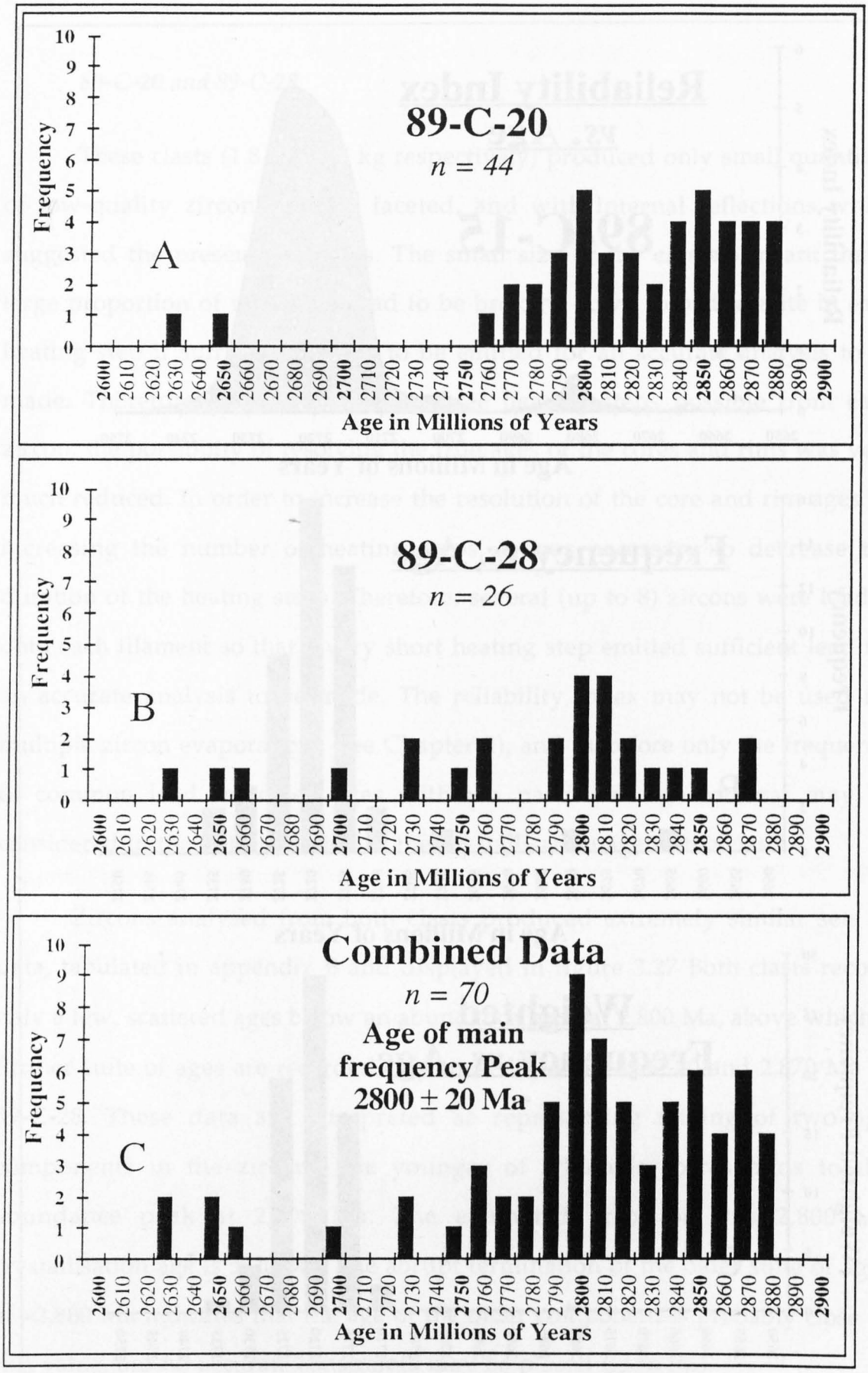

Figure 3.27 Frequency within a 10 Ma interval vs. age histogram for the Chinhoyi group 1 clasts 89-C-20 and 89-C-28. (a) data for 89-C-20 (b) data for 89-C-28 (c) combined data.

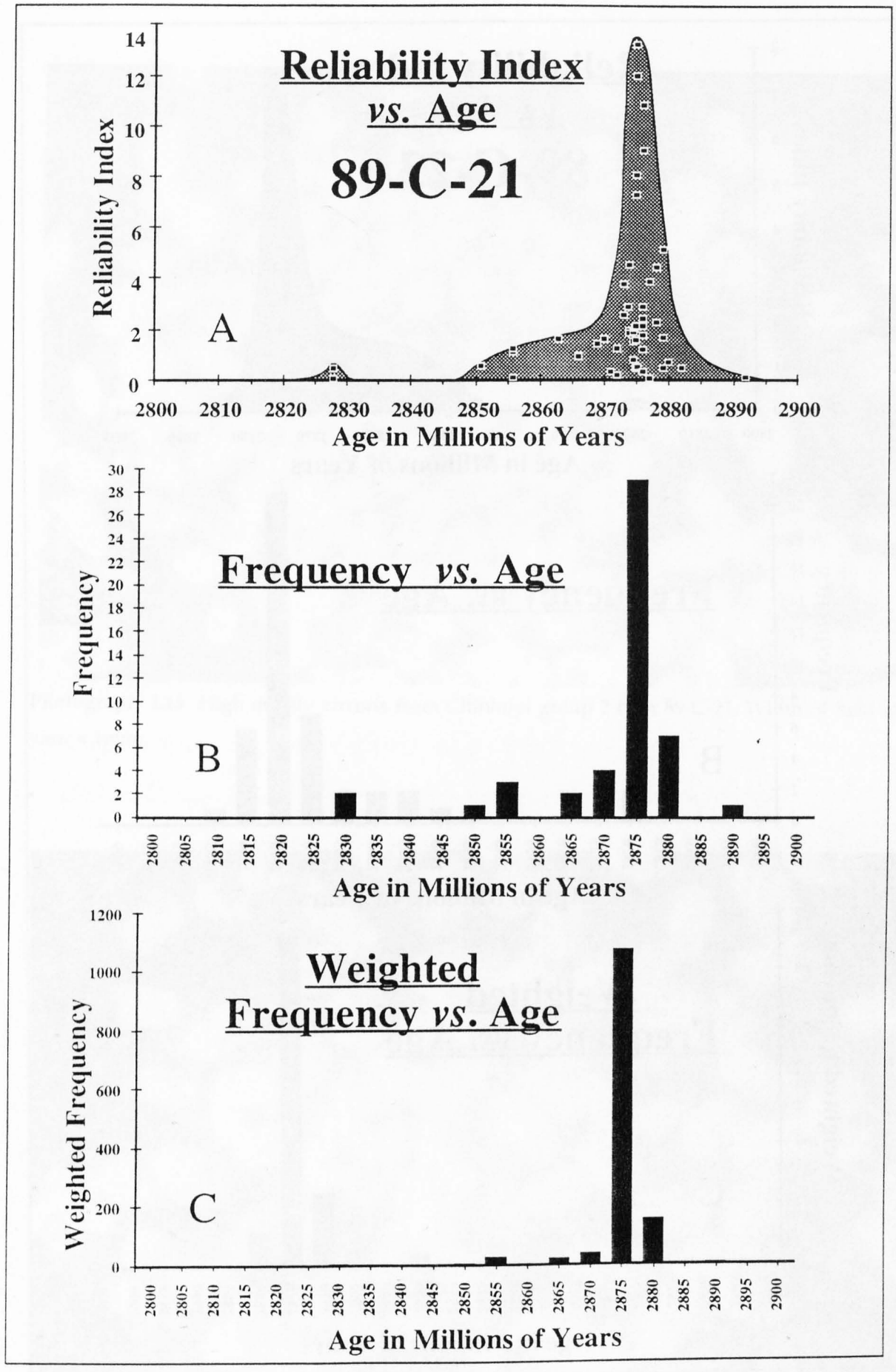

Figure 3.28 Zircon data from the Chinhoyi group 2 clast 89-C-21 (a) Index of reliability of data vs. age scatter graph; (b) Frequency within a 10 Ma interval vs. age histogram; (c) Weighted frequency vs. age histogram. See Chapter 2:4 for a full explanation of the use of these diagrams

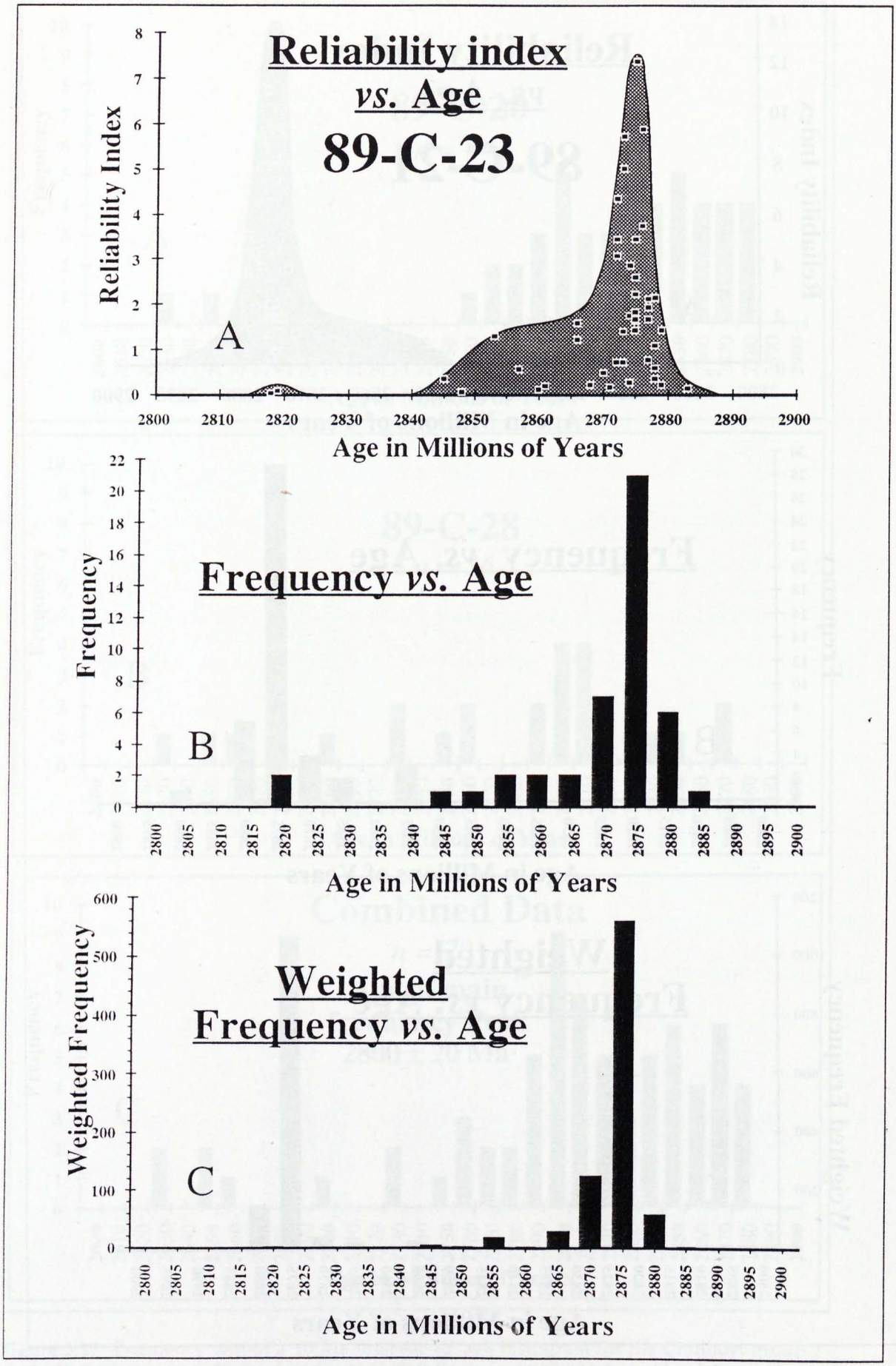

Figure 3.29 Zircon data from the Chinhoyi group 2 clast 89-C-23 (a) Index of reliability of data vs. age scatter graph; (b) Frequency within a 10 Ma interval vs. age histogram; (c) Weighted frequency vs. age histogram. See Chapter 2:4 for a full explanation of the use of these diagrams

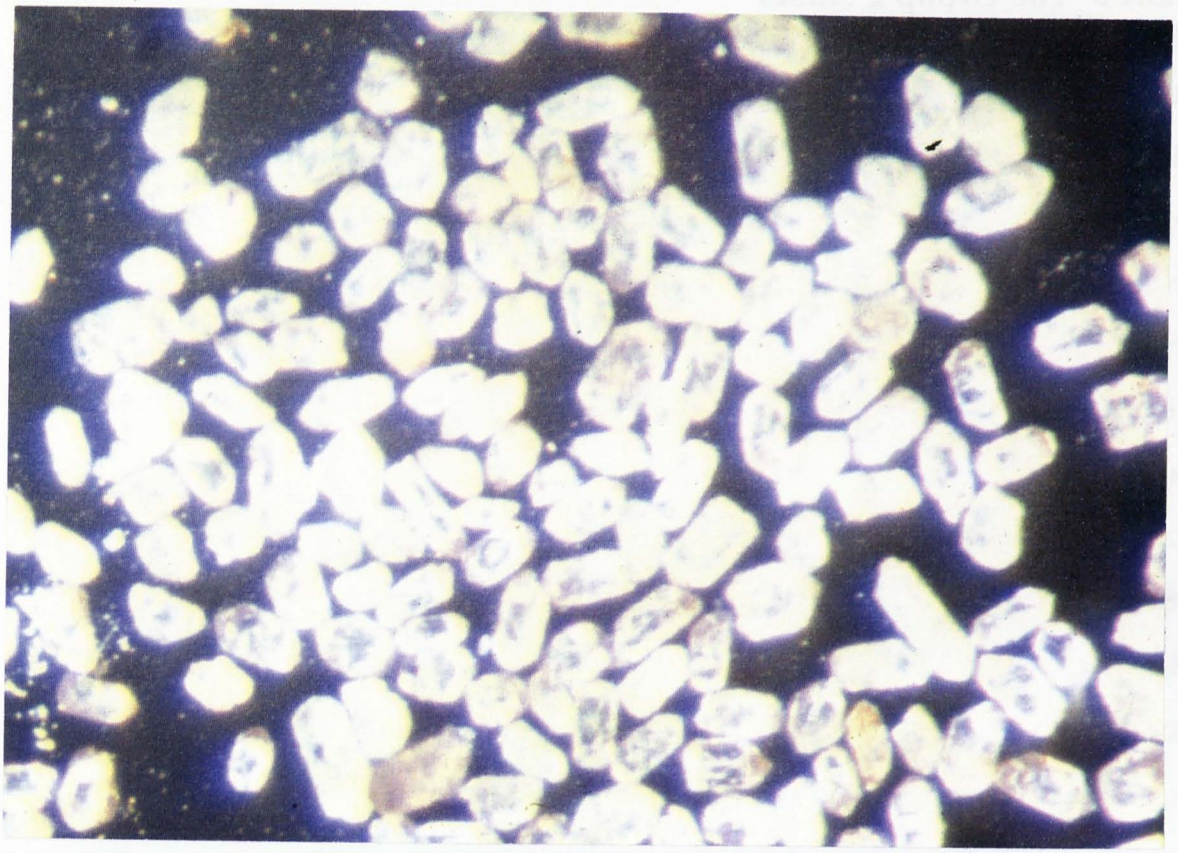

Photograph 3.13 High quality zircons from Chinhoyi group 2 clast 89-C-21. Width of field of view ≈ 1mm.

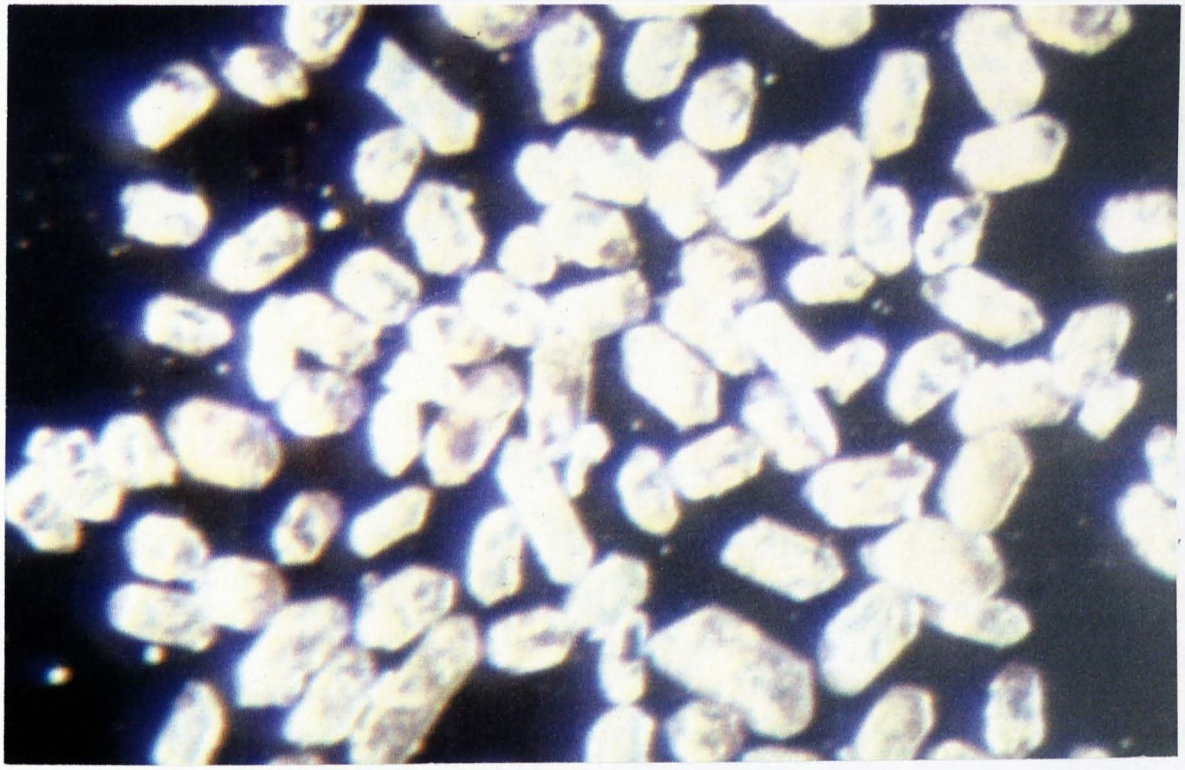

Photograph 3.14 High quality zircons from Chinhoyi group 2 clast 89-C-23. Width of field of view ≈ 1mm.

3:3.4 b The Group 2 clasts

89-C-21

This 3.5 kg clast provided a large separate of several hundred clear, pinkish crystals with well developed crystal faces, primary (magmatic) inclusions and magmatic growth zoning. No cores or rims were observed to this single phase of zircon crystallisation. Six zircons were analysed in a total of fifty-two heating steps, the common-lead corrected ages of which are tabulated in appendix B and plotted in figure 3.28. There is a single peak to the data, slightly skewed to the left. The weighted average age of all the points is 2875 Ma, and the 1 standard deviation error of all the points is ± 11 Ma. However, the ages younger than the main peak are considered to contain a younger component, rather than this error being entirely analytical. Therefore only the points within minimal contents of a younger component should be considered in the calculation of the error on the age of this peak. This is achieved by assuming that as the peak does not show "mixing" with an older component, the width of the older side of the frequency peak represents the half-width of a normal distribution, giving a width of ± 7 Ma to the peak if the point at 2,892 Ma is rejected as a low-reliability "flier". Therefore the 1 standard deviation error the age of this clast, calculated from the points between 2,868 and 2,882, is ± 3 Ma.

89-C-23

Like 89-C-21, this 2.9 kg clast also provided a large separate of several hundred clear, pinkish crystals with well developed crystal faces, primary (magmatic) inclusions and magmatic growth zoning. Again, no cores or rims were observed to this single phase of zircon crystallisation. Six zircons were analysed in a total of forty-five heating steps, the data from which are tabulated in appendix B and plotted in figure 3.29 There is a single peak to the data, and the weighted average age on all of these points is 2874 Ma, with a 1 standard deviation error of ± 14 Ma on all the points. The peak is skewed by

mixing between the main phase of zircon and a younger phase, and following the method detailed above for 89-C-21 width of the normal distribution is taken as ± 10 Ma, the points within which give a 1 standard deviation error of ± 3 Ma.

3:3.5 Summary of Data From Chinhoyi

The earliest record of continental crust from Chinhoyi is the extremely well constrained crystallisation age of two group 2 clasts at 2,875 ± 3 Ma (table 3.3). In terms of REE, the group 2 clasts conform to the low-alumina Archaean TTG model of Barker and Arth (1976), and thus represented an addition of new siliceous material to the continental crust, consistent with ≈ 10% partial melting of a metabasaltic precursor at a pressure of ≈ 8 kbar and a temperature of ≈ 1000°C (Rapp et al. 1991).

Sample	Pb-Pb Zircon Age
Group 1 **89-C-15**	2,720 ± 6 Ma
89-C-20 & 28 (combined data)	2,800 ± 20 *(rim)* ≥ 2,880 *(core)*
Group 2 **89-C-21**	2,875 ± 3 Ma
89-C-23	2,874 ± 3 Ma

Table 3.3 Summary table of Pb-Pb zircon data for the Chinhoyi clasts.

The next event recorded is in the group 1 clasts 89-C-20 and 89-C-28, at 2,800 ± 20 Ma. These clasts conform to the high-alumina TTG model of Barker and Arth, and also represent addition of new material to the continental crust. Their formation has been modelled by 10 to 40% partial melting of

amphibolite-facies metabasalt at pressures of ≈16 kbar (double the depth at which melting occurred to produce group 2), with residual garnet (± hornblende) buffering the HREE content of the melt at a low level (Barker and Arth, 1976; Martin 1986; Drummond and Defant, 1990; Rapp et al. 1991; Luais and Hawkesworth, 1994). These clasts record 2 phases of zircon growth, one at ≈ 2,880 Ma, and one at 2,800 ± 20 Ma. With the degree of alteration and deformation that these clasts have undergone, in the absence of Sm-Nd crustal residence data, it is not possible to determine whether the 2.8 Ga event was metamorphism of material intruded at 2,875 Ga, or if melts intruded at 2.8 Ga assimilated the older material, which is now recorded as xenocrystic cores. However, given the larger proportion of material of "rim" age present in these zircons, the latter explanation is preferred.

The youngest material recorded in the clasts is 2,720 ± 6 Ma for a group 1 tonalite.

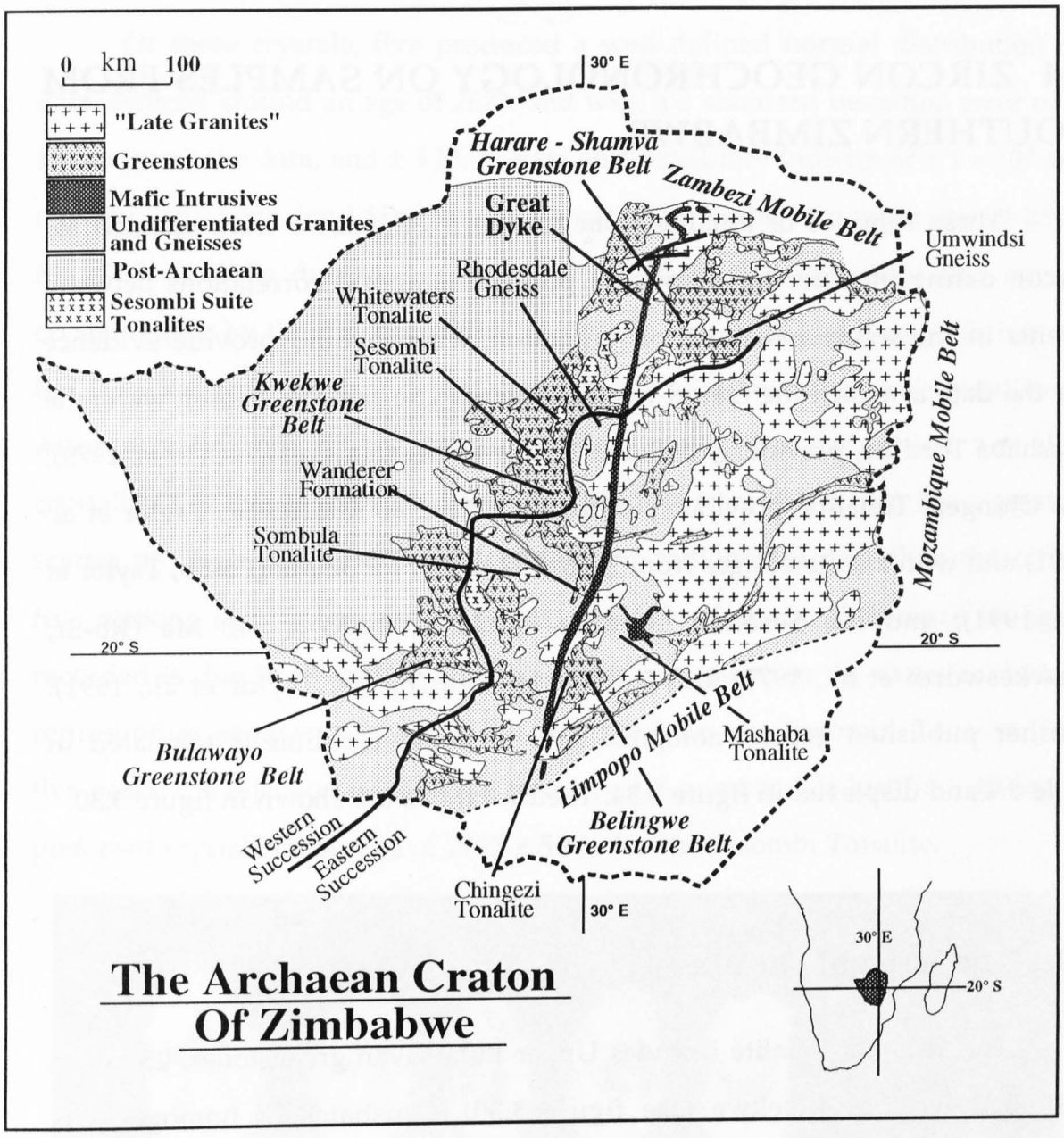

Figure 3.30 Geological sketch map of the Archaean Craton of Zimbabwe, showing the major geological divisions, the boundary between the eastern and western successions of Upper Bulawayan greenstones, and the locations of granites and greenstones dated in previous work (table 3.4) and this study (table 3.5).

3:4 ZIRCON GEOCHRONOLOGY ON SAMPLES FROM SOUTHERN ZIMBABWE.

Three samples of tonalite from Southern Zimbabwe were selected for zircon dating in order to investigate possible temporal correlations between events in the south and north of the craton, which would provide evidence for the date at which the craton was assembled. The samples chosen were; the Mashaba Tonalite, previously dated at 2,860 ± 60 Ma (Hawkesworth et al. 1979); the Chingezi Tonalite, previously dated at 2,772 ± 60 Ma (Rb-Sr, Taylor et al. 1991) and with a suite of ages from 2686 ± 94 to 2,874 ± 32 Ma (Pb-Pb, Taylor et al., 1991); and the Sesombi Tonalite, dated at 2,633 ± 140 Ma (Rb-Sr, Hawkesworth et al., 1975) and 2,579 ± 160 Ma (Pb-Pb, Taylor et al., 1991). Further published geochronological data on these tonalites is tabulated in table 3.4 and displayed in figure 3.34. Their locations are shown in figure 3.30.

3:4.1 The Sesombi Tonalite.

The Sesombi tonalite intrudes Upper Bulawayan greenstones, 25 km to the north-west of Kwekwe (see figure 3.30). Crushates of homogeneous tonalites previously used to construct Rb-Sr (Hawkesworth et al., 1975, which also describes sample localities) and Pb-Pb isochrons (Taylor et al., 1991) (sample numbers Rh-73-176, 178 and 179) were mixed in order to facilitate zircon separation procedures, to give a total sample weight of 5 kg, and the zircon was separated. The combined sample contained abundant clear, adamantine, pink zircon crystals, with well developed crystal faces and magmatic inclusions, and no visible cores or rims (photograph 3.15). Six zircons were analysed, in a total of 46 heating steps. Common-Pb corrected ages were calculated for each eating step, and these results are plotted in figure 3.31 and tabulated in appendix B.

Of these crystals, five produced a well defined normal distribution of data, centred around an age of 2673, and with a 1 standard deviation error of ± 18 Ma on all the data, and ± 5 Ma if data with reliability indicies of $< 1 \times 10^8$ are rejected. The sixth (and largest) crystal gave the slightly younger age of 2663 Ma. This may be due to disruption of the U-Pb systematics of this zircon crystal, either by the presence of inclusions, or a slight initial disequilibrium of the U-series decay system (see Chapter 2) at the time the zircon crystallised. Alternatively, one of the three samples mixed for separation actually crystallised at this slightly younger age. The data from this zircon has a greater scatter of "high reliability" (uncontaminated radiogenic) data than the other five zircons combined, and it seems probable that the difference in ages recorded is due to disturbance of this crystal, rather than the samples chosen representing separate phases of intrusion within the Sesombi Tonalite. On this basis, the rejection of the data from crystal number 1 is justified, giving a preferred crystallisation age of 2673 ± 5 Ma for the Sesombi Tonalite.

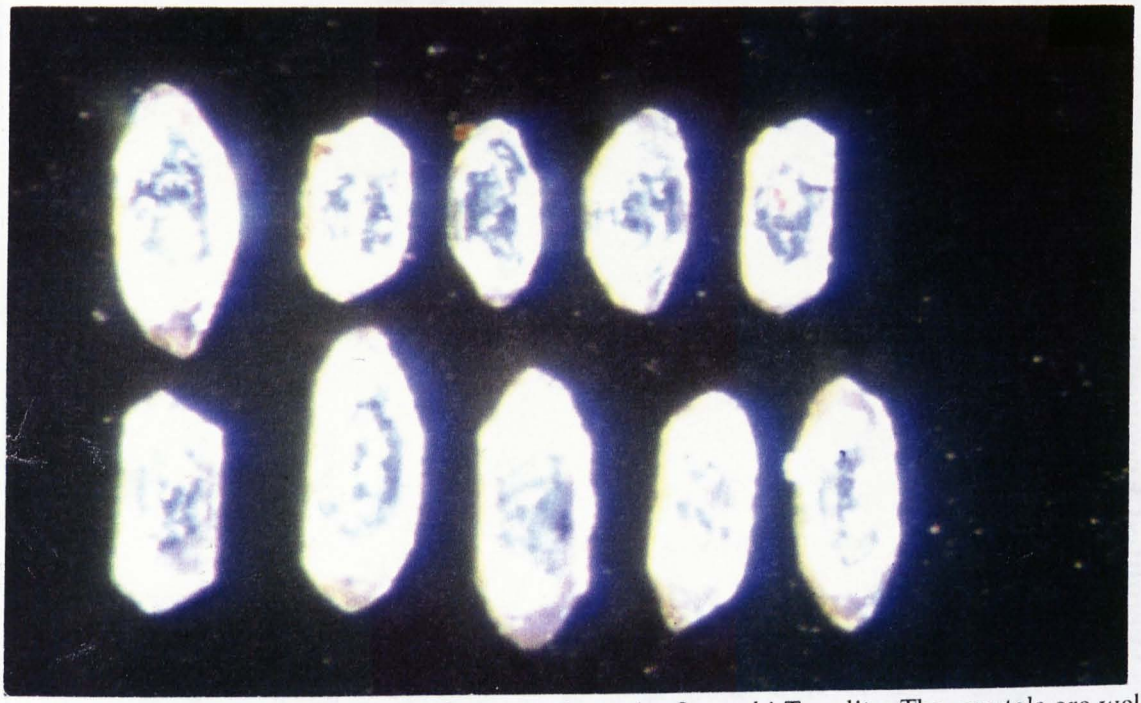

Photograph 3.15 Large, multi-faceted zircons from the Sesombi Tonalite. The crystals are well formed, up to 0.4 mm in length, with magmatic zoning and inclusions.

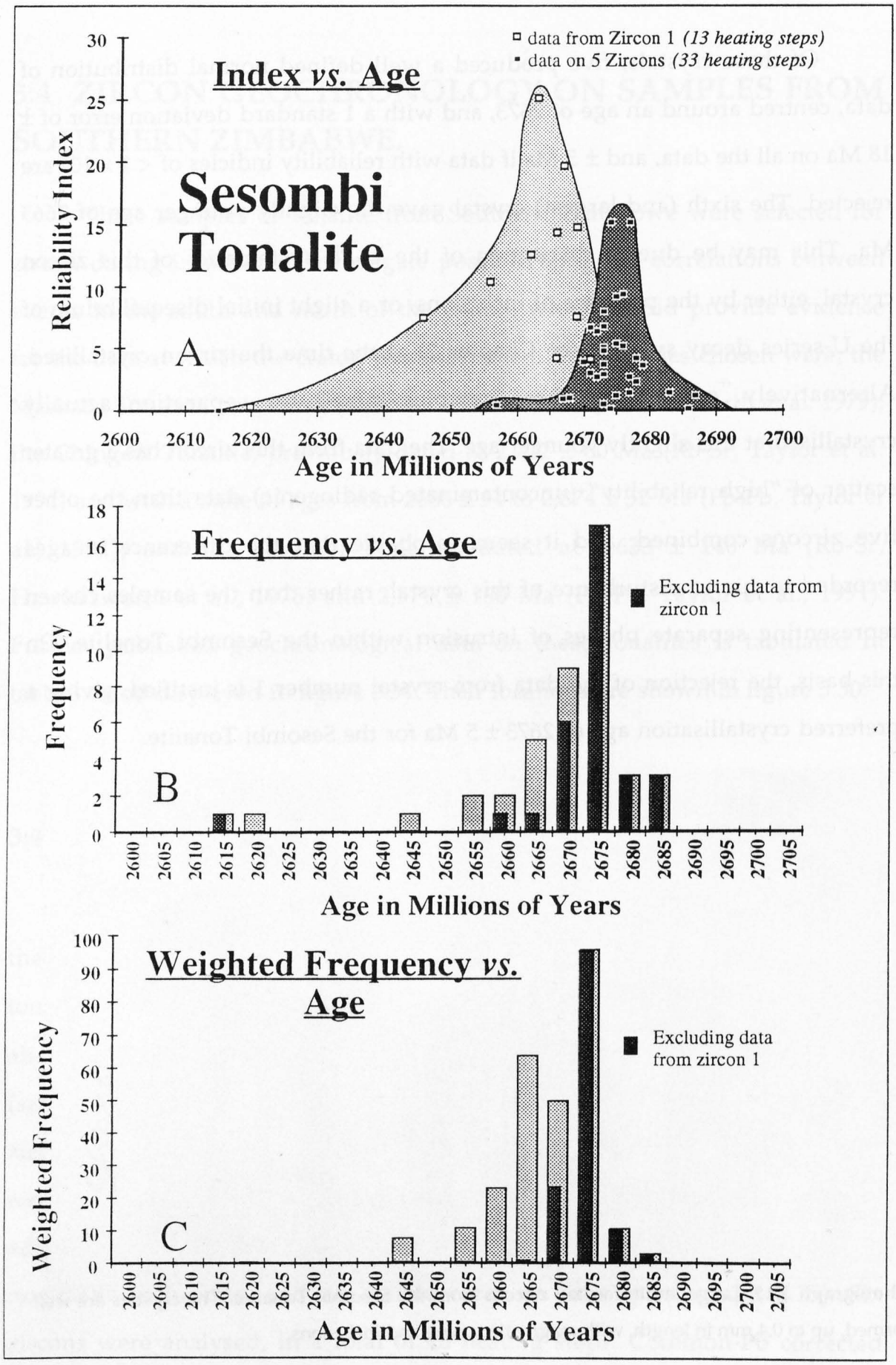

Figure 3.31 Zircon data from the Sesombi Tonalite (a) Index of reliability of data vs. age scatter graph; (b) Frequency within a 10 Ma interval vs. age histogram; (c) Weighted frequency vs. age histogram. See Chapter 2:4 for a full explanation of the use of these diagrams

3:4.2 The Chingezi Tonalite / Hokonui Formation.

The Chingezi Tonalite outcrops to the south-west of the Belingwe Greenstone belt, intruding the Lower Greenstones, cutting the basal (Bvute) formation, but apparently coeval with the overlying Hokonui formation. Exposures are found in which the tonalite intrudes the volcanics of the Hokonui formation, but also exposures occur in which agglomerates of the Hokonui formation brecciate the tonalite (Taylor et al. 1991). The range of ages obtained by Taylor et al. (1991) on the Chingezi Tonalite (table 3.4), together with the variations in chemistry reported in Luais and Hawkesworth (1994) strongly suggests that a variety of granitoids, intruded at different times, have been included within the term "Chingezi Tonalite", and that more detailed mapping is required if the relationships between the various intrusions present are to be fully understood. A sample of tonalite was taken from a volcanic breccia within the Hokonui formation, as it was hoped that dating of this sample would also constrain the date of formation of the coeval Lower Bulawayan greenstones of the Belingwe Greenstone Belt.

A 3.5 kg sample unfoliated tonalite (sample number 89-H-1) was collected from a very large (> 10 m) block of the Chingezi Tonalite within a coarse volcanic breccia of the Hokonui Formation, in the bed of the Mtshingwe river, ≈ 4.5 km to the north-west of the road bridge where the main Zvishavane-Bulawayo road crosses the river (Lat. 20° 24' S, Long. 29° 52' E). The metamorphic grade at this locality is very low (chlorite grade). The sample provided a small zircon separate, of less than 30 small clear and colourless zircons. Two of the larger zircons (zircons 2 and 3) were analysed individually, and a multiple load of 10 smaller zircons ("zircon 1") was also step-heated, to give the data displayed in figure 3.32 and tabulated in appendix B.

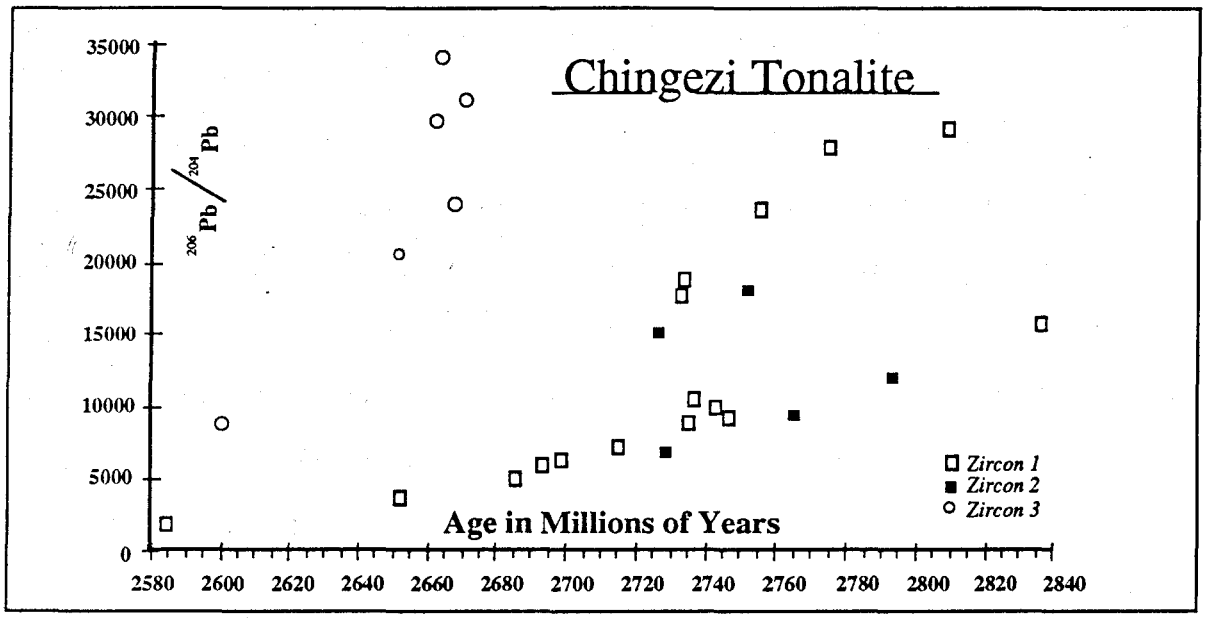

Figure 3.32 A graph of $^{206}Pb/^{204}Pb$ *vs.* age for zircons from 89-H-1, a sample of the Chingezi Tonalite collected from a volcanic breccia in the Hokonui Formation. 2 of the samples "zircon 1" (10 zircons heated within a single filament) and "zircon 2", a single crystal, gave suites of ages up to a maximum value of 2,840 Ma. The third crystal, "zircon 3", gives a clustering of data at 2660 Ma, and is rejected as a contaminant from the Sesombi Tonalite (figure 3.31).

The results are displayed in figure 3.32 as the $^{206}Pb/^{204}Pb$ ratio *vs:* common Pb corrected age. The higher the $^{206}Pb/^{204}Pb$ ratio, the less common Pb is present, and the "purer" the zircon analysed is. In general, it is expected that the $^{206}Pb/^{204}Pb$ ratio will increase with successive heating steps through a zircon crystal from the (often comparatively metamict and inclusion rich) rim to the core. These zircons were analysed in a series of extremely short deposition cycles in order to maximise the resolution of any zoning present, but as a consequence of this, the beam intensities were very low. Therefore for this rock (and also the Mashaba Tonalite) the $^{206}Pb/^{204}Pb$ ratio gives a clearer indication of the zonation of the zircons than the reliability index or frequency diagrams which are usually used in this work.

Zircons 1 and 2 gave suites of ages in which there is a general increase in $^{206}Pb/^{204}Pb$ ratio with age, up to a maximum age of 2,840 Ma. These data are interpreted as a *minimum* crystallisation age of ≥ 2,840 Ma for the Chingezi Tonalite, with the younger suite of ages representing partial re-setting through

lead loss. It is not possible to determine whether this lead loss was due to a thermal "event", or simply continuous diffusion from the metamict portions of these small crystals. The third zircon gave a cluster of ages at ≈ 2,660 Ma, a date younger than the Pb-Pb age of the brecciated tonalites in this locality (2,764 ± 30, calculated from data for "Locality 12" in Taylor et al., 1991). The lack of agreement between the data from this zircon and the other zircons analysed, combined with fact that the zircon gives a younger age than the Pb-Pb whole rock data (which will undergo open system behaviour and re-setting under far lower metamorphic conditions than zircon), strongly suggests that this zircon is a contaminant from another sample (probably the Sesombi Tonalite), and should be discounted in the calculation of the age of the Chingezi Tonalite.

3.4.3 The Mashaba Tonalite

A 2.5 kg sample of tonalite, from a weakly foliated homogeneous tonalitic sill cutting the ≈ 3.5 Ga Mashaba gneisses (sample number 89Zb-12, supplied by B.Luais) was crushed and the zircons extracted. The sample provided a small, very heterogeneous population of white, transparent zircons, with obvious cores and rims. A single, large (≈ 0.3 mm) crystal was heated in 16 steps, to provide the data displayed in figure 3.33, tabulated in appendix B. $^{206}Pb/^{204}Pb$ data for the zircons analysed are plotted against age, together with the corresponding $^{208}Pb/^{206}Pb$ ratios. ^{208}Pb is produced by the decay of ^{232}Th, while ^{206}Pb is produced by the decay of ^{238}U. Therefore the $^{208}Pb/^{206}Pb$ ratio may be used to give an indication of any zonation of Th/U ratios within the zircons analysed.

A suite of ages between 2.70 Ga and 3.25 Ga was recorded, and given the length of the time-span over which these ages are spread, combined with the lack of any statistically significant clusterings of data, no accurate inferences on the crystallisation history of this clast may be made, other than to say that the

main crystallisation event(s) occurred between 2,800 and 3,050 Ma, with a *minimum* age for the zircon cores of ≥ 3,250 Ma.

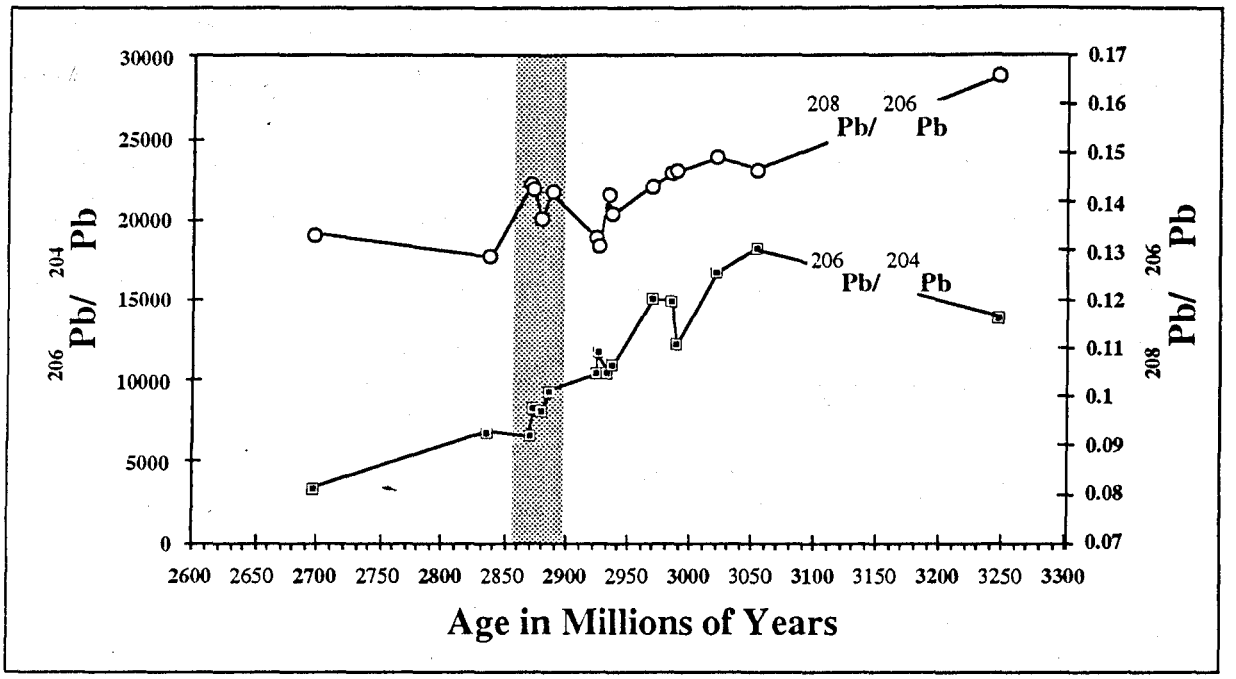

Figure 3.33 A graph of $^{206}Pb/^{204}Pb$ and $^{208}Pb/^{206}Pb$ *vs.* age for a single zircon from the Mashaba Tonalite (sample 89Zb-12, supplied by B.Luais). There is a suite of ages up to 3,250 Ma. The shaded region indicates the possible crystallisation date of a high $^{208}Pb/^{206}Pb$ phase of zircon at ≈ 2.87 Ga, coincident with the Rb-Sr age of the rock. (2860 ± 60 Ma).

The Mashaba Tonalite has been interpreted as representing a partial melt of earlier greenstones (Luais and Hawkesworth, 1994) and these cores may therefore give an indication of the minimum age of the source region. Alternatively, as the Mashaba tonalite intrudes the ≈ 3.5 Ga Tokwe gneisses, these ancient cores may be xenocrysts derived from the surrounding terrain. It is interesting to note that there is a clustering of four $^{207}Pb/^{206}Pb$ ages (the shaded region on figure 3.33) with high $^{208}Pb/^{206}Pb$ ratios, possibly indicating that this cluster of data represents a single phase of zircon crystallisation (Kober, 1987), at ≈ 2.87 Ga, the Rb-Sr age of this rock. However, without corroborating data from other zircons, this must be regarded as unproven. Unfortunately, the small size and complex crystallisation histories of the remaining few crystals prevented any further analysis of this sample, but a

larger (>10 kg) quantity of rock would provide more large crystals, and thus would allow accurate dating of complex crystallisation histories such as this.

3:5 DISCUSSION

Locality		Age
Shamva	89-S-26	*3.34 Ga*
	Group 1	
	89-S-14	**2,800 ± 20** (rim) **3,197 ± 10 Ma** (core) *2.98 Ga*
	89-S-23	**≈ 2,800 Ma ≈ 2,920 Ma ≥ 3,182 Ma** (core) *3.16 Ga*
	Group 2	
	89-S-12	**≈ 2,680 Ma 2,921 ± 10 Ma** *3.13 Ga*
	89-S-19	**≈ 2,650 Ma 2,920 ± 30 Ma** *3.17 Ga*
	89-S-25	**≈ 2,670 Ma 2,924 ± 5 Ma ≥ 3,116 Ma** (core) *3.20 Ga*
	All Group 2	**2,925 ± 10 Ma**
Chinhoyi	**Group 1**	
	89-C-15	**2,720 ± 6 Ma**
	89-C-20 & 28	**2,800 ± 20 Ma** (rim) **≈ 2,880 Ma** (core)
	Group 2	
	89-C-21	**2,875 ± 3 Ma**
	89-C-23	**2,874 ± 3 Ma**
Sesombi Tonalite		**2,673 ± 5 Ma**
Mashaba Tonalite		
	89-Zb-12	**2.95 ± 0.1 Ga** (rim) **> 3.25 Ga** (core)
Chingezi Tonalite		**> 2.84 Ga** (core)

Table 3.5. Summary table of geochronological work on Shamva, Chinhoyi, Sesombi, Mashaba and Chingezi carried out in this thesis. Zircon dates are in bold type, Sm-Nd T_{DM} model ages are in italics.

Using a combination of geochronological (zircon and Sm-Nd) and geochemical data, an outline of the history of the early continental crust of Northern Zimbabwe may be deduced. Table 3.5 summarises the geochronological data obtained in this study, and table 3.4 and figure 3.34 summarise some relevant previous geochronological work on both granitoids and supracrustals from throughout Zimbabwe.

LATE "GRANITES"		
Chilimanzi	Rb-Sr	2570±25 (9)
Chinamora	U-Pb Zircon	2601±14 (7)
UPPER BULAWAYAN		
Chinamora Post-Tectonic Tonalite	U-Pb Zircon	2664±6 (7)
Sombula Tonalite	Rb-Sr	2594±80 (3)
	Pb-Pb	2752±52 (2)
	Sm-Nd	2.74 Ga T_{DM} (2)
Sesombi Tonalite	Rb-Sr (*whole rock*)	2633±140 (4)
	Rb-Sr (*muscovite*)	2.61 Ga ±1% (10)
	Rb-Sr (*biotite*)	2.56 Ga ±1% (10)
	Rb-Sr (*feldspar*)	2.47 Ga ±1% (10)
	Pb-Pb	2579±164 (2)
	Sm-Nd	2.68 Ga T_{DM} (2)
Shamvaian Syn-depositional porphry	U-Pb Zircon	2672±12 (7)
White Waters Tonalite	Sm-Nd	2648±81 (6)
Wedza Tonalite	Rb-Sr	2680±104 (5)
	Zircon	2667±4 (7)
Greenstones		
Iron Mask Fm.	U-Pb Zircon	2713±15 (7)
	Zircon (SHRIMP)	2645±4 (8)
	Sm-Nd	2.91 Ga T_{DM} (5)
Arcturus Fm.	Pb-Pb	2659±4 (2)
	Sm-Nd	2.80 Ga T_{DM} (2)
Maparu Fm.	Zircon (SHRIMP)	2697± 9 (8)
Passaford Fm.	Zircon (SHRIMP)	2643 ± 8 (8)
MID-ARCHAEAN		
Chingezi Tonalite (Locality 8)	Pb-Pb	2800±76 (2)
	Sm-Nd	3.05 Ga T_{DM} (2)
(Locality 9)	Pb-Pb	2874±32 (2)
	Sm-Nd	2.95 Ga T_{DM} (2)
(Locality 10)	Pb-Pb	2825±100 (2)
(Localities 14-17)	Pb-Pb	2686±94 (2)
	Sm-Nd	2.98 Ga T_{DM} (2)
(in Hokonui vent agglomerate)	Pb-Pb	2764±30 (2*)
(All localities except 9 & vent)	Rb-Sr	2772±60 (2)
	Rb-Sr	2690±140 (4)
Rhodesdale Gneiss	Rb-Sr	2700±80 (3)
	Pb-Pb	2976±125 (3)
	Sm-Nd	2.99 Ga T_{DM} (2)
Umwindsi Gneiss	Rb-Sr	2860±135 (5)
Mashaba Tonalite	Rb-Sr	2860±60 (10)
Detrital Zircon Abundance Peak in Southern Zimbabwe	Zircon (SHRIMP)	3.2 Ga (1)

Table 3.4. Some previous geochronological work on Zimbabwe. (1)Dodson et al., 1988; (2)Taylor et al., 1991; (2*) calculated from data in Taylor et al. 1991; (3)Moorbath, 1977; (4)Hawkesworth et al., 1975; (5)Baldock and Evans, 1988; (6)NERC Geoscience Lab report 1990-'92; (7)Jelsma, 1993; (8)Nesbitt et al. (unpublished data); (9)Hickman, 1978; (10) Hawkesworth et al. 1979.

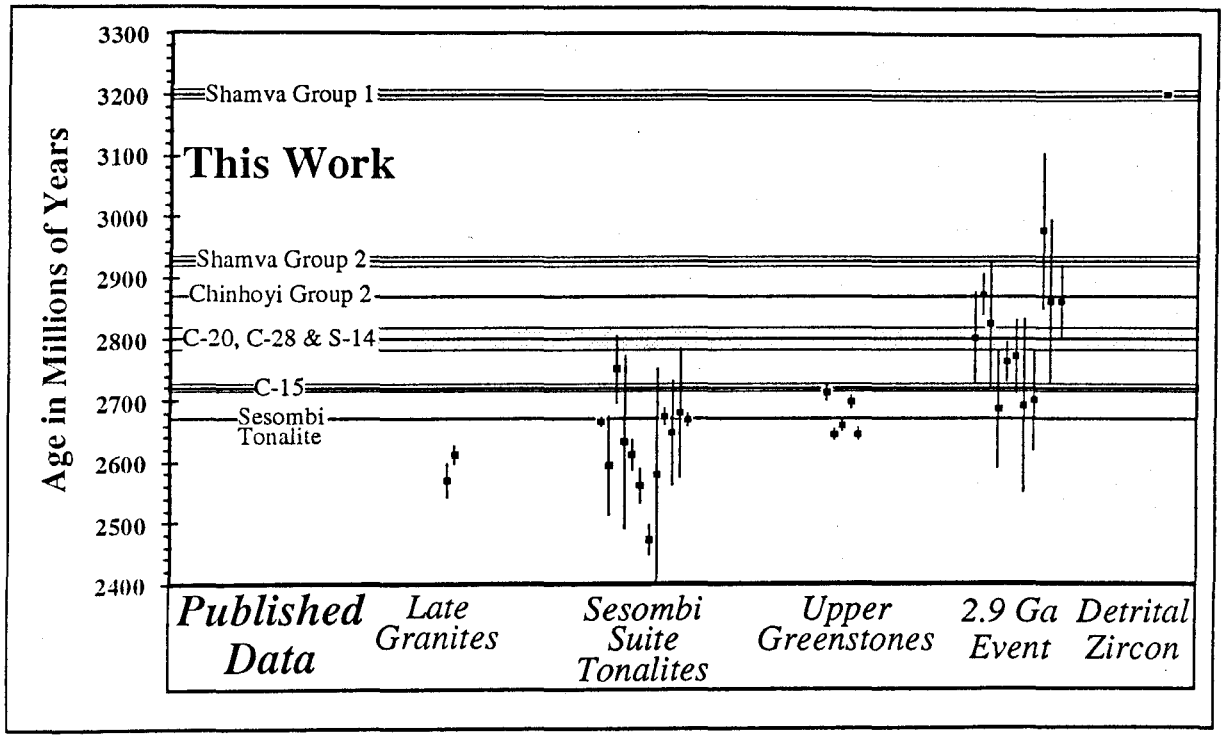

Figure 3.34 Shows the data presented in tables 3.5 and 3.5, comparing the zircon data obtained in this work (horizontal lines, with grey shading to represent error bars) with previously published data (black squares with vertical error bars)

Prior to this study, the only indications of continental material older than the Upper Bulawayan in Northern Zimbabwe were rare gneisses such as the Umwindsi Gneiss, dated at 2,860 ± 135 Ma (Rb-Sr, Baldock and Evans, 1988; table 3.4), and Sm-Nd TDM model ages up to 200 Ma greater than the extrusion age for Upper Bulawayan Greenstones such as the Iron Mask formation (table 3.4) indicating contamination with a pre-existing enriched crustal reservoir. There were no indications of the presence of material older than the ≈ 2.9 Ga Lower Bulawayan. One of the sample localities, Chinhoyi, has confirmed this view, with a crustal history extending only as far as 2,875 ± 3 Ma, whereas the clasts analysed from Shamva indicate a long and complex crustal history prior to the Lower Bulawayan.

The group 1 Shamva and Chinhoyi clasts 89-S-14, 89-C-20 and 28 show that assimilation of pre-existing continental crust by "juvenile" (ie new additions of material to the continental crust) TTG-suite magmas was common. The Shamva group 2 clasts show that intra-crustal melting episodes occurred in which existing crustal material was homogenised, and variable amounts of juvenile TTG added. In terms of Sm-Nd model ages, these processes will cause an averaging effect, such that material from two minor phases of crustal growth will be interpreted as a single, larger event of intermediate age. If the relative proportions of material are not known, then it is impossible to interpret whether the older component was small, and considerably older than the younger component, or large, and close in age to the younger component. Therefore Sm-Nd model ages on materials which average the composition of a portion of continental crust (such as granitoids produced by intra-crustal melting, or sediments) may overestimate the rate of late Archaean crust formation, and underestimate the maximum age of continental material present. The combined zircon and Sm-Nd data presented in this chapter for the Shamva region strongly suggest that the earliest nucleus of continental material in this region was extremely ancient, possibly several hundred million years older than the Sm-Nd T_{DM} model age of clast 89-S-26. The complex, multiply zoned zircons in this sample indicate that this age may be also be an average of several components, and should therefore be regarded as a minimum age. Zircon crystallisation dates demonstrate that the early crust was augmented in a frequent succession of episodes of TTG intrusion.

Unlike Shamva, the oldest clasts recorded from Chinhoyi give a well-defined crystallisation age of 2,875 ± 3 Ma. Sm-Nd analyses were not carried out on these clasts, so model ages are not available, but the lack of any cores within these zircons indicates that no older granitoids were assimilated. The earliest granitoids recorded were members of the low-alumina TTG suite,

while younger clasts were of the high alumina suite. Experimental and theoretical modeling (eg Rapp et al. 1991; Barker and Arth, 1976) of the formation of such granitoids indicates that both may be formed by partial melting of the same metabasite protolith, with depth of melting controlling the chemistry of the resultant melts - melting at ≈ 8 kbar giving the low alumina suite, and melting at pressures between 12 and 30 kbars giving the high alumina suite (Rapp et al. 1991). This increase in depth of melting is used in Chapter 4 in the construction of a model for the formation of early continental crust.

3:5.1 Temporal correlations between Chinhoyi, Shamva, and the rest of the Zimbabwe Craton.

The Shamva clasts record a crustal history (table 3.5) extending back as far as 3.34 Ga, with a significant episode of crustal growth indicated by zircon crystallisation at ≈3,200 Ma, Sm-Nd model ages and chemical modelling. This correlates well with a detrital zircon abundance peak of 3.2 Ga (Dodson et al. 1988) in the "Wanderer Formation" - sediments of similar (Upper Bulawayan) age (Tsomondo et al., 1992) in Southern Zimbabwe, possibly indicating that the "Shamva Terrain" and the Tokwe segment of Southern Zimbabwe were already joined by 3.2 Ga. The next episode recorded at Shamva is one of crustal re-working at ≈2,925 Ma, and the final event recorded is at 2,800 ± 20 Ma. By contrast, the Chinhoyi clasts record a shorter history, with the first recorded event at 2,875 ± 3 Ma, and subsequent events at 2,800 ± 20 and 2720 ± 6 Ma. This last age is identical within error of a U-Pb zircon age obtained on a rhyolite within the basal (Iron Mask) formation of the Shamva-Harare Greenstone belt (2,713 ± 15 Ma, Jelsma, 1993; table 3.4), indicating that one of the results of the "event" at this time was the simultaneous extrusion of greenstone-belt supracrustals and the intrusion of TTG-suite granitoids in Northern Zimbabwe.

A "2.9 Ga event" has been recorded in Southern Zimbabwe (Hawkesworth et al. 1979), and it is obviously of interest to determine whether this correlates with the 2,925 Ma event recorded at Shamva; the 2,875 ± 3 Ma event in Chinhoyi, or the 2,800 ± 20 Ma event recorded in both Shamva and Chinhoyi. Existing dates on Southern Zimbabwe using Rb-Sr and Pb-Pb isochron methods of dating are within error of any of these events (table 3.4). Unfortunately, attempts to obtain high-precision dates the Mashaba and Chingezi tonalites in this project were unsuccessful (section 3:4) due to the complexity of the zircons in the Mashaba Tonalite and the small size and rarity of zircons in the sample from the Chingezi Tonalite.

Syn-depositional porphyries within the Shamvaian sediments have been dated at 2672 ± 12 Ma (Jelsma, 1993 by U-Pb zircon; table 3.4), and the age of 2673 ± 5 Ma for the Sesombi Tonalite (this work; table 3.5), both confirms that the Shamvaian and Sesombi suites were indeed coeval, and also that the Wedza Suite of syn-deformational tonalites in the Harare area (dated at 2667 ± 4 Ma by U-Pb zircon, Jelsma, 1993) are coeval with the Sesombi Suite of tonalites. The dominance of supracrustal greenstone belts towards the west of the craton may indicate that the west is preserved at a higher structural level than the east. Therefore the observed structural differences between the weakly deformed Sesombi suite of tonalites in the west, and the often gneissose Wedza suite of tonalites to the east are interpreted as due to differences in erosion level through coeval suites of granitoids.

The Shamva group 2 clasts all record a poorly defined age during the Upper Bulawayan "event". The coincidence of these ages, both with each other and a known event strongly suggests that the recorded ages record a true episode of zircon crystallisation. This episode of zircon growth may have been caused by either the lower amphibolite facies metamorphism of the belt, the peak of which occurred at ≈ 2,650 Ma (Jelsma, 1993), or this youngest recorded phase of zircon may have crystallised from the same hydrothermal solutions

which caused the gold mineralisation seen at Shamva, which also occurred at this time.

3:5.2 Comment on the Applicability of the Kober Technique of Pb-Pb Zircon Dating Combined with a "Reliability Index" of Pb-Pb Data to the Archaean Tonalites in this Study

This study has demonstrated that for rocks with simple histories, such as the Sesombi Tonalite and some of the Chinhoyi clasts, the Kober technique allows very high precision (± 0.1 %) dating of Archaean granitoids, with sufficient data for a high precision date generally supplied by only 6 zircons, which may be analysed in a single day's machine-time. This rapid data acquisition, combined with the lack of any chemical procedures, gives the Kober technique an obvious advantage over conventional dissolution and U-Pb analysis of zircon. The reproducibility of the technique has been demonstrated by the close correspondence of the dates of the Chinhoyi clasts 89-C-21 and 89-C-23 (2875 ± 3 Ma and 2874 ± 3 Ma respectively), and a good correlation between U-Pb dissolution and the Kober technique has been illustrated by the agreement of dates for the Sesombi and Wedza Tonalites (2,673 ± 5 Ma (this study) and 2,667 ± 4 Ma (Jelsma, 1993) respectively).

Although the Kober Technique is capable of providing high precision analyses on zircons with simple histories, such crystals are rare in rocks with complex histories. An example of this is provided by Kroner and Todt (1988) in an investigation of the Barberton greenstone belt, where only 6 large, single stage zircons of suitable quality for dating by the Kober technique were extracted from more than 20 kg of sample. The usefulness of the "reliability index" in constraining complex crystallisation histories has been demonstrated in this study by the dating of the clasts from Shamva, where the use of the index allowed accurate constraints to be placed on samples with

complex, multi-stage crystallisation histories. Furthermore, use of the index was able to show that one of the zircons analysed from the Sesombi Tonalite had undergone a slight perturbation of its U-Pb systematics, allowing the data from this zircon to be discarded in the determination of the age of the tonalite.

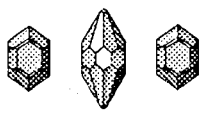

Chapter Four

Models for the Formation and Stabilisation of Archaean Continental Crust

4:1 INTRODUCTION

The study of granitoid clasts in Late Archaean sediments detailed in Chapter 3 has provided a unique insight into the longevity, rate of formation and chemistry of the early continental crust of northern Zimbabwe prior to the stabilisation of the craton between 2,700 and 2,600 Ma ago. Geochronological work has shown that the two regions studied had long and complex histories prior to the Upper Bulawayan "event", while geochemical data on the early crust indicates that it was dominated by Tonalite-Trondhjemite-Granodiorite (TTG) - suite granitoids, within which (at Chinhoyi), there appears to have been a temporal progression in granitoid chemistry, from low- to high-alumina TTG-suite granitoids. There is also a marked disparity between the chemistry of the early TTG dominated continental crust recorded both at Shamva and Chinhoyi, and the calc-alkaline granitoids which intruded most of the craton at the time of the Upper Bulawayan "event". Using this information, this chapter reviews models for the formation, growth and stabilisation of the Archaean Craton in Zimbabwe.

The chemical differences between the (sodic) TTG granitoids of the early continent and the (potassic) calc-alkaline granitoids of the Upper Bulawayan event which culminated in the stabilisation of the craton require separate

models to explain the formation of early continental crust and its stabilisation in the late Archaean. The model invoked for the formation of early continental crust considers the possible effects of a hotter Archaean mantle on the nature of Archaean tectonic processes, and requires that the earliest crust was composed primarily of TTG, formed by partial melting of metabasalt, with a temporal progression from the low-alumina suite TTG to the (dominant) high-alumina TTG suite. It should be stressed that within the craton, this progression was diachronous, and that high-alumina TTG granitoids were formed in the Shamva region at least 300 Ma before the low alumina TTG rocks at Chinhoyi.

The model invoked for the Upper Bulawayan "event" and crustal stabilisation incorporates the following factors : (i) the contemporaneous occurrence of the effects of the event over the entire craton. (ii) A magmatic progression from greenstone belt volcanism, to the intrusion of calc-alkaline granitoids, to the intrusion of "late granites" rich in radioactive elements. (iii) The formation of depleted sub-cratonic lithosphere. (iv) The chemical differences between "Archaean" and "Post-Archaean" sediments.

4:2 THE EARLY CONTINENTAL CRUST.

4:2.1 Archaean oceanic crust and tectonic regimes.

The petrogenetic models outlined in Chapter 3 indicate that Archaean TTG suite granitoids were formed by partial melting of amphibolite facies metabasalts, and the dominantly siliceous nature of Archaean continental crust indicates that the basaltic material was somehow removed from the site of generation of granitoid melts. Applying uniformitarian principles, oceanic crust would be capable of suppling the large volumes of basalt required, and this crust could be moved through the site of melt generation by subduction.

Therefore, any discussion of the processes by which Archaean continental crust was formed requires some understanding of Archaean oceanic crust and the processes by which it may have been created and destroyed.

Radiogenic heat production was between 2.65 and 3.4 times greater at 2.8 Ga (depending on the bulk K:U ratio which is taken for the Earth) than at present (Bickle, 1978). Unless the heat producing radioactive elements were somehow concentrated into the surface layers of the young planet (Galer and Goldstein, 1991), then the inevitable consequence is that the mantle was hotter in the Archaean than at the present day. Estimates vary for how much hotter the mantle may have been, with an upper limit of up to 450°C hotter, based on the extrusion temperatures of komatiites (eg Arndt, 1983). However, such temperatures would lead to the upper mantle being extensively partially molten to a depth of 250 km (Nisbet and Walker, 1982), and therefore the temperatures responsible for the formation of komatiites must have been anomalously high and localised, probably related to mantle plumes (Campbell et al. 1989). Temperatures in modern plumes are 200 to 300°C hotter than the present average mantle "potential temperature" of 1,280°C (McKenzie and Bickle, 1988). ("Potential temperatures" are temperatures corrected to one atmosphere pressure, eliminating the adiabatic increase of temperature as a function of depth within the mantle).

Mathematical models suggest that the differences between ambient mantle temperatures and temperatures within mantle plumes were similar in the Archaean to the present day (Campbell and Jarvis, 1984; Bickle, 1986; Campbell and Griffiths, 1992; Nisbet et al. 1993). Therefore, as shown in figure 4.1, Nisbet et al. (1993) used the calculated extrusion temperatures of komatiites, the products of Archaean plumes, to constrain the potential temperature of the Archaean mantle to ≈ 1600°C at the time of the extrusion of the Barberton greenstone belt (3.5 Ga; de Wit, 1992), and to ≈ 1500°C at the time of the extrusion of the Upper Greenstones of the Belingwe belt of

Zimbabwe (2,692 ± 9 Ma; Chauvel et al. 1993). Temperature estimates of plumes are based on the MgO content of komatiitic liquids, determined from glassy chilled margins or calculated from the forsterite contents of olivines. The calculations require that the olivines are at equilibrium with the liquid under investigation, and the olivine to liquid Mg to Fe partition coefficient must be precisely known. This coefficient depends on the temperature, pressure and oxygen fugacity at which the olivine crystallised. Thus the assumptions necessary to calculate an extrusion temperature introduce errors of ≈ ± 50°C to the calculated temperatures (figure 4.1). However, it should be noted that although the temperature estimates of Nisbet et al. are the most robust estimates available on the temperatures of Archaean plumes, a further set of calculations is required to relate these to average mantle temperatures.

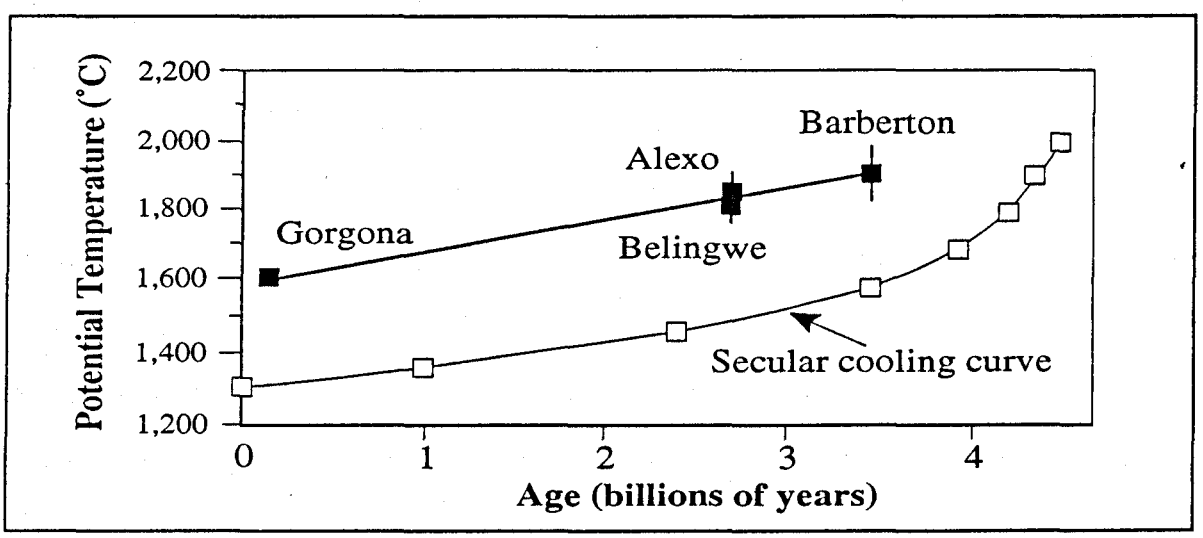

Figure 4.1 Potential temperatures of Archaean plumes estimated from komatiites. Plume temperatures are assumed to be ≈ 300°C higher than average mantle temperatures, thus closely relating the thermal evolution of the mantle to a secular cooling curve (after Nisbet et al. 1993).

Mathematical models (eg Campbell and Jarvis 1984, Nisbet and Walker, 1982) indicate that if ambient mantle potential temperatures in the Archaean were more than 200 to 250°C hotter than at present, mantle convection would have been chaotic, and an upper mantle partial melt zone would have encircled the globe. Therefore several authors (Galer, 1991; Campbell and Griffiths, 1992; Davies, 1992) estimate that the Archaean upper mantle was on

average only 50 to 150°C hotter than at present. The estimates of Campbell and Griffiths (1992) and Davies (1992) are based on the chemistry (MgO) of tholeiitic basalts dominant within the mafic sequences of greenstone belt volcanics. Recent detailed geochemical analysis of these basalts has indicated that these lavas were produced by melting under thick lithosphere (Arndt and Albarède, 1992), whereas Campbell and Griffiths (1992) used thermal models which assume that melting could proceed to similar depths as modern oceanic basalts. To achieve the same percentage of partial melting (and hence MgO content) at a greater depth requires higher potential temperatures. Therefore the comparatively low estimates of the temperature of the Archaean mantle made by Campbell and Griffiths (1992) and Davies (1992) are possibly underestimates of the true temperature.

When the error bars on the temperature estimates discussed above are considered, the upper limits of mantle temperature estimated by mathematical models and the lower limits of mantle temperature estimated from komatiite models overlap. In this thesis, this overlap of temperature estimates is taken as the most probable temperature of the Archaean mantle, giving a potential temperature for the mid-Archaean mantle of 1450°C ± 50°C, approximately 170°C hotter than the mantle today.

At the present day, the earth loses 65% of its heat through the construction and destruction of oceanic crust by plate tectonic processes (England and Bickle, 1984). Clearly, any uniformitarian model of the Archaean thermal regime should incorporate the dominant mechanism by which the mantle is cooled at the present day. However, because of the higher temperature of the Archaean mantle, the principle of uniformitarianism cannot be directly applied to Archaean plate tectonic processes. The effects of higher mantle temperature on Archaean tectonics are considered below.

The base of the lithosphere is thermally defined (McKenzie and Bickle, 1988), and therefore higher Archaean mantle temperatures would inevitably have lead to the Archaean oceanic lithosphere being thinner than modern oceanic lithosphere of similar age. Higher upper mantle temperatures cause increased melting at mid-ocean ridges, producing larger volumes of basic magmas, resulting in thicker oceanic crust (McKenzie and Bickle, 1988). Figure 4.2 shows a curve from Galer (1991) relating mantle potential temperature to the thickness of oceanic crust. This curve predicts that if the mantle was 170°C hotter than at present the resulting thickness of oceanic crust would have been ≈ 22 km. Therefore, Archaean oceanic plates would have contained a larger proportion (by a factor of two to three) of crust to lithospheric mantle than modern oceanic plates. The greater heat loss necessary from the mantle to accommodate the higher radiogenic heat production in the Archaean may have been accommodated by either greater ridge length (Hargraves, 1986), or by faster plate motion (Abbott and Hoffman, 1984; Christensen, 1985; Martin, 1986; Davies, 1992).

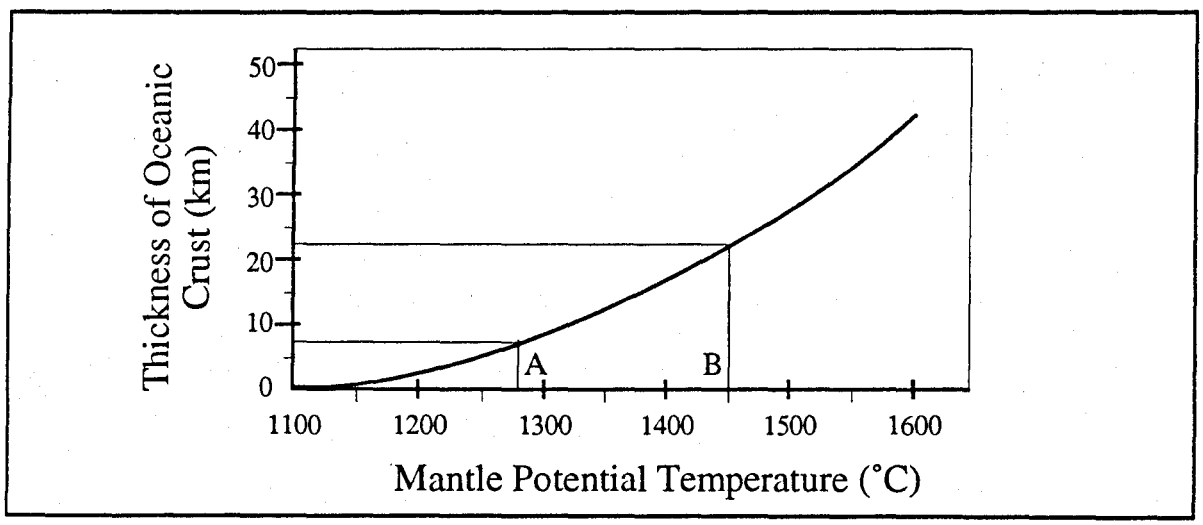

Figure 4.2 A curve relating mantle potential temperature to thickness of oceanic crust (after Galer, 1991), predicting (A) 7 km thick oceanic crust for a modern upper mantle potential temperature of 1280°C, and (B) ≈ 22 km thick oceanic crust for a 170°C hotter Archaean mantle.

The second factor which must be considered in any model of Archaean plate tectonics is the mechanism by which oceanic crust was returned to the

mantle. At the present day this is achieved by subduction, in which old (at the present day, the average age of oceanic crust upon subduction is 100 Ma (Parsons, 1982)), comparatively cold and dense oceanic lithosphere sinks into the underlying mantle, primarily by virtue of its density. However, there would have been major differences in the Archaean.

Modern basaltic oceanic crust has a density of 2.95 g cm^{-3} (Turcotte and Schubert, 1982), and the peridotites of the oceanic lithospheric mantle have (normative) densities of 3.33 to 3.34 g cm^{-3} (Hawkesworth et al. 1990). Therefore it is the lithospheric component of oceanic plates which raises the average density of the plate to a value at which subduction into the mantle is possible. In the Archaean (as discussed above) oceanic plates contained a larger proportion of oceanic crust to lithospheric mantle. Therefore Archaean oceanic plates would have had a lower density than modern oceanic plates. It has been argued that the density of Archaean oceanic plates could have been increased to a value at which subduction was possible if the Archaean oceanic crust was komatiitic (eg Arndt, 1983), thus facilitating subduction. However, this requires an implausibly hot mantle, and the residues of such melting, which would make up the oceanic lithospheric mantle, would be less dense than modern lithospheric mantle (Hawkesworth et al. 1990; Davies, 1992; 1993), again resulting in buoyant oceanic plates. The density of Archaean oceanic plates may have been further reduced if the larger amount of heat loss required from the mantle was being accommodated by faster plate motion. In this instance oceanic plates would be young (and therefore hot, with a relatively low density) on arrival at the site of plate destruction (Condie, 1986; Martin, 1986; Davies, 1992, 1993). In addition, the density of the oceanic crust may have been still further reduced by hydrothermal alteration (to the ≈ 500°C isotherm - the stability limit of serpentine) to values as low as low as 2.67 g/cm^3 (de Wit et al, 1992). To some extent, the lower density of Archaean oceanic plates would have been offset by the lower density and viscosity of the

hot Archaean mantle (Nisbet and Walker, 1982), but it is probable that the return of oceanic plates to the mantle was harder to achieve in the Archaean than at the present day.

Several authors have suggested models for the possible consequences of higher Archaean mantle temperatures and buoyant oceanic plates on plate tectonic processes. These models range from subduction processes similar to those operating at the present day, but with shallower angles of subduction and higher geotherms within subduction zones (Condie, 1986; Martin, 1986), to non-uniformitarian models in which the buoyancy of oceanic plates caused them to stack over sites where they entered the mantle to produce a pile of slabs of oceanic material.

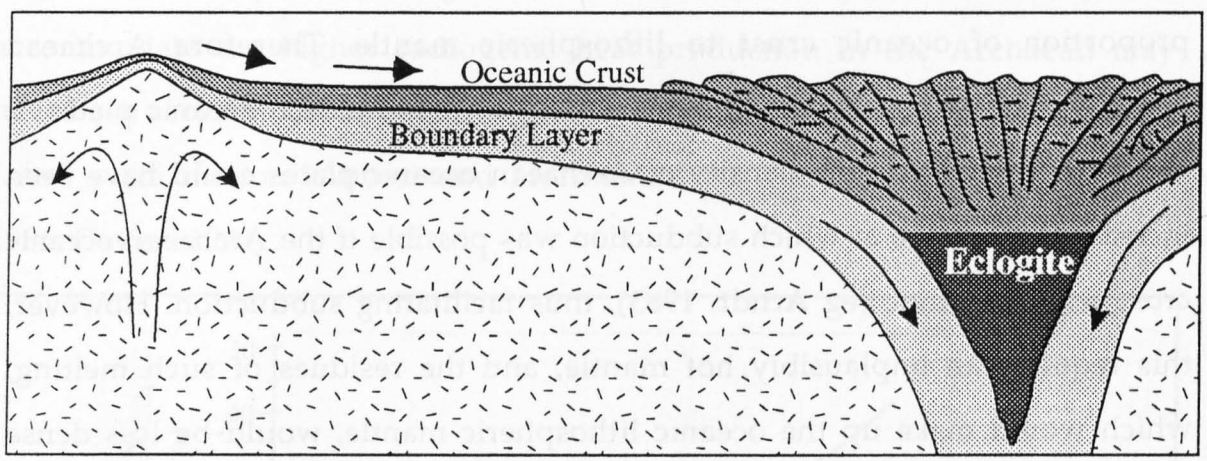

Figure 4.3 A non-uniformitarian model for Archaean plate tectonic processes (Davies, 1992) in which the inherent buoyancy of oceanic crust prevents it being easily returned to the mantle. Oceanic crust piles up over symmetrical "subduction" zones, and may only return into the mantle once it had entered the eclogite field.

Models have been proposed in which oceanic material was underthrust beneath a slab pile (Rapp, 1991; Davies, 1992) or obducted on top of it (de Wit et al. 1992). In either case, the base of the slab pile would eventually reach the eclogite or garnet granulite field, where it would have had a slight density excess over the underlying mantle (approximately 80 kg/m^3; Davies 1992), and so be capable of sinking into the underlying mantle, either in a continuous

process, or as periodic "drips" as the dense base of the slab pile delaminated (Davies, 1992).

The processes by which Archaean oceanic crust was destroyed may have been asymmetric, as with modern subduction zones, or they may have been symmetrical, as shown in figure 4.3. This model is clearly significantly different from recent subduction zones, and therefore the nomenclature of such sites of the destruction of oceanic crust becomes important. Simply to refer to them as subduction zones, with the modern implications of old, cold, dense lithosphere entering the mantle along Benioff Zones ignores the differences between Archaean and modern processes. However, use of terms such as "sites of return of oceanic plates to the mantle" seems unnecessarily clumsy. Here the sites and processes will be referred to as subduction, but with the caveat *s.l.* (*sensu lato*), indicating that all that is implied is the return of basic plates, produced at the Archaean equivalent of mid-ocean ridges, to the mantle.

In the following discussion of models for Archaean crust formation, Archaean subduction *s.l.* processes are shown as asymmetric. This is partly for reasons of clarity, and partly based on the consideration that for symmetrical subduction *s.l.* processes to occur, the colliding plates must have had the same density as each other. The age of plates is an important factor determining their densities, and it is considered unlikely that two colliding plates would necessarily be the same age. There would therefore have been a tendency for the older, denser plate to sink faster than the younger plate, thus developing an asymmetric system of subduction *s.l.*.

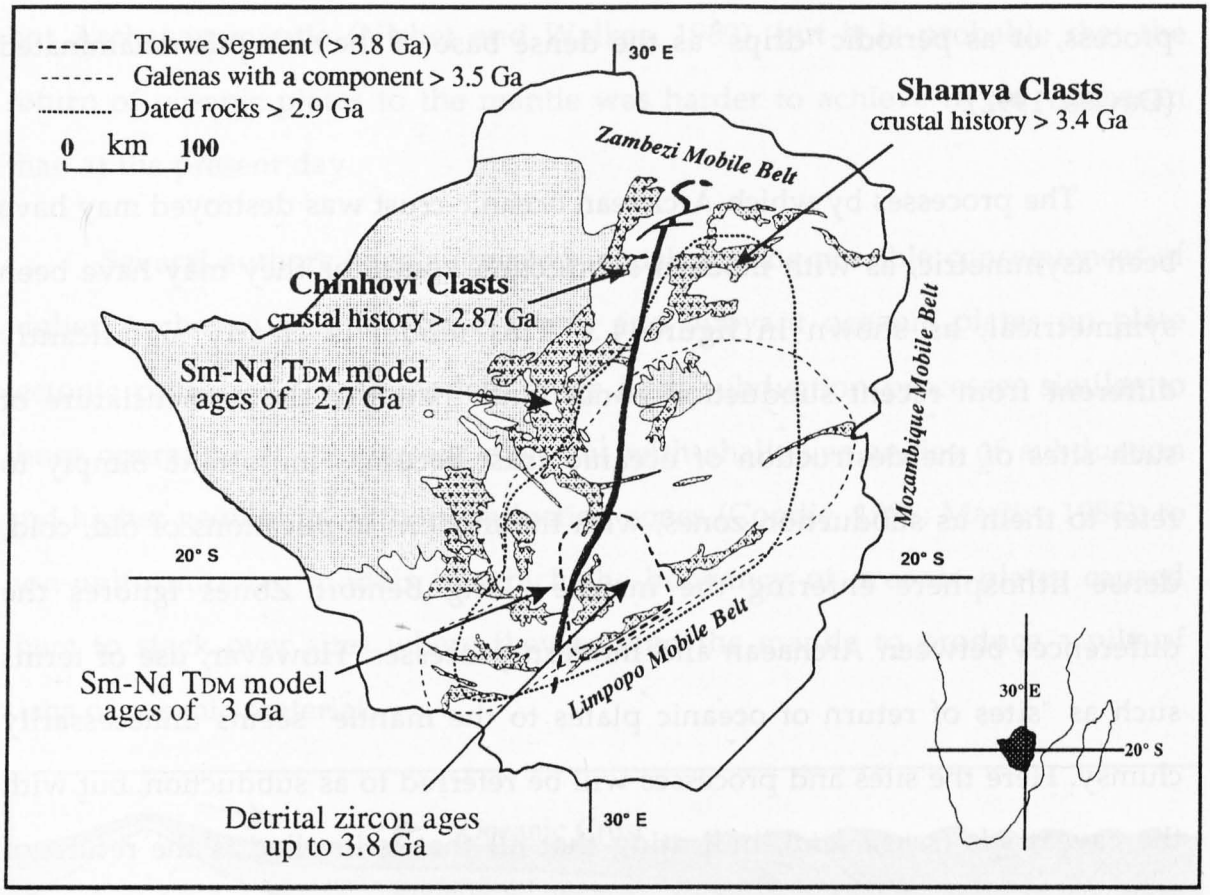

Figure 4.4 An age map of the Zimbabwe craton, showing the ≥ 3.8 Ga Tokwe segment, the area within which rocks older than 2.9 Ga have been recognised, and the region of "Kwekwe" type leads (analysed from galenas, Robertson, 1973) which contain a component ≥ 3.5 Ga old (Kramers and Foster, 1982). These demonstrate that the craton grew first to the north, and then to towards the north-west. However, there is insufficient data from the east of the craton to show how and when this portion of the craton formed.

4:2.2 Formation and growth of proto-continents.

Although the Sm-Nd T_{DM} model age of clast 89-S-26 sets a minimum age for continental crust within the Shamva region of 3.34 Ga, the date at which continental crust was first formed in the Shamva region is difficult to establish. At Chinhoyi, the earliest continental crust recognised has a well defined crystallisation age of 2,875 ± 3 Ma, almost 500 Ma younger than the minimum age for the oldest material in the Shamva region. The striking difference in duration of crustal histories recorded at the Shamva and Chinhoyi clast localities indicates that lateral growth of continental crust may

have occurred in the Archaean. When other isotope systems are taken into consideration throughout the Zimbabwe craton (figure 4.4), this does appear to be the case, with the continent nucleating with the Tokwe segment in the early Archaean, and then growing first to the north, and then to the north-west. However, this model is based on a relatively small data set, and further data are required, especially to the east of the craton, where dating would show if the growth of the craton was symmetrical (occurring on both flanks at the same time) or asymmetrical.

As the earliest history of the Shamva region is poorly constrained, the geochronology and geochemistry of the earliest material recorded from Chinhoyi is used in constructing a model for the initial formation of continental nucleii. It should be stressed that the models invoked require horizontal plate motions, and thus allow a diachronous progression of processes from the initial construction of continental crust at the margins of the young continent, (or at a new site of the generation of continental crust) to the processes by which older, thicker, more stable continental crust is augmented. Chinhoyi, at the margin of the craton, is used as an example of the processes by which continental crust is initially formed at a given locality. The oldest granitoids preserved at Chinhoyi are members of the low-alumina TTG suite (Chapter 3:3.2), such as the clasts 89-C-21 and 89-C-23, which have been dated (Chapter 3:3.5) to give a well constrained zircon crystallization age of 2,875 ± 3 Ma. The model invoked for the formation of this suite, based on experimental petrology carried out by Rapp et al. (1991) involves ≈ 10% partial melting of amphibolite facies metabasalt at a depth of ≈ 25 km (8 kbar) and a temperature of 1000°C (Chapter 3:3.3).

Such conditions would have been achieved early in the history of an Archaean subduction *s.l.* zone, by partial melting of thick oceanic crust underthrust beneath another oceanic plate (figure 4.5). This model requires a far higher geothermal gradient than is present in modern subduction zones,

which may have been achieved by a combination of the higher potential temperature of the Archaean mantle (Nisbet et al. 1993), subduction *s.l.* of younger, hotter oceanic crust (Condie, 1986; Martin, 1986; Davies, 1992, 1993), and the thin Archaean oceanic plate undergoing rapid conductive heating as it attempted to attain thermal equilibrium with the mantle (as Archaean oceanic plates were thinner, they would attain thermal equilibrium through conductive processes more rapidly than thicker modern plates).

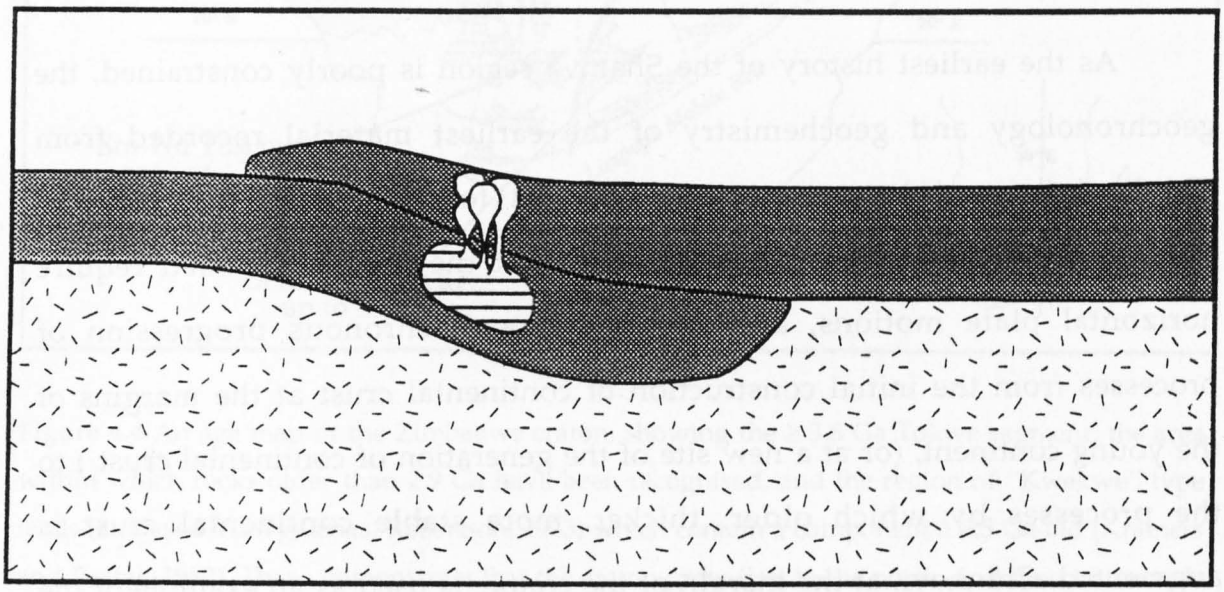

Figure 4.5 The production of the low-alumina TTG suite by partial melting of underthrust thick oceanic crust.

However, as has been discussed previously, Archaean oceanic plates would probably not have subducted *s.l.* efficiently, resulting in slabs of oceanic material stacking over subduction *s.l.* sites. As the slab pile grew by continued subduction *s.l.* of oceanic crust, the upper surface of new material introduced to the site by continued subduction *s.l.* would no longer be in contact with the hot base of young oceanic crust, but instead would be in contact with older, cooler material. Therefore, as a site of subduction *s.l.* evolved, the depth of melting would increase (figure 4.6).

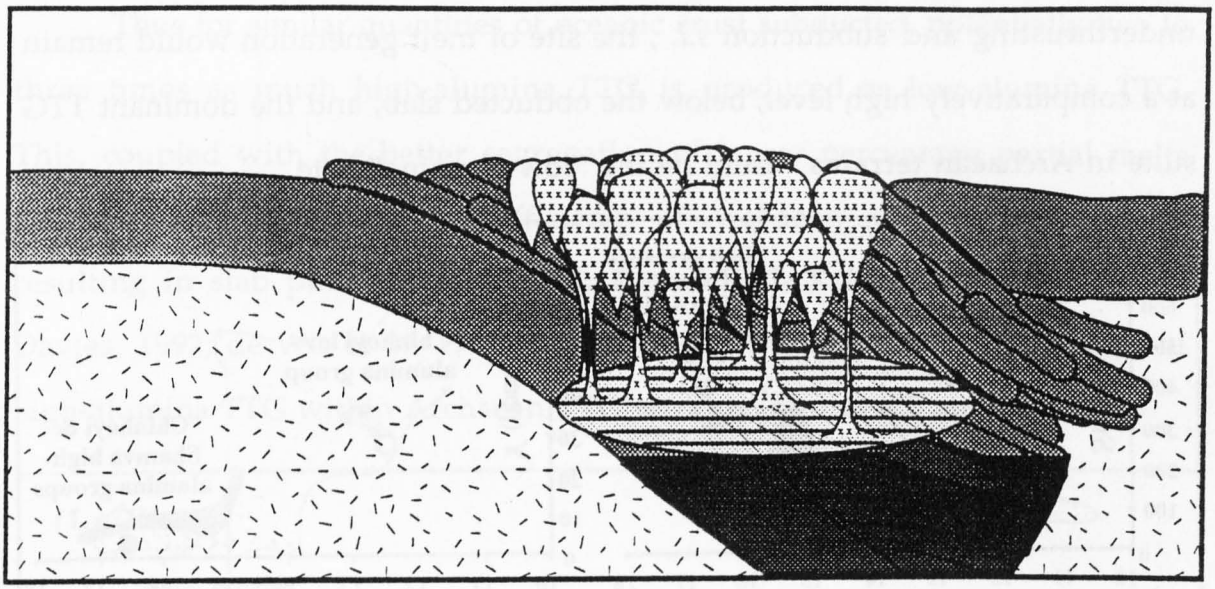

Figure 4.6 Generation of high alumina TTG ("X" hatching) by the partial melting of metabasalt in the base of pile of slabs of oceanic crust. The base of the pile is in the eclogite field (darkest shading) and can return to the mantle.

As the depth of melting increases, the increased pressure causes changes in the composition of the restite assemblage. At shallow levels, plagioclase is a major residual phase, and depletes the melts in Eu and Sr. As the depth of melting increases, plagioclase becomes increasingly less stable, and forms a progressively smaller proportion of the residual assemblage. Therefore as depth increases, negative Eu anomalies become less pronounced, and Sr abundances in the melts increase. Also, as depth increases, garnet becomes a stable phase within the residuum. The compatibility of HREE within this mineral means that as depth of melting increases, partial melts are increasingly likely to be depleted in HREE. Therefore a continuum of TTG compositions are possible, from a low pressure, Sr depleted "low-alumina" suite (plagioclase contains a high proportion of alumina, and thus melts produced where plagioclase was a major phase in the residuum have

relatively low Al_2O_3 contents), to a high pressure, HREE depleted "high-alumina" suite (Barker and Arth, 1976; Rapp et al. 1991). It is important to note that if slab piles grew by overthrusting of slabs of oceanic crust rather than by underthrusting and subduction *s.l.* , the site of melt generation would remain at a comparatively high level, below the obducted slab, and the dominant TTG suite in Archaean terrains would be the "low-alumina"suite.

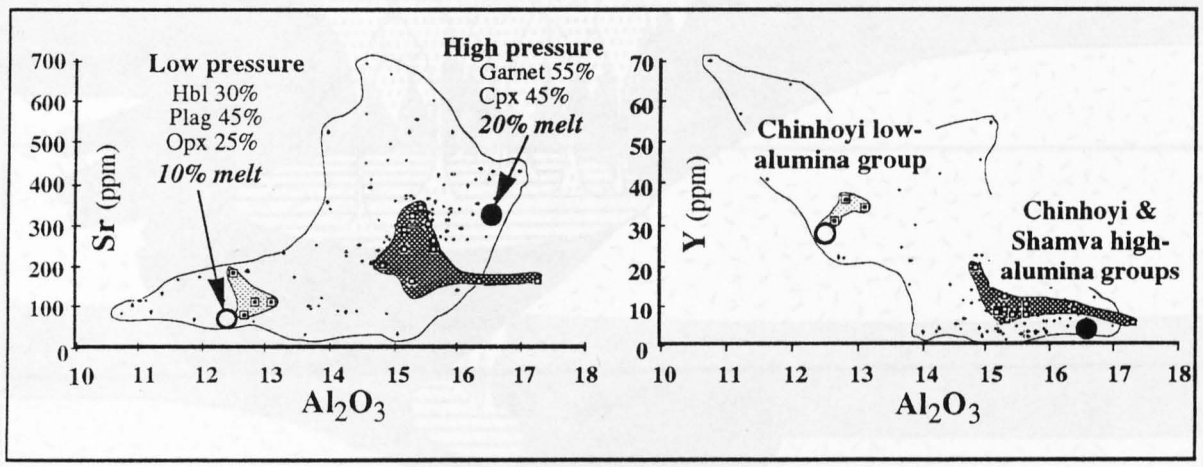

Figure 4.7 Sr and Y against Al_2O_3 for the Chinhoyi group 2 clasts (light shading) the Shamva and Chinhoyi group 1 clasts (dark shading), and granitoids from Southern Zimbabwe (unshaded; data supplied by B. Luais, pers. comm). The open circle is a 10% batch melt of amphibolite (major element composition from Rapp et al. 1991) with Sr and Y contents of modern MORB. The filled circle is a 20% batch melt of the same composition. Restite assemblages are based on experimental petrology detailed in Rapp et al. (1991). Distribution coefficients are given in appendix A.

Figure 4.7 shows the positive correlation of Sr with Al_2O_3, and the negative correlation of Y with Al_2O_3 which is predicted by this model. It is important to note that as the Al_2O_3 content, and hence the inferred depth of melting, increase the percentage of partial melting also increases from 10% partial melting to produce the low-alumina suite, to 20 to 30% to produce the high-alumina suite (Barker and Arth, 1976; Martin, 1986; Drummond and Defant, 1990; Rapp et al. 1991; Luais and Hawkesworth, 1994). At Chinhoyi, this transition between the production of low- and high-alumina TTG appears to have occurred in 75 (± 20) Ma, between the first crust formed (clasts 89-C-21

and 89-C-23), at 2,875 ± 3 Ma, and the first group 1 clasts (89-C-20 and 89-C-28) at 2,800 ± 20 Ma.

Thus for similar quantities of oceanic crust subducted, potentially two to three times as much high-alumina TTG is produced as low-alumina TTG. This, coupled with the better segregation of larger percentage partial melts (Wickham, 1987), and the low efficiency of Archaean subduction processes, resulting in slab piles (Kröner, 1985; Rapp, 1991; Kröner and Layer, 1992; Davies, 1992; de Wit et al. 1992) may have contributed to the dominance of high-alumina TTG within Archaean TTG terrains (figures 4.7 and 4.8).

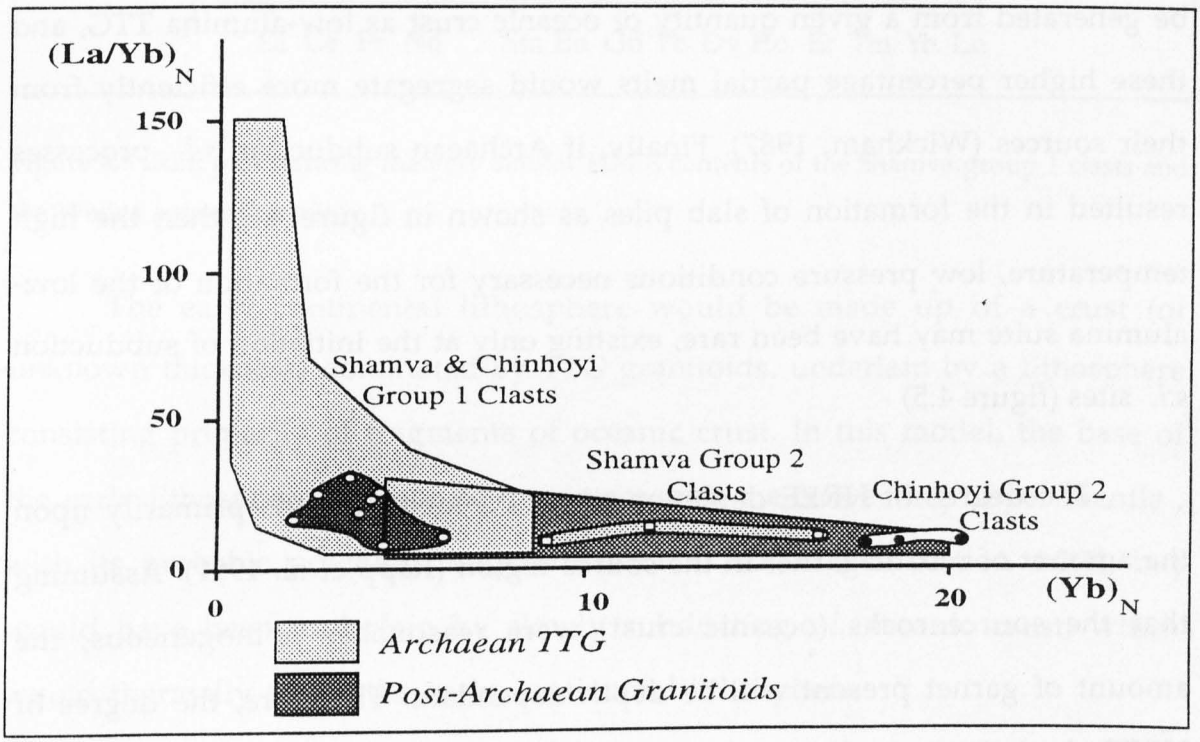

Figure 4.8 Chondrite normalised $(La/Yb)_N$ vs. $(Yb)_N$ for the Shamva and Chinhoyi clasts, relative to the Archaean and Post-Archaean granitoid fields of Martin (1986), showing that the low alumina TTG group 2 clasts of Chinhoyi group 2 plot well outside the usual field for Archaean TTG, with high $(Yb)_N$.

Graphs of La/Yb vs Yb are commonly used (eg Martin, 1986; 1993) in order to support the suggestion that the sources of Archaean TTG suite granitoid were at sub-crustal depths, with garnet as a major residual phase, resulting in steeply fractionated REE patterns and HREE depletion, in contrast

to more recent granitoids, which were generally formed by processes at higher levels, where garnet is not residual, resulting in less fractionated REE patterns, with less HREE depletion. However, it should be emphasised that the Archaean TTG field shown on figure 4.8 is only representative of the high-alumina suite. The low-alumina suite (Chinhoyi group 2) has low $(La/Yb)_N$ and high $(Yb)_N$ values, well outside the usual field for Archaean TTG. The dominance of the high alumina suite may be due to one or more of the following factors. The percentage of partial melting necessary to produce the high-alumina suite is two to three times greater than that for the low-alumina suite (figure 4.7), and thus two to three times as much high-alumina TTG may be generated from a given quantity of oceanic crust as low-alumina TTG, and these higher percentage partial melts would segregate more efficiently from their sources (Wickham, 1987). Finally, if Archaean subduction *s.l.* processes resulted in the formation of slab piles as shown in figure 4.6, then the high temperature, low pressure conditions necessary for the formation of the low-alumina suite may have been rare, existing only at the initiation of subduction *s.l.* sites (figure 4.5)

The degree of HREE depletion of a TTG melt depends primarily upon the amount of restitic garnet in the source region (Rapp et al. 1991). Assuming that the source rocks (oceanic crust) were reasonably homogeneous, the amount of garnet present will be depth dependant. Therefore, the degree of HREE depletion may be used as a crude indication of the depth at which melting occurred. Figure 4.9 shows that the HREE contents of the Shamva group 1 clasts, intruded at 3.2 and 2.8 Ga (Chapter 3:2.5), have extremely similar HREE contents to the 2.67 Ga Wedza suite of tonalites (Jelsma, 1993), strongly suggesting that from 3.2 to 2.67 Ga, the depth of melting (and thus the thickness of the overlying continental lithosphere) of the Shamva region had a reasonably constant thickness, within the range ≈ 50 to 70 km, the depth of the zone of optimum TTG melt generation (16 to 22 kbar, Rapp et al. 1991).

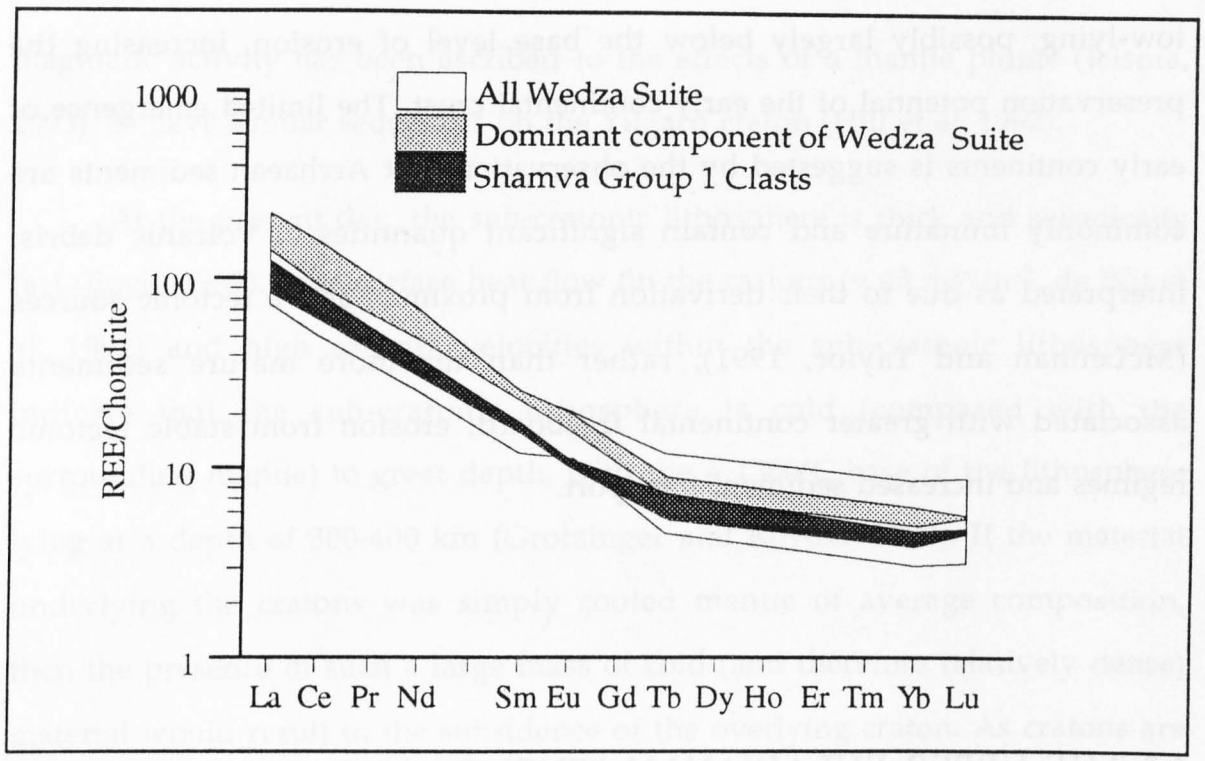

Figure 4.9 REE plot showing the very similar HREE contents of the Shamva group 1 clasts and the Wedza suite of tonalites.

The early continental lithosphere would be made up of a crust (of unknown thickness) dominated by TTG granitoids, underlain by a lithosphere consisting primarily of fragments of oceanic crust. In this model, the base of the early lithosphere will not be in contact with the convecting upper mantle , with its probable potential temperature of ≈ 1450°C (see section 4:2.1), but would have been underlain by slowly subducting *s.l.* oceanic crust, which would thermally shield the early continental lithosphere.

This study has demonstrated that at least fragments of the early continents were capable of surviving for long periods of time before their stabilisation. In the case of the Shamva region this was ≥ 670 Ma, from the minimum age of clast number 89-S-26 (see Chapter 3:2.4) to stabilisation in the Upper Bulawayan "event". The early continental crust would have resisted a direct return to the mantle by virtue of its low density. As the crust was underlain by a thick pile of slabs of oceanic crust, sited over subduction *s.l.* zones, the coolest part of the upper mantle, it may have been comparatively

low-lying, possibly largely below the base level of erosion, increasing the preservation potential of the early continental crust. The limited emergence of early continents is suggested by the observation that Archaean sediments are commonly immature and contain significant quantities of volcanic debris, interpreted as due to their derivation from proximal, active tectonic sources (McLennan and Taylor, 1991), rather than the more mature sediments associated with greater continental freeboard, erosion from stable tectonic regimes and increased sediment transport.

4:3 THE UPPER BULAWAYAN "EVENT" AND CONTINENTAL STABILISATION

The Upper Bulawayan "event" involved a sequence of mafic and felsic igneous events which cross-cutting relationships indicate were coeval over the entire area of the Zimbabwe Craton. However, this cross-cutting stratigraphy has yet to be confirmed by high resolution geochronology. The first recorded effects of the "event" were the extrusion of the "Iron Mask" greenstone belt volcanics within the Harare-Shamva greenstone belt at 2,713 ± 15 Ma (Jelsma, 1993), and associated intrusion of TTG suite granitoids (2,720 ± 6 Ma for the Chinhoyi clast 89-C-26; this study). The greenstones were intruded by the Sesombi and Wedza suites of syn-tectonic tonalites at 2,673 ± 5 Ma (this study) and 2,667 ± 4 Ma (Jelsma, 1993) respectively, and by a late- to post-tectonic suite of tonalite-granodiorite-monzogranites between 2,664 ± 6 Ma and 2,618 ± 7 Ma (Jelsma, 1993). The final felsic magmatic event before the stabilisation of the craton was the intrusion of the Chilimanzi suite of monzogranites (also known as the "Late Granites") at 2,601 ± 14 Ma (Jelsma, 1993). This series of

magmatic activity has been ascribed to the effects of a mantle plume (Jelsma, 1993), as have similar sequences on the Yilgarn craton (Hill et al. 1992).

At the present day, the sub-cratonic lithosphere is thick and seismically fast (Boyd, 1989). Low surface heat flow on the cratons (≈ 45 mWm^{-2}, de Wit et al. 1992) and high seismic velocities within the sub-cratonic lithosphere indicate that the sub-cratonic lithosphere is cold (compared with the surrounding mantle) to great depth, with the ≈ 1300°C base of the lithosphere lying at a depth of 300-400 km (Grotzinger and Royden 1990). If the material underlying the cratons was simply cooled mantle of average composition, then the presence of such a large mass of cold (and therefore relatively dense) material would result in the subsidence of the overlying craton. As cratons are emergent, this strongly suggests that the underlying material must be of inherently low density. The largest suites of xenoliths from the sub-cratonic lithosphere have higher $Mg^{\#}$ than those from oceanic lithosphere (Boyd, 1989). Geochemistry and petrology indicate these xenoliths may be interpreted as residua of an event which depleted them in FeO, TiO_2, CaO and Al_2O_3 (Herzberg, 1993). Re-Os isotope systematics indicate that this depletion occurred in the Archaean, rapidly and throughout the entire thickness of sub-cratonic lithosphere sampled by kimberlites (Walker et al. 1989; Pearson et al. 1993). Therefore the sub-cratonic lithosphere is not only thermally and mechanically defined but, particularly in Archaean areas, it is also chemically depleted. The FeO depletion of this material lowers its density by ≈ 1 %, equivalent to a temperature difference of 200°C to 400°C in homogeneous mantle (Hawkesworth et al. 1990). Therefore the depleted sub-cratonic mantle may be cooler than its surroundings, and yet still be buoyant. The depletion of the sub-cratonic mantle also means that it is refractory, protecting the overlying crust from magmatic and deformational events (Pollack, 1986).

Several authors have suggested that the depletion of the sub-cratonic lithosphere could be achieved by extracting a komatiitic melt from the mantle

(Bickle, 1986; Boyd, 1989; Hawkesworth et al. 1990; Takahashi, 1990; Herzberg 1992, 1993), although there are chemical mass balance problems in applying this model to komatiites of the Kaapvaal craton, which either require an anomalously siliceous source if they are residua of partial melting, or are cumulates from high percentage partial melts (Herzberg 1993). However, the volume of komatiite required is similar to the volume of the Archaean sub-cratonic lithosphere preserved today, and no such volume of material is seen on the surface (komatiites make up <2% of the Harare-Shamva greenstone belt; Jelsma, 1993). It has been suggested (Nisbet and Walker, 1982; Boyd, 1989) that at pressures ≥ 50 kbar, komatiitic liquids are more dense than their residuum, in which case most of the komatiite may have been returned directly to the mantle, with only a small percentage erupted by virtue of its low viscosity. The residuum would then underplate the young continents to form depleted lithosphere (Boyd,1989; Kröner and Layer, 1992). The temperatures necessary for komatiite formation are too high to have been widespread in the mantle, otherwise the mantle would have undergone extensive partial melting (Nisbet and Walker, 1982; Campbell and Griffiths, 1992; Davies, 1992). Instead it is inferred that komatiites were formed within anomalously hot mantle plumes (Campbell et al. 1989; Rapp et al. 1991; Nisbet et al. 1993; Davies, 1993). Therefore it is suggested that plumes are responsible for the formation of depleted material in the sub-cratonic lithosphere, and that lithosphere formation may be incorporated within a model for the stabilisation of the Zimbabwe craton in the Upper Bulawayan "event" in response to the effects of a plume.

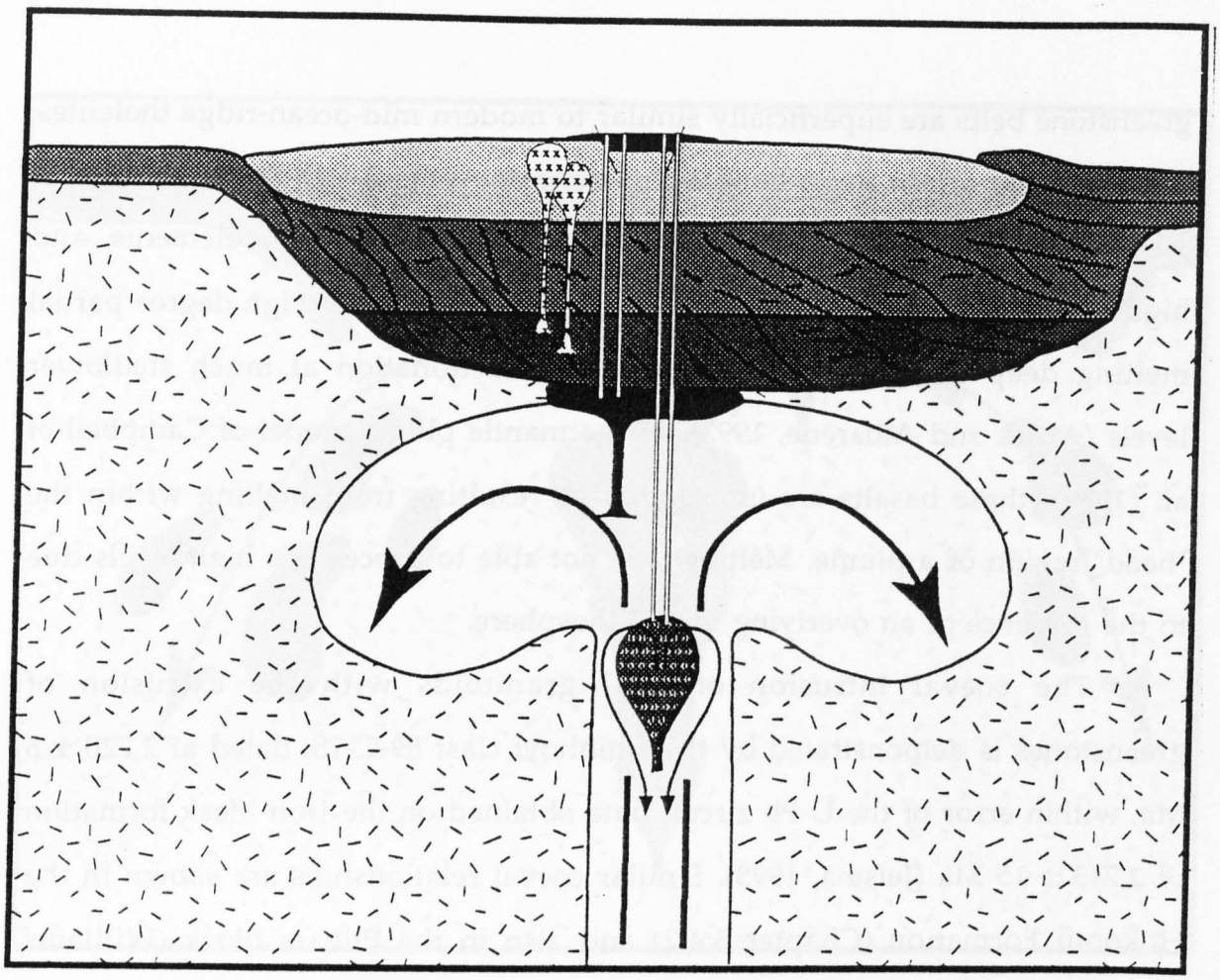

Figure 4.10 Northern Zimbabwe at 2.72 Ga. A plume under an early continent, showing eruption of komatiites from the plume tail region, with rising depleted residues of komatiite melting (white on black "0" hatching), and the generation of basaltic melts from the plume head region.

The first igneous products of the Upper Bulawayan event - the extrusion of greenstone belt volcanics - may be most readily attributed to the effects of a mantle plume. The basal sequences of greenstone belts contain komatiitic lavas, the ultramagnesian chemistry of which (up to 21% MgO in non-cumulate compositions in the Harare-Shamva greenstone belt, Jelsma, 1993) indicates extrusion temperatures of ≈ 1,500°C, and partial melting at temperatures of ≈ 1,750°C (Nisbet and Walker, 1982). Such extremely high temperatures must have been anomalous and localised within the mantle, if widespread partial melting of the upper mantle were not to result. Therefore, the hot "tail" region of an ascending mantle plume has been interpreted as the source of komatiite lavas (Campbell et al. 1989).

The formation of tholeiitic basalts within greenstone belts has also been attributed to the effects of a mantle plume. Although tholeiitic basalts in

greenstone belts are superficially similar to modern mid-ocean-ridge tholeiites, there are important geochemical differences. Archaean tholeiites have low Al_2O_3 contents (for a given $Mg^{\#}$), low levels of incompatible elements, and high Fe, Ni and Cr. Their formation has been modelled by high degree partial melting deep in the mantle, followed by fractionation at much shallower levels (Arndt and Albarède, 1992). In the mantle plume model of Campbell et al. (1989), these basalts are interpreted as resulting from melting within the "head" region of a plume. Melting was not able to proceed to high levels due to the presence of an overlying thick lithosphere.

The coeval intrusion of TTG granitoids with the extrusion of greenstones is demonstrated by the Chinhoyi clast 89-C-15, dated at 2,720 ± 6 Ma, within error of the U-Pb zircon date obtained on the Iron Mask formation of 2,713 ± 15 Ma (Jelsma, 1993). Similar coeval relationships are shown in the Hokonui Formation (Chapter 3:4.2) and also in the Pilbara block (Williams and Collins, 1990). Such TTG granitoids, coeval with greenstones, are interpreted as resulting from partial melting of fertile metabasalt in the base of the slab pile in response to heating by the plume, either by conduction, or by underplating of magmas. Given the close temporal relationship of the granites and greenstones, underplated basic magmas are considered the more probable heat source, as they are capable of supplying heat more rapidly than the conduction of a thermal pulse through the slab pile.

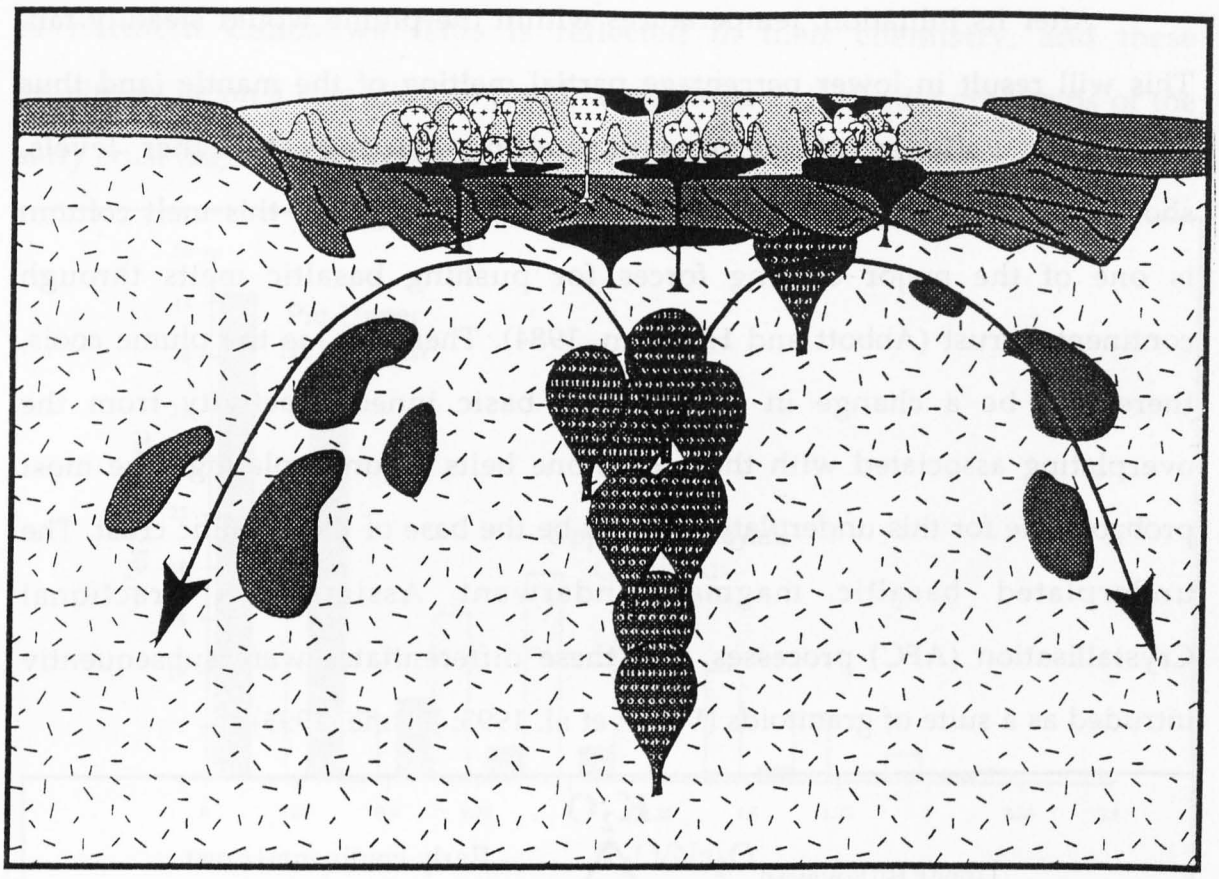

Figure 4.11 Northern Zimbabwe at 2.67 Ga. Continued plume activity under the continent results in the accelerated delamination of eclogite from the base of the early continent. Basalts intruded from the plume head region underplate the crust, and undergo AFC to produce a suite of calc-alkaline granitoids ("+" hatching).

Figure 4.11 shows a model for the situation under northern Zimbabwe at ≈ 2.67 Ga. The presence of the plume head beneath the young continent would increase the density contrast between the eclogitic root and the underlying mantle, thus accelerating the process of delamination. The response to this delamination would be uplift, causing erosion and the deposition of the Shamvaian sediments within basins sited over thick, subsiding, piles of greenstone belt volcanics. As the thermal pulse of conducted heat from the plume head passed up through the slab pile, fertile metabasalts would undergo partial melting, producing the Sesombi and Wedza suites of tonalites.

After its initiation, temperatures within the plume would steadily fall. This will result in lower percentage partial melting of the mantle (and thus decreasing volumes of melt), with melting starting at higher levels, shortening melt columns within the mantle. The length of this melt column is one of the major driving forces for pushing basaltic melts through continental crust (Abbott and Hoffman, 1984). Therefore, as the plume cools, there will be a change in the style of basic igneous activity from the overplating associated with the greenstone belts to underplating. The most probable site for this underplating would be the base of the tonalitic crust. The underplated basaltic magmas underwent Assimilation Fractional Crystallisation (AFC) processes, and these differentiates were subsequently intruded as a suite of granitoids (Vinyu et al. 1993; Jelsma, 1993).

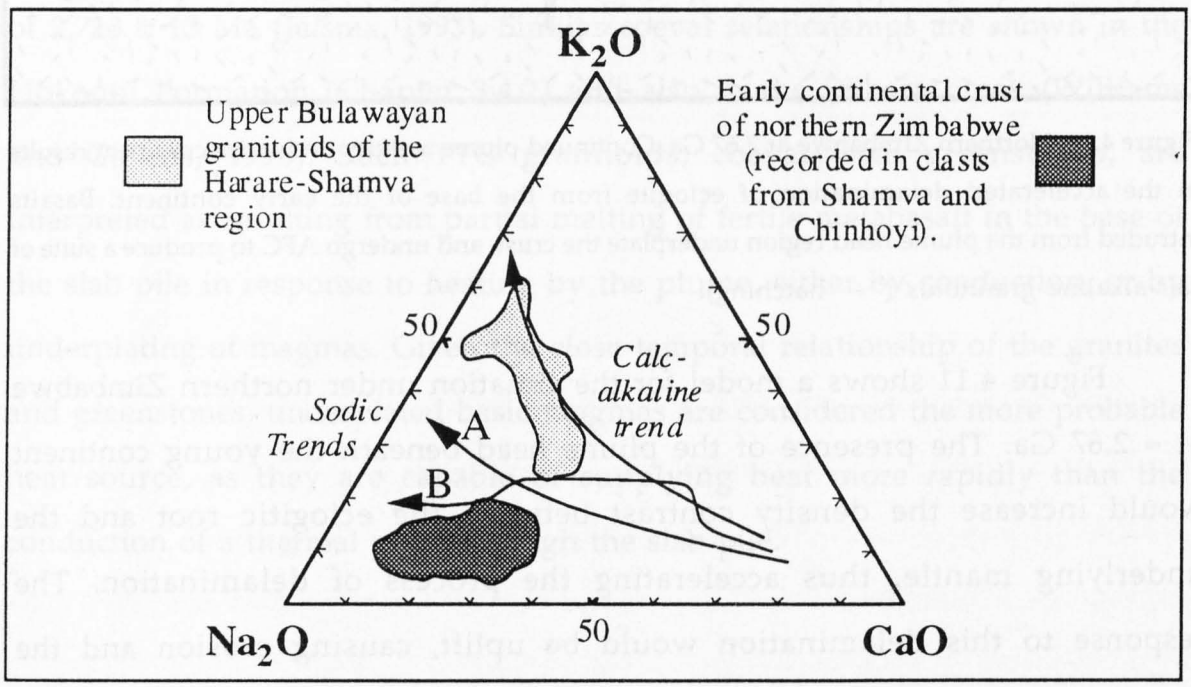

Figure 4.12 K_2O-Na_2O-CaO diagram showing that the Upper Bulawayan granitoids lie on a calc-alkaline trend, distinct from the sodic early continental crust. A - Sodic trend of Luais and Hawkesworth, 1994. B - Sodic trend of Barker and Arth, 1976. Data on early continental crust - this work; data on Upper Bulawayan granitoids from Snowden and Snowden, 1981 and Jelsma, 1993.

The granitoids of the Upper Bulawayan "event" are therefore produced by different process to the TTG-suites which formed the early continental crust

of northern Zimbabwe. This is reflected in their chemistry, and these granitoids lie on a calc-alkaline trend, as opposed to the sodic granitoids of the early crust (figures 4.12 and 4.13)

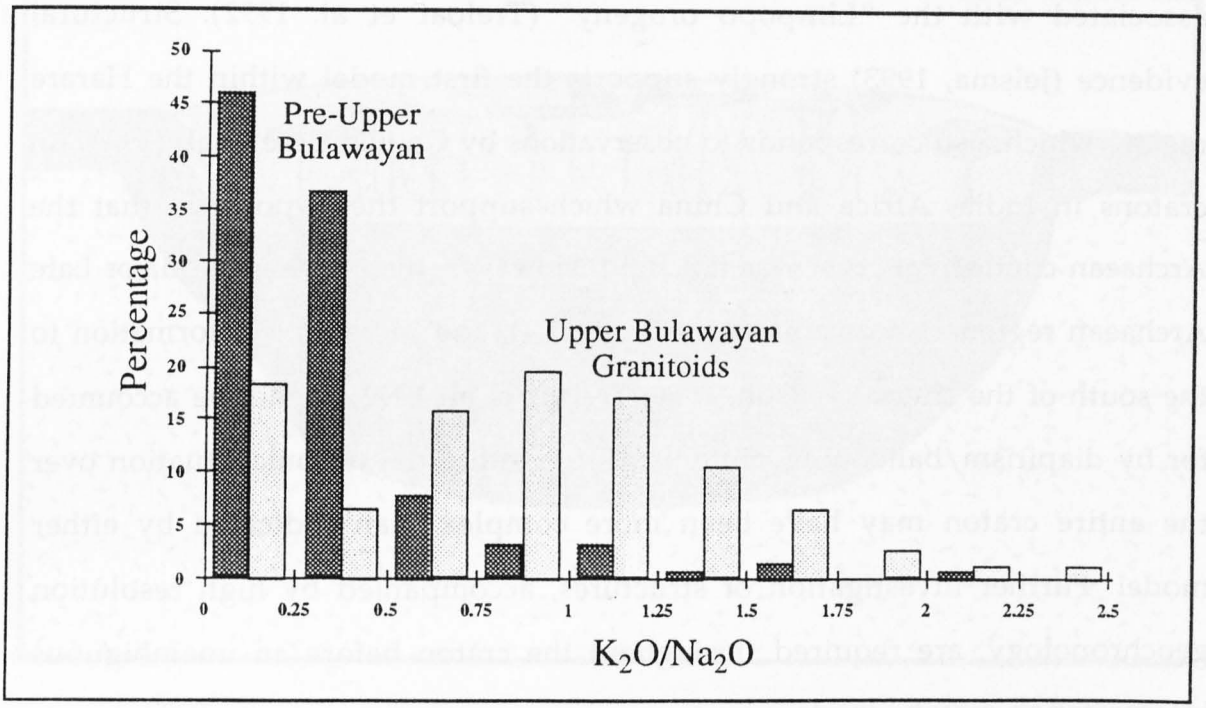

Figure 4.13 A histogram of percentage of sample set against K_2O/Na_2O for pre-Upper Bulawayan granitoids (this study; Luais and Hawkesworth, 1994; B. Luais, pers. comm) and Upper Bulawayan granitoids (Snowden and Snowden, 1981; Jelsma, 1993; B.Luais, pers. comm), clearly demonstrating the more potassic nature of the later Upper Bulawayan granitoids

The early members of this suite of granitoids are syn-deformational. This deformation resulted in the "dome and basin" pattern of granite batholiths with infolded synclinal greenstone belts which is preserved to the present day. There are two conflicting models for the tectonic regimes responsible for this deformation. In the first, deformation is achieved by vertical tectonics. As the granitoid plutons intruded, they progressively deformed their own margins and intervening country rocks in a large scale diapiric or ballooning plutonism interference pattern (Macgregor, 1951; Jelsma et al. 1993; Jelsma, 1993). This pattern may have been accentuated by a coeval downsagging of the comparatively dense greenstone belt materials into the underlying TTG crust, which had been warmed and softened by the intrusion of the granitoids (Peucat et al. 1993). The opposing model requires a

comparatively rigid crust, and states that the deformation is a fold interference pattern (Snowden and Bickle, 1976; Snowden, 1984), produced by horizontal tectonic forces (Bickle et al. 1980), possibly in response to deformation associated with the "Limpopo orogeny" (Treloar et al. 1992). Structural evidence (Jelsma, 1993) strongly supports the first model within the Harare region, which also corresponds to observations by Choukroune et al. (1993) on cratons in India, Africa and China which support the hypothesis that the Archaean continental crust was not rigid. However, the presence of major Late Archaean regional shear zones (see figure 1.4), and increasing deformation to the south of the craton (Wilson, 1990; Treloar et al. 1992) cannot be accounted for by diapirism/ballooning plutonism, suggesting the tectonic situation over the entire craton may have been more complex than indicated by either model. Further investigation of structures, accompanied by high resolution geochronology, are required throughout the craton before an unambiguous interpretation may be made.

Figure 4.14 is a model for the Zimbabwe craton at 2.6 Ga. The final stage of felsic magmatism on the Zimbabwe craton was the intrusion of the Chilimanzi suite of "Late granites". These are extensive, tabular intrusions of monzogranites, which outcrop over approximately 50% of the surface of the Zimbabwe craton at the present day. These late granites (figure 4.15) have higher contents of radioactive elements (Rb, K, Th, U) than granitoids intruded earlier in the Upper Bulawayan event, such as the Wedza Suite, lower abundances of trace elements concentrated in potassic and plagioclase feldspars (Ba and Sr), and higher contents of HREE. Major element modelling (Jelsma, 1993) suggests that they were formed by intra-crustal melting. This melting may have been in response to crustal thickening.

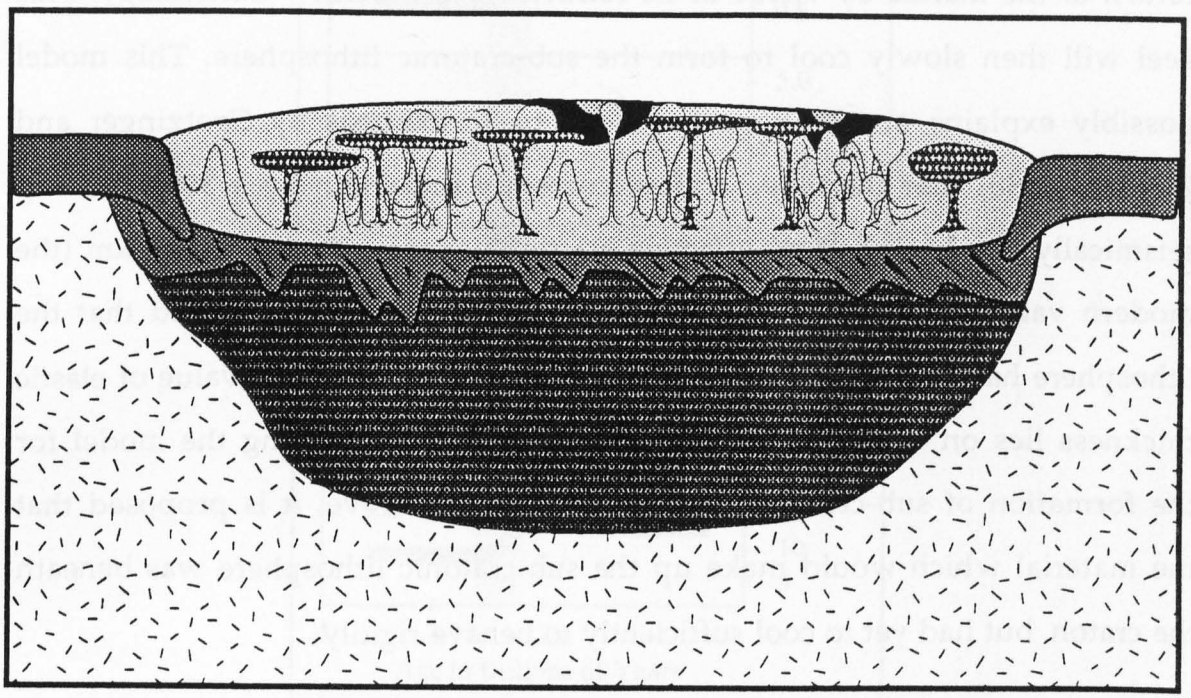

Figure 4.14 Northern Zimbabwe at 2.6 Ga. In response to magmatic and tectonic thickening, intra-crustal re-melting results in the formation of the "Late Granites" (white on black "+"). The continent is underlain by a depleted keel, formed from the residues of komatiite melting.

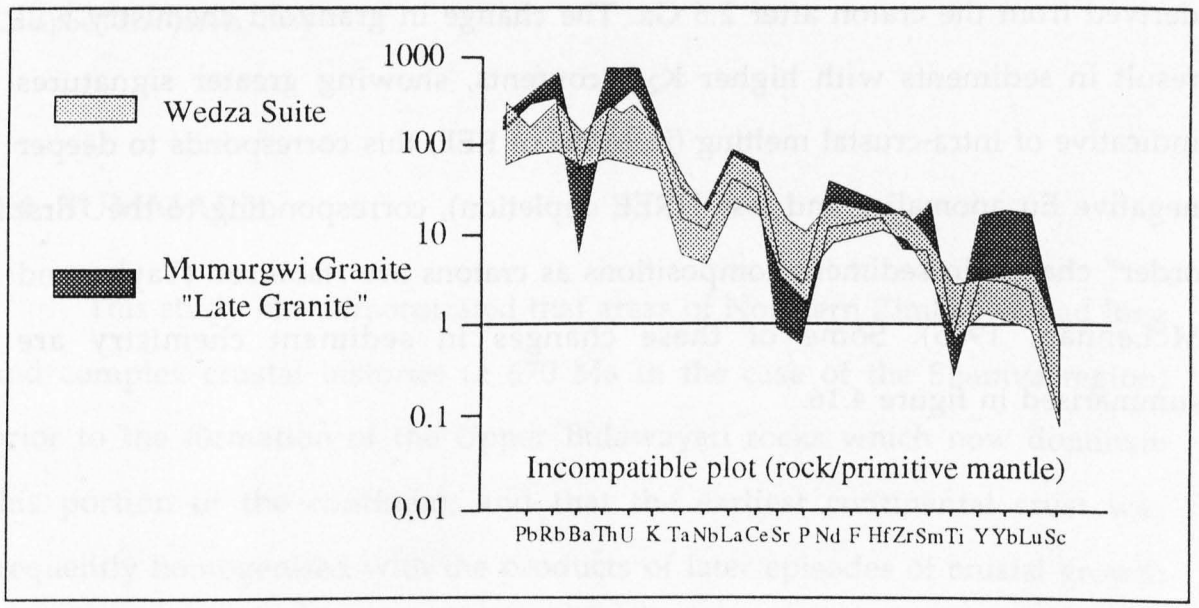

Figure 4.15 Incompatible element plot showing element patterns for the Wedza suite and the Mumurgwi granite, a "Late Granite" of the Chilimanzi suite (after Jelsma, 1993)

Accretion of depleted material from the plume tail beneath the continent results in the formation of a keel to the continent, which will resist return to the mantle by virtue of its refractory, low density mineralogy. This keel will then slowly cool to form the sub-cratonic lithosphere. This model possibly explains observations based on basin analysis by Grotzinger and Royden (1990) that the Slave craton, currently underlain by a 300 km deep seismically fast keel, had an effective elastic thickness of only 12 ± 4 km (the modern value is 100 ± 25 km) at 1.9 Ga. They therefore concluded that the lithosphere had not yet formed. Hoffman (1990) noted that this value of elastic thickness lies on a secular cooling curve. Therefore, invoking the model for the formation of sub-cratonic lithosphere detailed above, it is proposed that the material which would make up the sub-cratonic lithosphere was beneath the craton, but had yet to cool sufficiently to behave rigidly.

Due to the major changes in chemistry between the granitoids of the Upper Bulawayan event and those of the early crust, there will be sharp contrasts between sediments derived from the early continent, and sediments derived from the craton after 2.6 Ga. The change in granitoid chemistry will result in sediments with higher K_2O contents, showing greater signatures indicative of intra-crustal melting (in terms of REE, this corresponds to deeper negative Eu anomalies and less HREE depletion), corresponding to the "first order" change in sediment compositions as cratons are stabilised (Taylor and McLennan, 1985). Some of these changes in sediment chemistry are summarised in figure 4.16.

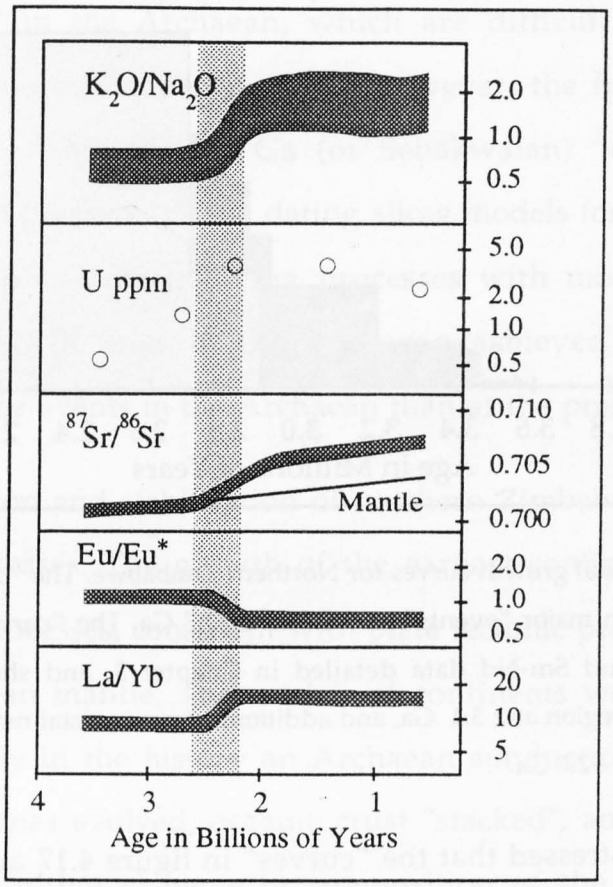

Figure 4.16 Changes in K_2O/Na_2O ratio, U abundance, $^{87}Sr/^{86}Sr$, Eu/Eu* and La/Yb with time, all showing major changes at the Archaean/Proterozoic boundary (light grey shading). After Campbell and Jarvis, 1984

4:4 SUMMARY

This study has demonstrated that areas of Northern Zimbabwe had long and complex crustal histories (≥ 670 Ma in the case of the Shamva region) prior to the formation of the Upper Bulawayan rocks which now dominate this portion of the continent, and that the earliest continental crust was frequently homogenised with the products of later episodes of crustal growth (see the discussion on clast 89-S-14 in Chapter 3:2.5). Using this information, a crustal growth curve for northern Zimbabwe may be constructed.

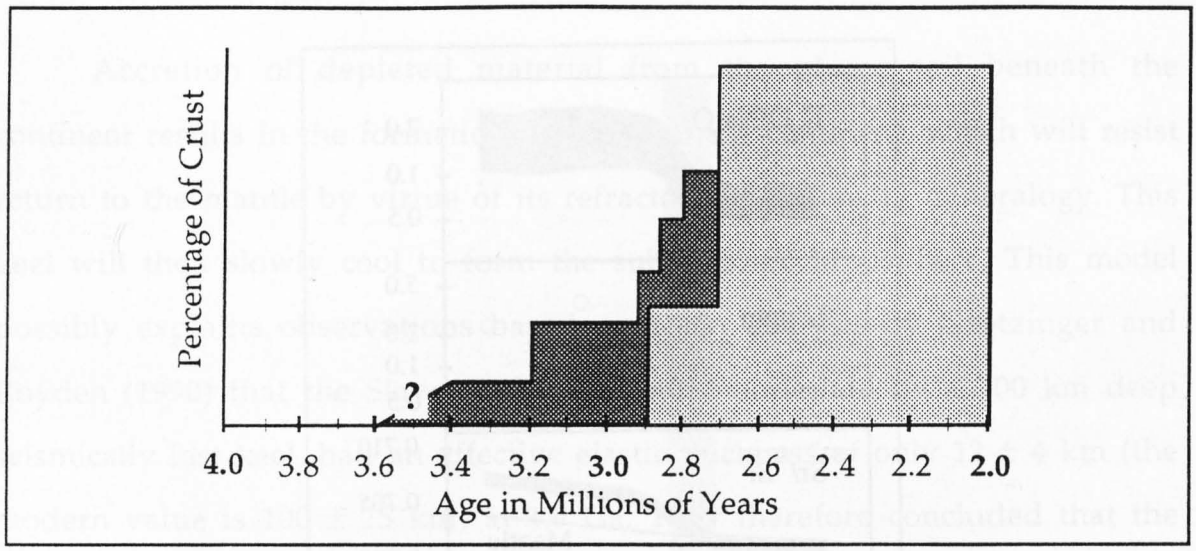

Figure 4.17 Cartoon crustal growth curves for Northern Zimbabwe. The "curve" in light shading shows crustal growth in major "events" at ≈ 2.9 and ≈2.7 Ga. The "curve" in dark shading is based on the zircon and Sm-Nd data detailed in Chapter 3, and shows the initiation of continental crust in the region at ≥ 3.4 Ga, and additions of new crustal materials at 3.2 Ga, 2.925 Ga, 2.875 Ga, 2.8 Ga and ≈ 2.7 Ga.

It should be stressed that the "curves" in figure 4.17 are just cartoons, as there is no constraint on the amount of continental crust generated in each event. The dark crustal growth curve, which proposes that crustal growth in the Archaean occurred in comparatively frequent small events, rather than major infrequent events has some support in other results of the application of high resolution geochronology to the Archaean. For example, the first dates obtained on the Tokwe segment of southern Zimbabwe (Chapter 1, figure 1.2) (by Rb-Sr isochron methods), indicated that this portion of crust may have been formed in a single major event at ≈ 3.5 Ga, with intra-crustal re-working at ≈ 3.35 Ga to form the Mont d'Or granodiorite (eg Moorbath and Taylor, 1981). However, these rocks have undergone later metamorphic events, resulting in partial re-setting of their isotope systematics and comparatively large errors. Recent zircon dating (Dodson et al. 1988; Compston et al. 1990) has suggested that the Tokwe segment may in fact have been formed by up to 6 magmatic events between 3.8 Ga and 3.2 Ga (Chapter 1, figure 1.2). Models based on the low-resolution isochron data, such as the Crustal Accretion Differentiation Superevents (CADS) of Moorbath (1977) require major crust-

forming "events" in the Archaean, which are difficult to explain by the application of uniformitarian principles. However, the frequent episodes of magmatism seen within the 3.5 Ga (or Sebakwaian) "event" in southern Zimbabwe by high precision zircon dating allow models for the construction of Archaean continental crust invoking processes with modern analogs, with higher crustal growth rates in the Archaean achieved by more frequent occurrences of these events in the Archaean than at the present day.

The formation and stabilisation of northern Zimbabwe are modelled as two separate processes. The growth of the earliest continental crust was by lateral accretion processes, consistent with plate tectonic processes modified by the hotter Archaean mantle. The nucleii of continents were formed of low-alumina TTG, early in the history an Archaean subduction *s.l.* zones. As the subduction *s.l.*. zones evolved, oceanic crust "stacked", and depth of melting increased. The resulting changes in composition of the restite assemblage resulted in the formation of high-alumina TTG suites, which became the dominant components of the early TTG terrains. Continental growth was probably by small, frequent addition of high-alumina TTG suite granitoids as new, fertile metabasalts in the underlying subducting *s.l.* pile of oceanic crust reached the optimum partial melting conditions (≈ 70 km and 1050°C, Rapp et al. 1991) for the generation of the high-alumina TTG suite. Temporal variations between the Chinhoyi and Shamva regions show that the early continents were capable of growth by lateral accretion.

Continental stabilisation was achieved predominantly by underplating processes in response to the interaction of a plume with a young proto-continent. The plume model for the stabilisation of northern Zimbabwe provides a coherent, integrated explanation of the features associated with the Upper Bulawayan event and continental stabilisation, from progressions of magmatic activity to lithosphere formation and changes in sediment compositions. Initially, the young hot plume causes greenstone belt volcanism

on the early continent. As temperatures in the plume fall, the plume derived melts increasingly underplate the early crust. Differentiates of these melts intrude as a calc-alkaline suite of granitoids, and vertical tectonic processes with downsagging of greenstone belts and diapiric (or ballooning plutonism) deformation cause the formation of "dome and basin" structures (granitoid batholiths and greenstone belts respectively). The final felsic igneous event is the intrusion of "Late Granites" - intracrustal remelts - in response to thickening of the crust. Material from the plume depleted by the extraction of komatiitic melts accretes beneath the continent to form a depleted, refractory keel. The major changes in the chemistry of granitoids, from the early, sodic TTG crust, to the potassic granitoids of the Upper Bulawayan "event" are responsible for the change in chemistry of sediments from "Archaean" to "Post-Archaean".

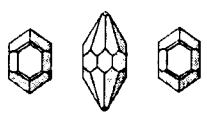

References

Abbott,D.H. & Hoffman,S.E. (1984). Archaean plate tectonics revisited. 1.Heat flow, spreading rate, and the age of subducting oceanic lithosphere and their effects on the origin and evolution of the continents. *Tectonics* Vol. 3 No.4 pp 429-448

Aleinikoff,J.N., Winegarden,D. & Walter,M. (1990). U-Pb ages of Zircon rims: a new analytical method using the air abrasion technique. *Chemical Geology (Isotope Geoscience Section)* Vol. 80 pp 351-363

Ansdell,K.M. & Kyser,T.K. (1993) Textural and chemical changes undergone by zircon during the Pb-evaporation technique. *American Mineralogist* Vol. 78 pp 36-41

Arkani-Hamed,J. & Jolly,W.T. (1989). Generation of Archaean tonalites. *Geology* Vol. 17 pp 307-310

Arndt,N.T. (1983). Role of a thin, komatiite-rich oceanic crust in the Archaean plate tectonic process. *Geology* Vol. 11 pp 372-375

Arndt,N.T. & Albarède,F. (1992). Archaean tholeiites: products of deep melting beneath a thick lithosphere. *Abstracts from the 29th international geological congress* I-1-02 02

Arth,A., Barker,F., Peterman,Z.E. & Frideman,I. (1978) Geochemistry of the gabbro - diorite - tonalite - trondhjemitic magmas. *Journal of Petrology* Vol.19 pp 289-316

Baldock,J.W. & Evans,J.A. (1988). Constraints on the age of Bulawayan group metavolcanic sequence - Harare greenstone belt, Zimbabwe. *Journal of African Earth Sciences* Vol.7 Nos. 5/6 pp 795-804

Barker, F. & Arth, J.G. (1976) Generation of trondhjemitic-tonalitic liquids and Archaean bimodal trondhjemite-basalt suites. *Geology* Vol. 4 pp 596-600.

Barker,F., Arth,J.G. & Hudson,T. (1981) Tonalites in crustal evolution. *Phil. Trans. R. Soc. Lond.* Vol. A 301 pp 293-303

Barth,S; Oberil, F & Meiler, M. (1989) U-Th-Pb systematics of morphologically characterized zircon and allanite: a high resolution isotopic study of the Alpine Rensen Pluton (Northern Italy). *Earth and Planetary Science Letters* Vol. 95 pp 235-254

Barton,J.M.(jr) & Van Reenen,D.D. (1992) When was the Limpopo Orogeny? *Precambrian Research* Vol. 55 pp 7-16

Benisek,A. & Finger, F. (1993) Factors controlling the development of prism faces in granite zircons: a microprobe study. *Contributions to Mineralogy and Petrology* Vol. 114 pp 441-451

Bickle,M.J. (1978) Heat loss from the Earth: a constraint on Archaean tectonics from the relation between Geothermal gradients and the rate of heat production. *Earth and Planetary Science Letters.* Vol. 40 pp 301-315

Bickle,M.J. (1986) Implications of melting for stabilisation of the lithosphere and heat loss in the Archaean. *Earth and Planetary Science Letters* Vol. 80 pp 314-324

Bickle,M.J., Martin,A. & Nisbet,E.G. (1975) Basaltic and peridotitic komatiites and stromatolites above a basal unconformity in the Belingwe greenstone belt, Rhodesia. *Earth and Planetary Science Letters* Vol. 27 pp 155-162

Bickle,M.J., Bettenay, L.F., Boulter,C.A., Groves,D.I. & Morant,P. (1980) Horizontal tectonic interaction of an Archaean gneiss belt and greenstones, Pilbara Block, Western Australia. *Geology* Vol. 8 pp 525-529.

Bickle,M.J., Arndt,N.T., Nisbet,E.G., Orpen,J.L., Martin,A., Keays,R.R. & Renner,R. (1993) Geochemistry of the igneous rocks of the Belingwe Greenstone Belt: Alteration, contamination and petrogenesis. *in Bickle,M.J.and Nisbet,E.G. (eds), The Geology of the Belingwe greenstone belt: a study of the evolution of the Archaean continental crust: Geol. Soc. Zimbabwe special publication 2 pp 175-213*

Black,L.P., Williams,I.S. & Compston,W. (1986) Four zircon ages from one rock; the history of a 3930 Ma. old granulite from Mt. Somes, Enderby Land, Antarctica Contributions *to mineralogy and petrology* Vol. 94

Blenkinsop,T.G., Fedo,C.M., Bickle,M.J., Eriksson,K.A., Martin,A., Nisbet,E.G. & Wilson,J.F. (1993) Ensilaic origin for the Ngezi Group, Belingwe greenstone belt, Zimbabwe. *Geology* Vol. 21 pp 1135-1138

Bogomolov,Y.S. (1991) Migration of lead in non-metamict zircon. *Earth and Planetary Science Letters* Vol. 107 pp 625-633

Bossart,P.J., Meier,M., Oberli,F. & Steiger,R.H. (1986) Morphology versus U-Pb systematics in Zircon: a high-resolution isotopic study of a zircon population from a Variscian dyke in the Central Alps. *Earth and Planetary Science Letters* Vol. 78 pp 339-354

Bowring,S.A., Williams,I.S. & Compston,W. (1989b) 3.96 Ga. gneisses from the Slave Province, Northwestern Territories, Canada *Geology* Vol. 17 pp 971-975

Boyd,F.R. (1989) Compositional distinction between oceanic and cratonic lithosphere *Earth and Planetary Science Letters* Vol. 96 pp 15-26

Byerley,G.B., Mrakovitch,J.V. & Malcuit, R.J. (1975) Use of fourier shape analysis in Zircon petrogenetic studies. *Geol. Soc. Am. Bull.* Vol. 86 pp 956-958

Campbell,I.H. & Jarvis,G.T. (1984) Mantle convection and early crustal evolution *Precambrian research* Vol. 26 pp 15-56

Campbell,I.H., Griffiths, R.W. & Hill, R.I. (1989) Melting in an Archaean mantle plume: heads it's basalts, tails it's komatiites. *Nature* Vol. 339 pp 697-699

Campbell,I.H. & Griffiths,R.W. (1992) The changing nature of mantle hotspots through time: Implications for the chemical evolution of the mantle. *Journal of Geology* Vol. 100 pp 497-523

Campbell,I.H. & Taylor,S.R.(1983) No water, no granites - no oceans, no continents *Geophysical Research Letters* Vol. 10 No. 11 pp 1061-1064

Chase,C.G. & Patchett,P.I. (1988) Stored mafic/ultramafic crust and early Archaean mantle depletion.*Earth and Planetary Science Letters* Vol. 91 pp 66-72

Chauvel,C., Dupre,B. & Arndt,N.T. (1993) Pb and Nd isotopic correlation in Belingwe komatiites and basalts. *in Bickle,M.J.and Nisbet,E.G. (eds), The Geology of the Belingwe greenstone belt: a study of the evolution of the Archaean continental crust: Geol. Soc. Zimbabwe special publication 2 pp 167-174*

Choukroune,P., Bouhallier,H. & Arndt,N. (1993) Archaean tectonics did not involve a modern lithosphere: examples from Indian, West African and Sino-Korean cratons. *Terra Nova* Volume 5 No.1 (abstract supplement) p 314

Christensen,U.R. (1985) Thermal evolution models for the Earth. *Journal of Geophysical Research* Vol. 90 No. B4 pp 2995-3007

Claoue-Long, J.C., Sobolev, N.V., Shatsky, V.S., Sobolev, A.V. (1991) Zircon response to diamond-pressure metamorphism in the Kokchetav massif, USSR. *Geology* Vol. 19 pp 710-713.

Cocherie,A.; Guerrot,C. and Rossi,Ph. (1992) Single-zircon dating by step-wise Pb evaporation: comparison with other geological techniques applied to the Hercynian granites of Corsica, France. *Chemical Geology (Isotope Geoscience section)* Vol. 101 pp 131-141.

Compston,W. & Kröner,A. (1988) Multiple zircon growth within early Archaean tonalitic gneiss from the ancient gneiss complex, Swaziland. *Earth and Planetary Science Letters* Vol. 87 pp 13-28

Compston,W. & Pidgeon,R.T. (1986) Jack Hills, evidence of more very old detrital zircons in Western Australia. *Nature* Vol. 321 pp 766-769

Compston,W., Dodson,M.H. & Williams,I.S. (1990) An ion probe zircon age for the Mushandikie Granite, Zimbabwe. *Australian National University, Research School of Earth Sciences Annual Report* p 32

Compston,W., Williams, I.S. & Meyer,C. (1984) U-Pb geochronology of zircons from lunar Breccia 73217 using a sensitive high mass-resolution ion microprobe. *Proceedings of the fourteenth lunar and planetary science conference, part 2. Journal of geophysical research.* Vol. 89 (supplement) pp B525-B534

Compston,W., Williams,I.S., Campbell,I.H. & Gresham,J.J. (1986) Zircon xenocrysts from the Kambalda volcanics: Age constraints and direct evidence for older continental crust below the Kambalda-Norseman greenstones. *Earth and Planetary Science Letters* Vol. 76 pp 299-311

Compston,W., Williams,I.S., Kirschvink,J.L., Zichao,Z. & Guogan,M. (1992) Zircon U-Pb ages for the Early Cambrian time scale *Journal of the Geological Society of London* Vol. 149 pp 171-184

Condie,K.C. (1986) Origin and early growth rate of continents. *Precambrian research* Vol. 32 pp 261-278

Condie,K.C. & Hunter,D.R. (1976) Trace element geochemistry of Archaean granitic rocks from the Barberton region, South Africa. *Earth and Planetary Science Letters* Vol.29 pp 389-400

Condie,K.C. & Wronkiewicz,D.J. (1990) The Cr/Th Ratio in Precambrian pelites from the Kaapvaal Craton as an index of craton evolution. *Earth and Planetary Science Letters.* Vol. 97 pp 256-267

Corfu,F. & Davis,D.W. (1991) Comment on "Archaean hydrothermal zircon in the Abitibi greenstone belt: Constraints on the timing of gold mineralization." by J.C. Claoue-Long, R.W. King & R. Kerrich. *Earth and Planetary Science Letters* Vol. 104 pp 545-522

Davies, G.F. (1992) On the emergence of plate tectonics. *Geology.* Vol. 20 pp 963-966

Davies, G.F. (1993) Conjectures on the thermal and tectonic evolution of the Earth. *Lithos* Vol. 30 pp 281-289

DePaulo & Wasserburg (1976) Nd isotopic variations and petrogenetic models. *Geophysical research letters* Vol. 3 pp 249-252

de Wit,M.J., Hart,R.J., Armstrong,R.A., de Ronde, C.E.J., Green, R.W.E., Tredoux,M., Peberdy,E. and Hart,R.A. (1992) Formation of an Archaean Continent. *Nature* Vol. 357 pp 553-562

de Wit,M.J. & Hart,R.A. (1993) Earth's earliest continental lithosphere, hydrothermal flux and crustal recycling. *Lithos* Vol. 30 pp 309-355

Dodson,M.H., Compston,W., Williams,I.S. & Wilson,J.F. (1988) A search for ancient detrital zircons in Zimbabwean sediments *Journal of the Geological Society of London* Vol. 145 pp 977 983

Drummond,M. S. & Defant, M.J. (1990) A model for trondhjemite-tonalite-dacite genesis and crustal growth via slab melting: Archaean to modern

comparisons. *Journal of Geophysical Research.* Vol. 95 No. B 13 pp 21,503 - 21,521

Ellam,R.M. & Hawkesworth,C.J.(1988) Is average continental crust generated at subduction zones? *Geology* Vol. 16 pp 314-317

England,P. & Bickle,M. (1984) Continental thermal and tectonic regimes during the Archaean. *The Journal of Geology* Vol. 92 pp 353-367

Fanning,C.M., Williams,I.S., McCulloch,M.T. & Compston,W. (1990) IDTIMS single grain analyses of ion-microprobed zircons; a comparison of U-Pb techniques through geologic time. *Geol. Soc. Australia Abstracts* p 33

Faure,G. (1986) Principles of isotope geology (2nd edition) *Wiley & Sons 589 pp.*

Feng,R., Machado,N & Ludden,J. (1993) Lead geochronology of zircon by LaserProbe - inductively Coupled Plasma Mass Spectrometery (LP-ICPMS). *Geochimica et Cosmochimica Acta* Vol. 57 pp 3479-3486

Froude,D.O., Ireland,T.R., Kinny,P.D., Williams,I.S., Compston,W., Williams,I.R. & Myers,J.S. (1983) Ion microprobe identification of 4,100-4,200 myr - old terrestrial zircons *Nature* Vol. 304 pp 616-618

Fryer,B.J., Jackson,S.E. & Longerich, H.P. (1993) The application of Laser Ablation Microprobe - Inductively Coupled Mass spectrometery (LAM-ICP-MS) to in-situ (U)-Pb geochronology. *Chemical Geology* Vol. 109 pp 1-8

Galer,S.J.G. (1991) Interrelationships between continental freeboard, tectonics and mantle temperature. *Earth and Planetary Science Letters* Vol. 105 pp 214-228

Galer,S.J.G. & Goldstein,S.L. (1991) Early mantle differentiation and its thermal consequences. *Geochimica et Cosmochimica Acta* Vol. 55 pp 227-239

Gaudette,H.E., Vitrac-Michard,A. & Allègre,C.J. (1981) North American Precambrian history recorded in a single sample: high resolution U-Pb systematics of the Potsdam sandstone detrital zircons, New York State. *Earth and Planetary Science Letters* Vol. 54 pp 248-260

Gentry,R.V., Sworski,T.J., McKown,H.S., Smith,D.H., Eby,R,E. & Christie,W.H. (1982) Differential lead retention in Zircons: implications for nuclear waste containment. *Science* Vol. 216 p 297

Glikson,A.Y. & Jahn,B-M. (1985) R.E.E. and L.I.L. elements, Eastern Kaapvaal Shield, South Africa: Evidence for crustal evolution by three stage melting. *Geol. Assoc. Canada Special Paper 28 - Evolution of Archaean supracrustal sequences, Edited by L.D.Ayres; P.C.Thurston; K.D.Card; W.Weber*

Gromet,L.P. & Silver,L. (1983) Rare Earth Element distributions among minerals in a granodiorite and their petrogenetic implications. *Geochimica et Cosmochimica Acta* Vol. 47 pp 925-939

Grotzinger,J. & Royden,L. (1990) Elastic strength of the Slave Craton at 1.9 Gyr and implications for the thermal evolution of the continents. *Nature* Vol. 347 pp 64-66

Hamilton, P.J. (1977) Sr isotope and trace element studies on the Great Dyke and Bushveld mafic phase and their relation to early Proterozoic magma genesis in Southern Africa. *Journal of Petrology* Vol. 18 pp 24-52

Hamilton,P.J., O'Nions,R.K & Evenson,N.M. (1977) Sm-Nd dating of Archaean basic and ultrabasic volcanics. *Earth and Planetary Science Letters* Vol. 36 pp 263-268

Hanchar,J.M. & Miller,C.F. (1992) Interpretation of crustal histories using zircon zonation patterns. *Goldschmidt conference abstract volume* p A-46

Hansen,B.T. & Friderichsen,J.D. (1989) The influence of recent lead loss on the interpretation of disturbed U-Pb systems in zircons from igneous rocks in East Greenland. *Lithos* Vol. 23 pp 209-223

Hanson,G.N. (1978) The application of trace elements to the petrogenesis of igneous rocks of granitic composition. *Earth and Planetary Science Letters* Vol. 38 pp 26-43

Hargraves,R.B. (1986) Faster spreading or greater ridge length in the Archaean? *Geology* V.14 pp 750-752

Harris,N.W.B., Hawkesworth,C.J., P. Van Calsteren & F. McDermott (1987) Evolution of continental crust in Southern Africa. *Earth and Planetary Science Letters* Vol. 83 pp 85-93

Harrison,M.T. & Watson,E.B. (1983) Kinetics of zircon dissolution and zirconium diffusion in granitic melts of variable water content. *Contributions to Mineralogy and Petrology* Vol. 84 pp 66-72

Hawkesworth,C.J., Bickle, M.J., Gledhill,A.R., Wilson,J.F. & Orpen,J.L. (1979) A 2.9 B. y. event in the Rhodesian Archaean. *Earth and Planetary Science Letters*.. Vol. 43 pp 258-297.

Hawkesworth,C.J., Kempton,P.D., Rogers,N.W., Ellam,R.M. and Van Calsteren,P.W. (1990) Continental mantle lithosphere, and shallow level enrichment processes in the Earth's mantle. *Earth and Planetary Science Letters*. Vol. 96 pp 256-268.

Hawkesworth,C.J., Moorbath,S. & O'Nions,R.K. (1975) Age relationships between greenstone belts and granites in the Rhodesian Archaean craton. *Earth and Planetary Science Letters* Vol. 25 pp 251-261

Heaman,L.M., Bowins,R. & Crocket,J. (1990) The chemical composition of igneous zircon suites: implications for geochemical tracer studies. *Geochimica et Cosmochimica Acta* Vol. 5 pp 1597-1607

Helmstaedt,H.; Padgham,W.A. & Brophy,J.A. (1986) Multiple dykes in Lower Kam Group, Yellowknife greenstone belt: Evidence for Archaean sea-floor spreading? *Geology* Vol. 14 pp 562-566

Herzberg,C.T. (1993) Lithosphere peridotites of the Kaapvaal craton. *Earth and Planetary Science Letters* Vol. 120 pp 13-29

Herzberg,C.T. (1992) Depth and degree of melting of komatiites. *Journal of Geophysical Research* Vol. 97 pp 4521-4540

Hickman,M.H. (1978) Isotopic evidence for crustal reworking in the Rhodesian Archaean craton, Southern Africa *Geology* Vol. 6 pp 214-216

Hickman,M.H. (1974) 3,500 myr-old granite in Southern Africa. *Nature* Vol. 251 pp 295-296

Hill,R.I., Campbell,I.H., Davies,G.F. & Griffiths,R.W. (1992) Mantle plumes and continental tectonics. *Science.* Vol. 256 pp 168-193

Hoffman, P.F. (1990) Archaean continental plates - old and young mantle roots. *Nature* Vol. 347 pp 19-20

Hunter,D.R., Barker,F. & Millard, H.T. (Jr). (1978) The geochemical nature of the Archaean ancient gneiss complex and granodiorite suite, Swaziland: A preliminary study. *Precambrian research* Vol. 7 pp 105-127

Hunter,D.R., Barker,F. & Millard, H.T. (Jr). (1984) Geochemical investigation of Archaean bimodal and Dwalile metamorphic suite, Ancient gneiss complex, Swaziland. *Precambrian research* Vol. 24 pp 131-155

Jahn,B-M. & Condie,K.C. (1976) On the age of the Rhodesian Greenstone belts. *Contributions to Mineralogy and Petrology* Vol. 57 317-330

Jahn,B-M.; Glikson,A.Y.; Peucat,J.J. & Hickman,A.H. (1981) R.E.E. Geochemistry and isotopic data of Archaean Silicic volcanics and granitoids from the Pilbara Block, Western Australia; implications for early crustal evolution *Geochimica et Cosmochimica Acta* Vol. 45 pp 1633-1652

Jelsma,H.A. (1993) Granites and Greenstones in northern Zimbabwe: tectono-thermal evolution and source regions. *PhD thesis at Institute of Earth Sciences, Vrije Universiteit, the Netherlands 268 pages*

Jelsma,H.A.; Van der Beek,P.A. & Vinyu.M.L. (1993) Tectonic evolution of the Bindura-Shamva greenstone belt (northern Zimbabwe): progressive deformation around diapiric batholiths. *Journal of Structural Geology* Vol. 15 pp 163-176.

Johnston,A.D. & Wyllie,P.J. (1988) Constraints on the origin of Archaean Trondhjemites based on phase relations of Nuk gneisses with H2O at 15 kbar *Contributions to Mineralogy and Petrology* Vol. 100 pp 35-46

Kamber,B.S., Kramers,J.D. & Rollinson,H.R. (1993) The triangle shear zone, a Proterozoic kill-joy in the tectonic models for the Archaean Limpopo mobile belt. *Terra Nova* Vol. 5 No.1 (abstract supplement) p 316

Kinny,P.D. & Wyborn,D. (1990) High resolution ion-probe analyses of rare earth elements in zircons *Australian National University Research School of Earth Sciences Annual Report* pp 28

Kinny,P.D., Williams,I.S., Compston,W. & Bristow,J.W. (1986) Archaean zircon xenocrysts from the Jwaneng kimberlite pipe, Botswana. *Geol. Soc. Australia abstracts* Vol. 16 pp 267-269

Kober,B. (1986) Whole-grain evaporation for $^{207}Pb/^{206}Pb$-age investigations on single zircons using a double-filament thermal ion source. *Contributions to Mineralogy and Petrology* Vol. 93 pp 482-490

Kober,B. (1987) Single-zircon evaporation combined with Pb+ emitter bedding for $^{207}Pb/^{206}Pb$-age investigations using thermal ion mass spectroscopy, and implications to zirconology. *Contributions to Mineralogy and Petrology* Vol. 96 pp 63-71

Kober,B., Pidgeon,R.T. & Lippolt,H.J. (1989) Single zircon dating by stepwise Pb-evaporation constrains the Archaean History of detrital zircons from the Jack Hills, Western Australia. *Earth and Planetary Science Letters* Vol. 91 pp 286-296

Kosztolanyi,C. (1965) Nouvelle methode d'analyse isotopique des zircons a' l'etat naturel apres attaque directe sur le filament. *Compt. Rend. Acad. Sci.* Vol.261 pp 5849-5851

Kramers,J.D. & Foster,R.P. (1982) A reappraisal of lead isotope investigations of gold deposits in Zimbabwe. *in Gold 1982, R.P. Foster (Ed.)* pp 569-582

Krogh,T.E. (1973) A low contamination method for hydrothermal decomposition of zircon and extraction of U and Pb for isotopic determinations. *Geochimica et Cosmochimica Acta* Vol. 37 pp 485-494

Krogh,T.E. (1982a) Improved accuracy of U-Pb zircon ages by the creation of more concordant samples using an air abrasion technique. *Geochimica et Cosmochimica Acta* Vol. 46 pp 637-649

Krogh,T.E. (1982b) Improved accuracy of U-Pb zircon dating by selection of more concordant fractions, using a high gradient magnetic separation technique. *Geochimica et Cosmochimica Acta* Vol. 46 pp 631-635

Kröner, A. (1985) Evolution of the Archaean continental crust. *Ann. rev. earth planet. sci.* Vol. 13 pp 49-74

Kröner, A. & Todt,W. (1988) Single Zircon dating constraining the maximum age of the Barberton Greenstone belt, Southern Africa. *Journal of Geophysical Research* Vol. 93 No. B.12, pp 15,329-15,337

Kröner,A. & Layer,P.W. (1992) Crust formation and plate motion in the early Archaean. *Science* Vol. 256 pp 1405-1411

Kusky,T.M. & Kidd,W.S.F. (1992) Remnants of an Archaean oceanic plateau, Belingwe greenstone belt, Zimbabwe. *Geology* Vol. 20 pp 43-46

Lister,G.S. & Snoke,A.W. (1984) S-C mylonites. *Journal of Structural Geology* Vol. 6 pp 617-638

Luais,B. & Hawkesworth,C.J. (1994) The generation of continental crust: an integrated study of crust-forming processes in the Archaean of Zimbabwe. *Journal of Petrology* Vol. 35 pp 43-93

Macgregor,A.M. (1951) Some milestones in the Precambrian of Southern Rhodesia. *Trans. Geol. Soc. S. Africa* Vol. 54 pp xxvii-lxxi

Martin,H. (1993) The mechanisms of petrogenesis of the Archaean continental crust - comparison with modern processes *Lithos* Vol. 30 pp 373-388

Martin.H. (1986) Effect of steeper Archaean geothermal gradient on geochemistry of subduction- zone magmas. *Geology* Vol. 14 pp 753-756

Maas,R., Kinny,P., Williams,I.S., Froude, D.O. & Compston,W. (1992) The Earth's oldest known crust: A geochronological and geochemical study of 3,900-4,200 Ma old detrital zircons from Mt. Narryer and Jack Hills, Western Australia. *Geochimica et Cosmochimica Acta* Vol. 56 pp 1281-1300

McDonough,W.F. & Frey,F.A. (1989) Rare earth elements in upper mantle rocks. *in* B.R. Lipin & G.A.McKay (eds) Geochemistry & mineralogy of rare earth elements. *Reviews in Mineralogy* Vol. 21 pp 99-145

McDonough,W.F. & Ireland,T.R. (1993) Intraplate origin of komatiites inferred from trace elements in glass inclusions *Nature* Vol. 365 pp 432-434

McKenzie,D. & Bickle,M.J. (1988) The volume and composition of melt generated by extension in the lithosphere. *Journal of Petrology* Vol. 29 pp 625-679

McLaren,A.C., Fitzgerald,J.D., Williams,I.S. (1990) The microstructure of zircon and its influence on the Pb/U age measured by the ion microprobe. *Geol. Soc. Australia Abstracts* Vol. 27 p 65

McLennan,S.M. & Taylor,S.R. (1991) Sedimentary Rocks and Crustal Evolution: Tectonic setting and secular trends. *Journal of Geology* Vol. 99 pp 1-21

Moorbath,S. (1977) Ages, isotopes and evolution of Precambrian continental crust. *Chemical Geology* Vol. 20 pp 151-187

Moorbath,S., Wilson,J.F. & Cotterill,P. (1976) Early Archaean age for the Sebakwean group at Selukwe, Rhodesia. *Nature* Vol. 264 pp 536-538

Moorbath,S., Wilson,J.F., Goodwin,R. & Humm,M. (1977) Further Rb-Sr and isotope data on early and late Archaean rocks from the Rhodesian craton *Precambrian research* Vol. 5 pp 229-239

Moorbath,S. & Taylor,P.N. (1981) Isotopic evidence for continental Growth in the Precambrian. *in Developments in Precambrian Geology 4: (A.Kröner ed.) "Precambrian plate tectonics"* Chapter 20

Moorbath,S., Taylor,P.N. & Jones.N.W. (1986) Dating the oldest terrestrial rocks: Fact and fiction. *Chemical Geology (Isotope Geoscience Section* Vol. 57 pp 63-86

Moorbath,S., Taylor,P.N., Orpen,J.L., Treloar,P. & Wilson,J.F. (1987) First direct radiometric dating of an Archaean stromatolitic limestone. *Nature* Vol. 326 pp 865-867

Mortensen,J.K., Roddick,J.C. & Parrish,R.R. (1992) Evidence for high levels of unsupported radiogenic ^{207}Pb in Zircon from a granitic pegmatite: implications for interpretation of discordant U-Pb data. *American Geophysical Union/Canadian Geophysical Union/Mineralogical Society of America Spring meeting book of Abstracts (Supplement to Eos, April 7, 1992)*

Nagaswa,H. (1970) Rare Earth concentrations in zircon and apatites and their host dacites and granites. *Earth and Planetary Science Letters* vol. 9 pp 359-364

NERC geoscience lab report (1991-1992) *Studies in Economic geology: Gold mineralization in Zimbabwe* p18

Nesbitt et al. unpublished data, tabulated in Jelsma (PhD thesis), 1993 p 176.

Nesbitt, H.W. & Young, G.M. (1984) Prediction of some weathering trends of plutonic and volcanic rocks based on thermodynamic and kinetic considerations. *Geochimica et Cosmochimica Acta* Vol. 48 pp 1523-1534

Nisbet,E.G. (1982) Definition of "Archaean" - comment and a proposal on the recommendations of the international subcommission on Precambrian stratigraphy. *Precambrian research* Vol. 19 pp 111-118

Nisbet,E.G., Bickle,M.J. & Martin,A. (1977) The mafic and ultramafic lavas of the Belingwe greenstone belt. *Journal of Petrology* Vol. 18 pp 521-566.

Nisbet,E.G. & Walker,D. (1982) Komatiites and the structure of the Archaean mantle. *Earth and Planetary Science Letters* Vol. 60 pp 105-113

Nisbet,E.G., Cheadle,M.J., Arndt,N.T. & Bickle,M.J. (1993) Constraining the potential temperatures of the Archaean mantle: A review of the evidence from komatiites.*Lithos* Vol. 30 pp 291-307

O'Connor,J.T. (1965) A classification for Quartz-Rich igneous rocks based on feldspar ratios. *U.S.Geol. Survey prof. Paper (Geol. Survey Research 1965)* 525-B pp 79-84

Ono, A. (1976) Chemistry and zoning of zircon from some Japanese Granitic rocks. *J.Japan Assoc. Min. Petro. Econo. Geol.* Vol. 71 pp 6-17

Othman,D.B., Polve,M. & Allègre,C.J. (1984) Nd-Sr isotopic composition in granulites and constraints on the evolution of the lower continental crust. *Nature* Vol. 307 pp 510-515

Parrish,R.R. (1987) An improved micro-capsule for Zircon Dissolution in U-Pb geochronology *Chemical Geology (Isotope Geoscience Section)* Vol. 66 pp 99-102

Parsons,B. (1982) Causes and consequences of the relation between area and age of the ocean floor *Journal of Geophysical Research* Vol. 87 pp 289-302

Pearson,D.G., Shirey,S.B., Carlson,R.W., Boyd,F.R., Pokhilenko,N.P & Nixon,H.P. (1993) Re-Os isotope evidence for the formation of ancient lithospheric mantle linked to crust building beneath southern Africa and Siberia. *Terra Nova* Vol. 5 No.1 (abstract supplement) p 40

Peucat,J.J., Gruau,G., Martin,H., Auvray,B., Foucrcade,S., Choukroune,H., Bouhallier,H. & Jayananda,M. (1993) A 2.5 Ga mega-plume in South-India? *Terra Nova* Vol. 5 No.1 (abstract supplement) p 321

Pidgeon,R.T. (1992) Recrystallization of oscillatory zoned zircon: Some geochronological and petrological implications. *Contributions to Mineralogy and Petrology* Vol. 110 pp 463-47

Pollack,H.N. (1986) Cratonization and the thermal evolution of the mantle. *Earth and Planetary Science Letters* Vol. 80 pp 175-182

Potts,P.J., Williams Thorpe,O., Isaacs,M.C., Wright, D.W. (1985) High precision instrumental neutron activation analysis of geological samples employing simultaneous counting with boh planar and coaxial detectors. *Chemical Geology* Vol. 48, pp 145-155

Pupin, J.P. (1980) Zircon and granite petrology. *Contributions to Mineralogy and Petrology,* Vol. 73 pp 207-220

Rapp, R,P., Watson, E.B. & Miller, C.F. (1991) Partial melting of Amphibolite/Eclogite and the origin of Archaean Trondhjemites and Tonalites. *Precambrian research* Vol. 51 pp 1-25

Rapp, R.P. (1991) Origin of Archaean Granitoids and Continental Evolution. *Eos* Vol. 72 No. 20 pp 225-227

Ridley,J.R. (1992) The thermal causes and effects of voluminous, late Archaean monzogranite plutonism. *"The Archaean: Terrains, processes and metallogeny." University of Western Australia publication 22* pp 275-285

Robertson,D.K. (1973) A model discussing the early history of the Earth based on a study of lead isotope ratios from veins in some Archaean cratons of Africa *Geochimica et Cosmochimica Acta* Vol. 37 pp 2099-2124

Roddick, J.C., Loveridge, W.D. & Parrish, R.R. (1987) Precise U-Pb Dating at the sub-nanogram Pb level. *Chemical Geology (Isotope Geoscience Section)* Vol. 66 pp 111-121

Roering,C., Van Reenen,D.D., Smit,C.A., Barton,J.M.(jr), DeBeer,J.H., De Wit,M.J., Stettler,E.H., Van Schalkwyk,J.F., Stevens,G. & Pretorius,S. (1992) Tectonic model for the evolution of the Limpopo Belt. *Precambrian Research* Vol. 55 pp 539-552

Rudnick,R.L. & Taylor,S.R. (1986) Geochemical constraints on the origin of Archaean tonalitic-trondhjemitic rocks and implications for lower crustal composition. *from: Dawson, J.B., Carswell, D.A.,Hall, J. & Wedepohl,K.H. (eds) The nature of the Lower continental crust. Geol soc. Special publication No. 24* pp. 179-191

Schärer,U. & Allègre,C.J. (1985) Determination of the age of the Australian continent by single grain analysis of Mount Narryer metaquartzite. *Nature* Vol. 315 pp 52-55

Snowden,P.A. (1984) Non-Diapiric Batholiths in the North of the Zimbabwe Shield *in "Precambrian plate tectonics Illustrated", Edited by A.Kröner and R.Greiling, Published in Stuttgart* pp 135-145

Snowden,P.A. & Bickle,M.J. (1976) The Chinamora Batholith - diapiric intrusion or interference fold? *Journal of the Geological Society of London* Vol. 132 pp 131-137

Snowden,P.A., Snowden,D.V. (1981) Petrochemistry of late Archaean granites of the Chinamora Batholith, Zimbabwe. *Precambrian research* Vol. 16 pp 103-129

Speer, J. A. (1980) Zircon *Reviews in Mineralogy* pp 67-112

Stacey,J.S. & Kramers,J.D. (1975) Approximation of terrestrial lead isotope evolution by a two stage model. *Earth and Planetary Science Letters* Vol. 26 pp 207-221

Stagman,J.G. (1961) The geology of the country around Sinoia and Banket, Lomagundi district. *Rhodesia geological survey bulletin No. 49*

Stidolph,P.A. (1977) The geology of the country around Shamva. *Rhodesia geological survey bulletin No. 78*

Sun,S.-s. & McDonough, W.F. (1989) Chemical and isotopic systematics of oceanic basalts: implications for mantle composition and processes. *From* Saunders,A.D. & Norry,M.J. (eds) Magmatism in the ocean basins, *Geological society special publication* No. 42, pp 313-345

Takahashi,E. (1990) Speculations on the Archaean mantle: missing link between komatiite and depleted garnet peridotite. *Journal of Geophysical Research* Vol. 95 pp 15941-15954

Taylor,P.N., Jones,N.W. & Moorbath,S. (1984) Isotopic assessment of relative contributions from crust and mantle sources to the magma genesis of Precambrian granitoid rocks. *Philos. Trans. R. Soc. London* Vol. A 310 pp 605-625

Taylor,P.N., Kramers,J.D., Moorbath,S., Wilson,J.F., Orpen,J.L. & Martin,A. (1991) Pb/Pb, Sm-Nd and Rb-Sr geochronology in the Archaean craton of Zimbabwe. *Chemical Geology (Isotope Geoscience Section)* Vol. 87 pp 175-196

Taylor,S.R. & McLennan,S.M. (1985) The continental crust: its composition and evolution.*312 pp Blackwell, Oxford.*

Treloar,P.J. (1988) The geological evolution of the Magondi mobile belt, Zimbabwe. *Precambrian research* Vol. 38 pp 55-73

Treloar,P.J., Coward,M.P. & Harris,N.B.W. (1992) Himalayan-Tibetan analogies for the evolution of the Zimbabwe Craton and Limpopo Belt. *Precambrian research* Vol. 55 pp 571-587

Tsomondo,J.M., Wilson,J.F & Blenkinsop,T.G. (1992) Reassesment of the early Archaean Selukwe Nappe, Zimbabwe. *"The Archaean: Terrains, processes and metallogeny." University of Western Australia publication 22* pp 123-135

Turcotte,D.L. & Schubert,G. (1982) Geodymamics:applications of continuum physics to geological problems pp 450.

Van Breemen,O. & Hawkesworth,C.J. (1980) Sm-Nd isotopic study of garnets and their metamorphic host rocks. *Trans. R. Soc. Edinburgh Earth Sci.* Vol. 71 pp 97-102

Vavra,G. (1992) Quantification of zircon growth kinematics: A new approach using zircon morphology as a petrogenetic tracer. *Goldschmidt Conference Abstracts* p A - 117

Vinyu,M.L., Jelsma,H.A., Beunk,F.F. & Kramers, J.D. (1993) The petrogenetic evolution of granitoids and associated xenoliths form the Late Archaean Shamva-Harare greenstone belt, Zimbabwe. *Terra Nova* Vol. 5 No.1 (abstract supplement) p 40

Walker,R.J., Carlson,R.W., Shirey,S.B. & Boyd,F.R. (1989) Os, Sr, Nd and Pb isotope systematics of Southern African peridotite xenoliths: Implications for the chemical evolution of the sub-continental mantle. *Geochimica et Cosmochimica Acta* Vol. 53 pp 1583-1595

Watson,E.B. (1979) Zircon saturation in felsic liquids: Experimental results and applications to trace element geochemistry. *Contributions to Mineralogy and Petrology* Vol. 70 pp 407-419

Watson,E.B. & Harrison, T.M. (1983) Zircon saturation revisited: Temperature and composition effects in a variety of crustal magma types. *Earth and Planetary Science Letters* Vol. 64 pp 295-304

Watson,E.B. & Harrison, T.M. (1984) Accessory minerals and the geochemical evolution of crustal magmatic systems: A summary and prospectus of experimental approaches. *Physics of the Earth and Planetary interiors* Vol. 35 pp 19-30

Wendt, J.I., Milisenda,C.C. & Kröner,A. (1993a) Multiple recycling of TTG rocks form the Ancient Gneiss complex of Swaziland: A compilation of U-Pb zircon data and Sm-Nd systematics. *Terra Nova* Vol. 5 No.1 (abstract supplement) p 41

Wendt,I., Wendt,J.I. & Tuttas,D. (1993b) Determination of U-Pb ages of zircons by direct measurement of the $^{210}Pb/^{206}Pb$ ratio. *Chemical Geology (Isotope Geoscience Section)* Vol. 106 pp 467-474

Wendt,J.I., Wendt,I. & Tuttas,D. (1992) Dating of Archaean zircons using $^{210}Pb/^{206}Pb$ measurement for the direct determination of U-Pb ages.*American Geophysical Union/Canadian Geophysical Union/Mineralogical Society of America Spring meeting book-of Abstracts (Supplement to Eos, April 7, 1992)*

Wetherill, G.W. (1956) An interpretation of the Rhodesia and Witwatersrand age patterns. *Geochimica et cosmochimica acta* Vol. 9 pp 290-292

Wickham,S.M. (1987) The segregation and emplacement of granitic magmas *Journal of the Geological Society of London* Vol. 144 pp 281-297

Williams,I.S., Collins,W.J. (1990) Granite- Greenstone terrains in the Pilbara block, Western Australia, as coeval volcano-plutonic complexes; evidencé from U-Pb Zircon dating of the Mount Edgar Batholith. *Earth and Planetary Science Letters* Vol. 97 pp 41-43

Williams,I.S., Compston,W., Black,L.P., Ireland,T.R. & Foster,J.J. (1984) Unsupported radiogenic Pb in zircon: a case anomalously high Pb-Pb, U-Pb and Th-Pb ages. *Contributions to Mineralogy and Petrology* . Vol. 88 pp 322-327

Wilson,J.F. (1973) Granites and gneisses of the area around Mashaba, Rhodesia. *Special Publication of the Geological Society of South Africa* No. 3 pp 79-84

Wilson,J.F. (1979) A preliminary reappraisal of the Rhodesian Basement Complex *Special Publication of the Geological Society Of South Africa* Number 5 pp 1-23

Wilson,J.F. (1981) Zimbabwe. *in Developments in Precambrian Geology 2 - Precambrian of the southern hemisphere* pp 454-488

Wilson,J.F. (1990) A craton and its cracks: some of the behaviour of the Zimbabwe block from the late Archaean to the Mesozoic in response to horizontal movements and the significance of some mafic dyke fracture patterns *Journal of African Earth Sciences* Vol. 10 No. 3 pp 483-501

Zeitler,P.K. & Chaimberlain,C.P. (1991) Petrogenetic and tectonic significance of young leucogranites from the Northwestern Himalaya, Pakistan. *Tectonics* Vol. 10 pp 729-741

Appendix A

Major, trace and rare earth element data

Sample powder preparation.

Samples were spilt into 5 cm cubes using a hydraulic splitter, removing any severely weathered material. The remaining cubes were rinsed in distiled water to remove possible surface contamination. The cubed samples were then crushed in a hardened steel jaw-crusher, and a representative 100g portion of the crushate taken by cone and quartering. This was powdered in an agate-lined tema swing mill for ≈ 15 minutes to a powder of less than 200 mesh grain size.

XRF sample preparation and analysis.

Major and trace element analysis was carried out at Oxford University, using a Phillips PW1400 x-ray fluorescence spectrometer, and the data processed using a PDP11 minicomputer. The x-rays were generated using a Rh tube, and the analysing crystals used were LiF 220, LiF 200, PE and PX1. Mass absorption was corrected for using De Jongh's formula (major element analyses), and the Rh Compton scatter peak (trace elements). The concentrations of the elements Co, Cr, V and Ba were corrected for the Fe, Mn and Ti absorption edges and line overlaps.

Major element analyses were performed on glass disks prepared by fusing a mixture of 1.000g rock powder and 5.0000g lithium metaborate-tetraborate mixture (spectroflux 100B) in a zirconia grained Pt - 5% Au alloy crucible in a muffle furnace at 1175°C for 5 minutes. The melt was poured into a Pt - Au alloy casting mould, and quenched over a jet of air. The flux had

been pre-dried at 600°C for at least 12 hours, and the sample powder pre-ignited at 1000°C for a minimum of 20 hours. Crucibles were cleaned in hot 6M HCl, and rinsed in distilled water.

Trace element analyses were carried out on pressed powder pellets prepared by mixing ≈ 10g of rock powder and ≈ 1ml Mowiol binder in an agate pestle and mortar. The mixture was pressed into a 3cm diameter pellet in a hydraulic press at a pressure of 105 Pa for 30 seconds. The pellets were dried for 12 hours at 80°C before analysis.

XRF Major and Trace Element Data Tables

Shamva Sediments

	89-S-2	89-S-3	89-S-4	89-S-5	89-S-6
SiO2	75.07	71.94	70.68	75.70	75.29
TiO2	0.32	0.43	0.35	0.31	0.24
Al2O3	11.32	11.12	10.44	11.37	13.8
Cr2O3	0.02	0.04	0.02	0	0
Fe2O3T	4.20	5.96	4.54	4.77	2.19
MnO	0.08	0.12	0.17	0.07	0.04
MgO	2.19	3.15	2.22	1.28	0.51
CaO	2.63	3.97	7.94	2.37	2.13
Na2O	2.75	2.17	2.34	3.07	5.24
K2O	1.44	1.21	1.23	1.05	0.73
P2O5	0.06	0.07	0.06	0.04	0.07
Total	100.08	100.18	99.99	100.03	100.24
Zn	49.1	55.7	43.6	44.1	31.6
Cu	13.4	36.6	20.2	80.1	3.3
Ni	64.9	84.5	60.4	5.1	4.2
Co	13.6	21.9	17.3	6.2	4.6
Cr	133.6	218.6	137.2	0.7	4.2
V	60.5	92.3	75.1	0.1	12.9
Ba	471.7	341.4	314.9	181.5	344.3
Ga	11.4	11.1	9.6	20.4	15.6
Rb	29.6	26.4	31	14.8	22.3
Sr	129.9	161.5	153.9	184.5	233.3
Y	12.2	15.2	12.4	13.2	7.8
Zr	69.9	82.7	65.7	520.3	133.1
Nb	4.7	4.2	3.6	25.9	3.9
Pb	18	14.6	11	14.6	11.1
Th	5.5	6.8	4.5	11.4	2.8
U	2.4	3.3	2.5	3.3	1.5

Shamva Clasts

	Group 1						Group 2	
	89-S-14	89-S-15	89-S-22	89-S-23	89-S-24	89-S-27	89-S-12	89-S-13
SiO2	73.20	72.69	71.03	73.15	73.20	75.51	75.72	77.18
TiO2	0.19	0.28	0.33	0.2	0.21	0.06	0.19	0.09
Al2O3	15.27	15.41	15.61	15.14	15.16	14.8	13.6	13.66
Cr2O3	0	0	0	0	0	0	0	0
Fe2O3T	1.85	2.21	2.94	2.11	2.19	0.60	2.04	0.90
MnO	0.03	0.03	0.05	0.04	0.04	0.01	0.03	0.02
MgO	0.69	0.68	1.06	0.86	0.69	0.11	0.48	0.23
CaO	2.69	2.64	3.12	1.9	2.33	1.73	1.66	1.51
Na2O	5.48	5.18	4.85	5.47	5.44	5.67	5.28	6.18
K2O	0.72	1.02	1.1	1.14	0.92	1.48	0.83	0.41
P2O5	0.06	0.09	0.09	0.06	0.06	0.02	0.05	0.04
Total	100.19	100.23	100.19	100.08	100.24	99.99	99.89	100.22
Zn	18.9	31.6	33.2	23	23	7.2	19.2	11.2
Cu	2.6	0.2	0.3	-0.4	5.4	1	28.1	3.9
Ni	1.9	3.3	6	2.9	2.3	1.2	4	1.9
Co	4.3	2.7	7	3.3	3.5	0.7	1.1	-0.3
Cr	1.9	6.6	10.6	-0.4	2	-1.6	2.2	-1.2
V	17.7	19.6	32.9	16.7	14.7	4.3	14.7	5.7
Ba	340	431.3	511	463.2	333.2	416.6	403.8	332.4
Ga	15.6	18.1	17.5	16.4	16.9	15	14.1	14.6
Rb	15	20.9	31.5	23.7	26.5	30	23.1	7.6
Sr	327.2	345.1	264.6	292.3	241.9	205.6	187.3	227
Y	9.4	8.1	8	9.4	8.6	19.7	31.6	6.9
Zr	90	156.6	124.7	120.1	125.3	53.5	130.4	71.2
Nb	4.3	4.3	4.1	3.8	3.9	4.9	10.9	5.1
Pb	22.7	21.8	23.6	19.3	16.9	20.7	27	21.3
Th	8.6	14.3	14	8.7	7.7	10.6	25.2	3.8
U	1.2	2	2	1.6	1.1	3.6	6.1	1.3

Shamva Group 2 Clasts

	89-S-17	89-S-18	89-S-19	89-S-20	89-S-25	89-S-26	89-S-28	89-S-29	89-S-30
SiO2	76.90	74.57	77.71	75.88	76.38	76.36	76.75	75.33	76.59
TiO2	0.1	0.21	0.11	0.2	0.1	0.11	0.15	0.19	0.08
Al2O3	13.68	14.27	13.07	13.39	13.78	13.81	13.1	13.61	13.95
Cr2O3	0	0	0	0	0	0	0	0	0
Fe2O3T	0.98	1.92	1.31	2.14	1.23	0.94	1.47	1.68	0.76
MnO	0.02	0.04	0.02	0.03	0.02	0.01	0.03	0.03	0.02
MgO	0.22	0.62	0.32	0.6	0.24	0.22	0.47	0.74	0.19
CaO	1.99	2.97	1.21	2.05	1.76	2.19	2.68	2.08	2.74
Na2O	5.68	4.58	5.52	5.08	5.95	5.68	4.77	5.18	5.40
K2O	0.35	0.76	0.73	0.67	0.46	0.45	0.5	0.7	0.34
P2O5	0.03	0.05	0.02	0.05	0.03	0.07	0.04	0.06	0.03
Total	99.95	99.99	100.02	100.09	99.95	99.83	99.95	99.61	100.10
Zn	10.3	16.4	12.3	18.3	10.4	10.1	13.6	18.4	8.8
Cu	6.4	1.8	8.2	26	21.1	3.4	3.3	0.6	3.5
Ni	0.4	2.4	1.8	3.3	2.1	2.6	1.9	2.6	3.4
Co	2.1	1.9	2.1	2.5	1.8	2.2	1.8	2	2.1
Cr	-0.6	1.5	-0.6	1.9	0.3	1.1	0.8	1.4	1
V	8.1	15.9	7.9	12.8	7.1	7	9.7	13.6	8.7
Ba	366.5	656.1	221	249.6	295.4	245.2	207.2	247.8	251.6
Ga	13.7	14.5	11.2	14.7	14.5	12	12.8	14.8	11.9
Rb	5.3	18.6	21.8	14.4	8.6	8.2	9.7	14.6	3.8
Sr	228.9	218.1	282	293.2	291.5	340.9	250.6	232.5	363.3
Y	12.5	9.1	17.9	28.9	21	11.9	15.5	12	8.9
Zr	84.4	115.4	80.7	126.1	82.4	97.5	102.4	105.8	93
Nb	2.7	3.8	7.1	11.6	6.6	3.4	5.7	6.1	2.7
Pb	24	19.6	30.2	26.9	27.5	33.2	20.6	20.1	20.1
Th	14.7	7.3	32.2	32.3	23.1	23.2	14.6	10.3	6
U	1.5	0.7	6.2	5.7	5.2	4.2	3.1	1.4	0.6

Chinhoyi Sediments

	89-C-1	89-C-2	89-C-3	89-C-4	89-C-5	89-C-6	89-C-7	89-C-13
SiO2	66.71	69.16	72.00	73.26	71.27	68.87	69.04	54.29
TiO2	0.43	0.56	0.36	0.41	0.46	0.4	0.39	1.71
Al2O3	11.54	15.73	14.39	15.39	14.75	15.38	15	13.17
Cr2O3	0.01	0.01	0.02	0.01	0.02	0	0	0.03
Fe2O3T	16.73	4.74	3.98	3.42	3.98	4.24	4.12	15.47
MnO	0.12	0.08	0.1	0.05	0.08	0.05	0.08	0.26
MgO	3.72	2.07	1.64	1.31	1.34	3.49	2.83	5.29
CaO	0.1	0.54	1.04	0.46	1.94	2.31	2.31	7.84
Na2O	bd	7.01	4.04	3.50	4.05	2.08	3.31	1.31
K2O	1.05	0.08	1.95	2.18	2.17	3.11	2.89	1.19
P2O5	0.1	0.13	0.12	0.09	0.11	0.14	0.14	0.17
Total	100.51	100.11	99.64	100.08	100.17	100.07	100.12	100.73
Zn	105.4	170.6	36.3	44.9	30.7	56.7	89.5	92
Cu	36.4	5.9	13.1	13.4	71.9	1	-0.4	34
Ni	22	15.3	23.4	28.8	40.1	21.1	21.3	85.3
Co	11.6	13	11	11.2	14.1	9.5	10.7	52.9
Cr	60.4	24.9	104.8	67.1	91.3	24.6	27	176.5
V	68.2	68.6	62.9	58.6	65.9	48	39.4	364.6
Ba	166.3	13.9	544.6	541.3	626	367.1	508.4	196.1
Ga	14.2	12.8	15	15.7	14	16.8	15.1	16.1
Rb	27.9	-4.1	55.4	63.3	53.7	83.3	77.5	43.5
Sr	24.5	106.2	243.4	235.8	193.7	99.2	95.2	90.8
Y	11.4	10.6	13.5	14.4	12.4	13.8	13.8	36.6
Zr	98.5	132	84	95.6	102.9	125.5	130.4	94.6
Nb	6	5.3	3.8	4.7	4.8	6.6	7.1	4.8
Pb	4.1	4.5	13.3	9.3	7.9	11.2	9.7	15.5
Th	10	0.1	bd	3.4	4.9	5.9	8	0.7
U	1.7	2.3	2.8	2.1	1.8	4.1	4.4	1.5

Chinhoyi Group 1 Clasts

	89-C-15	89-C-16	89-C-19	89-C-20	89-C-24	89-C-28
SiO2	69.89	71.05	72.23	70.74	68.14	70.54
TiO2	0.37	0.34	0.3	0.26	0.44	0.27
Al2O3	16.35	15.28	15.34	15.54	17.26	15.61
Cr2O3	0	0	0	0	0.01	0
Fe2O3T	3.26	3.77	2.45	2.73	2.69	2.98
MnO	0.05	0.05	0.03	0.05	0.07	0.04
MgO	1.28	1.2	1.27	1.35	1.51	1.08
CaO	1.88	1.41	0.91	2.37	3	2.19
Na2O	5.37	5.67	6.15	6.13	6.03	5.93
K2O	1.76	1.39	1.16	0.99	1.03	1.32
P2O5	0.12	0.11	0.09	0.1	0.14	0.11
Total	100.33	100.26	99.94	100.26	100.32	100.07
Zn	17.9	19.9	19.8	18	25	17.5
Cu	8.7	3.1	21.5	20.4	-0.1	9.7
Ni	7.2	6	5	7.1	17.8	4.4
Co	4.3	5.5	5.1	8.1	10.9	5.1
Cr	0.8	1.9	7	1.3	41.8	0.5
V	56.1	41.4	36.5	29.4	44.2	46.9
Ba	592.9	375.2	466	423.8	202.9	510
Ga	16.2	14.6	15	13.8	18.2	15.5
Rb	44.9	33.7	27	19.4	21.3	29.6
Sr	168	167.6	136.8	302.7	170.7	241.5
Y	9.2	12.6	6.9	9.8	6	10.9
Zr	102.2	111.3	116.5	84.8	147.3	92.4
Nb	4.3	4.5	4.3	3	1.8	3.5
Pb	8.1	7.3	7.4	9.5	23.3	8
Th	3.4	4.5	5.4	0.6	1.6	1.7
U	1.4	2.8	2	1	0	1.5

	Chinhoyi Group 2 Clasts				Felsite
	89-C-21	89-C-22	89-C-23	89-C-29	89-C-27
SiO2	75.49	77.41	75.76	76.60	74.55
TiO2	0.26	0.26	0.26	0.25	0.29
Al2O3	13.09	12.48	12.63	12.8	12.89
Cr2O3	0	0	0	0	0
Fe2O3T	2.54	2.22	2.76	2.77	2.65
MnO	0.05	0.02	0.04	0.02	0.05
MgO	0.76	0.7	1.1	0.52	1.42
CaO	1.72	0.66	1.66	0.92	2.59
Na2O	5.13	5.57	5.15	5.18	4.23
K2O	1	0.68	0.67	1.11	1.35
P2O5	0.04	0.05	0.04	0.04	0.07
Total	100.07	100.05	100.07	100.21	100.09
Zn	12.4	12.2	20.2	10.7	20.7
Cu	32.6	61.2	17.4	5.4	18.9
Ni	1.2	4.5	3.7	2.7	6.2
Co	4.1	6.6	7.4	1.2	5.8
Cr	-1	2	1.2	0	4.4
V	16.5	20.7	18.6	11.7	34.3
Ba	337.3	282.3	202.1	310.7	400.6
Ga	12.1	11.5	11.4	12.4	11.6
Rb	22.6	13.7	10.3	31.8	30.2
Sr	111.4	183.5	83.4	115.8	166.5
Y	34.1	29.2	30.7	36.3	27.9
Zr	198.6	183.1	181.1	177.4	143.7
Nb	8.6	8.4	7.5	8.2	7.4
Pb	9.2	9.3	8.9	8	9.7
Th	16.8	15.5	13.8	16.3	13.1
U	5.3	4.2	2.4	4.5	3.4

Instrumental Neutron Activation Analysis (INAA)

Analytical Technique.

INAA was carried out in order to determine the concentrations of the Rare Earth Elements (REE) La, Ce, Nd, Sm, Eu, Tb, Yb and Lu; also Th, Co, Ta, and Hf. 0.3 g of rock powder was weighed into a polythene capsule and sealed. Nine samples and two standards were stacked into a cylinder, with weighed lacquered iron foil between each capsule to monitor the neutron flux variation along the length of the cylinder. The standards used included the irradiation standard AC(OURS).

Samples were irradiated in the core tube at the Imperial College reactor centre, Ascot, in a thermal flux of 5 x 10^{12} n cm^2 sec^{-1} for 24 - 30 hours. The samples were left for one week before analysis to allow short lived radioactive isotopes to decay; details of counting conditions, peak fitting, calibration and corrections are described in Potts et al. (1985).

INAA Data Tables

Shamva Neutron Activation Data

	sediment	Group 1				Group 2			
	89-S-3	89-S-14	89-S-22	89-S-23	89-S-24	89-S-19	89-S-20	89-S-25	89-S-26
La	18.3	18.9	28	27.3	24.8	20.6	41.7	40.7	34
Ce	33.9	35.2	48.3	46.4	44.1	42.4	83.4	76.3	69.2
Nd	14.6	13.4	16	17	15.8	16.4	31.8	25.5	29
Sm	2.52	2.32	2.25	2.51	2.21	2.74	5.55	4	5.8
Eu	0.69	0.57	0.63	0.61	0.57	0.39	0.67	0.52	0.61
Tb	0.37	0.24	0.19	0.26	0.21	0.48	0.83	0.6	0.67
Yb	1.36	0.67	0.62	0.75	0.72	1.54	2.8	2.01	0.64
Lu	0.22	0.11	0.11	0.11	0.11	0.27	0.41	0.3	0.1
Th	7.87	8.73	14.8	10.4	9.78	33.7	36.4	27.4	26.6
U	3.64	1.18	1.7	1.29	2.43	7.74	5.67	5.34	3.86
Ta	0.36	0.41	0.45	0.25	0.37	0.92	1.7	0.85	0.53
Hf	2.19	2.82	3.51	3.52	3.78	3.09	4.35	3.27	3.41
Na2O	2.35	5.49	4.96	5.57	5.15	5.36	5.08	5.97	5.67
Rb	43	23	40	21	30	28	19	18	15
Cs	0.71	0.54	1.31	0.55	0.61	0.31	0.42	0.27	0.25
Co	22.7	2.9	5.5	3	2.7	1.6	0.3	1.5	1.6
Fe2O3	5.8	1.8	2.9	2.1	2.1	1.2	2	1.2	0.9
Sc	13.7	2.7	2.8	3.1	2.5	2	3.6	2.7	1.1
Cr	243	5	11	4	6	3	8	4	7

Chinhoyi Neutron Activation Data

	Sediment	Group 1				Group 2			
	89-C-4	89-C-16	89-C-19	89-C-20	89-C-24	89-C-21	89-C-22	89-C-29	89-C-27
La	15.9	17	17.8	9.8	9	39.2	33.9	40.3	33.4
Ce	33.5	33.6	29.8	198.7	18.3	71.3	68	73.2	62.6
Nd	13.9	16.1	11.7	10	9.5	29.3	25	31.5	24.8
Sm	2.53	2.55	1.86	1.74	1.8	4.99	4.4	5.49	4.38
Eu	0.82	0.65	0.46	0.53	0.67	1.06	0.96	0.86	1.07
Tb	0.33	0.3	0.19	0.21	0.18	0.83	0.73	0.93	0.72
Yb	1.05	1.06	0.47	0.77	0.36	3.17	3.05	3.45	2.72
Lu	0.16	0.15	0.09	0.11	0.05	0.5	0.44	0.53	0.41
Th	5.11	5.42	6.36	2.17	1.88	17.3	17.1	19.2	14.5
U	1.7	1.37	1.46	0.72	0.4	3.95	3.49	4.31	3.49
Ta	0.37	0.33	0.33	0.22	0.07	0.96	0.91	0.93	0.8
Hf	2.5	3.3	3.3	2.5	3.75	6.09	5.55	5.69	4.6
Na2O	4	5.64	6.23	6.21	5.95	5.08	5.37	5.02	5.32
Rb	82	42	38	31	29	32	22	43	41
Cs	2.15	0.85	0.55	0.67	0.3	0.36	na	0.4	0.77
Co	10.4	6	5.5	6.6	10.5	3	3.7	2.1	4.9
Fe2O3	3.3	3.6	2.4	2.7	2.5	2.4	2.1	2.7	2.6
Sc	8.4	4.5	4.1	3.9	6	6.8	6.5	7.5	6.4
Cr	75	7	10	7	45	6	6	7	10

Standards (Whin Sill) analysed in this study compared with accepted values (from Potts et al. 1985)

	Standards		Accepted Values
La	25.5	25.8	25.5
Ce	52.1	51.9	57.5
Nd	30.9	30.7	32.9
Sm	6.25	6.43	7.27
Eu	2.09	2.09	2.25
Tb	1.00	1.01	1.09
Yb	2.40	2.46	2.54
Lu	0.38	0.36	0.39
Th	2.84	2.94	3.05
U	0.52	0.58	0.9
Ta	1.13	1.13	1.26
Hf	4.65	4.57	4.93
Na2O	2.65	2.68	2.7
Rb	35	34	35.3
Cs	1.06	1.19	1.03
Co	48.8	48.8	47.4
Fe2O3	13.4	13.2	12.62

List of values used to normalise REE data to chondrite in this thesis.

Element	C1 Chondrite (ppm)
La	0.237
Ce	0.612
Pr	0.095
Nd	0.467
Sm	0.153
Eu	0.058
Gd	0.2055
Tb	0.0374
Dy	0.2540
Ho	0.0566
Er	0.1655
Tm	0.0255
Yb	0.170
Lu	0.0254

After Sun and McDonough, 1989

List of partition coefficients used in this thesis.

	Cpx	Opx	Garnet	Hornblende		Plagioclase		Allanite
				FC	*PM*	*FC*	*PM*	
Sr	0.2	0.085	0.013	0.022	0.36	4.4	0.26	
Ba	0.05	0.029	0.022	0.044	0.33	0.31	0.6	
Y	0.03	0.09	16	12	1.9	0.055	0.6	100
Rb	0.03	0.027	0.034	0.014	0.22	0.04	0.06	
Ni	4.8		1.2	12	7.3	0.38	0.1	
Zr	0.35		0.5	0.45	0.45	0.01	0.25	1
Nb	0.3		0.2	1.3	1.3	0.025	0.025	2
La	0.1	0.5	0.04	0.74	0.2	0.4	0.13	960
Ce	0.2	0.15	0.08	1.52	0.3	0.27	0.11	940
Nd	0.4	0.22	0.2	4.26	0.8	0.21	0.07	750
Sm	0.6	0.27	1	7.77	1.1	0.13	0.05	620
Eu	0.6	0.17	0.98	5.14	1.3	2.15	1.3	56
Gd	0.7	0.34	3.8	10	1.8	0.097	0.04	440
Tb	0.7		7.5	11	2	0.09	0.037	270
Dy	0.7	0.46	11	13	2	0.064	0.031	200
Er	0.6	0.65	16	12	1.9	0.055	0.026	100
Yb	0.6	0.86	21	8.38	1.7	0.049	0.024	54
Lu	0.6	0.9	21	6	1.5	0.046	0.023	41

FC = fractional crystallisation, PM = partial melting. Coefficients reported in Luais and Hawkesworth (1994), which contains a complete reference list.

Appendix B

Pb-Pb zircon and Sm-Nd Procedures and Data Tables

Zircon Separation and Loading for the Kober Technique

Sample preparation.

Whole rock samples are split into small cubes, using a hydraulic splitter. The cubes are then cleaned in distilled water, to remove any possible surface contamination, and once dry, are crushed to small chips using a jaw crusher. The size of the crushate is then reduced to ≤ 1mm using a disk grinder. The dust sized fraction (which would clog filters later in the separation process) is removed from the crushate by rinsing in water, and the sample is then dried under a heat lamp. A zircon rich concentrate is then prepared from the crushate by two stages of flotation in heavy liquids, followed by magnetic separation. Individual zircons are then hand-picked and placed on filaments for analysis by the Kober Technique.

Heavy mineral concentration.

The separation of heavy minerals is carried out by flotation in two overflow-type centrifuges, the larger of which was built as part of this project.

Figure App. 1 shows the large centrifuge. The centrifuge pot (4.5 litre capacity) is axially driven at 2,800 RPM by a 450 V electric motor. The centrifuge is constructed within a fume cupboard, as it was initially to be run using the heavy liquid bromoform ($CHBr_3$; density $\approx$ 2.9 g/cm^3), which is toxic, both by contact and inhalation, and requires trichloroethane ($C_2H_3Cl_3$) as a solvent. However, the heavy liquid used is an aqueous solution of the salt sodium polytungstate, diluted to a density of 2.8 g/cm^3, which has the advantages of being non-toxic, and easy to recover from heavy-liquid saturated separates, simply using distilled water as a solvent.

The sample is mixed with heavy liquid in the bowl above the centrifuge, and the resulting slurry is passed down into the centrifuge. Minerals with densities $\geq$ 2.8 g/cm^3 (eg zircon, sphene, apatite, monazite, pyroxenes, biotite, hornblende) are retained within the centrifuge, and minerals less dense than 2.8 g/cm^3 (eg feldspars and quartz) are washed out of the centrifuge pot as further heavy liquid is added, to be collected in a sump. The heavy liquid is filtered from the light minerals (the filtration process is speeded by use of a rotary vacuum pump), and pumped back up into a header tank, from where it is mixed with more crushate.

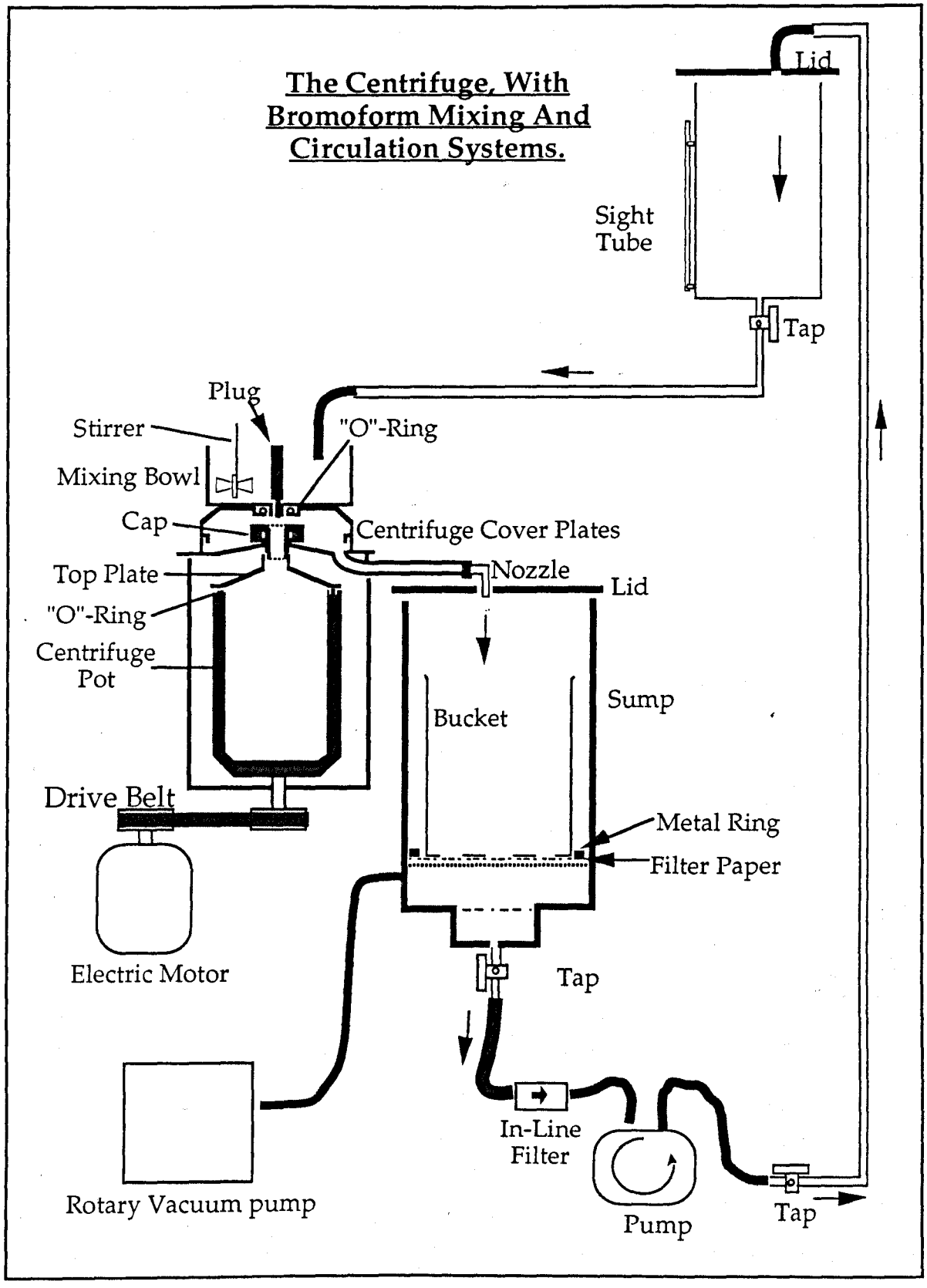

Figure App .1 Schematic diagram of the large centrifuge used in this work for the first stage in the preparation of a zircon-rich separate.

Once all the sample has been processed in this way, the bucket containing the light minerals is removed, and the light minerals are rinsed to recover the heavy liquid that they are saturated in. A second bucket is placed in the sump. The centrifuge assembly is stripped down, and the remaining heavy liquid and minerals are blown out of the centrifuge pot and into the sump using compressed air (figure App 2).

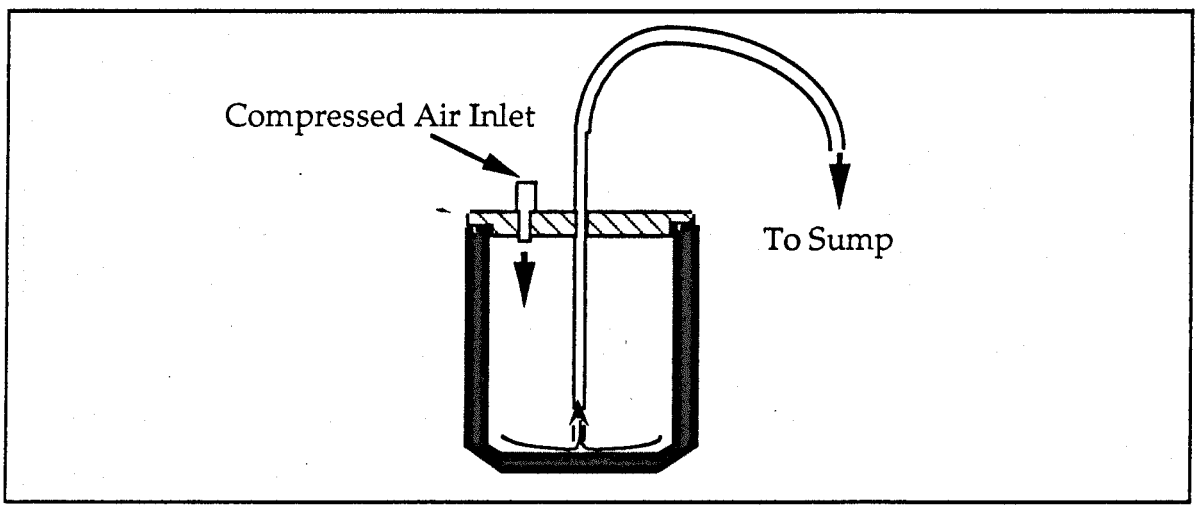

Figure App 2 Apparatus used to remove liquid and heavy minerals from the centrifuge pot

The dense separate is then rinsed in distilled water to extract any remaining sodium polytungstate. The water used to rinse the separates is then evaporated until it reaches the required density of 2.8 g/cm^3. In this way, over 95% of the sodium polytungstate may be recovered.

The dense separate is then processed in a small centrifuge (which operates on the same principle as the large centrifuge), using the heavy liquid di-iodo-methane (CH_2I_2; density ≈ 3.3 g/cm^3), which is recovered from the separates using trichloroethane as a solvent. The dense separate consists of zircon, sphene, apatite, monazite, sulphides, magnetite and metal "swarf" from the disk grinder. Magnetite and swarf are removed using a magnet, and the remaining material is passed several times through a Frantz electromagnetic separator, with the intensity of separation gradually increasing, removing minerals with magnetic properties such as sphene and monazite, to produce a zircon rich

separate, from which zircons may be hand-picked and loaded onto filaments for analysis.

Loading Filaments for the Kober Technique

Filament preparation

The evaporation filament (the filament into which the zircon is loaded) must be folded into a "canoe" to receive the zircon. This canoe is made by the following method.

The material used for the evaporation filament is 0.7 mm wide zone-refined Re. Before a strip of filament wire is welded onto its holder, a dent approximately 5 mm long is made at its centre, using the indentor (a modified letter "I" from a printing set) shown in figure App 3a. The filament is then welded to a holder, following normal filament making procedures. The dent in the filament is used as guide to fold the filament into a steep, symmetrical "v" shape, using a pair of tweezers, the spacing of teeth on which is approximately 0.7 mm. The ends of this "v" are then pressed together using a flat-faced pair of tweezers, to create a "canoe". The filament is then outgassed at 4.5 A for 10 minutes under high vacuum (> 10^{-6} torr).

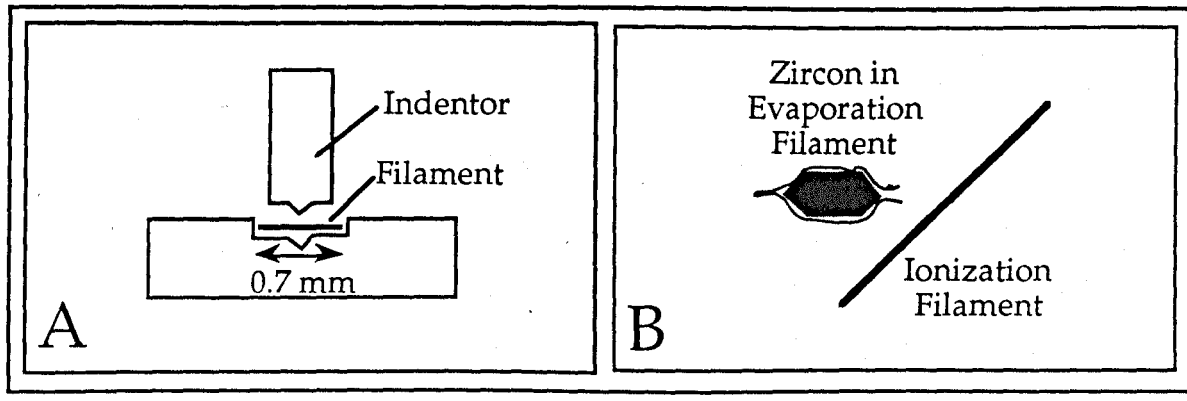

Figure App 3 (a) apparatus used to indent filaments as part of the process of crimping zircons into filaments. (b) sketch showing the optimum positioning of evaporation and ionization filaments.

The zircon is loaded into the filament by placing a drop of (teflon distilled) water in the "canoe" and placing a zircon into this. The zircon (usually) floats on the surface tension of the drop of water. As the water evaporates, the zircon is drawn down into the canoe, which is carefully folded up around the zircon using narrow, flat faced tweezers to produce a finished filament as shown in photo 2.1. The filament is then loaded onto the magazine, and carefully aligned with the ionisation filament (also 0.7 mm Re) as shown in figure App 3b, allowing the zircons to be analysed by the incremental heating technique described in Chapter 2. Analyses of the zircons were carried out on a Finnigan MAT 261 solid source, multi-collector mass spectrometer, interfaced with a HP 9836 computer using software designed by D.W. Wright and P.W.C. van Calsteren. Angling the ionisation filament as shown in figure App 3b (H. Chapman, pers. comm) was found to greatly increase beam intensities. There is probably an optimum separation of ionisation and evaporation filaments at any given emission temperature to allow the maximum amount of material from the zircon to plate the ionisation filament during a deposition cycle, and angling the ionization filament probably increases beam intensities by maximizing the surface area at the critical separation distance.

The zircon standards were run against the standard NBS 983, loaded onto 0.7 mm Re filaments with silica gel and phosphoric acid, and analysed on the Finnigan MAT 261 solid source, multi-collector mass spectrometer. The standard was assumed to have the isotope ratios $^{208}Pb/^{206}Pb = 0.013619 \pm 0.000024$, $^{207}Pb/^{206}Pb = 0.071201 \pm 0.000040$, $^{204}Pb/^{206}Pb = 0.000371 \pm 0.000020$. The standard was shown to be sensitive to addition of common Pb, and estimated loading blanks (figure App 4) were found to correspond closely to

spiked loading blank analyses carried out at this time (P.W.C. van Calsteren, pers. comm.)

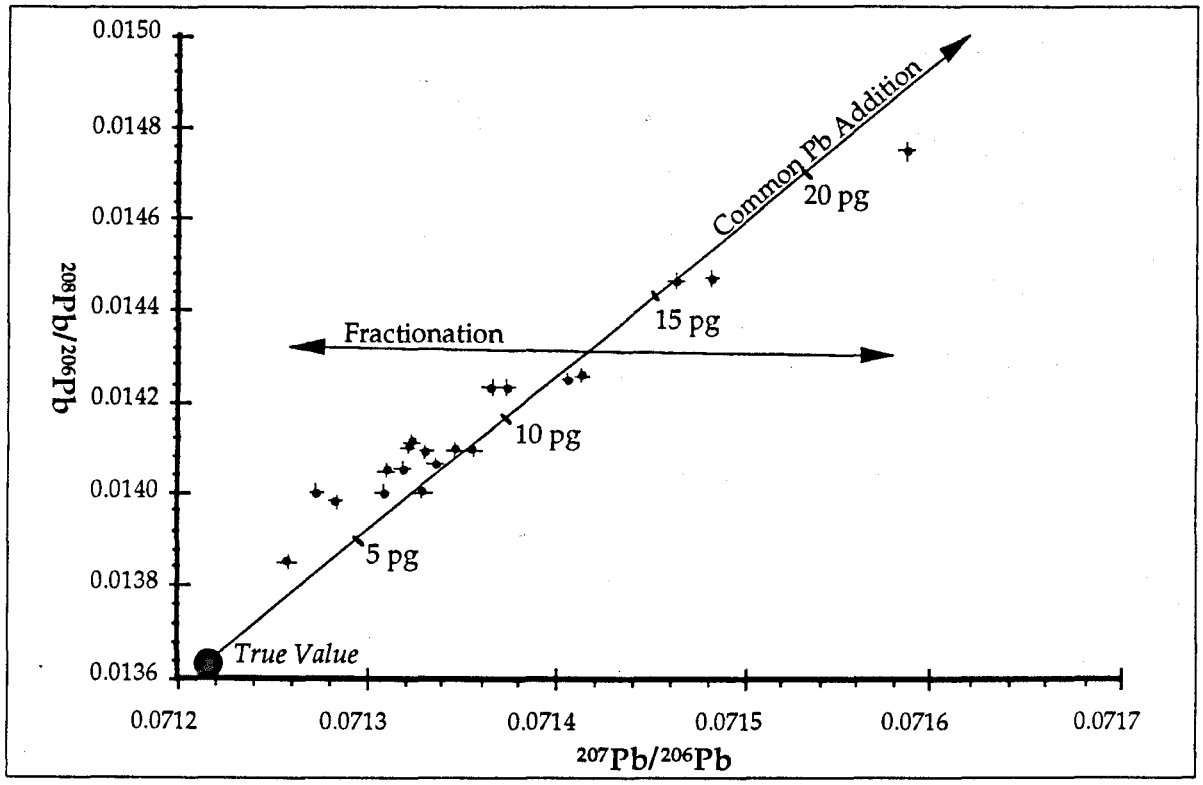

Figure App 4 Some analyses of the standard NBS 983 carried out during this thesis, showing the vectors for addition of common Pb (with the estimated amount of contamination in pico-grams), and fractionation.

89-S-14

Zircon	208/206	207/206	error in 7/6	204/206	Age	Index ($*10^8$)
Red Crystals						
2	0.16549	0.21730	62	0.000401	2926	0.04
	0.15495	0.21976	6	0.000183	2963	0.96
	0.10801	0.22999	5	0.000036	3049	5.43
	0.10407	0.23956	6	0.000021	3115	8.20
	0.13306	0.25058	27	0.000013	3187	2.83
	0.14889	0.25553	54	0.000014	3218	1.34
4	0.05019	0.21045	10	0.000112	2899	0.89
	0.03622	0.22437	15	0.000074	3006	0.87
	0.05504	0.23341	4	0.000163	3062	1.50
	0.08413	0.24108	5	0.000106	3119	1.92
	0.11302	0.24869	7	0.000061	3173	2.49
	0.13042	0.25010	21	0.000057	3181	0.83
	0.14198	0.25270	10	0.000027	3200	3.69
	0.14971	0.25375	52	0.000026	3205	0.73
5	0.07936	0.18404	42	0.000361	2649	0.07
	0.06935	0.20368	22	0.000161	2840	0.28
	0.05662	0.21840	12	0.000120	2959	0.71
	0.06478	0.22476	15	0.000142	3003	0.47
	0.07183	0.23148	6	0.000176	3048	0.98
	0.08513	0.23912	12	0.000036	3111	2.27
	0.10611	0.24501	14	0.000022	3151	3.22
	0.11457	0.24526	11	0.000021	3153	4.29
	0.13390	0.25207	7	0.000008	3197	16.07
6	0.12103	0.24341	27	0.000137	3132	0.27
8	0.08338	0.21899	31	0.000175	2958	0.19
	0.08092	0.22725	5	0.000038	3030	5.05
	0.07866	0.23164	25	0.000039	3060	1.01
	0.08085	0.23433	7	0.000034	3079	4.47
	0.08945	0.23787	15	0.000053	3102	1.22
	0.09610	0.24025	9	0.000035	3119	3.07
	0.10270	0.24356	4	0.000046	3140	6.19
	0.09038	0.23514	97	0.000059	3083	0.18
18	0.11673	0.21369	15	0.000152	2920	0.44
	0.07316	0.22129	19	0.000367	2960	0.14
	0.03666	0.22121	28	0.000149	2977	0.24
	0.03499	0.22232	19	0.000196	2982	0.26
	0.03733	0.22273	15	0.000156	2987	0.43
	0.04270	0.22520	7	0.000121	3008	1.22
	0.05332	0.23209	16	0.000076	3061	0.85
	0.07004	0.23773	14	0.000074	3099	0.96
	0.09590	0.24542	3	0.000031	3153	9.90
	0.12267	0.25268	11	0.000011	3201	8.34
	0.12812	0.25318	88	0.000018	3203	0.62
White Crystals						
3	0.08726	0.20208	179	0.000383	2806	0.01
9	0.07306	0.18937	220	0.000194	2717	0.02
	0.07829	0.19106	26	0.000118	2739	0.32
	0.08292	0.19418	13	0.000081	2770	0.94
	0.08041	0.19487	16	0.000068	2777	0.93

89-S-14 (continued)

Zircon	208/206	207/206	error in 7/6	204/206	Age	Index ($*10^8$)
9 (cont)	0.07538	0.19421	19	0.000074	2771	0.72
	0.07274	0.19175	9	0.000102	2747	1.10
	0.08261	0.19543	13	0.000102	2778	0.78
	0.06694	0.19461	19	0.000084	2773	0.64
11	0.11199	0.19232	11	0.000326	2729	0.27
	0.11195	0.19683	20	0.000225	2778	0.22
	0.11450	0.19861	24	0.000144	2801	0.29
	0.11208	0.19834	16	0.000120	2801	0.52
	0.11743	0.19784	27	0.000117	2797	0.32
	0.11980	0.19937	14	0.000142	2808	0.50
	0.12282	0.19940	7	0.000085	2813	1.66
	0.11795	0.19892	10	0.000037	2813	2.86
	0.13640	0.19993	15	0.000029	2822	2.23
	0.18908	0.20336	30	0.000015	2852	2.22
12	0.08733	0.17609	11	0.000265	2586	0.36
	0.10893	0.18777	14	0.000113	2711	0.61
	0.10698	0.19142	9	0.000108	2743	1.01
	0.11266	0.19584	9	0.000073	2784	1.46
	0.11927	0.19783	39	0.000066	2802	0.39
	0.11647	0.19711	10	0.000075	2795	1.33
	0.11869	0.19806	38	0.000070	2803	0.38
	0.11795	0.19786	24	0.000058	2802	0.73
	0.11550	0.19994	39	0.000047	2822	0.54

89-S-23

Zircon	208/206	8/6 error	207/206	7/6 error	204/206	4/6 error	Age	Index ($*10^8$)
1	0.11584	304.3	0.23341	102.5	0.000276	40.5	3054	0.00
	0.25082	335.6	0.24946	7.1	0.000032	2.2	3179	0.44
	0.28041	158.9	0.24785	3.8	0.000042	1.2	3168	0.62
	0.27262	287.0	0.24736	2.9	0.000037	2.1	3165	0.94
	0.28992	175.6	0.24800	1.8	0.000024	0.8	3171	2.38
	0.33358	487.7	0.24974	2.5	0.000018	1.3	3182	2.21
2	0.21397	142.7	0.20619	14.4	0.000285	9.9	2849	0.02
	0.24176	211.3	0.22058	3.6	0.000031	0.2	2982	0.88
	0.23422	335.2	0.22072	3.4	0.000017	1.3	2984	1.74
6	0.30883	0.7	0.21643	2.6	0.000079	0.9	2954	0.49
	0.30563	9.2	0.21651	1.2	0.000065	0.7	2955	1.32
7	0.11796	2.0	0.21401	1.7	0.000024	0.7	2934	2.48
10	0.08939	2.1	0.16297	1.8	0.000485	3.7	2424	0.12
	0.93975	1.5	0.17404	1.3	0.000407	0.8	2548	0.19
	0.11248	1.7	0.19336	1.4	0.000254	1.6	2745	0.29
	0.12219	0.9	0.20754	1.1	0.000127	1.0	2875	0.74
	0.13166	0.2	0.21120	0.2	0.000126	0.2	2904	3.45
	0.12848	3.4	0.21398	3.3	0.000062	1.0	2930	0.49
11	0.18669	1.6	0.17953	1.5	0.000998	2.4	2532	0.07
	0.14887	1.9	0.18642	0.9	0.000684	2.1	2636	0.17
	0.14742	1.2	0.19140	0.9	0.000569	1.4	2695	0.20
	0.15644	0.8	0.19940	0.7	0.000496	1.5	2772	0.29
	0.13504	2.5	0.21039	0.6	0.000614	32.1	2852	0.28
	0.14458	1.1	0.21864	1.2	0.000466	1.1	2930	0.17
12	0.11900	1.8	0.19778	1.5	0.000140	1.0	2794	0.49

89-S-23 (continued)

Zircon	208/206	error in 8/6	207/206	error in 7/6	204/206	error in 4/6	Age	Index (*10^8)
13	0.11700	1.0	0.19481	0.9	0.000259	0.6	2757	0.43
	0.14177	1.2	0.19887	1.5	0.000251	1.8	2793	0.26
	0.14687	3.2	0.20018	3.3	0.000242	3.1	2804	0.13
15	0.07079	6.6	0.22678	1.4	0.000090	0.7	3022	0.80
	0.08061	1.6	0.23419	1.9	0.000030	0.3	3079	1.72
	0.05603	2.8	0.23673	3.5	0.000031	58.0	3095	0.92
	0.04672	1.4	0.23951	1.0	0.000032	0.7	3114	3.25
16	0.11475	0.3	0.20120	0.9	0.000366	0.7	2801	0.31
	0.13382	0.6	0.23236	0.6	0.000080	0.4	3062	2.22
	0.13545	1.6	0.23906	1.2	0.000064	0.5	3109	1.27
17	0.17801	3.7	0.20955	2.9	0.000219	1.9	2882	0.16
	0.25408	0.2	0.21364	0.4	0.000058	1.1	2922	3.89
20	0.10066	11.6	0.19836	11.4	0.000355	5.1	2778	0.02
	0.12691	20.1	0.21281	1.2	0.000046	2.3	2923	1.79

Shamva Group 2

89-S-25

	208/206	error in 8/6	207/206	error in 7/6	204/206	error in 4/6	Age	Index (*10^8)
1	0.16637	169.7	0.21519	21.6	0.000036	2.1	2942	1.29
2	0.12768	194.1	0.21322	25.4	0.000411	95.3	2893	0.10
	0.14180	96.9	0.21242	18.0	0.000073	2.7	2918	0.76
	0.14193	33.6	0.21272	8.7	0.000112	1.5	2917	1.02
	0.12868	101.1	0.21263	6.2	0.000010	0.4	2925	16.37
3	0.13809	28.1	0.19817	11.3	0.000120	1.3	2799	0.73
	0.20622	26.0	0.20924	7.6	0.000063	0.5	2894	2.09
	0.19361	0.6	0.20870	52.0	0.000063	0.4	2888	0.30
4	0.20038	45.8	0.24169	19.1	0.000720	8.5	3076	0.07
	0.20356	1.6	0.24337	3.5	0.001118	857.0	3056	0.26
5	0.12317	16.4	0.16983	8.0	0.000604	4.4	2479	0.21
	0.14744	57.9	0.19202	31.0	0.000280	5.4	2730	0.12
9	0.13846	737.8	0.21148	202.7	0.000497	132.0	2872	0.01
	0.15113	710.4	0.21847	169.6	0.000864	194.1	2893	0.01
	0.14296	50.8	0.21002	39.0	0.000099	0.2	2897	0.26
	0.13210	59.5	0.21251	18.7	0.000131	3.0	2913	0.41
	0.13285	270.5	0.21450	19.3	0.000140	14.2	2928	0.37
10	0.10259	20.1	0.19115	16.6	0.000724	7.8	2675	0.08
	0.09818	32.9	0.19186	27.9	0.000755	17.9	2679	0.05
	0.07441	2.5	0.21996	3.0	0.000209	0.4	2963	1.60
	0.07452	13.3	0.22070	13.3	0.000189	1.8	2970	0.40
	0.06101	17.3	0.24001	7.7	0.000052	0.9	3116	2.50
	0.06487	39.6	0.23736	6.7	0.000072	0.4	3097	2.07
11	0.16981	307.8	0.21349	1030.0	0.000080	10.7	2926	0.01
12	0.08555	45.8	0.18414	21.0	0.000432	12.9	2463	0.11
	0.10326	18.0	0.18702	7.2	0.000306	3.0	2683	0.45
	0.16427	26.7	0.20314	9.5	0.000131	1.2	2839	0.80

89-S-12

Zircon	208/206	error in 8/6	207/206	error in 7/6	204/206	error in 4/6	Age	Index ($*10^8$)
1	0.13350	85.7	0.20152	146.6	0.000153	3.2	2842	0.04
	0.11711	17.9	0.20644	20.0	0.000050	0.9	2873	1.01
	0.10627	26.4	0.21047	25.2	0.000063	1.2	2904	0.63
	0.10197	38.9	0.21178	37.6	0.000017	0.6	2917	1.54
	0.10289	28.2	0.21242	30.0	0.000036	0.4	2921	0.93
	0.10305	17.8	0.21197	22.3	0.000013	0.3	2920	3.50
	0.10497	14.7	0.21198	9.1	0.000044	0.7	2917	2.52
	0.10303	12.3	0.21252	15.2	0.000052	0.7	2920	1.27
	0.10025	9.3	0.21210	16.1	0.000012	0.3	2921	5.11
2	0.12237	25.4	0.17969	24.1	0.000377	1.4	2607	0.11
	0.11868	12.8	0.18163	7.3	0.000340	1.3	2660	0.40
	0.12462	25.1	0.18775	31.2	0.000262	2.2	2695	0.12
	0.01266	13.6	0.19232	21.8	0.000198	2.1	2742	0.23
	0.13413	8.4	0.19713	9.1	0.000090	0.6	2794	1.22
	0.17352	78.0	0.20825	10.8	0.000392	1.2	2856	0.24
	0.18844	23.9	0.20747	13.2	0.000059	0.7	2880	1.29
	0.20696	7.3	0.20833	9.6	0.000050	0.8	2888	2.08
	0.21227	8.6	0.20828	10.6	0.000057	0.9	2887	1.65
	0.21762	21.2	0.20892	22.1	0.000083	0.9	2890	0.54
	0.23007	23.4	0.20852	8.2	0.000036	0.5	2891	3.42
	0.24594	18.6	0.20894	10.6	0.000030	0.6	2894	3.12
	0.25263	22.6	0.20869	19.1	0.000017	0.5	2894	3.14
	0.02530	25.5	0.20948	20.1	0.000017	0.4	2900	2.97
	0.25274	27.8	0.20926	20.7	0.000018	0.3	2898	2.74
3	0.10909	14.3	0.18769	36.6	0.000140	0.4	2708	0.20
	0.11675	120.8	0.19323	94.5	0.000072	1.3	2762	0.15
	0.11990	15.5	0.19942	15.7	0.000052	1.2	2817	1.23
	0.12224	27.0	0.20494	81.0	0.000031	0.7	2863	0.40
	0.11711	46.0	0.20923	24.3	0.000027	0.9	2897	1.50
	0.13017	34.8	0.21331	39.5	0.000021	0.9	2929	1.18
	0.11908	47.4	0.21517	49.7	0.000088	1.8	2937	0.23
4	0.16246	81.6	0.17546	64.8	0.000322	4.5	2573	0.05
	0.13747	63.0	0.17905	71.4	0.000200	5.1	2622	0.07
	0.14060	32.0	0.18311	15.6	0.000026	0.4	2679	2.47

89-S-19

Zircon	208/6	8/6 error	207/6	7/6 error	204/6	error in 4/6	Age	Index ($*10^8$)
1	0.09714	941.9	0.18996	964.1	0.000207	206.6	2720	0.01
	0.13267	659.7	0.19540	66.5	0.000153	152.7	2773	0.10
	0.12220	4310.6	0.18829	632.7	0.000146	145.8	2712	0.01
	0.14507	1078.0	0.19792	4725.8	0.000155	154.9	2794	0.00
	0.14396	431.5	0.19967	1010.1	0.000150	150.2	2809	0.01
	0.18297	136.3	0.21701	107.6	0.000145	145.5	2946	0.06
2	0.19584	22.5	0.22032	12.4	0.000983	982.7	2987	0.08
	0.14976	24.0	0.21837	27.1	0.000678	678.4	2910	0.05
	0.15112	1.4	0.21603	1.6	0.000393	393.1	2917	1.62
	0.16758	3.2	0.22189	0.5	0.000576	575.8	2945	3.47
3	0.11836	6.6	0.18734	5.7	0.000756	755.5	2636	0.23
	0.11774	1.8	0.19844	1.5	0.000500	499.9	2763	1.33
	0.12596	29.0	0.20280	2.8	0.000459	458.7	2804	0.78
	0.12288	34.9	0.20053	3.0	0.000409	408.9	2790	0.82
4	0.12587	37.6	0.20809	31.2	0.000179	178.9	2874	0.18
	0.12852	9.6	0.21006	5.3	0.000143	143.2	2893	1.32
	0.13603	7.8	0.21238	10.0	0.000144	144.4	2911	0.69
5	0.15527	3.9	0.21638	3.4	0.000357	357.2	2923	0.82
	0.15599	4.1	0.21787	3.0	0.000246	245.7	2944	1.36
6	0.10035	16.0	0.17483	17.7	0.000266	266.4	2573	0.21
	0.09821	8.0	0.17085	9.0	0.000276	275.8	2532	0.40
	0.09753	4.8	0.17055	5.0	0.000268	268.4	2529	0.75
	0.15526	9.2	0.20365	4.7	0.000161	160.7	2840	1.32
7	0.14723	63.4	0.18690	40.6	0.000503	503.1	2660	0.05
8	0.14210	14.3	0.20677	23.4	0.000405	405.1	2843	0.11
9	0.10421	86.7	0.20128	128.7	0.000261	261.4	2812	0.03
10	0.10865	122.8	0.20068	129.6	0.000309	309.0	2802	0.02
	0.14997	9.8	0.21624	2.1	0.000283	282.7	2928	1.68
11	0.13850	3.4	0.20769	18.4	0.000165	165.0	2872	0.33
12	0.14526	36.2	0.21248	49.9	0.000062	61.7	2919	0.32
13	0.14714	13.2	0.20934	7.1	0.000248	248.2	2878	0.57
	0.14739	6.5	0.20916	30.7	0.000273	272.7	2874	0.12
	0.14687	4.2	0.20858	2.1	0.000209	208.7	2875	2.30
	0.14720	3.7	0.20871	3.9	0.000282	282.5	2870	0.91
	0.13728	1.4	0.21577	168.3	0.000114	114.0	2939	0.05
14	0.14729	20.0	0.21357	1.7	0.000366	365.8	2900	1.61
	0.13464	109.2	0.21313	137.2	0.000372	371.6	2897	0.02
15	0.14581	4.5	0.21573	3.7	0.000074	73.7	2943	3.67
18	0.15350	188.5	0.21212	256.6	0.000437	437.1	2882	0.01
	0.18432	114.4	0.22147	132.9	0.000990	989.9	2906	0.01
	0.22664	25.5	0.23256	11.2	0.001876	1875.9	2912	0.05
	0.16119	3.9	0.21626	38.3	0.000364	363.8	2921	0.07
	0.16257	307.1	0.21636	316.1	0.000116	116.3	2944	0.03
19	0.12422	811.9	0.22313	886.2	0.000423	423.3	2968	0.00
	0.15260	38.5	0.21250	24.4	0.000505	504.6	2879	0.08
	0.14726	13.0	0.21206	10.4	0.000307	307.3	2894	0.31
	0.14994	7.7	0.21513	3.4	0.000234	233.6	2924	1.26
	0.16472	17.1	0.22045	6.2	0.000339	338.6	2955	0.48

Chinhoyi Group 1

89-C-15

zircon	208/206	error in 8/6	207/206	error in 7/6	204/206	error in 4/6	Age	Index ($*10^8$)
1	0.16237	50.1	0.18855	10.7	0.000126	1.2	2716	0.74
	0.16941	15.5	0.19601	19.3	0.000679	1.7	2722	0.08
	0.15096	43.7	0.19128	49.4	0.000330	2.9	2718	0.06
	0.14432	16.2	0.19014	26	0.000233	1.9	2719	0.17
	0.13218	46.9	0.18822	20.9	0.000032	0.5	2723	1.49
	0.12297	37.7	0.18809	35.7	0.000030	1.2	2722	0.94
	0.12160	27.0	0.18788	26.3	0.000038	1.0	2720	1.01
	0.11513	29.4	0.18829	32.3	0.000038	2.4	2723	0.82
2	0.16237	17.1	0.18855	10.7	0.000126	1.2	2716	0.74
	0.17341	10.8	0.18841	8	0.000099	0.7	2718	1.26
	0.16687	8.7	0.18822	4.3	0.000090	0.7	2717	2.58
	0.16042	7.7	0.18894	6.5	0.000121	0.8	2720	1.28
	0.15845	8.9	0.18958	11.5	0.000151	1.2	2723	0.58
	0.18029	20.8	0.19044	10.9	0.000194	2.0	2725	0.47
3	0.17450	6.7	0.18699	6.6	0.000323	0.5	2681	0.47
	0.17023	10.8	0.18680	69	0.000023	0.4	2712	0.62
	0.16487	16.6	0.18709	14.9	0.000023	0.5	2715	2.92
	0.16702	14.4	0.18719	8.6	0.000033	0.9	2714	3.55
	0.16151	27.7	0.18843	24.8	0.000019	0.5	2726	2.08
	0.16429	133.4	0.18920	72.7	0.000022	1.3	2733	0.62
4	0.15335	37.6	0.18792	38.3	0.000034	1.2	2721	0.76
	0.15167	27.6	0.18733	26.8	0.000034	0.8	2716	1.08
	0.15080	47.3	0.18916	42.2	0.000027	1.0	2732	0.87
	0.16389	23.9	0.19151	26.3	0.000384	1.8	2715	0.10
	0.15802	3.2	0.18963	6.2	0.000649	0.7	2669	0.25
	0.16503	4.9	0.19088	10.5	0.000344	0.3	2714	0.28
	0.15998	6.2	0.19019	4.9	0.000263	0.1	2715	0.78
	0.15902	6.2	0.18939	17.9	0.000146	1.3	2722	0.38
	0.15607	16.4	0.18958	19.3	0.000144	1.5	2723	0.36
	0.15771	6.4	0.18967	5.8	0.000211	1.0	2717	0.82
6	0.15430	9.3	0.18898	4.8	0.000152	0.6	2717	1.37
	0.15929	5.7	0.18930	6.5	0.000178	1.1	2717	0.87
	0.15523	8.7	0.18894	5.7	0.000142	0.5	2718	1.24
	0.15993	6.3	0.18941	6.3	0.000063	18.4	2730	2.52
	0.15085	1.0	0.18819	13.9	0.000083	0.7	2717	0.87
	0.15315	4.4	0.18798	5.7	0.000060	0.7	2718	2.91
	0.15213	4.4	0.18775	6.6	0.000031	0.3	2719	4.94
	0.16190	9.2	0.18799	6	0.000039	1.9	2721	4.28
	0.16618	14.3	0.18800	8.2	0.000027	0.4	2722	4.56
	0.15738	17.4	0.18798	8.5	0.000023	0.4	2723	5.22
	0.16946	12.8	0.18826	9.7	0.000048	1.2	2722	2.15
	0.16793	14.7	0.18838	15.5	0.000015	0.4	2726	4.16
	0.16309	19.1	0.18777	23.9	0.000018	0.5	2721	2.32
	0.15784	6.9	0.18828	15.2	0.000015	0.2	2725	4.52

89-C-20

zircon	208/206	error in 8/6	207/206	error in 7/6	204/206	error in 4/6	Age	Index ($*10^8$)
2	0.17884	16.5	0.20436	18.2	0.000035	2.3	2858	1.57
4	0.24817	73.8	0.22394	7.9	0.002281	4.4	2799	0.06
	0.18092	28.1	0.20708	46.7	0.000875	3.7	2798	0.02
	0.19508	11.7	0.21156	9.1	0.000996	2.4	2823	0.11
	0.20026	7.2	0.21372	3.0	0.001051	3.9	2835	0.32
	0.25910	29.6	0.23436	15.9	0.002291	6.2	2884	0.03
	0.16314	33.8	0.20347	19.5	0.000105	1.5	2844	0.49
	0.17001	7.8	0.20459	9.1	0.000114	0.9	2852	0.96
	0.18957	15.3	0.20859	13.5	0.000283	1.8	2868	0.26
	0.21757	42.1	0.21471	31.8	0.000659	4.2	2882	0.05
	0.18496	40.8	0.20560	30.8	0.000014	0.7	2870	2.32
	0.19745	38.6	0.20668	16.1	0.000011	0.3	2879	5.43
3	0.16841	19.5	0.20117	15.6	0.000619	3.0	2774	0.10
	0.18120	56.7	0.20833	15.0	0.000842	15.4	2812	0.08
	0.17444	20.7	0.20659	8.2	0.000538	1.6	2827	0.23
	0.16842	15.2	0.20510	13.9	0.000332	1.4	2835	0.22
	0.21789	39.9	0.22240	26.0	0.001530	14.8	2860	0.03
	0.16864	25.3	0.20477	26.0	0.000163	1.3	2849	0.24
	0.17173	261.9	0.20919	214.6	0.000168	5.6	2883	0.03
	0.17636	122.0	0.20655	12.4	0.000112	1.0	2868	0.72
6	0.20053	14.6	0.19497	83.3	0.001245	7.9	2651	0.01
	0.17329	13.8	0.19811	13.3	0.000410	2.0	2769	0.18
	0.16412	16.3	0.19940	17.1	0.000221	1.6	2798	0.27
	0.16593	16.0	0.20091	15.9	0.000228	4.5	2811	0.28
	0.17104	23.9	0.20456	19.7	0.000314	1.9	2833	0.16
	0.18095	45.5	0.21202	36.3	0.000686	2.6	2857	0.04
	0.20349	33.0	0.22244	49.6	0.001461	8.9	2868	0.01
7	0.16246	16.1	0.18295	7.7	0.000430	2.7	2631	0.30
	0.14428	11.9	0.19381	12.2	0.000119	0.5	2762	0.69
	0.14767	6.2	0.19362	9.0	0.000101	0.9	2778	1.10
	0.14910	4.9	0.19548	7.9	0.000070	0.6	2782	1.81
	0.14466	9.2	0.19654	4.1	0.000056	0.5	2792	4.39
	0.13833	10.4	0.19659	9.2	0.000052	0.5	2793	2.08
	0.14294	6.5	0.19733	7.0	0.000052	0.4	2799	2.76
	0.13811	7.4	0.19680	4.1	0.000051	0.5	2794	4.83
	0.13704	11.5	0.19886	9.9	0.000051	0.3	2812	1.97
	0.13380	2.7	0.19906	5.8	0.000037	0.3	2815	4.62
	0.18232	12.7	0.21465	6.8	0.000950	2.0	2853	0.15
	0.15000	8.1	0.20378	5.2	0.000030	0.3	2854	6.31
	0.14474	6.5	0.20265	6.3	0.000518	0.3	2797	0.31
	0.14290	8.3	0.20304	8.3	0.000069	0.6	2844	1.76
	0.15037	32.3	0.20372	8.3	0.000097	7.1	2847	1.25
	0.14943	103.3	0.20481	67.9	0.000058	1.2	2860	0.25
	0.14095	120.7	0.19919	274.4	0.000037	1.7	2816	0.10

89-C-28

Zircon	208/206	error in 8/6	207/206	error in 7/6	204/206	error in 4/6	Age	Index ($*10^8$)
1	0.18500	32.4	0.19622	29.9	0.000597	3.4	2734	0.06
	0.18244	47.5	0.19532	38.6	0.000551	4.2	2730	0.05
	0.16274	18.9	0.19789	26.1	0.000110	1.1	2798	0.35
	0.16853	88.7	0.19893	38.6	0.000115	2.5	2806	0.22
	0.16402	14.0	0.20012	20.6	0.000139	1.5	2813	0.35
	0.11589	48.0	0.20084	23.6	0.000117	1.6	2822	0.36
2	0.15284	43.5	0.18119	34.0	0.000087	1.3	2653	0.34
	0.13934	113.2	0.18213	277.8	0.000069	3.6	2664	0.05
	0.14571	113.2	0.18576	69.2	0.000067	1.5	2698	0.21
4	0.20520	12.1	0.19204	3.7	0.001149	1.6	2634	0.24
	0.24197	21.7	0.21612	6.8	0.002132	3.4	2746	0.07
	0.17765	8.3	0.20039	13.0	0.000671	2.4	2762	0.11
	0.16162	4.7	0.19917	5.1	0.000263	1.3	2794	0.74
	0.16865	7.9	0.20026	5.9	0.000310	2.6	2798	0.55
	0.16657	9.7	0.19956	49.0	0.000251	1.0	2798	0.08
	0.16206	7.6	0.19968	5.4	0.000251	1.0	2789	0.74
	0.16315	11.0	0.19915	8.5	0.000175	1.2	2802	0.67
	0.16435	4.0	0.20021	6.8	0.000180	1.1	2810	0.82
	0.16820	3.0	0.20164	9.3	0.000255	2.4	2814	0.42
	0.17743	29.1	0.20481	20.4	0.000461	8.8	2821	0.11
	0.16215	12.9	0.20038	11.1	0.000733	1.1	2755	0.12
	0.16168	11.7	0.20138	10.0	0.000059	0.5	2831	1.69
	0.16529	9.8	0.20225	7.9	0.000059	0.7	2839	2.14
	0.17548	12.9	0.20320	10.6	0.000059	0.7	2846	1.59
	0.16473	20.7	0.20544	11.1	0.000039	0.5	2866	2.29
	0.17760	17.3	0.20613	13.4	0.000054	1.1	2870	1.38

89-C-23

zircon	208/206	error in 8/6	207/206	error in 7/6	204/206	error in 4/6	Age	Index (*10^8)
2	0.14935	15.0	0.20663	15.5	0.000011	0.3	2878	5.83
	0.13005	3.6	0.20616	3.0	0.000013	0.2	2875	25.84
4	0.13926	5.2	0.20584	2.2	0.000010	0.3	2872	43.37
5	0.13065	5.1	0.20633	3.7	0.000007	0.2	2876	37.38
6	0.12975	6.4	0.20355	4.4	0.000018	0.2	2853	12.93
	0.12271	5.1	0.20509	6.0	0.000011	0.2	2866	15.83
7	0.15301	8.7	0.20266	4.4	0.000301	1.0	2819	0.76
	0.13795	6.8	0.20321	3.8	0.000076	0.5	2845	3.47
	0.13610	4.8	0.20442	4.1	0.000045	0.3	2857	5.46
	0.13458	5.2	0.20534	2.7	0.000031	0.3	2866	12.11
	0.13624	13.8	0.20623	12.7	0.000029	0.3	2874	2.69
	0.13171	3.1	0.20592	1.6	0.000018	0.1	2872	34.41
	0.13215	2.6	0.20593	2.0	0.000016	0.2	2872	30.76
	0.13292	2.5	0.20604	1.4	0.000014	0.2	2873	50.08
	0.13097	3.4	0.20593	1.8	0.000010	0.1	2873	56.98
	0.13126	4.5	0.20621	4.6	0.000013	0.1	2875	16.43
	0.13233	19.4	0.20650	8.3	0.000015	0.2	2877	7.77
	0.13028	4.4	0.20647	5.0	0.000012	0.9	2877	16.64
	0.13099	6.5	0.20661	2.6	0.000018	0.2	2877	21.20
	0.13157	3.7	0.20658	3.5	0.000013	0.2	2878	21.40
	0.13520	25.3	0.20722	41.7	0.000017	0.5	2883	1.37
	0.13512	10.3	0.20676	3.3	0.000028	0.3	2878	10.87
	0.14181	13.0	0.20718	5.0	0.000059	1.0	2878	3.40
	0.13872	8.9	0.20681	6.8	0.000010	0.3	2879	14.17
8	0.14567	41.0	0.20062	25.0	0.000139	0.7	2818	0.29
	0.14285	60.0	0.20390	23.0	0.000109	0.6	2848	0.40
	0.13839	16.0	0.20464	27.0	0.000020	0.2	2861	1.81
	0.13670	22.0	0.20460	28.0	0.000033	0.2	2860	1.07
	0.13626	15.0	0.20545	23.0	0.000021	0.1	2868	2.12
	0.13461	34.7	0.20581	31.4	0.000019	0.5	2871	1.68
	0.13515	23.0	0.20603	8.9	0.000016	0.3	2873	7.03
	0.13550	7.3	0.20585	11.7	0.000018	0.2	2870	4.86
	0.13692	6.8	0.20614	4.5	0.000032	0.3	2872	7.03
	0.13363	3.7	0.20612	4.0	0.000014	0.3	2874	17.54
	0.13552	6.6	0.20617	5.1	0.000014	0.3	2875	14.26
	0.13725	4.2	0.20608	3.5	0.000020	0.3	2873	14.00
	0.13850	9.7	0.20713	9.5	0.000053	0.6	2879	2.00
	0.13699	5.3	0.20627	4.7	0.000012	0.2	2875	18.15
	0.13668	5.4	0.20626	6.3	0.000010	0.2	2875	16.64
	0.13611	3.3	0.20609	3.4	0.000010	0.6	2874	28.55
	0.13639	4.7	0.20609	4.8	0.000006	0.1	2875	34.31
	0.13717	11.9	0.20618	6.8	0.000007	0.2	2875	22.17
	0.13614	3.0	0.20616	2.4	0.000006	0.1	2875	73.78
	0.13876	8.7	0.20639	7.5	0.000007	0.1	2877	19.33
	0.13819	7.7	0.20634	4.8	0.000004	0.2	2876	58.64

89-C-21

zircon	208/206	error	207/206	error	204/206	error	Age	Index ($*10^8$)
1	0.11673	11.4	0.20327	8.5	0.000022	0.4	2851	5.35
	0.11840	11.0	0.20471	8.8	0.000007	0.2	2863	16.16
	0.12362	15.7	0.20650	4.2	0.000005	0.2	2878	44.12
	0.11587	34.2	0.20608	33.3	0.000007	0.4	2875	4.48
4	0.13918	41.9	0.20604	30.7	0.000020	0.4	2872	1.59
	0.14022	15.6	0.20685	16.6	0.000013	0.5	2879	4.54
7	0.13953	60.2	0.20089	65.5	0.000057	1.9	2828	0.27
	0.13426	2.4	0.20398	3.6	0.000026	0.2	2856	10.88
	0.13409	4.4	0.20515	7.6	0.000014	0.3	2866	9.51
	0.13524	11.6	0.20576	7.3	0.000011	0.4	2872	12.64
	0.13402	9.2	0.20554	6.7	0.000009	0.5	2870	16.04
	0.13477	26.6	0.20713	26.1	0.000008	0.4	2882	4.69
	0.13316	5.5	0.20594	4.3	0.000006	0.1	2873	37.31
	0.13099	8.4	0.20658	8.9	0.000007	0.2	2879	16.49
9	0.16241	267.5	0.21987	462.9	0.000470	6.2	2939	0.00
	0.13495	22.6	0.20454	20.2	0.000076	1.0	2856	0.65
	0.13388	19.2	0.20584	11.4	0.000028	0.4	2871	3.14
	0.13207	25.1	0.20646	18.6	0.000017	0.3	2876	3.25
	0.13203	13.0	0.20628	7.0	0.000009	0.3	2875	15.89
	0.13052	5.4	0.20624	5.6	0.000008	0.2	2875	21.09
	0.12924	4.1	0.20637	5.3	0.000009	0.2	2876	21.11
	0.13332	13.5	0.20635	6.3	0.000009	0.2	2876	17.64
	0.13428	85.4	0.20872	136.6	0.000009	0.6	2892	0.85
	0.13582	5.0	0.20134	2.4	0.000087	0.7	2828	4.80
10	0.13168	3.2	0.20419	2.1	0.000038	0.2	2856	12.43
	0.14843	43.8	0.20917	14.1	0.000241	2.7	2877	0.29
	0.13372	4.9	0.20547	2.5	0.000043	0.3	2866	9.21
	0.13255	5.1	0.20548	3.8	0.000018	0.2	2869	14.23
	0.13288	7.5	0.20596	4.3	0.000009	0.1	2873	25.32
	0.13302	13.3	0.20633	6.2	0.000007	0.1	2876	24.24
	0.13352	11.5	0.20643	5.9	0.000004	0.1	2877	38.23
	0.13042	6.1	0.20628	6.5	0.000005	0.1	2876	28.80
	0.13185	6.1	0.20649	7.2	0.000006	0.1	2878	22.79
	0.13211	6.0	0.20620	2.9	0.000004	0.1	2876	90.14
	0.13176	6.0	0.20597	4.9	0.000005	0.4	2874	44.65
	0.12945	3.7	0.20607	2.4	0.000003	0.0	2875	119.92
	0.13254	3.4	0.20611	3.2	0.000004	0.0	2875	80.32
	0.13296	8.9	0.20681	35.5	0.000004	0.1	2880	6.97
11	0.13078	14.3	0.20612	3.8	0.000003	0.1	2875	80.40
	0.13022	3.8	0.20625	3.2	0.000004	0.7	2875	72.39
	0.12963	3.7	0.20622	28.0	0.000003	0.0	2876	12.21
	0.13095	6.5	0.20620	3.3	0.000003	0.1	2876	108.03
	0.13114	4.7	0.20604	2.7	0.000003	0.1	2875	132.46
	0.13340	9.5	0.20655	6.5	0.000003	0.1	2879	51.08
	0.13700	9.9	0.20650	6.0	0.000032	0.4	2875	5.16
	0.13569	5.4	0.20638	4.2	0.000030	0.2	2875	8.03
	0.13504	2.8	0.20635	2.4	0.000027	0.3	2875	15.34
	0.13485	1.9	0.20636	1.9	0.000026	0.1	2875	20.35
	0.13470	1.5	0.20635	2.0	0.000026	0.1	2875	19.01
	0.13464	0.6	0.20627	1.9	0.000027	0.2	2874	19.57
	0.13461	1.5	0.20628	2.0	0.000027	0.1	2874	18.33
	0.13456	1.3	0.20625	1.3	0.000027	0.1	2874	28.56

Sesombi Tonalite

Zircon	208/208	error in 8/6	207/206	error in 7/6	204/206	error in 4/6	Age	Index (*10^8)
1	0.10420	5.2	0.17501	11.2	0.000103	1.1	2594	0.86
	0.10188	7.6	0.17711	75.0	0.000050	0.5	2620	0.27
	0.10322	5.3	0.17964	4.5	0.000030	0.2	2646	7.40
	0.10353	3.8	0.18059	4.6	0.000021	0.2	2656	10.34
	0.10596	8.3	0.18120	4.9	0.000016	0.4	2662	12.44
	0.11706	5.8	0.18171	4.1	0.000012	0.3	2667	19.66
	0.12233	4.7	0.18133	2.8	0.000014	0.2	2663	25.04
	0.12615	5.9	0.18162	6.0	0.000012	0.2	2666	14.27
	0.12086	10.4	0.18190	10.0	0.000013	0.1	2669	7.48
	0.11530	6.7	0.18197	4.3	0.000016	0.2	2669	14.67
	0.11517	15.2	0.18222	18.4	0.000013	0.2	2671	4.08
	0.11293	12.0	0.18168	15.1	0.000016	0.4	2666	4.13
2	0.09263	3.5	0.18348	6.6	0.000149	0.9	2668	1.02
3	0.09120	8.7	0.17445	16.6	0.000076	0.8	2592	0.79
	0.08673	4.7	0.18123	3.0	0.000032	0.4	2661	10.35
	0.09506	12.1	0.18228	6.3	0.000024	0.5	2671	6.65
	0.10845	5.5	0.18280	8.2	0.000024	0.5	2676	5.16
	0.10535	11.5	0.18254	9.7	0.000021	0.4	2673	5.02
	0.10512	5.3	0.18244	6.9	0.000018	0.4	2673	7.94
	0.10845	3.0	0.18253	4.6	0.000014	0.4	2674	15.03
	0.11073	11.4	0.18306	18.8	0.000015	0.4	2679	3.61
	0.11312	13.7	0.18275	6.0	0.000011	0.2	2677	15.11
	0.10528	25.0	0.18413	29.1	0.000028	4.3	2687	1.23
4	0.07266	30.5	0.18218	37.5	0.000010	1.0	2672	2.67
	0.08153	162.6	0.18076	119.4	0.000024	1.7	2657	0.35
	0.09052	46.9	0.18359	42.1	0.000017	1.0	2683	1.42
5	0.10554	9.5	0.18248	15.1	0.000078	1.1	2667	0.85
	0.09983	9.2	0.18219	8.2	0.000032	0.3	2670	3.85
	0.09819	7.5	0.18261	4.4	0.000036	13.7	2672	6.34
	0.09935	5.2	0.18258	5.7	0.000026	0.5	2673	6.75
	0.10305	5.8	0.18272	4.3	0.000026	0.5	2675	9.10
	0.10600	10.2	0.18276	6.3	0.000017	0.3	2676	9.28
	0.11204	14.2	0.18311	21.4	0.000034	1.1	2677	1.36
	0.12175	5.6	0.18263	6.0	0.000057	0.4	2671	2.95
	0.12804	7.8	0.18299	14.4	0.000026	0.6	2677	2.65
10	0.10296	85.4	0.18563	59.0	0.000271	2.9	2674	0.06
	0.09446	42.2	0.17998	97.8	0.000330	12.7	2615	0.03
	0.09367	62.5	0.18269	54.7	0.000040	11.2	2673	0.45
	0.10014	6.1	0.18252	9.2	0.000023	0.5	2673	4.79
	0.09631	4.9	0.18272	7.9	0.000024	2.7	2675	5.30
	0.09501	18.3	0.18298	20.4	0.000021	0.5	2678	2.32
	0.09782	1.3	0.18262	11.9	0.000030	0.6	2673	2.83
	0.10594	11.1	0.18316	7.6	0.000032	0.3	2678	4.17
	0.11946	120.0	0.18565	152.7	0.000161	5.6	2686	0.04
	0.10711	19.8	0.18257	10.0	0.000027	0.5	2673	3.69
	0.12022	17.8	0.18300	19.2	0.000046	1.0	2675	1.14

Mashaba Tonalite

89Zb-12

208/206	error in 8/6	207/206	error in 7/6	204/206	error in 4/6	Age	Index ($*10^8$)
0.13345	15.7	0.18853	14.5	0.000300	1.0	2697	0.23
0.12877	28.6	0.20304	43.6	0.000146	1.5	2836	0.16
0.14361	24.0	0.20712	26.8	0.000153	2.4	2869	0.24
0.14263	7.7	0.20730	48.5	0.000121	1.0	2873	0.17
0.13627	30.1	0.20793	56.3	0.000123	2.3	2878	0.14
0.14219	9.9	0.20885	31.1	0.000107	11.1	2886	0.30
0.13253	14.8	0.21323	17.2	0.000096	1.3	2922	0.60
0.13083	5.3	0.21343	12.4	0.000085	0.8	2924	0.95
0.14130	14.4	0.21459	15.5	0.000096	1.3	2932	0.67
0.13728	8.5	0.21515	7.4	0.000092	0.1	2936	1.48
0.14333	18.5	0.21913	19.2	0.000066	0.9	2968	0.79
0.14563	11.8	0.22121	6.8	0.000067	0.6	2984	2.20
0.14639	29.5	0.22196	46.0	0.000081	1.1	2988	0.27
0.14902	21.7	0.22624	20.0	0.000060	1.5	3021	0.83
0.14661	10.6	0.23060	10.7	0.000055	2.5	3052	1.70
0.12693	6.2	0.24012	7.7	0.000127	1.0	3111	1.02
0.16588	24.0	0.26080	14.6	0.000072	2.1	3247	0.95

Chingezi Tonalite - Hokonui Formation

Zircon	208/206	error in 8/6	207/206	error in 7/6	204/206	error in 4/6	Age	Index ($*10^8$)
1	0.08092	26.0	0.19253	14.7	0.000106	1.5	2765	0.64
	0.08080	13.0	0.19259	8.8	0.000083	0.8	2793	1.37
	0.08542	92.3	0.19180	7.3	0.000055	0.5	2752	2.47
	0.08791	22.9	0.19008	1.5	0.000145	62.1	2728	4.76
	0.08910	30.6	0.18891	28.6	0.000066	1.6	2726	0.53
2	0.12914	7.4	0.17898	7.4	0.000508	2.6	2584	0.27
	0.11833	5.1	0.18322	5.9	0.000271	0.6	2652	0.63
	0.11356	4.3	0.18600	4.5	0.000197	0.6	2686	1.13
	0.11051	4.7	0.18647	6.9	0.000166	0.9	2693	0.87
	0.11000	9.2	0.18693	6.6	0.000158	0.2	2699	0.96
	0.10739	10.3	0.18860	5.2	0.000140	1.1	2715	1.37
	0.10543	4.4	0.19053	3.6	0.000112	0.6	2735	2.49
	0.10187	8.8	0.19139	7.5	0.000100	1.2	2743	1.33
	0.10187	8.5	0.19197	7.1	0.000107	7.0	2747	1.31
	0.10087	6.2	0.19054	9.0	0.000095	0.9	2737	1.17
	0.09873	1.8	0.18960	11.1	0.000056	0.8	2733	1.60
	0.09796	9.7	0.18974	15.2	0.000053	0.6	2734	1.25
	0.09673	7.7	0.19202	12.1	0.000042	0.8	2755	1.97
	0.09143	12.5	0.19429	11.2	0.000036	0.8	2775	2.49
	0.09142	12.5	0.19836	30.1	0.000034	0.6	2809	0.97
	0.09268	67.3	0.20201	85.8	0.000064	18.8	2836	0.18
3	0.11026	14.0	0.17571	14.1	0.000114	1.3	2600	0.62
	0.12114	12.7	0.18043	12.5	0.000049	0.5	2651	1.64
	0.12537	20.0	0.18138	27.3	0.000034	0.8	2662	1.09
	0.13014	20.6	0.18209	17.6	0.000042	1.0	2667	1.36
	0.13453	13.2	0.18155	27.8	0.000029	0.6	2663	1.23
	0.13666	9.9	0.18223	13.7	0.000032	0.5	2670	2.28

Chinese Granulite

Chinese Granulite

Zircon	208/206	error in 8/6	207/206	error in 7/6	204/206	error in 4/6	Age	Index ($*10^8$)
1	0.15327	39.7	0.16488	25.8	0.000026	0.1	2503	1.49
2	0.22732	25.9	0.16818	17.2	0.000002	0.1	2538	24.33
	0.16699	9.0	0.16760	13.4	0.000001	0.0	2533	64.81
	0.22676	13.9	0.16733	7.9	0.000009	0.1	2530	13.97
3	0.17065	8.0	0.16767	7.7	0.000016	0.2	2532	8.17
	0.20023	9.3	0.16747	5.0	0.000013	0.3	2531	15.59
4	0.19169	11.6	0.16699	16.8	0.000012	0.3	2526	5.10
5	0.20590	16.7	0.16766	9.7	0.000021	0.2	2531	4.96
6	0.21186	20.2	0.16627	42.9	0.000018	0.5	2518	1.32
7	0.15135	20.9	0.16738	4.2	0.000004	1.0	2531	61.28
	0.17804	6.3	0.16729	7.4	0.000006	1.5	2530	22.80
	0.18099	33.8	0.16802	42.9	0.000010	4.3	2536	2.30
	0.18616	8.5	0.16738	7.9	0.000005	0.2	2531	24.86
	0.18914	16.2	0.16730	1.2	0.000005	0.2	2530	177.54
	0.19173	10.5	0.16775	16.5	0.000008	3.6	2534	8.06
	0.19468	20.9	0.16677	15.8	0.000010	5.0	2524	6.32
	0.19642	20.8	0.16712	17.0	0.000003	0.2	2528	20.75
	0.20139	23.9	0.16747	13.9	0.000004	0.2	2532	16.00
	0.20533	25.0	0.16776	27.7	0.000003	0.2	2535	12.21
	0.20901	14.0	0.16735	10.7	0.000003	0.1	2531	32.37

Fractionation Experiment

Fractionation Experiment

Temperature	208/206	error in 8/6	207/206	error in 7/6	204/206	error in 4/6	Age
1250°C	0.13700	9.9	0.20650	6.0	0.000032	0.4	2875.2
1260°C	0.13569	5.4	0.20638	4.2	0.000030	0.2	2874.6
1265°C	0.13504	2.8	0.20635	2.4	0.000027	0.3	2874.6
1270°C	0.13485	1.9	0.20636	1.9	0.000026	0.1	2874.7
1275°C	0.13470	1.5	0.20635	2.0	0.000026	0.1	2874.6
1280°C	0.13464	0.6	0.20627	1.9	0.000027	0.2	2874.0
1285°C	0.13461	1.5	0.20628	2.0	0.000027	0.1	2874.0
1290°C	0.13456	1.3	0.20625	1.3	0.000027	0.1	2873.8
1295°C	0.13453	1.9	0.20617	1.9	0.000027	0.1	2873.2
1300°C	0.13457	1.0	0.20608	1.6	0.000026	0.2	2872.5
1305°C	0.13450	0.9	0.20605	1.3	0.000025	0.1	2872.4
1310°C	0.13441	1.8	0.20603	1.0	0.000024	0.1	2872.3
1315°C	0.13432	1.5	0.20597	1.0	0.000022	0.1	2872.0
1320°C	0.13419	0.6	0.20591	1.0	0.000020	0.1	2871.7

Sm-Nd procedure

Sm-Nd analyses were performed at Clermont-Ferrand by Béatrice Luais. For each analysis, approximately 100-160 mg of rock powder was weighed into a screw-top Savillex teflon bomb, with a ^{150}Nd-^{149}Sm double spike, in order to obtain Nd isotope compositions and concentrations, and Sm concentrations by isotope dilution analysis from the same dissolution of sample. The acids used for digestion were: 3ml of HCl (12M), 2 ml HNO_3 (14M), 3 ml concentrated HF. The Savillex bomb was covered with the screw top and left for approximately one month (cool), followed by a few days on a hot plate at 80-100°C to insure complete dissolution, before being evaporated to dryness. The residue was dissolved in 3ml aqua regia (2/3 HCl +1/3 HNO_3), then evaporated to dryness. The residue was then dissolved in 10ml 6M HCl, left on the hot plate for 1-2 days, until no visible residue was present. It was then evaporated to dryness.

This residue is dissolved in 2.5M HCl, centrifuged, and loaded onto cationic exchange columns, from which the REE fraction was collected. The REE fraction was evaporated to dryness, then dissolved in 0.25M HCl and loaded onto columns of teflon powder coated with HDEHP. Nd was eluted with 0.25M HCl and then Sm with 0.6M HCl. These two fractions were then evaporated to dryness .

Outgassed triple Re-Ta filaments with central Re and Ta sides were used for Nd analysis on a Micromass VG54E mass spectrometer. The Nd fraction was dissolved in 3µl H_2O and loaded on one of the Ta side filament.

Outgassed single Ta filaments are used for Sm analysis. The Sm fraction was dissolved with few µl of H_2O and loaded with H_3PO_4 on a Ta filament.

The value of the $^{146}Nd/^{144}Nd$ ratio is used for the mass fractionation correction of the Nd isotopic composition by normalizing to

$^{146}Nd/^{144}Nd$=0.7219 Nd isotope composition was then subsequently corrected to $^{145}Nd/^{144}Nd = 0.348417$

Nd isotope composition values obtained for La Jolla standard during this period of time were:

$^{143}Nd/^{144}Nd = 0.511855 \pm 7$
$^{143}Nd/^{144}Nd = 0.511851 \pm 7$
$^{143}Nd/^{144}Nd = 0.511838 \pm 7$
$^{143}Nd/^{144}Nd = 0.511863 \pm 6$
$^{143}Nd/^{144}Nd = 0.511855 \pm 6$
$^{143}Nd/^{144}Nd = 0.511861 \pm 7$

Giving an average value of 0.511854 ± 9 (1 std. dev. error), compared with the recommended value of 0.511850. During the same run, $^{150}Nd/^{144}Nd$ ratios were analysed for Nd contents. For separate Sm runs, the $^{149}Sm/^{147}Sm$ ratios were analysed for Sm contents. The reproducibility on the $^{147}Sm/^{144}Nd$ ratio is estimated to be 0.2%.

Sm-Nd data table

	Sm ppm	Nd ppm	$^{147}Sm/^{144}Nd$	$^{143}/^{144}Nd$ *measured*	±	$^{145}/^{144}Nd$ *measured*	$^{143}Nd/^{144}Nd$ *corrected*
Shamva sediments							
89-S-3	2.55	13.10	0.117670	0.511164	7	0.348401	0.511141
89-S-6	2.01	12.33	0.098478	0.510866	7	0.348411	0.510857
Shamva clasts							
89-S-14	2.26	13.26	0.103042	0.510897	9	0.348393	0.510862
89-S-23	2.45	15.42	0.095907	0.510616	7	0.348391	0.510578
89-S-12	4.89	26.72	0.110540	0.510943	8	0.348392	0.510906
89-S-19	2.71	14.96	0.109737	0.510896	6	0.348406	0.510880
89-S-25	3.88	23.48	0.099983	0.510669	8	0.348387	0.510625
89-S-26	5.58	26.33	0.128074	0.511185	8	0.348392	0.511148